DEVELOPMENT OF NOVEL STRATEGIES TO FILL THE EMPTY DRUG PIPELINE FOR SCHISTOSOMIASIS: FROM DRUG SENSITIVITY ASSAY DEVELOPMENT TO PRECLINICAL STUDIES

Inauguraldissertation
zur
Erlangung der Würde eines Doktors der Philosophie
vorgelegt der
Philosophisch-Naturwissenschaftlichen Fakultät
der Universität Basel

von

Flavio Christopher Lombardo

aus Italien

2020

Originaldokument gespeichert auf dem Dokumentenserver der Universität Basel
https://edoc.unibas.ch

Genehmigt von der Philosophisch-Naturwissenschaftlichen Fakultät

auf Antrag von

Prof. Dr. Jennifer Keiser, Prof. Dr. Britta Lundström-Stadelmann

Basel, 17/12/2019

Prof. Dr. Martin Spiess
The Dean of Faculty

Acknowledgments

First of all, I would like to express my sincere gratitude to Prof. Dr. Jennifer Keiser for giving me the opportunity to be part of this exciting research group and to work in this very interesting field of research, for her patience, precious support and all the considerate guidance. I could not have wished for a better professor.

I would also like to thank everybody on my thesis committee: Prof. Dr. Britta Lundström-Stadelmann, Prof. Dr. Andreas Hierlemann and Prof. Dr. Pascal Mäser, for agreeing to be part of my committee and for their contribution of time to this very important moment of my career.

A warm thank you to Valentin Buchter, Alexandra Probst and Anna Van Beek for their encouragement and support offered during the process of writing this thesis and for proofreading it.

Special thanks go to Gordana Panic who introduced me to the topic when I first joined the team and to the fantastic wormy group: Cécile Häberli, Valerian Pasche, Valentin Buchter, Alexandra Probst, Sophie Welsche, Marta Palmeirim, Ladina Keller, Chandni Patel, Emmanuel Mrimi, Stefan Biendl, Anna Van Beek, Jantine Brussee, Daniela Hofmann, Eveline Hürlimann, Miriam Bolz and all the Zivis. Thank you to all the wormy friends - thanks for all the fun we had together, it was great sharing a lab and office with you guys!

The chip / EIS projects discussed in this dissertation would not have been possible without Mario Modena and Paolo Ravaynia from the Professor Hierlemann's group at ETH Basel, who designed and provided the various platform prototypes and contributed valuable inputs and ideas to the project. Thank you for the fruitful collaboration and all the hard work you put into the project.

I would like to thank Professor Dr. Beatrice Perissutti from the University of Trieste for the very pleasant collaboration leading to the manuscript presented in Chapter IV of this thesis. Not only did she provide the praziquantel derivative, but she also contributed time and valuable inputs.

Thank you to all the friends in the MPI! My work would not have been the same without you!

And finally, last but by no means least, my deep appreciation goes to my partner Alexandra and to my family; their love and support has been unconditional all these years. Grazie mille!

Sincerely,

Flavio C. Lombardo

Table of Contents

Table of abbreviations 1

Summary 2

1. Introduction 4
  - 1.1 Background 4
    - 1.1.1. *Schistosoma mansoni* life cycle 5
    - 1.1.2. Epidemiology 7
    - 1.1.3. Pathology 8
    - 1.1.4. Diagnosis, treatment and prevention 10
    - 1.1.5. Praziquantel 12
  - 1.2. Current challenges in the field 14
  - 1.3. Anti-schistosomal drug screening 15
    - 1.3.1. Drug repurposing 17
  - 1.4. Polymorphism 18
  - 1.5. Electrical impedance spectroscopy (EIS) 20
  - 1.6. Liver microtissues 22
  - 1.7. Aim and objectives of the thesis 25

Chapter 1: Life cycle maintenance and drug-sensitivity assays for early drug discovery in *Schistosoma mansoni* 34

Chapter 2: Parallelized Impedance-Based Platform for Continuous Dose-Response Characterization of Antischistosomal Drugs 56

Chapter 3: Evaluation of human liver microtissues for drug screening on *Schistosoma mansoni* schistosomula 69

Chapter 4: Activity and pharmacokinetics of a praziquantel crystalline polymorph in the *Schistosoma mansoni* mouse model 77

2 General discussion 85

2.1 Advances in in silico drug screenings 87

2.2 EIS-based real time drug screening on *Schistosoma mansoni* 90

2.3 Incorporation of liver microtissues into the drug screening procedure 97

2.4 Praziquantel and derivatives 102

3 Conclusion and outlook.. 107

Table of abbreviations

DALY	Disability Adjusted Life Years
PZQ	Praziquantel
OXE	Oxethazaine
FLUT	Flutamide
PROCAB	Procarbazine hydrochloride
TAM	Tamoxifen citrate
AURO	Auranofin
TERF	Terfenadine
MOA	Mechanism of Action
API	Active Pharmaceutical Ingredient
CYPs	Cytochromes P450
IC_{50}	Inhibitory concentration 50%
WBR	Worm Burden Reduction
WB	Worm Burden
WHO	World Health Organization
MDA	Mass Drug Administration
PHH	Primary Human Hepatocytes
$T_{1/2}$	Half-life
C_{max}	Maximum concentration
t_{max}	Time at maximum concentration
AUC	Areal Under the Curve
LC-MS/MS	Liquid Chromatography coupled with triple quad mass spectrometry
MRM	Multiple Reaction Monitoring

Summary

Schistosomiasis is a neglected tropical disease caused by *Schistosoma* spp. parasites. It affects more than 200 million people and 700 million more are at risk. Over 10’000 people die every year because of the disease, but this number might be a big underestimation. While the disease is endemic in 78 countries and affects mostly poor communities without access to clean water, the highest prevalence for the disease is found in sub-Saharan Africa with over 85% of the overall occurrences. Children are at especially high risk of exposure through activities such as playing or bathing in infested water bodies.

Schistosomiasis is a debilitating disease; the loss of productivity and mortality associated with the disease have a negative effect on the emerging countries' economies, which causes people to be stuck in a negative feedback loop of poverty and public health problems. Poor sanitation and unawareness of the general population are the main reasons for the transmission of schistosomiasis. The first symptoms of the disease are red bumps on the skin, usually appearing a few hours after infection and sometimes followed by mild fever and nausea. However, the chronic effects are more serious. In fact, children affected by the disease often show developmental delays and adults may develop chronic hepatic damage and eventually liver failure. There is only one drug available for mass drug administration (MDA) campaigns: praziquantel. There is growing evidence of a decreasing efficacy of praziquantel against *Schistosoma* spp. There is no vaccine available and the drug pipeline to treat schistosomiasis is empty.

The overwhelming prevalence of schistosomiasis in the developing world and the absence of novel drug candidates against the disease are provoking fear of resistance emergence among the handful of laboratories involved in the fight against this neglected tropical disease (NTD). The research of novel compounds moves slowly and one of the main reasons for this is the difficulty in finding a reliable and faster drug screening method that would increase the drug screening output and the concordance between laboratories involved in the drug screening process.

During my PhD, I worked on different projects tackling schistosomiasis, searching for ways to speed up drug screening processes and to contribute to the currently empty

drug pipeline. I worked on a protocol, in which we detail all the aspects of the drug screening procedure, with the aim to familiarize new laboratories with the procedures as we do them here at Swiss TPH, in order to decrease the methodological fragmentation in the field. I worked on the development of novel drug screening platforms and new methods to identify potential drug candidates. In collaboration with the Department of Biosystems Science and Engineering (D-BSSE) of ETH located in Basel, we developed a novel platform for antischistosomal drug screening based on microfluidic electrical impedance spectroscopy (EIS). Also, I worked on a human liver microtissue-based system to assess the liver metabolism for extending the standard drug screening assays *in vitro* on NTS to prodrugs, and to evaluate the liver metabolism's effect on the compounds' activity on NTS *in vitro*. I first validated the system with praziquantel and then quantified the amount of compound metabolised and tested the effect of the liver metabolites on NTS *in vitro* with other compounds that are approved for human medicine. Finally, in an attempt to resolve the issue of praziquantel's low solubility, I collaborated with the University of Trieste in the development and testing of a novel formulation of praziquantel. This novel praziquantel formulation was based on a polymorph co-crystal provided by the University of Trieste. I tested this formulation derivative *in vivo* and *in vitro* to compare it to the standard praziquantel to evaluate its activity. I quantified praziquantel enantiomers by LC-MS/MS in mice plasma and compared the pharmacokinetics of the standard praziquantel with the polymorph praziquantel derivative. In this thesis, all of the above-mentioned projects are contextualised and discussed.

1. Introduction

1.1. Background

Schistosomiasis is a neglected tropical disease and it is a morbidity associated with *Schistosoma* spp. infections. Schistosomes are the only known trematodes which possess dioecious reproduction and are able to reproduce sexually in the definitive host, while they reproduce asexually in the intermediate host (McManus et al., 2018). There are five main human *Schistosoma* species, which are commonly associated with the disease, namely: *Schistosoma haematobium, S. mansoni, S. japonicum, S. mekongi* and *S. intercalatum,* although the first three account for more than 90% of all the schistosomiasis cases (Gryseels et al., 2006). It is estimated that more than 779 million individuals in 78 countries are at risk of contracting the disease (Keiser, 2010, Utzinger et al., 2011). The most endangered countries are the ones in sub-Saharan Africa with over half of all the schistosomiasis infections (Colley et al., 2014, Gryseels et al., 2006, Holding, 2003, Keiser, 2010, King, 2017). In sub-Saharan Africa, it is estimated that more than 10,000 deaths per year are due to schistosomiasis. The main reasons for the disease endemicity in these countries is the lack of sanitation-infrastructures and the presence of uninformed individuals and unawareness (Gryseels et al., 2006).

According to the Global Burden of Disease Study, schistosomiasis caused a loss of 1.4 million disability-adjusted life years in 2017 (GBD 2017). The individuals infected with the disease, in most cases, will survive, but the liver damage can be dramatic, leading to hepatic cirrhosis and an increased risk of contraction of other diseases (Feldmeier et al., 1994). On top of this co-morbidity, schistosomiasis can lead to infertility, haematuria, impaired growth, anaemia and mental retardation (Tucker et al., 2013, Lewis and Tucker, 2014, Colley et al., 2014).

The main cause for the disease is the presence of eggs released by the female schistosomes that remain embodied in the host organs, mostly the liver. Those eggs are released by the parasites in the order of a few dozens to hundreds per day, depending on the *Schistosoma* species; many of those eggs are excreted by the host but the ones remaining embedded are the cause of the disease (McManus et al., 2018, Elbaz and Esmat, 2013). The eggs have a specific morphology that helps the microscopic distinction of the species during diagnostic screenings (Gray et al., 2011).

Every species has a specific localisation of the adults, which also helps the identification of the parasite species. However, the parasite localisation can vary depending on the animal model used (Keiser, 2010).

1.1.1. *Schistosoma mansoni* life cycle

Schistosoma are dioecious, digenetic, parasitic flatworms, and have a syncytial tegument and a ventral and oral sucker (Olson et al., 2003). The adult worms are about 1-2 cm long, and possess a blind digestive tract, reproductive organs and a primitive neuromuscular system. Sexual dimorphism is evident: the male is wide with a tegument patterned by distinct tubercles, while the female is longer and streamlined (Hockley, 1973, Buchter et al., 2018). The life cycle of the parasite is a complex one and only a few institutions worldwide have it in-house (Keiser, 2010). The life cycle includes both asexual and sexual reproduction in an intermediate and definitive host, respectively.

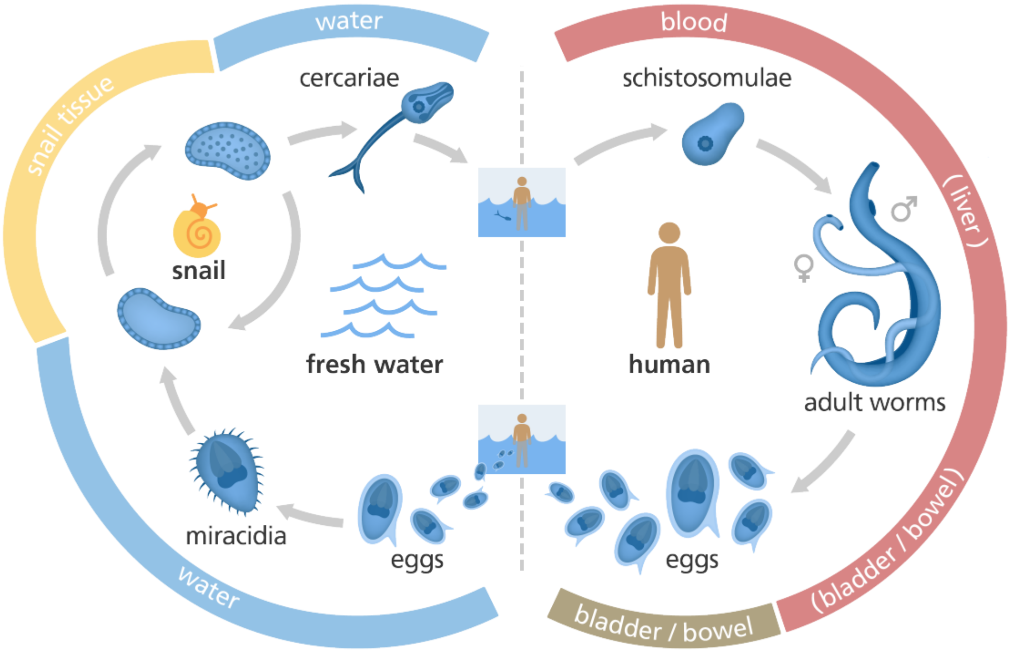
water
blood
snail tissue
cercariae
schistosomulae
(liver)
♂
♀
snail
fresh water
human
adult worms
miracidia
eggs
eggs
water
bladder / bowel
(bladder / bowel)

Figure 1 Schematic representation of the *S. mansoni* life cycle. Figure adapted from yourgenome.org/facts/what-is-schistosomiasis.

Flagellated, fork-tailed cercariae, the infectious freshwater swimming stage of the parasite, are chemotactically attracted by the human's (definitive host) skin due to its release of L-arginine (Haas et al., 2002) and/or skin lipids (Shiff et al., 1972). The cercariae can survive in fresh water for 24-48 hours without feeding due to their glycogen reserves (Morley, 2011). Once the cercariae reach the host, the parasites penetrate the host's skin, which activates a series of biochemical mechanisms causing them to shed their tail and their glycocalyx (McKerrow and Salter, 2002). They are from this moment on known as schistosomula. The schistosomula enter the blood circulation and, driven by the blood pressure, reach the lungs and the heart. Schistosomula will mature for up to 3 weeks in the lungs. Eventually, from here the schistosomula will reach the liver, where, over a period of about 7 weeks, they mature into a sexually dimorphic species and pair, living in constant copula, which can last for many years (Gryseels et al., 2006, Jamieson, 2017) . Once this stage is reached, the paired adults leave the liver through the portal vein and parasitize the mesenteric veins.

There are reports indicating that *Schistosoma* spp can live up to 30 years in the human host (Tucker et al., 2013, Lewis and Tucker, 2014, Colley et al., 2014, Gryseels et al., 2006).

The adult schistosomes feed on blood; the ingested volume is ~100 nL for males and ~900 nL for females per day (Skelly et al., 2014). Ingested erythrocytes are lysed by gut proteases present in the digestive tract. Proteomic analysis of the gut identified an amino acid transporter, ion, and lipid transporters (Skelly et al., 2014). Specialised channels on the surface of the parasites acquire glucose. The catabolic product of the haemoglobin degradation is heme, which could be toxic for the parasites (Skelly et al., 2014). Consequently, a not very well understood process of regurgitation excretes heme back into the host circulation, since schistosomes lack the anus (Skelly et al., 2014).

The females of *Schistosoma* spp. shed eggs that extravasate the mesenteric veins, pass through the wall of the intestines via the Peyer's patches to the intestinal lumen and eventually end up in the feces (Turner et al., 2012). Due to poor sanitation and hygiene standards in the affected countries, the eggs end up contaminating water bodies. Ciliated miracidia develop inside those eggs and once favourable conditions are present, they hatch. The ciliated miracidia are chemotactically attracted by their intermediate host, the *Biomphalaria glabrata* water snails and penetrate them. Once inside the intermediate host, the miracidia transform into sporocysts and reproduce asexually, leading to shedding of thousands of sporocyst every day, which eventually develop into cercariae, the infectious stage of the schistosomes' life cycle (Jamieson, 2017). Cercariae can survive in open water for a period longer than 24 hours and eventually infect their definitive host, thereby completing the cycle (Figure 1) (Jamieson, 2017, Morley, 2011).

The replication of the life cycle of the parasite in a laboratory setting has been an essential achievement for a better understanding of the host-parasite dynamics and is a fundamental pillar for the research on novel compounds that would deter schistosomiasis (Keiser, 2010, Lombardo et al., 2019). In a laboratory environment the entire cycle requires about 4 months to be completed, and at that point, it can also be reproduced every month by having numerous batches simultaneously (Lombardo et al., 2019).

1.1.2. Epidemiology

One of the objectives set by the WHO is the elimination of schistosomiasis within the year 2020. The objective will not be reached, but the overall prevalence in many sub-Saharan countries has been decreasing steadily, in some settings dramatically (Rollinson et al., 2013). The reason for this partial success were the mass drug administration (MDA) campaigns, started in early 2000, which distributed hundreds of millions of therapeutic doses (of praziquantel) over the years (Wang and Liang, 2015). Although the MDAs do not prevent helminthic reinfection, the overall prevalence has decreased, for example by ~30% in Mali between 2003 and 2010, and in Lebanon schistosomiasis transmission has been eliminated (Miguel and Kremer, 2004, Rollinson et al., 2013) (Figure 2). Some endemic countries, such as Zanzibar, will most likely reach the goal of disease elimination as soon as 2025 (Knopp et al., 2019). A more realistic goal for the elimination of transmission is 2030 (Fenwick and Jourdan, 2016).

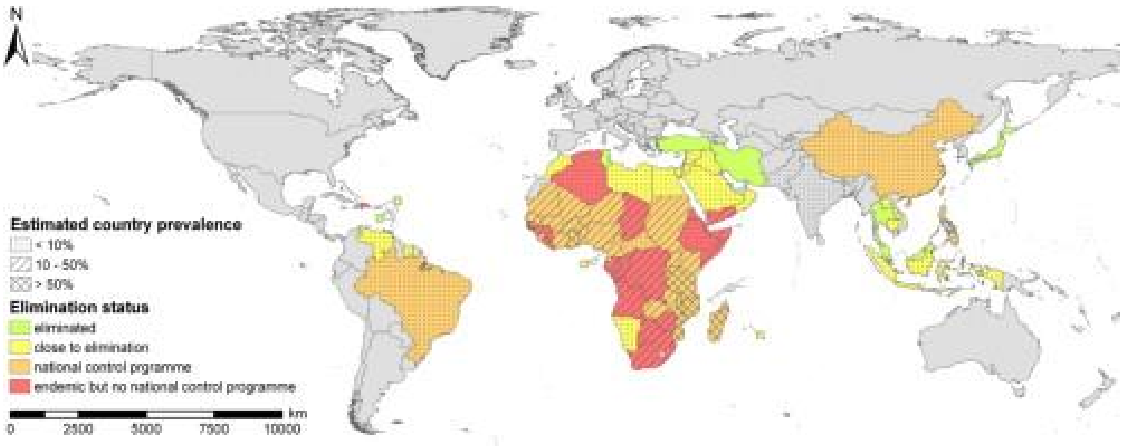
N
Estimated country prevalence
< 10%
10 - 50%
> 50%
Elimination status
eliminated
close to elimination
national control prgramme
endemic but no national control programme
km
0
2500
5000
7500
10000

Figure 2: Distribution of schistosomiasis in the world and the countries that have been determined to have achieved the elimination of the burden (Rollinson et al., 2013)

The countries in which the prevalence of the disease is still high are usually lacking adequate sanitation infrastructures and have poor healthcare systems (Figure 2). This poverty-loop makes the infection and eventually reinfection extremely likely to happen, especially in children 5-12 years old (Bustinduy et al., 2017, Coulibaly et al., 2017). However, there is an overall increase of interest as well as a growing awareness of the disease and health education (Miguel and Kremer, 2004). There are also global initiatives, such as Water, Sanitation and Hygiene (WASH), which help alleviate the poverty cycle caused by schistosomiasis (McMichael, 2019, McManus et al., 2018). In endemic areas, schistosomiasis can also be associated with other parasitic infections. Such a condition is known as polyparasitism, and it can lead to exacerbation of the symptoms (Ezeamama et al., 2008, McKenzie, 2005). Overall, the contribution of the MDAs was important in the reduction of schistosomiasis prevalence. However, more work has be conducted to eliminate the disease.

1.1.3. Pathology

The cercariae penetrate the host's skin within an average of seven minutes after contact (Haas and Haeberlein, 2009, Gryseels et al., 2006). Within one hour after cercarial penetration through the skin, there is generally an ectodermal manifestation characterized by general rash with maculopapular lesions, known as "swimmer's itch" (Bouree and Caumes, 2004). This is characterized by sensation of itch and red swollen regions of the skin. Once the schistosomula successfully penetrated the human skin, an acute, then a chronic phase follows. The acute phase, called also Katayama syndrome, provokes general flu-like symptoms such as myalgia, fever, fatigue, nausea, abdominal pain, urticaria and eosinophilia, but sometimes the acute phase can be asymptomatic (de Jesus et al., 2002, Maizels and Yazdanbakhsh, 2003). In the animal model, those symptoms are hardly detected. These symptoms are caused by the immune system reacting to the parasite and are generally short-term and mild. Symptoms of acute schistosomiasis can develop a few weeks after the schistosome parasite first burrows into the skin of the human host, when the first parasite eggs are trapped in the liver and spleen. Those symptoms arise due to the activity of elements of the humoral immunity such as macrophages and basophils. The incremental differentiation of the CD4 T cells into Th2 T cells drives the macrophages to exacerbate the inflammatory microenvironment and causes fibrogenesis in the *Schistosoma* eggs milieu in the liver by upregulation of Fizz1, Ym-1 and Arg-1 (Wilson et al., 2006).

In the chronic phase of schistosomiasis, symptoms can persist for years. Symptoms of chronic schistosomiasis include: abdominal pain, hepatomegaly, haematochezia or haematuria (Gryseels et al., 2006). In rare events, eggs have been found in the brain or the cerebrospinal fluid (CSF) causing inflammation and seizures. This condition is known as neuroschistosomiasis; in most cases it is due to ectopic egg dissemination of *Schistosoma japonicum* (Ross et al., 2012).

S. haematobium is localised in the blood vessels surrounding the bladder. A common complication is an increased risk of co-morbidities, especially in women, such as haematuria and increased risk of contracting HIV (Feldmeier et al., 1994). Moreover, chronic infection with *S. haematobium* increases the risk of chronic inflammation that could eventually lead to squamous cell carcinoma of the bladder (SCC), due to the eggs trapped in the tissue.

Schistosoma mansoni has not been associated with increased risk of developing hepatocarcinoma, but it is well known to cause periportal fibrosis and consequent hepatosplenomegaly (Nacif-Pimenta et al., 2019). Recently, a correlation between the levels of splenomegaly could be predicted by the altered proportion of blood elements, such as the proportion of leukocytes. The enlargement of the spleen is directly proportional to the level of leukopenia (Vasconcellos et al., 2018).

1.1.4. Diagnosis, treatment and prevention

Routine screening for schistosomiasis is usually conducted by analysis of stool smear specimens (2-10 mg) based on methods such as Kato Katz or urine filtration and by optical microscopy to identify eggs (Gray et al., 2011). This allows the identification of the infecting *Schistosoma* species due to the morphological distinguishing trait of the eggs' spine (Gray et al., 2011). However, trained operators are required for the stool analysis. The stool based analysis method can introduce an operator bias, and it can be laborious. The Kato-Katz and urine filtration methods are recommended by WHO for schistosomiasis when the intensity of infection is high, but their sensitivity varies with prevalence and intensity of infection, because if less eggs are present in the sample they can go undetected by the operator, leading to an underestimation of the infection level (Gray et al., 2011). A sensitive PCR based assay has been developed for the detection of *Schistosoma* spp. DNA in biological samples from feces and plasma. This approach has the potential to provide a test for diagnosing schistosomiasis in all phases of infection (immediate, acute or chronic phase of infection). This diagnostic test is particularly important because egg detection can take up to two months post infection (Gray et al., 2011). There are also other techniques such as ELISA that allow the detection of IgG, IgM, or IgE against soluble worm antigen or soluble egg antigen, indirect haemagglutination, or immunofluorescence (Gray et al., 2011). However, these techniques are less sensitive and specific than PCR and stool or urine sample analysis (Gray et al., 2011). The circulating cathodic antigen (CCA) and the circulating anodic antigen (CAA) are both applied to diagnose active infections and for evaluation of drug efficiency. There are emerging detection methods based on point-of-care-circulating cathodic antigen (POC-CCA) on biological samples, which have been shown to be sensitive in field settings in high and middle endemic areas. However, the performance of the POC is still debated in low endemic areas (Kittur et al., 2016).

Preventive chemotherapy against schistosomiasis has been going on since the early 2000 (Inobaya et al., 2014). The WHO organises annual or biannual MDA campaigns for preventive chemotherapy. MDAs aim to reduce the morbidity and mortality associated with the infection with *Schistosoma* spp. and to prevent new infections by limiting the transmissions by reduction of the overall prevalence in the population

(Inobaya et al., 2014). Over 200 million doses are distributed each year to the schistosomiasis endemic countries (Inobaya et al., 2014). MDAs are often implemented in combination with other strategies, such as intermediate host control. Using molluscicides is a common method for elimination of the intermediate host. One of the main chemicals used for this purpose is niclosamide, which is also the only WHO recommended molluscicide (Inobaya et al., 2014).

Praziquantel has always been the drug of choice for these administration campaigns, because of the low cost of the therapy and the well-known efficacy of this drug as well as the ease of administration and the minor side effects (Inobaya et al., 2014). The preventive chemotherapy is based on a single dose of 40 mg/kg of praziquantel. This drug regimen has 66-95% efficacy for MDA programs, egg reduction rate (ERR) above 90% and cure rate (CR) above 70% (Gryseels et al., 2006). However, double-dose praziquantel treatments achieved ERR above 95% and CR above 90% (Munisi et al., 2017). The WHO recommends a dosage regimen of 60 mg/kg orally for *S. japonicum* and *S. mekongi* and a 40 mg/kg praziquantel dose for *S. mansoni, S. haematobium*, and *S. intercalatum* (Gryseels et al., 2006). There is still a debate whether a double dose with 40-60 mg/kg praziquantel therapy could provide some benefit over a single dose treatment. King *et al.* suggested in a systematic review that a double dose of praziquantel administered 2-8 weeks after the first dosage would justify the additional costs sustained by increasing the cure rates of the treatment in the case of *S. mansoni* infection, but in the case of *S. haematobium* this is still unclear (King et al., 2011). This increased cure rate after double therapy could be due to the development of the parasites in infected individuals, who had juvenile stage parasites (which are not susceptible to praziquantel) at the time of administration of the first dose, which had developed into susceptible developmental stages by the time of administration of the second dose (Cioli et al., 2014). However, because praziquantel is not effective for the prevention of reinfection, because it does not kill the young parasites and because many of the people infected are still not reached by the MDAs, the disease elimination objectives could not be reached (Inobaya et al., 2014). In addition, praziquantel drug efficacy is decreasing, making the research for novel drug candidates necessary (Doenhoff et al., 2008).

A problem related to the current treatment with praziquantel is the bitter taste and the size of the oral pills (600 mg). Those two issues make the praziquantel paediatric compliance difficult. Because children (10-13 yrs.) are the most exposed population to the infection in schistosomiasis endemic countries (Hajissa et al., 2018), there are currently some efforts to make the formulation more child friendly, for example by removing the inactive stereoisomer S-praziquantel from the current formulation, thereby reducing the pill size (Cioli et al., 2014).

1.1.5. Praziquantel

Praziquantel has an interesting history. It is the only drug available today as effective treatment against schistosomiasis, next to oxamniquine, which has seen the insurgence of resistant parasite strains and is therefore no longer used. Praziquantel is listed by the WHO as essential medicine and it has been recommended for MDA since the mid-80s (Colley et al., 2014). It was discovered in 1971, from a collaboration between Bayer and Merck, in Germany. When the compound was first discovered among a library of about 400 pyrazinoisoquinolines as potential tranquilizers, it was used for veterinary practice. A few years later, its broad-spectrum activity against several helminths and cestodes was discovered and human clinical trials established that the drug was indeed safe and effective for use in human medicine (Campbell and Rew, 2013). The drug was very expensive at first, but it rapidly became cheaper and cheaper with the increased competitive chemical power of China and Korea. Praziquantel is the latest cornerstone against schistosomiasis. Nowadays, hundreds of millions of doses of praziquantel are used routinely every year to treat schistosomiasis in human and veterinary medicine. The fact that this drug is used for both human and animal medicine implies an increased risk of resistance development, because of the high evolutionary pressure posed on the *Schistosoma* spp parasites. Praziquantel's mechanism of action is not yet completely understood, but the most accredited opinion is an effect on the calcium channels on the tegument of the parasites (Olliaro et al., 2014).

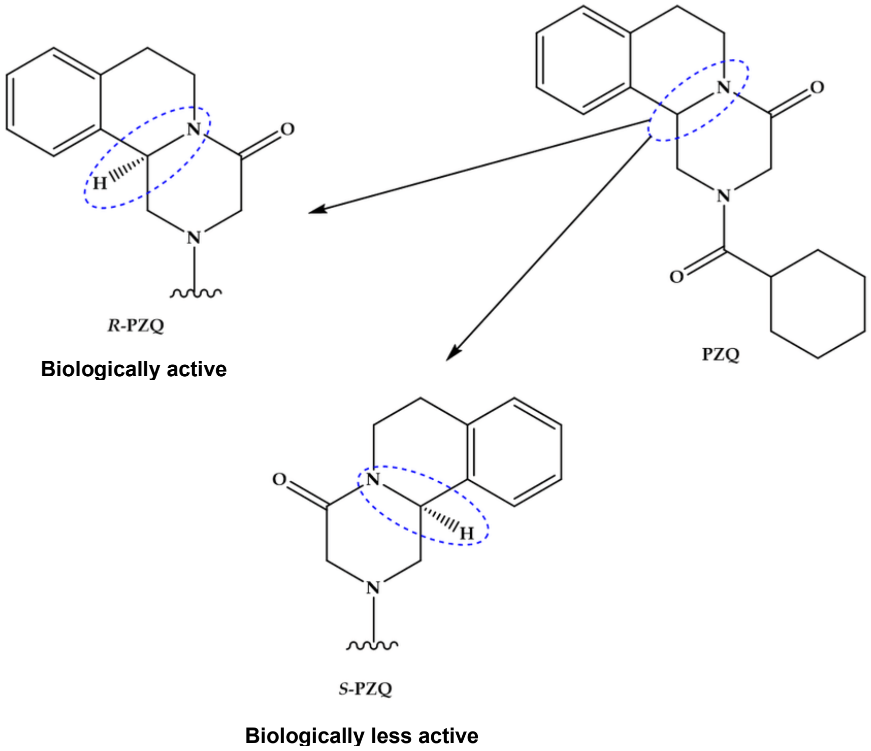

Figure 3 Molecular structure of praziquantel with its stereocentre (Gouveia et al., 2018). The stereocentre is highlighted in blue. The two enantiomers have different biological effects. R-praziquantel is biologically active while S-praziquantel is less active.

Voltage-gated Ca^{2+} channels (VGCCs) and in particular the beta subunits of the VGCC are known as one of the potential molecular targets of praziquantel (Jeziorski and Greenberg, 2006). It has been demonstrated that, if these channels are specifically antagonized by nicarpidine and nifedipine, the adult worms survive doses of praziquantel otherwise lethal (Doenhoff et al., 2008).

Praziquantel is a safe drug with a good safety window, but it also has drawbacks, such as poor efficacy against juvenile stages of the parasites, poor formulation compliance in children due to bitter taste and tablet size and very erratic pharmacokinetic profiles. In consequence, rounds of multiple doses are necessary to clear the infection (Doenhoff et al., 2008, Cioli and Pica-Mattoccia, 2003).

The commercial formulation of praziquantel is a racemate (both the R- and S-enantiomers are present each in 50%) (Figure 3), since the active pharmaceutical ingredient (API) possesses a stereocentre. Maximum concentrations are reached at about 60-120 minutes post oral intake with an overall bioavailability of about 80%. Only

R- praziquantel is the active component (Figure 3). However, some authors claim that S- praziquantel has some activity *in vivo* against *S. haematobium* (Kovac et al., 2017, McManus et al., 2018). The drug undergoes extensive liver first pass metabolism and is later processed into the inactive main human metabolites trans-4-hydroxy-praziquantel and cis-4-hydroxy-praziquantel by the two P-450 isozymes 2B1 and 3A that oxidise xenobiotics (Doenhoff et al., 2008, McManus et al., 2018).

1.2. Current challenges in the field

Schistosomiasis is a global disease, which affects over 200 million individuals, yet there is only one treatment currently available and the drug pipeline is empty. There is no vaccine available (Lewis and Tucker, 2014, Ricciardi and Ndao, 2015) and the research for new antischistosomal vaccines or drugs relies on a handful of academic laboratories (Keiser, 2010). However, in the last ten years, global awareness of the disease has been increasing and some new public and private partnerships (PPP), such as Drugs for Neglected Diseases Initiative (DNDi) and Medicine for Malaria Venture (MMV) and collaboration programs are being established in a number of academic settings (Chatelain and Ioset, 2011, Nwaka and Hudson, 2006).

Nonetheless, finding alternative drugs against schistosomiasis is not an easy task. There are many challenges related to the complex nature of the parasite’s life cycle, which requires two hosts, and to the biology of the parasite, which is so variable depending on the parasite stage (Lombardo et al., 2019). There are problems regarding the availability of parasites, which at this point, is still too limited to perform high throughput drug screenings (Lombardo et al., 2019).

In addition, the current gold standard for drug screening is based on phenotypic assessment by microscope visual scoring (Ramirez et al., 2007). This method does not allow medium or high throughput and it suffers from operator bias, which makes this screening method slow and subjective (Lombardo et al., 2019). It has been reported that less than 20% of drug hits identified by a lab are confirmed by other laboratories (Panic et al., 2015b, Mansour et al., 2016).

Many alternatives to the standard drug screening method have been proposed, but none of these technologies spread. NTS drug screening methods based on microthermal calorimetry (Manneck et al., 2011), colorimetric assay (Panic et al., 2015a), as well computer aided image recognition and photogram-image subtraction (Paveley et al., 2012) have been proposed. Each of these methods has some drawbacks and the lack of other laboratories using the same technique is a cause of conflicting results, variance and fragmentation in the field. In the case of the calorimetric assay, one of the main limitations was the high number of parasites needed, which made this technique difficult to implement (Manneck et al., 2011). Also, calorimetric assays are often based on expensive dyes, therefore low-resource settings could not afford them (Panic et al., 2015a, Lalli et al., 2015). This is also a problem with the computer aided phenotypic screenings on NTS, which are based on high computational power and sophisticated algorithms and/or devices that can be costly and difficult to implement (Paveley et al., 2012).

1.3. Anti-schistosomal drug screening

It is not known, at the moment, if the sex of the adult worm is already determined at the level of the eggs, as suggested by some authors (Sotillo et al., 2015). However, some authors reported a genetic trait at the cercarial stage that is essential for the development of female parasites (Spotila et al., 1987). There are also authors suggesting that it is the presence of schistosomes of the opposite sex, which makes the parasites develop into sexually mature adults (Hernandez et al., 2004). Another theory assumes that the maturation into male or female is determined by components of the definitive host's immune response (Hernandez et al., 2004).

NTS represent an important stage for the entire drug discovery procedure, as illustrated in (Chapter I) of this thesis. Because NTS can be obtained in high numbers (in contrast to the adult stage parasites that are isolated from animal hosts in the range of dozens per mouse (Lombardo et al., 2019)), they are considered an important organism for drug discovery and drug development. Ideally, a drug that is effective *in vitro* on NTS would be active on adult stage parasites *in vitro* and hopefully *in vivo*. This ideal drug would lower the risk of reinfection, since the drug would be active against the juvenile stages of the parasites that are not targeted by praziquantel (Cioli et al., 2014). NTS are obtained by mechanical transformation, by passing snail-shed-cercariae through a pair of 10 mL syringes connected by a plastic Luer-Lok connector. During this coerced passage, the cercariae become tailless. At this point, the genetic profile of the NTS is very different from the one of naturally occurring schistosomula after skin penetration. For this reason, some researchers analysed the transcriptomic difference between those mechanically and the naturally obtained schistosomula. Protasio *et al.* (Protasio et al., 2013) noticed that the profile differs in the expression of some proteases, which are expressed in naturally occurring schistosomula, but not in the mechanically obtained ones (Protasio et al., 2013). However, after 12-24 hours incubation, the expression profiles of the mechanically transformed schistosomula become similar to the ones of naturally occurring schistosomula (Protasio et al., 2013).

New drug candidates are tested *in vitro* at first on NTS at 10 μM and then the ones, which showed efficacy, called hits, are tested on adult *Schistosoma* again at 10 μM. IC_{50} curves are calculated to evaluate the potency of the compounds (Chapter I). During the drug screening on NTS and adult stage parasites, a trained operator gives scores from 0 to 3 depending on the morphology and the behaviour of the parasites after drug testing. When the operator assigns a 0, this score indicates that the compound tested was active leading to parasite death. If the operator assigns a score of 3, the parasites are viable with an optimal behaviour, indicating that the compound tested was not active against the parasites (Lombardo et al., 2019). Those lead compounds can at this point be tested in mice harbouring *S. mansoni* infection, in order to evaluate the potential effect *in vivo*, generally at 200 mg/kg (Chapter I). Unfortunately, many compounds that are active *in vitro*, fail to show activity *in vivo* or they show high toxicity (Pasche et al., 2018, Panic et al., 2015b, Panic and Keiser, 2018).

An approach to identify novel active compounds is to test “brute-force” libraries with huge numbers of compounds within the shortest time possible to observe a change in the phenotype of the target cell or organism (phenotypic screening). Many pharma-companies are currently using this approach to test millions of compounds in a limited amount of time (Swinney, 2013). Generally, these approaches are relying on high-throughput (HTS) screenings and automatized methods (Wildey et al., 2017). These large-scale approaches can hardly be applied to the drug screening against schistosomiasis, because of the complexity of the parasite's life cycle and because, at the moment, it is not possible to grow the parasite stages *in vitro* without the intermediate and definitive host.

A more recent approach for drug screenings consists of *in silico* drug prediction for both phenotypic drug screenings and target-based drug screenings. Thanks to the advances in computer technologies, life sciences and increased understanding of the parasites' biology, the acquired knowledge from decades of drug screenings and structure identification led to the availability of millions of molecular structures, now stored in freely available online databases (Liu et al., 2013, Wishart et al., 2006, Terstappen and Reggiani, 2001). Computer algorithms can scan these databases in a short time in order to identify possible molecular fits against molecules and vice versa. Each *in silico* fit can be subsequently tested and verified. With the recent advances in machine learning algorithms or neural networks, it is also possible to generate a molecule from the target by molecular computer-aided design (mol-CAD). This latter approach is estimated to be the next generation for drug screening procedures (Olivecrona et al., 2017). This could be useful in settings with low resources such as the field of neglected tropical diseases (NTDs) and rare diseases, both underfunded. These approaches could reduce the amount of drug screenings necessary to obtain interesting drug candidates, because the molecules are produced to fit to specific molecular targets or specific molecular targets are identified from known chemical structures (Plouffe et al., 2008).

1.3.1. Drug repurposing

Drug repurposing is a very interesting aspect of drug development. It is based on the idea of "recycling" established drugs by employing them against other diseases or against other organisms than they were originally intended for. Drug repurposing has important advantages, such as reducing the costs associated with the research and the development of a drug *ex novo* as well as reducing the time-to-market for potential lead candidates (Panic et al., 2014). Moreover, additional information, such as chemical, pharmacokinetic and analogue properties have already been determined and are usually available (Oprea et al., 2011). In addition, computer aided screening can facilitate this process, by finding other molecular targets for already marketed drugs in publicly available databases (Liu et al., 2013). For example, thalidomide was initially marketed in the 50s-60s' to treat morning sickness during pregnancy, but was re-used as therapy against brain tuberculosis (Buonsenso et al., 2010) and as cancer drug (Liu et al., 2013). Due to the limited resources funding the research of novel candidates in NTDs, drug repurposing has become an essential part of the drug development process. In our laboratory, many compounds come from a series of potential drug candidates for other diseases and/or conditions. These compounds were tested for their effects against schistosomiasis and in many cases interesting compounds were identified (Cowan and Keiser, 2015, Panic et al., 2014, Panic and Keiser, 2018, Gouveia et al., 2018, Panic et al., 2015b).

1.4. Polymorphism

Polymorphism is a characteristic that is intrinsic in the structure of compounds. Every compound has a specific number of possible conformations (Figure 4), in which the crystalline structure can be set. Those altered special dispositions of the constituents of the crystal lattice make it possible to generate new versions of a compound with modified chemical and physical properties, but keeping its molecular formula.

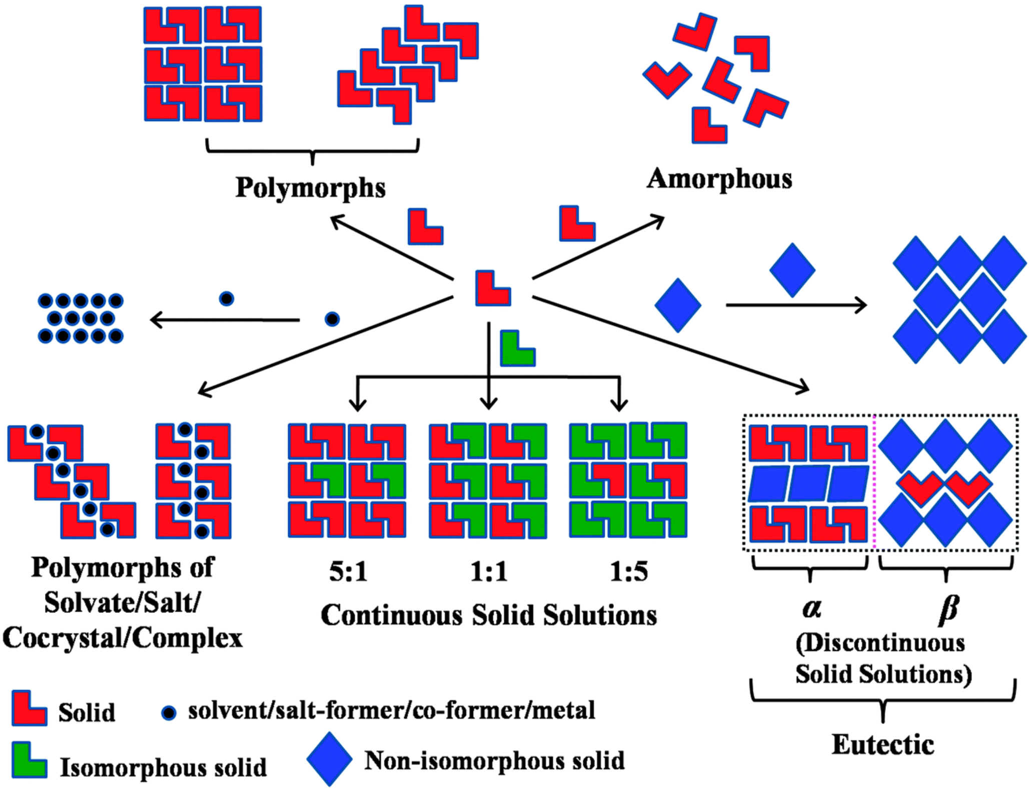
Polymorphs
Amorphous
Polymorphs of Solvate/Salt/ Cocrystal/Complex
5:1
1:1
1:5
Continuous Solid Solutions
α
β
(Discontinuous Solid Solutions)
Eutectic
Solid
solvent/salt-former/co-former/metal
Isomorphous solid
Non-isomorphous solid

Figure 4: In this schematic the various configurations of a compound are reported. Figure from https://newdrugapprovals.org/category/polymorph/

Polymorphs differ in numerous important drug properties such as drug efficacy, bioavailability, and even toxicity (Raza, 2014). For example, the praziquantel polymorph we used in this work (Chapter IV) has been shown to possess double the solubility of the standard praziquantel (Beatrice et al., 2017, Zanolla et al., 2018b).

Compounds can be of amorphous structure without a crystalline reticulate and they can undergo a series of chemo-physical rearrangements of their reticule in order to increase their stability. Polymorphs are an example of such a transition. Polymorphism can be of two types: monotropic and enantiotropic. In the monotropic type, the stability of one of the polymorphic forms is stable at temperatures below the melting point of the drug. In contrast, an enantiotropic polymorph can have several stable forms at different temperatures. Gibbs free energy (ΔG) determines the relative stability and it is the driving force for the polymorphic transformations at constant temperature and pressure (Figure 4).

There are some examples of important marketed polymorph drugs: Axitinib is a drug marketed for treatment of renal cell carcinoma (RCC) with over 200 reported polymorphic forms. The drug is an inhibitor of the vascular-endothelial-growth-factor-receptors (VEGFRs) kinase, expressed mostly in endothelial cells. However, the most thermodynamically stable form of the API is the polymorphic form, known as XLI; this drug is currently marketed as polymorph with the name Inlyta (INN) by Pfizer® (EMA, 2012).

Polymorphs of a drug can reveal information on the drug that were not known before. Therefore, this could expand the possibilities offered by many of the drug candidates (Zanolla et al., 2018a, Raza, 2014). This approach could also lower the costs associated with developing novel drugs. This is particularly important in drug discovery in the settings of neglected tropical diseases, which are, by definition, underfunded (Keiser, 2010).

I tested a polymorph derivative of praziquantel, in which the structure of the API is kept the same as in the commercial praziquantel. This, according to the literature, can have many different advantages over the standard drug formulation. Moreover, the drug had already been pre-tested in our lab *in vitro* and *in vivo* in a small trial and we observed interesting results, which suggested proceeding to further testing with this drug. I therefore extensively tested the praziquantel polymorph *in vitro* and *in vivo* in order to compare its activity and its pharmacokinetics to the ones of the standard commercial praziquantel (Chapter IV).

1.5. Electrical impedance spectroscopy (EIS)

Electrical impedance defines a measure to quantify the resistance offered by a circuit when an alternating current (AC) is applied. In the international system, Electrical Impedance (EI) is measured in Ohm (Ω). However, it is often symbolised as Z and it may be represented by writing its magnitude and phase in the form $|Z|\angle\theta$. EIS has been used in many biological applications already, such as a micro- flow cytometry devices that can evaluate the differentiation of cells by their size (Cheung et al., 2005). In another application, Gomez et al. showed a device based on EIS to evaluate the viability status of bacteria, in which products of the bacterial metabolism modified conductivity of the medium (Gomez et al., 2001). In another study, an EIS-based platform allowed continuous analysis of the growth rate of cell colonies in real time (Chawla et al., 2018).

The electrical impedance can be represented on a Cartesian plain. The impedance can give information on the magnitude and phase of the passing AC current. The impedance measurement is dependent on the frequency of the AC. Therefore, to analyse the behaviour of Z and the phase (angle of the Z function), one single frequency at the time can be used, or as well multiple frequencies.

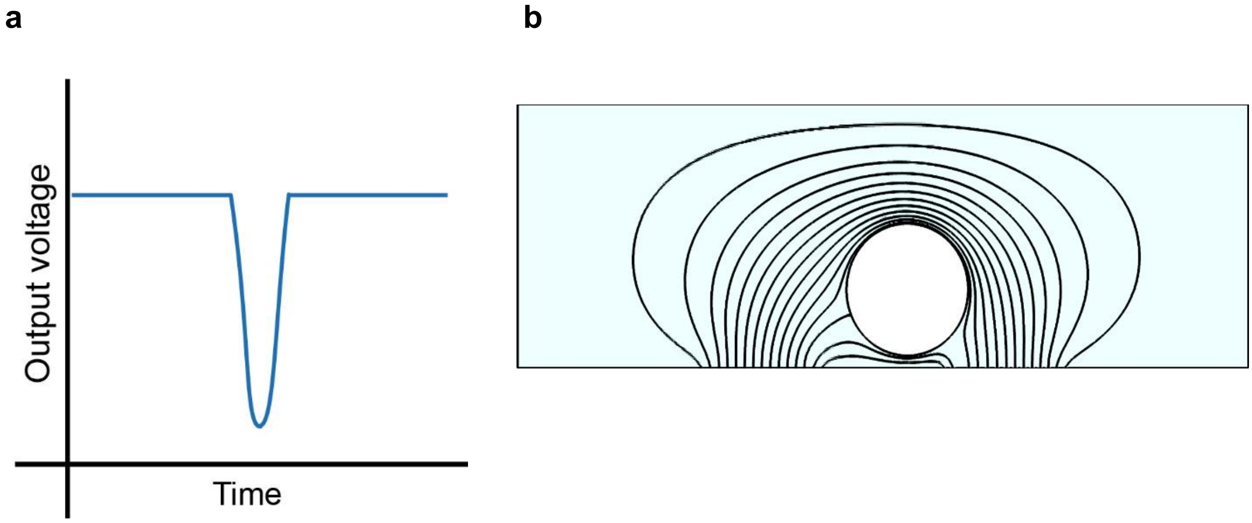

Figure 5: Schematic representation of the electrical impedance spectroscopy signal

in (a), where the output of the voltage is changing after the recording of a single movement of an NTS. (b) Schematic representation of the electric fluid between two co-planar electrodes, as used in the platform described in Chapter II.

EIS can be used to analyse the dielectric properties of elements in a circuit, since Z can provide information on the magnitude and the phase of the resistance. Therefore, a biological cell as well as a biological organism can be considered as a dielectric element (Pethig, 1985). EIS calculates the impedance of a sample by applying an AC current through a range of frequencies and measuring the resulting voltage. Hence, a complex and element-specific spectrum of readings can be acquired from each biological element (Chawla et al., 2018). For these reasons, impedance based spectroscopy is a very interesting technique that provides not only information on the dimension of the biological entity analysed, but also on its dielectric properties and resistivity. EIS is a non-destructive technique that is being used in many different fields such as cell viability and/or differentiation measurements (d'Entremont et al., 2002) or abasic DNA detection (Heinrich et al., 2018). It is used also in agronomy to evaluate the presence of fertile seeds from ones that are not (Zhang et al., 2011). We decided to implement an electrical impedance based platform that allows the measurement of NTS motility for drug screening (Chapter II). The parasites' motility is one of the most important parameters to be assessed in parasite scoring (Lombardo et al., 2019). To measure NTS motility, a pair of coplanar electrodes can be used for measuring conductivity variations of the medium caused by parasite movements between the electrodes. To measure the signal fluctuations caused by the NTS, an AC voltage is applied on one of the two co-planar electrodes, and the current flowing through the sensing volume is then acquired at the other electrode and converted to voltage through a transimpedance amplifier. The magnitude and the frequency of the voltage give indications on the intensity and frequency of the NTS movements, respectively. Therefore, this method can be applied for the evaluation of the NTS viability, by analysis of the motility, for example to assess a compound activity (Chapter II).

1.6. Liver microtissues

Drug metabolism *in vivo* and pharmacokinetic prediction are among the greatest incognita to overcome once a novel lead compound reaches the animal testing phase. Therefore, choosing the correct *in vitro* and *in vivo* model for more accurate drug prediction is crucial (Wang et al., 2015, Pampaloni and Stelzer, 2009). Liver microtissues represent a novel cell-culture technology that is surging and its usage could be highly beneficial for toxicity testing and metabolic testing of novel compounds, since liver microtissues possess expression of the whole P450 cytochrome family (CYPs) comparable to *in vivo* (Kim et al., 2015, Chiba et al., 2009). This *in vitro* model offers many advantages over conventional standard cell cultures (Wagner et al., 2013, Bale et al., 2016, Messner et al., 2013, Pampaloni and Stelzer, 2009). It has been shown, in fact, that the structural cell organisations present in the human liver are also present in the tridimensional liver microtissue-based cell cultures, in both monocultures and in multi-cellular-cultures (with endothelial cells (ELC) and Kupffer cells) (Figure 6) (Bell et al., 2018, Messner et al., 2013). These cells, especially hepatic primary cells, are variable (since they are taken from donor livers) and therefore they might better reflect the natural human genetic variability and proteome than standard cell line cultures (Simon et al., 2018, Messner et al., 2013, Pampaloni and Stelzer, 2009).

In a study from Olson *et al.* (Olson et al., 2000) it has been demonstrated that 43 % of toxic effects in humans were correctly predicted by tests in rodents, whereas this percentage increased to 63 % when liver primary microtissue models were used (Olson et al., 2000, Proctor et al., 2017). Another practical advantage is that those liver microtissues can be kept *in vitro* for 4-5 weeks, without risk of de-differentiation (Simon et al., 2018, Ramaiahgari et al., 2017); many studies are reporting stable expression of the key proteins for the liver functionality (Leite et al., 2012, Yokoyama et al., 2018).

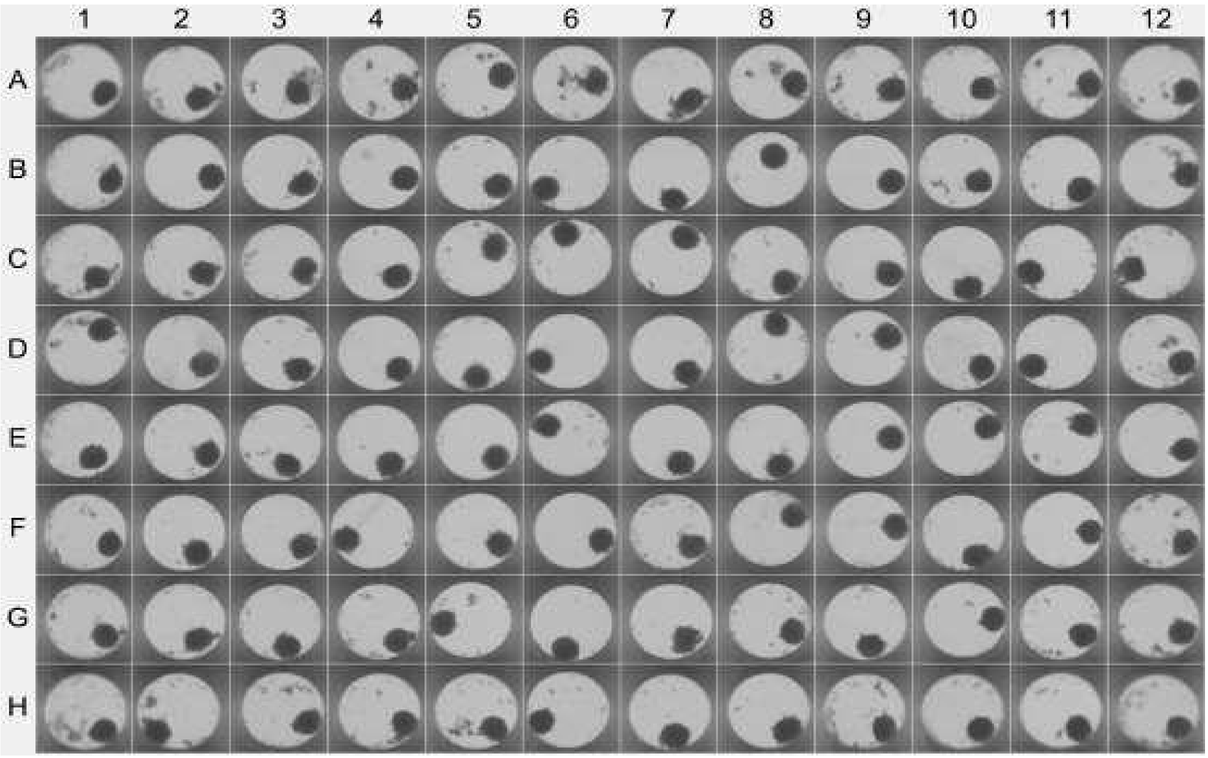

Figure 6 Image of a human liver microtissue plate. The plate is scanned during quality control by Insphero®. Each well contains a liver microtissue of 250-350 µm diameter.

Liver microtissues represent the human *in vivo* situation more closely compared to the standard animal model (most often rodents, and primates in the latest pre-clinical phases of drug development) and standard cell cultures (Proctor et al., 2017). In addition, liver microtissues are easy to handle and some “body-on-a-chip” prototypes for drug testing are being evaluated for drug screening and drug toxicity in more detail (Foster et al., 2019).

Each batch of multidonor human liver microtissues is obtained by pooling ten different livers from deceased donors (accidents, cardiovascular complications). Five donors are female and five donors are male. The livers are mashed and pooled together. Some cellular components, such as the immune cells i.e. Kupffer cells, are removed from the homogenate. Afterwards the cells are cryopreserved. Eventually, cellular seeds are distributed in special U-bottom wells where the liver cells aggregate in tridimensional spherical microtissues by gravity and cell polarisation (Kim et al., 2015, Jiang et al., 2019, Kermanizadeh et al., 2019).The quality control ensures homogeneity of the batch, and tests are performed to evaluate overall viability of the batch, dimension of the aggregates and the

expression of key enzymes such as P450 cytochromes (Figure 6).
Given all the advantages of the liver microtissues over the standard cell cultures, we validated this platform as a tool in antischistosomal drug screening, as explained in Chapter III of this work.

1.7. Aim and objectives of the thesis

The aim of this thesis was to study ways to overcome some of the limitations present in the *Schistosoma* spp. drug-screening pipeline, such as the low throughput and the subjectivity of the drug screening. We published a collection of protocols to uniform the drug screening procedure in *Schistosoma mansoni* with the aim to lessen the fragmentation between research groups involved in the search for novel antischistosomal drugs. Together with the D-BSSE of the ETH in Basel, more specifically with the Bio Engineering Laboratory led by Professor Dr. Andreas Hierlemann, I worked on the development of a novel device that could overcome some of the drawbacks linked to the laborious and subjective gold standard phenotypic drug screening procedure on *Schistosoma* spp.. This collaboration was essential for the development of a novel platform based on electrical impedance (EIS) for real-time measurement of NTS viability through motility readout. We developed a drug screening procedure based on primary human microtissues to extend the standard drug screenings on NTS to prodrugs and other compounds, assess the compound's cytotoxicity and to evaluate the effect of the liver CYPs on the compound’s activity *in vitro* on NTS. Finally, in collaboration with the University of Trieste I also evaluated a novel formulation of a polymorph of the racemic praziquantel *in vivo* and *in vitro*. To summarize, our aim was to

I. Make drug screening more uniform across different labs by providing a collection of procedures to detail our in-house drug screening in *Schistosoma mansoni* (Chapter I).

II. Improve the current drug screening procedure and overcome its previously identified limitations by developing novel drug screening systems: an EIS-based drug screening platform (Chapter II) and an approach incorporating human liver microtissues in the screening process (Chapter III).

III. Explore ways to improve the drawbacks of praziquantel and contribute to the currently empty drug pipeline by demonstrating the possibilities offered by a polymorph formulation (Chapter IV).

References

BALE, S. S., MOORE, L., YARMUSH, M. & JINDAL, R. 2016. Emerging *in vitro* liver technologies for drug metabolism and inter-organ interactions. *Tissue Eng Part B Rev,* 22**,** 383-394.

BEATRICE, P., PASSERINI, N., TRASTULLO, R., KEISER, J., ZANOLLA, D., ZINGONE, G., VOINOVICH, D. & ALBERTINI, B. 2017. An explorative analysis of process and formulation variables affecting comilling in a vibrational mill: The case of praziquantel. *Int J Pharm,* 533**,** 402-412.

BELL, C. C., DANKERS, A. C. A., LAUSCHKE, V. M., SISON-YOUNG, R., JENKINS, R., ROWE, C., GOLDRING, C. E., PARK, K., REGAN, S. L., WALKER, T., SCHOFIELD, C., BAZE, A., FOSTER, A. J., WILLIAMS, D. P., VAN DE VEN, A. W. M., JACOBS, F., HOUDT, J. V., LÄHTEENMÄKI, T., SNOEYS, J., JUHILA, S., RICHERT, L. & INGELMAN-SUNDBERG, M. 2018. Comparison of hepatic 2D sandwich cultures and 3D spheroids for long-term toxicity applications: a multicenter study. *Toxicological Sciences,* 162**,** 655-666.

BOUREE, P. & CAUMES, E. 2004. Cercarial dermatitis. *Presse Med,* 33**,** 490-3.

BUCHTER, V., HESS, J., GASSER, G. & KEISER, J. 2018. Assessment of tegumental damage to *Schistosoma mansoni* and *S. haematobium* after in vitro exposure to ferrocenyl, ruthenocenyl and benzyl derivatives of oxamniquine using scanning electron microscopy. *Parasites & vectors,* 11**,** 580-580.

BUONSENSO, D., SERRANTI, D. & VALENTINI, P. 2010. Management of central nervous system tuberculosis in children: light and shade. *Eur Rev Med Pharmacol Sci,* 14**,** 845-53.

BUSTINDUY, A. L., STOTHARD, J. R. & FRIEDMAN, J. F. 2017. Paediatric and maternal schistosomiasis: shifting the paradigms. *Br Med Bull,* 123**,** 115-125.

CAMPBELL, W. C. & REW, R. S. 2013. *Chemotherapy of parasitic diseases*, Springer Science & Business Media.

CHATELAIN, E. & IOSET, J. R. 2011. Drug discovery and development for neglected diseases: the DNDi model. *Drug Des Devel Ther,* 5**,** 175-81.

CHAWLA, K., MODENA, M. M., RAVAYNIA, P. S., LOMBARDO, F. C., LEONHARDT, M., PANIC, G., BURGEL, S. C., KEISER, J. & HIERLEMANN, A. 2018. Impedance-based microfluidic assay for automated antischistosomal drug screening. *ACS Sens*.

CHEUNG, K., GAWAD, S. & RENAUD, P. 2005. Impedance spectroscopy flow cytometry: On-chip label-free cell differentiation. 65A**,** 124-132.

CHIBA, M., ISHII, Y. & SUGIYAMA, Y. 2009. Prediction of hepatic clearance in human from *in vitro* data for successful drug development. *The AAPS journal,* 11**,** 262-276.

CIOLI, D. & PICA-MATTOCCIA, L. 2003. Praziquantel. *Parasitology Research,* 90**,** S3–S9.

CIOLI, D., PICA-MATTOCCIA, L., BASSO, A. & GUIDI, A. 2014. Schistosomiasis control: praziquantel forever? *Mol Biochem Parasitol,* 195**,** 23-9.

COLLEY, D. G., BUSTINDUY, A. L., SECOR, W. E. & KING, C. H. 2014. Human schistosomiasis. *The Lancet,* 383**,** 2253-64.

COULIBALY, J. T., PANIC, G., SILUE, K. D., KOVAC, J., HATTENDORF, J. & KEISER, J. 2017. Efficacy and safety of praziquantel in preschool-aged and school-aged children infected with *Schistosoma mansoni*: a randomised controlled, parallel-group, dose-ranging, phase 2 trial. *Lancet Global Health,* 5**,** E688-E698.

COWAN, N. & KEISER, J. 2015. Repurposing of anticancer drugs: *in vitro* and *in vivo* activities against *Schistosoma mansoni*. *Parasit. Vectors.,* 8**,** 417.

D'ENTREMONT, M. I., PAULSON, A. T. & MARBLE, A. E. 2002. Impedance spectroscopy: An accurate method of differentiating between viable and ischaemic or infarcted muscle tissue. *Medical and Biological Engineering and Computing,* 40**,** 380-387.

DE JESUS, A. R., SILVA, A., SANTANA, L. B., MAGALHAES, A., DE JESUS, A. A., DE ALMEIDA, R. P., RÊGO, M. A., BURATTINI, M. N., PEARCE, E. J. & CARVALHO, E. M. 2002. Clinical and immunologic evaluation of 31 patients with acute schistosomiasis mansoni. *J The Journal of infectious diseases,* 185**,** 98-105.

DOENHOFF, M. J., CIOLI, D. & UTZINGER, J. 2008. Praziquantel: mechanisms of action, resistance and new derivatives for schistosomiasis. *Curr Opin Infect Dis,* 21**,** 659-67.

ELBAZ, T. & ESMAT, G. 2013. Hepatic and intestinal schistosomiasis: review. *J Adv Res,* 4**,** 445-52.

EMA 2012. CHMP assessment report - Axitinib.

EZEAMAMA, A. E., MCGARVEY, S. T., ACOSTA, L. P., ZIERLER, S., MANALO, D. L., WU, H. W., KURTIS, J. D., MOR, V., OLVEDA, R. M. & FRIEDMAN, J. F. 2008. The synergistic effect of concomitant schistosomiasis, hookworm, and trichuris infections on children's anemia burden. *PLoS Negl Trop Dis,* 2**,** e245.

FELDMEIER, H., KRANTZ, I., POGGENSEE, G. J. I. J. O. S. & AIDS 1994. Female genital schistosomiasis as a risk-factor for the transmission of HIV. 5**,** 368-372.

FENWICK, A. & JOURDAN, P. 2016. Schistosomiasis elimination by 2020 or 2030? *Int J Parasitol,* 46**,** 385-8.

FOSTER, A. J., CHOUHAN, B., REGAN, S. L., ROLLISON, H., AMBERNTSSON, S., ANDERSSON, L. C., SRIVASTAVA, A., DARNELL, M., CAIRNS, J., LAZIC, S. E., JANG, K.-J., PETROPOLIS, D. B., KODELLA, K., RUBINS, J. E., WILLIAMS, D., HAMILTON, G. A., EWART, L. & MORGAN, P. 2019. Integrated *in vitro* models for hepatic safety and metabolism: Evaluation of a human liver-chip and liver spheroid. *Archives of Toxicology,* 93**,** 1021-1037.

GO´MEZ, R., BASHIR, R., SARIKAYA, A., LADISCH, M. R., STURGIS, J., ROBINSON, J. P., GENG, T., BHUNIA, A. K., APPLE, H. L. & WERELEY, S. 2001. Microfluidic Biochip for Impedance Spectroscopy of Biological Species. *Biomedical Microdevices,* 3**,** 201-209.

GOUVEIA, M. J., BRINDLEY, P. J., GÄRTNER, F., COSTA, J. M. C. D. & VALE, N. 2018. Drug Repurposing for Schistosomiasis: Combinations of Drugs or Biomolecules. *Pharmaceuticals (Basel, Switzerland),* 11**,** 15.

GRAY, D. J., ROSS, A. G., LI, Y. S. & MCMANUS, D. P. 2011. Diagnosis and management of schistosomiasis. *BMJ,* 342**,** d2651.

GRYSEELS, B., POLMAN, K., CLERINX, J. & KESTENS, L. 2006. Human schistosomiasis. *The Lancet,* 368**,** 1106–1118.

HAAS, W., GRABE, K., GEIS, C., PACH, T., STOLL, K., FUCHS, M., HABERL, B. & LOY, C. 2002. Recognition and invasion of human skin by *Schistosoma mansoni* cercariae: the key-role of L-arginine. *Parasitology,* 124**,** 153-67.

HAAS, W. & HAEBERLEIN, S. 2009. Penetration of cercariae into the living human skin: *Schistosoma mansoni* vs. *Trichobilharzia szidati*. *Parasitology Research,* 105**,** 1061-1066.

HAJISSA, K., MUHAJIR, A., ESHAG, H. A., ALFADEL, A., NAHIED, E., DAHAB, R., ALI, S. M., MOHAMMED, M., GAAFAR, M. & MOHAMED, Z. 2018. Prevalence of schistosomiasis and associated risk factors among school children in Um-Asher Area, Khartoum, Sudan. *BMC Res Notes,* 11**,** 779.

HEINRICH, F., RIEDEL, M. & LISDAT, F. 2018. Detection of abasic DNA by means of impedance spectroscopy. *Electrochemistry Communications,* 90**,** 65-68.

HERNANDEZ, D. C., LIM, K. C., MCKERROW, J. H. & DAVIES, S. J. 2004. *Schistosoma mansoni*: sex-specific modulation of parasite growth by host immune signals. *Exp Parasitol,* 106**,** 59-61.

HOCKLEY, D. J. 1973. Ultrastructure of the tegument of *Schistosoma*. *Adv Parasitol,* 11**,** 233-305.

HOLDING, C. 2003. Schistosomiasis under scrutiny. *Genome Biology,* 4**,** 9005.

INOBAYA, M. T., OLVEDA, R. M., CHAU, T. N., OLVEDA, D. U. & ROSS, A. G. 2014. Prevention and control of schistosomiasis: a current perspective. *Research and reports in tropical medicine,* 2014**,** 65-75.

JAMIESON, B. G. 2017. *Schistosoma: Biology, pathology and control*, CRC Press.

JEZIORSKI, M. & GREENBERG, R. 2006. Voltage-gated calcium channel subunits from platyhelminths: Potential role in praziquantel action. *International journal for parasitology,* 36**,** 625-32.

JIANG, J., MESSNER, S., KELM, J. M., VAN HERWIJNEN, M., JENNEN, D. G. J., KLEINJANS, J. C. & DE KOK, T. M. 2019. Human 3D multicellular microtissues: An upgraded model for the in vitro mechanistic investigation of inflammation-associated drug toxicity. *Toxicology Letters,* 312**,** 34-44.

KEISER, J. 2010. In vitro and in vivo trematode models for chemotherapeutic studies. *Parasitology,* 137**,** 589-603.

KERMANIZADEH, A., BROWN, D. M., MORITZ, W. & STONE, V. 2019. The importance of inter-individual Kupffer cell variability in the governance of hepatic toxicity in a 3D primary human liver microtissue model. *Scientific Reports,* 9**,** 7295.

KIM, J. Y., FLURI, D. A., MARCHAN, R., BOONEN, K., MOHANTY, S., SINGH, P., HAMMAD, S., LANDUYT, B., HENGSTLER, J. G., KELM, J. M., HIERLEMANN, A. & FREY, O. 2015. 3D spherical microtissues and microfluidic technology for multi-tissue experiments and analysis. *J Biotechnol,* 205**,** 24-35.

KING, C. H. 2017. The evolving schistosomiasis agenda 2007-2017—Why we are moving beyond morbidity control toward elimination of transmission. *PLOS Neglected Tropical Diseases,* 11**,** e0005517.

KING, C. H., OLBRYCH, S. K., SOON, M., SINGER, M. E., CARTER, J. & COLLEY, D. G. 2011. Utility of Repeated Praziquantel Dosing in the Treatment of Schistosomiasis in High-Risk Communities in Africa: A Systematic Review. *PLOS Neglected Tropical Diseases,* 5**,** e1321.

KITTUR, N., CASTLEMAN, J. D., CAMPBELL JR, C. H., KING, C. H., COLLEY, D. G. J. T. A. J. O. T. M. & HYGIENE 2016. Comparison of *Schistosoma mansoni* prevalence and intensity of infection, as determined by the circulating cathodic antigen urine assay or by the Kato-Katz fecal assay: a systematic review. 94**,** 605-610.

KNOPP, S., PERSON, B., AME, S. M., ALI, S. M., HATTENDORF, J., JUMA, S., MUHSIN, J., KHAMIS, I. S., MOHAMMED, K. A., UTZINGER, J., HOLLENBERG, E., KABOLE, F. & ROLLINSON, D. 2019. Evaluation of integrated interventions layered on mass drug administration for urogenital schistosomiasis elimination: a cluster-randomised trial. *Lancet Glob Health*.

KOVAC, J., VARGAS, M. & KEISER, J. 2017. *In vitro* and *in vivo* activity of R- and S-praziquantel enantiomers and the main human metabolite trans-4-hydroxy-praziquantel against *Schistosoma haematobium*. *Parasit Vectors,* 10**,** 365.

LALLI, C., GUIDI, A., GENNARI, N., ALTAMURA, S., BRESCIANI, A. & RUBERTI, G. 2015. Development and validation of a luminescence-based, medium-throughput assay for drug screening in *Schistosoma mansoni*. *PLoS Negl. Trop. Dis.,* 9**,** e0003484.

LEITE, S. B., WILK-ZASADNA, I., ZALDIVAR, J. M., AIROLA, E., REIS-FERNANDES, M. A., MENNECOZZI, M., GUGUEN-GUILLOUZO, C., CHESNE, C., GUILLOU, C., ALVES, P. M. & COECKE, S. 2012. Three-dimensional HepaRG model as an attractive tool for toxicity testing. *Toxicol Sci,* 130**,** 106-16.

LEWIS, F. A. & TUCKER, M. S. 2014. Schistosomiasis. *Digenetic Trematodes,* 766**,** 47-75.

LIU, Z., FANG, H., REAGAN, K., XU, X., MENDRICK, D. L., SLIKKER, W. & TONG, W. 2013. *In silico* drug repositioning – what we need to know. *Drug Discovery Today,* 18**,** 110-115.

LOMBARDO, F. C., PASCHE, V., PANIC, G., ENDRISS, Y. & KEISER, J. 2019. Life cycle maintenance and drug-sensitivity assays for early drug discovery in *Schistosoma mansoni*. *Nature Protocols,* 14**,** 461-481.

MAIZELS, R. M. & YAZDANBAKHSH, M. 2003. Immune Regulation by helminth parasites: cellular and molecular mechanisms. *Nature Reviews Immunology,* 3**,** 733-744.

MANNECK, T., BRAISSANT, O., HAGGENMULLER, Y. & KEISER, J. 2011. Isothermal microcalorimetry to study drugs against *Schistosoma mansoni*. *Journal of Clinical Microbiology,* 49**,** 1217-25.

MANSOUR, N. R., PAVELEY, R., GARDNER, J. M. F., BELL, A. S., PARKINSON, T. & BICKLE, Q. 2016. High throughput screening identifies novel lead compounds with activity against larval, juvenile and adult *Schistosoma mansoni*. *PLoS Negl. Trop. Dis.,* 10**,** e0004659.

MCKENZIE, F. E. 2005. Polyparasitism. *International journal of epidemiology,* 34**,** 221-223.

MCKERROW, J. & SALTER, J. 2002. Invasion of skin by *Schistosoma* cercariae. *Trends in Parasitology,* 18**,** 193-195.

MCMANUS, D. P., DUNNE, D. W., SACKO, M., UTZINGER, J., VENNERVALD, B. J. & ZHOU, X.-N. 2018. Schistosomiasis. *Nature Reviews Disease Primers,* 4**,** 13.

MCMICHAEL, C. 2019. Water, Sanitation and Hygiene (WASH) in Schools in Low-Income Countries: A Review of Evidence of Impact. *International journal of environmental research and public health,* 16**,** 359.

MESSNER, S., AGARKOVA, I., MORITZ, W. & KELM, J. M. 2013. Multi-cell type human liver microtissues for hepatotoxicity testing. *Archives of Toxicology,* 87**,** 209-213.

MIGUEL, E. & KREMER, M. 2004. Worms: Identifying impacts on education and health in the presence of treatment externalities. *Econometrica,* 72**,** 159-217.

MORLEY, N. J. 2011. Thermodynamics of cercarial survival and metabolism in a changing climate. *Parasitology,* 138**,** 1442-52.

MUNISI, D. Z., BUZA, J., MPOLYA, E. A., ANGELO, T. & KINUNG'HI, S. M. 2017. The efficacy of single-dose versus double-dose praziquantel treatments on *Schistosoma mansoni* infections: its implication on undernutrition and anaemia among Primary Schoolchildren in two on-shore communities, Northwestern Tanzania. *BioMed research international,* 2017**,** 7035025-7035025.

NACIF-PIMENTA, R., DA SILVA ORFANÓ, A., MOSLEY, I. A., KARINSHAK, S. E., ISHIDA, K., MANN, V. H., COELHO, P. M. Z., DA COSTA, J. M. C., HSIEH, M. H., BRINDLEY, P. J. & RINALDI, G. 2019. Differential responses of epithelial cells from urinary and biliary tract to eggs of *Schistosoma haematobium* and *S. mansoni*. *Scientific Reports,* 9**,** 10731.

NWAKA, S. & HUDSON, A. 2006. Innovative lead discovery strategies for tropical diseases. *Nature Reviews Drug Discovery,* 5**,** 941-955.

OLIVECRONA, M., BLASCHKE, T., ENGKVIST, O. & CHEN, H. 2017. Molecular de-novo design through deep reinforcement learning. *Journal of Cheminformatics,* 9**,** 48.

OLLIARO, P., DELGADO-ROMERO, P. & KEISER, J. 2014. The little we know about the pharmacokinetics and pharmacodynamics of praziquantel (racemate and R-enantiomer). *Journal of Antimicrobial Chemotherapy,* 69**,** 863-870.

OLSON, H., BETTON, G., ROBINSON, D., THOMAS, K., MONRO, A., KOLAJA, G., LILLY, P., SANDERS, J., SIPES, G., BRACKEN, W., DORATO, M., VAN DEUN, K., SMITH, P., BERGER, B. & HELLER, A. 2000. Concordance of the toxicity of pharmaceuticals in humans and in animals. *Regul Toxicol Pharmacol,* 32**,** 56-67.

OPREA, T. I., BAUMAN, J. E., BOLOGA, C. G., BURANDA, T., CHIGAEV, A., EDWARDS, B. S., JARVIK, J. W., GRESHAM, H. D., HAYNES, M. K., HJELLE, B., HROMAS, R., HUDSON, L., MACKENZIE, D. A., MULLER, C. Y., REED, J. C., SIMONS, P. C., SMAGLEY, Y., STROUSE, J., SURVILADZE, Z., THOMPSON, T., URSU, O., WALLER, A., WANDINGER-NESS, A., WINTER, S. S., WU, Y., YOUNG, S. M., LARSON, R. S., WILLMAN, C. & SKLAR, L. A. 2011. Drug repurposing from an academic perspective. *Drug Discovery Today: Therapeutic Strategies,* 8**,** 61-69.

PAMPALONI, F. & STELZER, E. H. 2009. Three-dimensional cell cultures in toxicology. *J Biotechnology* 26**,** 117-138.

PANIC, G., DUTHALER, U., SPEICH, B. & KEISER, J. 2014. Repurposing drugs for the treatment and control of helminth infections. *Int J Parasitol Drugs Drug Resist,* 4**,** 185-200.

PANIC, G., FLORES, D., INGRAM-SIEBER, K. & KEISER, J. 2015a. Fluorescence/luminescence-based markers for the assessment of *Schistosoma mansoni* schistosomula drug assays. *Parasit Vectors,* 8**,** 624.

PANIC, G. & KEISER, J. 2018. Acting beyond 2020: better characterization of praziquantel and promising antischistosomal leads. *Curr Opin Pharmacol,* 42**,** 27-33.

PANIC, G., VARGAS, M., SCANDALE, I. & KEISER, J. 2015b. Activity Profile of an FDA-Approved Compound Library against *Schistosoma mansoni*. *Plos Neglected Tropical Diseases,* 9.

PASCHE, V., LALEU, B. & KEISER, J. 2018. Screening a repurposing library, the Medicines for Malaria Venture Stasis Box, against *Schistosoma mansoni*. *Parasit. Vectors.,* 11**,** 298.

PAVELEY, R. A., MANSOUR, N. R., HALLYBURTON, I., BLEICHER, L. S., BENN, A. E., MIKIC, I., GUIDI, A., GILBERT, I. H., HOPKINS, A. L. & BICKLE, Q. D. 2012. Whole organism high-content screening by label-free, image-based Bayesian classification for parasitic diseases. *PLoS Negl Trop Dis,* 6**,** e1762.

PETHIG, R. 1985. Dielectric and Electrical Properties of Biological Materials. *Journal of Bioelectricity,* 4**,** vii-ix.

PLOUFFE, D., BRINKER, A., MCNAMARA, C., HENSON, K., KATO, N., KUHEN, K., NAGLE, A., ADRIÁN, F., MATZEN, J. T., ANDERSON, P., NAM, T.-G., GRAY, N. S., CHATTERJEE, A., JANES, J., YAN, S. F., TRAGER, R., CALDWELL, J. S., SCHULTZ, P. G., ZHOU, Y. & WINZELER, E. A. 2008. *In silico* activity profiling reveals the mechanism of action of antimalarials discovered in a high-throughput screen. 105**,** 9059-9064.

PROCTOR, W. R., FOSTER, A. J., VOGT, J., SUMMERS, C., MIDDLETON, B., PILLING, M. A., SHIENSON, D., KIJANSKA, M., STROBEL, S., KELM, J. M., MORGAN, P., MESSNER, S. & WILLIAMS, D. 2017. Utility of spherical human liver microtissues for prediction of clinical drug-induced liver injury. *Archives of Toxicology,* 91**,** 2849-2863.

PROTASIO, A. V., DUNNE, D. W. & BERRIMAN, M. 2013. Comparative study of transcriptome profiles of mechanical- and skin-transformed *Schistosoma mansoni* schistosomula. *PLoS Negl. Trop. Dis.,* 7**,** e2091.

RAMAIAHGARI, S. C., WAIDYANATHA, S., DIXON, D., DEVITO, M. J., PAULES, R. S. & FERGUSON, S. S. 2017. From the Cover: Three-Dimensional (3D) HepaRG Spheroid Model With Physiologically Relevant Xenobiotic Metabolism Competence and Hepatocyte Functionality for Liver Toxicity Screening. *Toxicol Sci,* 159**,** 124-136.

RAMIREZ, B., BICKLE, Q., YOUSIF, F., FAKOREDE, F., MOURIES, M. A. & NWAKA, S. 2007. Schistosomes: challenges in compound screening. *Expert Opin Drug Discov,* 2**,** S53-61.

RAZA, K. 2014. Polymorphism: The Phenomenon Affecting the Performance of Drugs. *SOJ Pharmacy & Pharmaceutical Sciences*.

RICCIARDI, A. & NDAO, M. 2015. Still hope for schistosomiasis vaccine. *Human Vaccines & Immunotherapeutics,* 11**,** 2504-2508.

ROLLINSON, D., KNOPP, S., LEVITZ, S., STOTHARD, J. R., TCHUEM TCHUENTÉ, L.-A., GARBA, A., MOHAMMED, K. A., SCHUR, N., PERSON, B., COLLEY, D. G. & UTZINGER, J. 2013. Time to set the agenda for schistosomiasis elimination. *Acta Tropica,* 128**,** 423-440.

ROSS, A. G., MCMANUS, D. P., FARRAR, J., HUNSTMAN, R. J., GRAY, D. J. & LI, Y.-S. J. J. O. N. 2012. Neuroschistosomiasis. 259**,** 22-32.

SHIFF, C. J., CMELIK, S. H. W., LEY, H. E. & KRIEL, R. L. 1972. The influence of human skin lipids on the cercarial penetration responses of *Schistosoma haematobium* and *Schistosoma mansoni*. *The Journal of Parasitology,* 58**,** 476-480.

SIMON, M., LISA, F., M., L. V., KATRIN, R., CLAUDIA, E., MAGDALENA, B., M., K. J., MAGNUS, I.-S. & WOLFGANG, M. 2018. Transcriptomic, Proteomic, and Functional Long-Term Characterization of Multicellular Three-Dimensional Human Liver Microtissues. *Applied In Vitro Toxicology,* 4**,** 1-12.

SKELLY, P. J., DA'DARA, A. A., LI, X.-H., CASTRO-BORGES, W. & WILSON, R. A. 2014. Schistosome feeding and regurgitation. *PLoS pathogens,* 10**,** e1004246-e1004246.

SOTILLO, J., PEARSON, M., BECKER, L., MULVENNA, J. & LOUKAS, A. 2015. A quantitative proteomic analysis of the tegumental proteins from *Schistosoma mansoni* schistosomula reveals novel potential therapeutic targets. *Int J Parasitol,* 45**,** 505-16.

SPOTILA, L. D., REKOSH, D. M., BOUCHER, J. M. & LOVERDE, P. T. 1987. A cloned DNA probe identifies the sex of *Schistosoma mansoni* cercariae. *Molecular and Biochemical Parasitology,* 26**,** 17-20.

SWINNEY, D. C. 2013. Phenotypic vs. target-based drug discovery for first-in-class medicines. *Clin Pharmacol Ther,* 93**,** 299-301.

TERSTAPPEN, G. C. & REGGIANI, A. 2001. *In silico* research in drug discovery. *Trends in Pharmacological Sciences,* 22**,** 23-26.

TUCKER, M. S., KARUNARATNE, L. B., LEWIS, F. A., FREITAS, T. C. & LIANG, Y. S. 2013. Schistosomiasis. *Curr Protoc Immunol,* 103**,** Unit 19 1.

TURNER, J. D., NARANG, P., COLES, M. C. & MOUNTFORD, A. P. J. P. P. 2012. Blood flukes exploit Peyer's patch lymphoid tissue to facilitate transmission from the mammalian host. 8**,** e1003063.

UTZINGER, J., N'GORAN, E. K., CAFFREY, C. R. & KEISER, J. 2011. From innovation to application: Social–ecological context, diagnostics, drugs and integrated control of schistosomiasis. *Acta Tropica,* 120, Supplement 1**,** S121-S137.

VASCONCELLOS, L. S., PETROIANU, A., ROMEIRO, J. R., TAVARES JUNIOR, W. C. & RESENDE, V. 2018. Correlation between the values of circulating blood elements with the size of spleen in the presence of schistosomal splenomegaly. *Acta Cir Bras,* 33**,** 1103-1109.

WAGNER, I., MATERNE, E. M., BRINCKER, S., SUSSBIER, U., FRADRICH, C., BUSEK, M., SONNTAG, F., SAKHAROV, D. A., TRUSHKIN, E. V., TONEVITSKY, A. G., LAUSTER, R. & MARX, U. 2013. A dynamic multi-organ-chip for long-term cultivation and substance testing proven by 3D human liver and skin tissue co-culture. *Lab Chip,* 13**,** 3538-47.

WANG, L., CHIANG, C., LIANG, H., WU, H., FENG, W., QUINNEY, S. K., LI, J. & LI, L. 2015. How to choose *in vitro* systems to predict *in vivo* drug clearance: a system pharmacology perspective. *BioMed research international,* 2015**,** 857327-857327.

WANG, W. & LIANG, Y. 2015. Mass drug administration (MDA) for schistosomiasis. *The Journal of Infectious Diseases,* 211**,** 848-9.

WILDEY, M. J., HAUNSO, A., TUDOR, M., WEBB, M. & CONNICK, J. H. 2017. Chapter Five - High-Throughput Screening. *In:* GOODNOW, R. A. (ed.) *Annual Reports in Medicinal Chemistry.* Academic Press.

WILSON, M. S., MENTINK-KANE, M. M., PESCE, J. T., RAMALINGAM, T. R., THOMPSON, R. & WYNN, T. A. 2006. Immunopathology of schistosomiasis. *Immun. Cell Biol.,* 85**,** 148-154.

WISHART, D. S., KNOX, C., GUO, A. C., SHRIVASTAVA, S., HASSANALI, M., STOTHARD, P., CHANG, Z. & WOOLSEY, J. 2006. DrugBank: a comprehensive resource for *in silico* drug discovery and exploration. *J Nucleic acids research,* 34**,** D668-D672.

YOKOYAMA, Y., SASAKI, Y., TERASAKI, N., KAWATAKI, T., TAKEKAWA, K., IWASE, Y., SHIMIZU, T., SANOH, S. & OHTA, S. 2018. Comparison of Drug Metabolism and Its Related Hepatotoxic Effects in HepaRG, Cryopreserved Human Hepatocytes, and HepG2 Cell Cultures. *Biol Pharm Bull,* 41**,** 722-732.

ZANOLLA, D., PERISSUTTI, B., PASSERINI, N., CHIEROTTI, M. R., HASA, D., VOINOVICH, D., GIGLI, L., DEMITRI, N., GEREMIA, S., KEISER, J., CERREIA VIOGLIO, P. & ALBERTINI, B. 2018a. A new soluble and bioactive polymorph of praziquantel. *Eur J Pharm Biopharm,* 127**,** 19-28.

ZANOLLA, D., PERISSUTTI, B., PASSERINI, N., CHIEROTTI, M. R., HASA, D., VOINOVICH, D., GIGLI, L., DEMITRI, N., GEREMIA, S., KEISER, J., CERREIA VIOGLIO, P. & ALBERTINI, B. 2018b. A new soluble and bioactive polymorph of praziquantel. *European Journal of Pharmaceutics and Biopharmaceutics,* 127**,** 19-28.

ZHANG, Q., ZHU, D., HOU, R., PAN, D., WANG, X., SUN, Z. & WANG, C. Study on the Characteristic of Electrical Impedance Spectroscopy of Soybean Seeds and the Detection of Seed Viability. 2011 Berlin, Heidelberg. Springer Berlin Heidelberg, 631-636.

Chapter I:

Life cycle maintenance and drug-sensitivity assays for early drug discovery in *Schistosoma mansoni*

nature protocols

PROTOCOL

https://doi.org/10.1038/s41596-018-0101-y

Life cycle maintenance and drug-sensitivity assays for early drug discovery in *Schistosoma mansoni*

Flavio C. Lombardo[1,2,3], Valérian Pasche[1,2,3], Gordana Panic[1,2], Yvette Endriss[1,2] and Jennifer Keiser[1,2*]

Drug discovery for schistosomiasis is still limited to a handful of academic laboratories worldwide, with only a few novel antischistosomal lead compounds being actively researched. Despite recent international mobilization against the disease to stimulate and promote antischistosomal drug discovery, setting up a drug-screening flow with schistosome parasites remains challenging. Whereas numerous different protocols to obtain and cultivate schistosomes have been published, those describing the drug-screening process are scarce, and none gather together parasite cultivation and early drug discovery procedures. To help overcome this hurdle, we provide here a set of integrated methods either adapted from already-published protocols or based on our long-term experience in schistosomiasis research. Specifically, we detail the establishment and maintenance of the complex and several-week-long *Schistosoma mansoni* life cycle in a laboratory setting, as well as the means of retrieving and culturing the parasites at their relevant life stages. The in vitro and in vivo assays that are performed along the drug-screening cascade are also described. In these assays, which can be performed within 5 d, the effect of a drug is determined by phenotypic assessment of the parasites' viability and morphology, for which stage-specific scoring scales are proposed. Finally, the modalities for testing and evaluating a compound in vivo, constituting a procedure lasting up to 10 weeks, are presented in order to go from in vitro hit identification to the selection of early lead candidates.

Introduction

In May 2012, the World Health Organization (WHO) put forth an ambitious goal to eliminate schistosomiasis, a debilitating parasitic disease caused by trematodes of the *Schistosoma* genus, as a public health problem by 2020 (WHO, https://www.who.int/neglected_diseases/9789241564540/en/). To fulfill this mandate, treatment coverage using the only drug available, praziquantel (PZQ), would need to expand from 35 to 75% of school-aged children in at-risk areas (WHO, https://www.who.int/neglected_diseases/news/WHO_urges_increased_access_to_praziquantel/en/). Yet, because of concerns about drug resistance, along with the drug's other drawbacks, the scientific community has recognized an urgent need for the development of new treatments[1,2]. Despite the pressing need, however, no new drug candidates are currently close to reaching market. As one of the neglected tropical diseases, the drug discovery pipeline for schistosomiasis is, by extension, underfunded[3]. Nonetheless, drug discovery efforts have been extensive in the academic community[4–7]. Moreover, recent product-development partnerships, such as the Drugs for Neglected Diseases *initiative* (DND*i*) and the Medicines for Malaria Venture (MMV), have been productive in securing compound libraries to be tested against a broad range of infectious diseases, including schistosomiasis, which has resulted in an array of hit compounds for the disease[8–10]. Hence, this is a key moment to expand antischistosomal drug discovery efforts.

This protocol aims to support these efforts by providing the necessary basics for establishing a screening cascade. Specifically, it details the procedures used at the Swiss Tropical and Public Health Institute (Swiss TPH) to establish the complex *S. mansoni* life cycle in the laboratory, obtain the relevant life-stage parasites, integrate them into an in vitro and in vivo drug-screening cascade, and lay out best-practice phenotypic assay evaluation procedures. As fewer than 30 institutions worldwide host an in-house *S. mansoni* life cycle[11], different culturing conditions and various screening techniques are being successfully used. The fact that we focus here on the protocols currently used at the Swiss TPH should therefore neither overshadow nor discredit alternative methods, which we discuss when applicable.

---

[1]Department of Medical Parasitology and Infection Biology, Swiss Tropical and Public Health Institute, Basel, Switzerland. [2]University of Basel, Basel, Switzerland. [3]These authors contributed equally: Flavio C. Lombardo, Valérian Pasche. *e-mail: jennifer.keiser@swisstph.ch

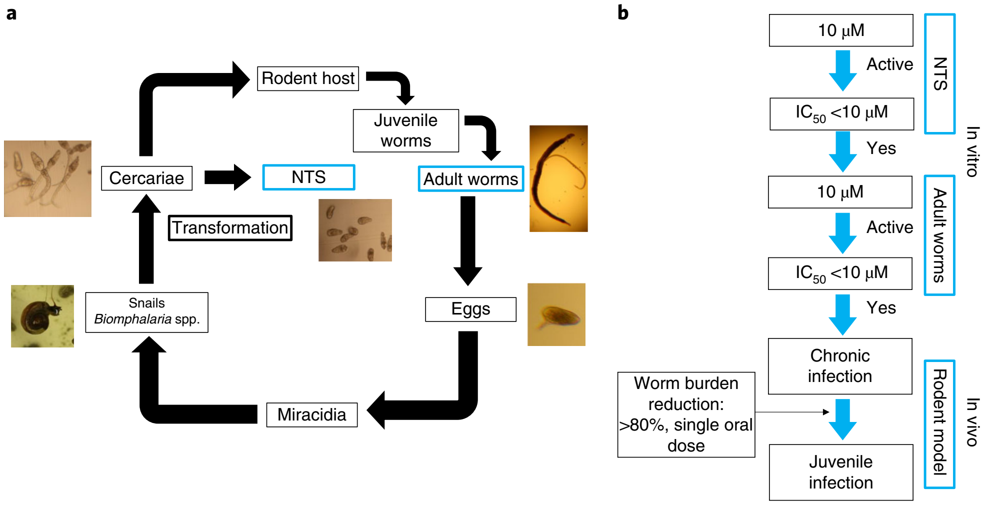

Fig. 1 | Overview of the protocol. a, The *S. mansoni* life cycle (Steps 1-38) requires that eggs obtained from an infected rodent be exposed to water to hatch as miracidia (Steps 11–28), which infect *Biomphalaria glabrata* snails. After a few weeks of asexual reproduction, *S. mansoni* cercariae emerge after snails are exposed to light (Steps 29-34). A cercarial suspension can then be collected to infect a mouse or hamster (Steps 35-38). The life stages used in the drug-screening cascade are indicated in blue boxes in the figure. For other *Schistosoma* species, please refer to Supplementary Table 1. **b**, The antischistosomal screening cascade starts with a pre-screen of compounds on NTS at 10 µM (can be adjusted) (Steps 51-55). Active compounds are tested on adult-stage worms (Steps 72–78) in vitro, and the most active from this screen are further tested in mice harboring *S. mansoni* chronic infection (Steps 79-82). The activity of the compounds that show worm burden reduction >80% can be further characterized on mice bearing juvenile worms.

Development of the protocol

Methods for breeding and maintaining *Biomphalaria glabrata* snails and schistosomes in laboratories have been established since the 1950s[12,13]. The procedure described here to maintain an *S. mansoni* life cycle is based on these original methods, with several modifications over time[11–16], as this life cycle has been running for more than 50 years at the Swiss TPH.

Since the 1970s, different techniques for mechanical cercarial transformation have been described[17–19]. In this protocol, we propose a transformation method adapted from Milligan and Jolly[20] (see video therein) and Colley and Wikel[17], which consists of a series of washing steps and repeated passage between two connected syringes.

Despite recent advances in automated or quantitative methods for drug screening on the different *S. mansoni* stages, there is no broadly accepted consensus on automated assays. Therefore, drug sensitivity assays based on phenotypic evaluation of adult worms have formed the basis of standard operating procedures recommended by the UNICEF/UNDP/World Bank/WHO Special Program for Research and Training in Tropical Diseases (TDR) since 2007[11,21]. However, when screening large libraries of chemical compounds, huge quantities of parasites are required. A medium-throughput phenotypic screening procedure based on schistosomula assessment was proposed by Abdulla et al.[22]. This approach was later applied by Mansour and Bickle[23], and modified to be suitable for screening large libraries of compounds. Assessing the viability of the parasite after drug exposure is essential to determining the effect of a drug candidate[11]. For this reason, we adapted the phenotypic scoring scale described by Ramirez et al.[21] and Abdulla et al.[22] for the assessment of newly transformed schistosomula (NTS) in vitro[11,24].

Overview of the procedure

The first part of the procedure (Steps 1–38) details how to set up and maintain the *S. mansoni* life cycle (Fig. 1a), which comprises setting up a *B. glabrata* snail life cycle (Steps 1–10), obtaining *S. mansoni* eggs from the infected hamsters (Steps 11–16), hatching the miracidia from the eggs and infecting the snails (Steps 17–28), inducing cercarial shedding from the snails (Steps 29–34), and infecting mice or hamsters with *S. mansoni* cercariae (Steps 35–38). Once the life cycle is established, it is possible to conduct the in vitro and in vivo screening.

The drug-screening process (depicted in Fig. 1b) often starts with a pre-screen of the compound library on the larval-stage worms, which are more abundant and easier to obtain. This stage of the protocol therefore begins with the production of larval-stage parasites, hereafter referred to as NTS (Steps 39–50). The drug assay setup, as well as the drug assay evaluation procedure, is then detailed (Steps 51–55). Only the compounds that are found to be active on NTS are tested on the primary target of interest, the adult-stage worms (Steps 72–78). In the last part of the protocol, the methods for testing and evaluating the activity of lead candidates in a mouse model are presented (Steps 79–86).

Alternative methods

Establishment and maintenance of a schistosome life cycle

The methods for establishing a schistosome life cycle vary slightly, depending on the *Schistosoma* species and lab conventions. At Swiss TPH, we generally use a Liberian *S. mansoni* strain, *B. glabrata* (Egyptian) for snail infection, coupled with an *S. mansoni*—hamster or *S. mansoni*—mouse infection model, as described in the Procedure. Variations to the protocols required for *S. haematobium* and *S. japonicum* are described in Supplementary Table 1, in addition to various mouse strain options. We also cite the optimal snail size for infection with miracidia (4–6 mm), development period until cercarial shedding (5–6 weeks) and length of exposure to light to induce cercarial shedding (3–4 h) that we have found to be effective in our drug discovery work[7,9,25,26]. However, this could vary from lab to lab for a number of reasons, such as the *Schistosoma* or snail strains chosen. We therefore recommend that readers experiment and determine their own optimal conditions.

In our experience, the RJHan:AURA hamster (Janvier Labs) is optimal for life cycle maintenance because of its ability to harbor many parasites for a sufficient period of time. However, the alternative rodent hosts listed in Supplementary Table 1 are also suitable.

Research groups that do not want to undertake the task of establishing a life cycle can make use of the NIH National Institute of Allergy and Infectious Diseases (NIAID) Schistosomiasis Resource Center, which maintains a variety of schistosome–snail and schistosome–rodent infections, available freely to any research team that requests them (http://www.afbr-bri.com/schistosomiasis/).

Cercarial transformation

The time requirement for the cercarial transformation using two connected syringes followed by a saline rinse is, in our experience, much shorter than those for other procedures based on pipetting or vortexing[16,18] to trigger separation of the cercarial head from the tail, or using a Percoll gradient[16,27] to rinse the tails.

In vitro drug testing

This procedure allows a certain flexibility and some modifications to it may be required to meet the reader's needs. For example, Basch medium can be used instead of M199 medium for larval-stage assays[11]. Also, the drug concentration range (10–100 µM) and the duration of each assay will depend on the type of drug being tested. Whereas a screen at 10 µM might be suitable for synthetic compounds, a test concentration of ≥100 µM might be more suitable to test sublethal effects of natural product derivatives[28].

Although phenotypic screenings based on microscopy as a readout are beneficial for researchers working in low-resource facilities, they are laborious and undeniably subjective[11]. Intensive research has been conducted to overcome these limitations, and various automated readout alternatives have been proposed. These include notably *S. mansoni* NTS drug assays using luminescent[29] or fluorescent markers[30,31], label-free microcalorimetry[32] or other methods based on electrical recordings[33,34]. In parallel, the development of computer-assisted image analysis is expected to improve the readout of phenotypic assays[22,35,36].

In vivo studies

We commonly use NMRI outbred mice for in vivo experiments, as they are more amenable to testing in larger numbers, easy to handle and can maintain an *S. mansoni* infection for a long period. As stated, we have listed alternative mouse models in Supplementary Table 1. It has been noted that drug efficacy can vary depending on the mouse strain used, and the reason for this variation is not clear[37,38]. It is also debatable whether inbred versus outbred mice are preferred[38]. Inbred mice would reduce experimental variability, but the results may be less reproducible across other breeds and species.

For infection of mice, the concentration of cercariae per injection we use (100 cercariae per mouse), as well as the 7-week infection period, has been optimized for our NMRI mouse strain.

If researchers desire to use other strains, they might need to adjust these parameters. Instead of subcutaneous injection with the cercarial suspension, mice can alternatively be infected by dipping the tail or the shaved abdomen directly into a Petri dish with a cercarial suspension or by percutaneous exposure[12,16,39]. Whereas these techniques allow the development of a natural infection, the parasite load cannot be fully controlled. In addition, the fact that these infection methods require animals to be anesthetized or restrained might be an issue in regard to ethical requirements. On that last concern, the paddling method proposed by Dettmann et al.[40] might provide an alternative, as it allows mouse infection without prior shaving.

In studies with schistosomes, portal perfusion is often used to flush out the adult worms. This technique has been well described[15,16,41]. However, in this protocol, we collect the worms from the mesenteric veins manually. It has the advantage that it is a fairly straightforward method to adopt for labs that are completely new to the process. It also ensures that all worms have been collected. In addition, one can visualize the localization of the worms after drug treatment. For example, the worms can lose their adherence from the mesenteric veins and be shifted to the liver (liver shunt). This could indicate partial activity of a drug[25]. On the other hand, the method we describe has the main disadvantage of being more time consuming as compared to the portal perfusion methods[41].

Applications

Several parts of this protocol are not restricted to antischistosomal drug discovery and can be useful to research teams working in other fields and with other parasites. The methods for establishing and maintaining a *Biomphalaria* snail cycle in a controlled environment can be used by malacologists, for example, in behavioral or ecological studies[42,43]. Schistosomes and their intermediate hosts are model organisms often used in the field of evolutionary biology and host–parasite interactions[44,45]. Similarly, NTS can be useful not only for the analysis of schistosome development but also for a range of biological studies, including genomic and transcriptomic analysis[46–48]. Nonetheless, the reader should note that NTS are not completely identical to the schistosomula present in the host after natural infection. However, only minor differences in morphology, antigenic profile and gene expression have been identified between NTS and 'natural' schistosomula[46,49,50]. Also, at the host–parasite interface, studies investigating hosts' immunity toward helminths—notably characterized by a shift from Th1 to Th2 immune responses—can use *S. mansoni*–mouse infection models[51]. Such immunological studies are also very relevant for developing a potential vaccine, which could prevent continuous reinfections with the parasite[52].

Advantages and limitations

The drug-screening process for *Schistosoma* spp. comes with a few challenges that may hinder research groups (especially in low-resource settings) from establishing their own screening flow. First, as target-based screening for schistosomiasis is still under development[53], antischistosomal drug discovery relies essentially on whole-organism drug sensitivity assays. Although more efficient at producing successful first-in-class compounds[54], whole-organism screening necessitates regular access to parasites that can neither reproduce nor be maintained in vitro for very long[11]. Therefore, a life cycle with both the intermediate and the definitive hosts—snails (e.g., *Biomphalaria spp.* for *S. mansoni*) and rodents (hamsters or mice), respectively—must be established and maintained. Moreover, only a limited number of adult-stage schistosomes (the most relevant parasite life stage for drug screening) can be collected from rodents, and only several weeks after infection. This is not an issue when only a handful of compounds are to be tested, but it poses an ethical and resource bottleneck when screening large compound libraries. This limitation is partly addressed by first screening compounds on NTS. The cercarial transformation method used to produce them and which is presented hereafter is reliable, fast and simple to execute.

Second, as there is no consensus on an acceptable automated reading system, the gold standard method of determining the antischistosomal activity of a drug is still direct observation using an optical microscope, which is simple and low-tech but subjective and laborious[23]. The post-drug exposure assessment of the parasites in vitro is therefore particularly important for the selection of lead candidates. Nonetheless, drug-screening results can vary greatly from lab to lab; a recent study showed that when two independent laboratories tested the same set of compounds, <30% of their hits overlapped[25]. This may be in great part due to differences in evaluation outcomes. In this protocol, we aim to minimize this by providing a graphic guide to parasite viability scoring.

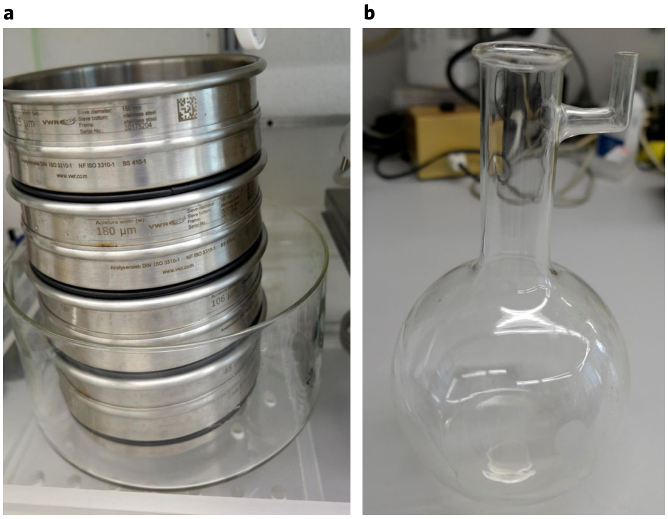

Fig. 2 | Equipment required for collecting eggs and hatching the miracidia. a, Four stainless-steel sieves (45–425 µm) (Step 15). **b**, 0.5-L side-arm flask (Step 18).

Third, the lead selection process described here is rather simple, and it is based on activity thresholds. However, additional tests can be performed to increase the chances of successful in vitro–in vivo translation, such as metabolic or enzymatic assays[23].

Experimental design

Note on animal experimentation

Many parts of this procedure include work on laboratory rodents. Compulsory certifications in animal experimentation are required in many countries, and we also recommend prior practical training. Untrained personnel may improperly inject the material, causing harm to the animal or themselves. We also encourage the reader to comply with the 3Rs principles for in vivo experimental design and statistical analysis, as well as to adhere to the ARRIVE guidelines for reporting animal research[55]. National laws and institutional regulatory board guidelines must be followed.

Establishment and maintenance of a schistosome life cycle

This part of the protocol comprises four essential steps, namely establishing a *B. glabrata* snail cycle (Steps 1–10), hatching miracidia for infecting snails (Steps 11–28), shedding and collecting of the cercariae (Steps 29–34), and infecting the rodent host with the collected cercariae (Steps 35–38). For the snail cycle, simple aquarium systems are used, with ecological water, ambient temperature and light cycle. Snails are kept until they start to produce eggs. Half of them are moved to a new tank containing flat, square polystyrene pieces on which they lay eggs. The eggs are then collected and placed in breeding tanks (Steps 1–10). The other half of the snails are collected for infection with *S. mansoni* (Steps 21–28). To infect the snails, the schistosome eggs are recovered from a saline solution of blended liver of an infected hamster that has been previously filtered (Steps 11–17) (Fig. 2a). The eggs are then placed in warm water in a covered side-arm flask (Fig. 2b) where the side arm is exposed to lamp light (Steps 18–23). After the hatched miracidia swim to the side arm, the suspension is collected and placed in well plates together with snails of appropriate size (4–6 mm) to infect them (Steps 24–28). After 5–6 weeks, the infected snails normally start to shed cercariae. The cercariae are collected by placing the snails under a neon lamp for a couple of hours (Steps 29 and 30) (Fig. 3 (**i**)). The cercariae are shed optimally for 2–4 weeks. Snail shedding of cercariae is highest in the first 2 weeks after initial shedding. After that, the persistence of the infection is highly variable, ranging anywhere from 4 weeks to 3 months. The collected cercarial suspension is then used to infect hamsters by subcutaneous injection (Steps 35–38). After the 7 weeks required for establishing a patent infection, the infected livers can be used to continue the cycle (Steps 11–28).

Cercarial transformation and adult worm collection

Mechanical stress is used to transform cercariae into NTS. The cercarial suspension (Fig. 3 (**ii–iv**)) is pushed between two interconnected syringes, followed by a cold rinse to separate heads from tails

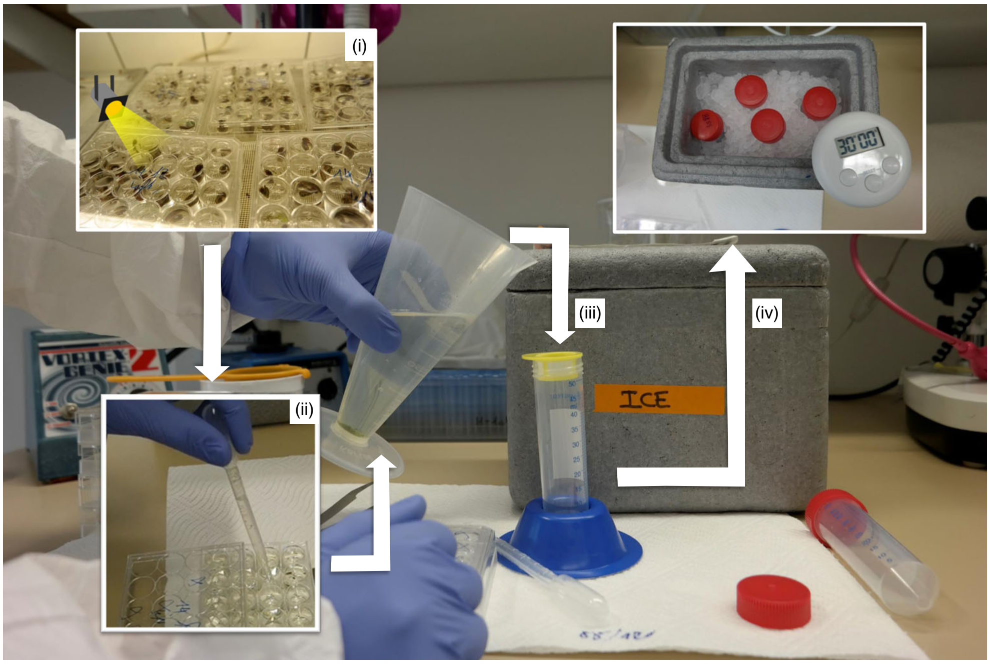

Fig. 3 | Collection of *S. mansoni* cercariae for transformation to NTS. (**i**) Snails are first exposed to light (Step 30). (**ii**) The snails are removed (Step 32), and the pond water containing the cercaria shed by the snails is collected (Step 33). (**iii**) The cercarial suspension is allowed to sediment at RT and is then poured through a 100-μm filter (yellow) into a 50-mL tube (Step 3). (**iv**) The suspension is cooled on ice for 30 min (Step 39) to immobilize the cercariae.

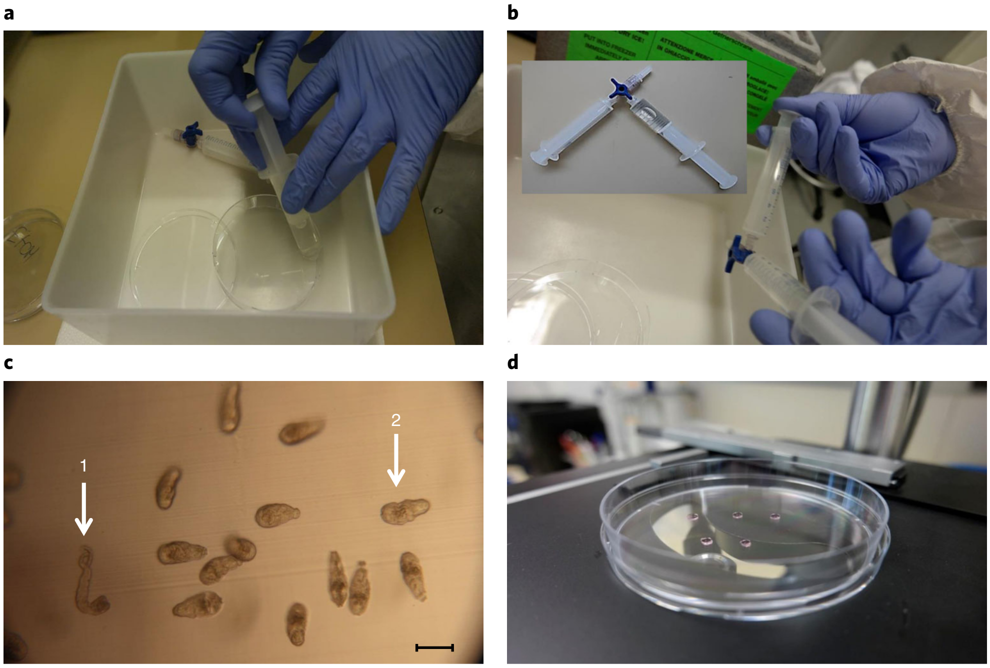

Fig. 4 | Transformation of cercariae to NTS. **a**, One syringe is filled with cercarial suspension (Step 43). **b**, The syringes are connected (inset) and the contents are pushed back and forth vigorously, three to four times (Step 43). **c**, Most (>90%) of the heads should be separated from the tails. This can be directly visualized under the microscope (Step 43). After several washing steps, the NTS are counted and the suspension is adjusted to the desired concentration (Step 49); tails (1) can be distinguished from the NTS (2). Scale bar, ~100 μm. **d**, Counting the NTS (Step 50).

(Steps 39–50) (Fig. 4). An overnight incubation in culture medium is required to complete the transformation. To obtain adult worms for drug screening, laboratory rodents (hamsters or mice) are injected subcutaneously with the collected cercarial suspension (Steps 35–38). The animals are then

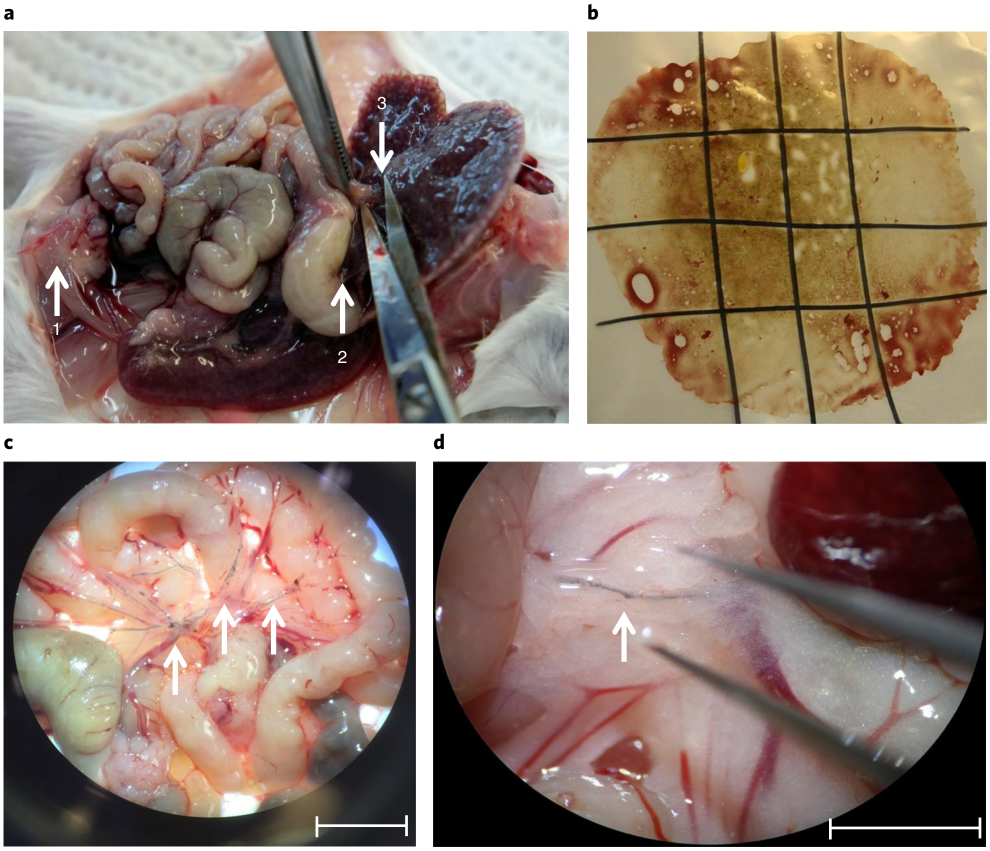

Fig. 5 | *S. mansoni* adult worm recovery. a, The intestines are excised by cutting at the distal part of the rectum (1) and the esophagus (2). The operator must hold the portal vein firmly closed, while excising the liver, to avoid blood spill resulting in the loss of adult worms (3). **b**, The liver is excised and placed between two transparent plastic layers and pressed vigorously. A grid is drawn on the plastic foil to facilitate worm localization (Step 69). **c**, The intestines are excised and placed under a dissection microscope. **d**, Zoomed-in view at ×1.8 magnification. The adult worms present in the mesenteric veins and indicated by the white arrows in **c** and **d** are then collected (Step 70). Scale bars, ~1 cm. For all our experiments involving laboratory animals, we were granted ethical and experimental approval from both the Canton Basel-Stadt and the Swiss federal veterinary authorities (license no. 2070). A certification for animal experimentation was required for all the operators involved.

euthanized, the mesenteries are excised and the adult worms are directly collected from the rodent mesenteric veins using flat-tip tweezers and a dissecting microscope (Steps 67–71) (Fig. 5). The collected worms are incubated with culture medium and can be used for ~2 weeks after the dissection.

In vitro drug testing

When screening large compound libraries, initial efficacy tests on NTS are helpful in selecting candidate compounds of interest. We first describe a pre-screen assay at a mono-concentration to assess the antischistosomal activity of a compound (Steps 51–55). The parasite viability is evaluated over 3 d post compound exposure and compared to the negative control wells containing the highest concentration of the solvent, dimethyl sulfoxide (DMSO) (Steps 51–55). Hits are further tested to determine their 50% inhibitory concentration (IC_{50}). We use a benchmark of $IC_{50} < 10\ \mu M$ to select compounds to test on adult worms, as drug concentrations higher than this are rarely found in vivo with realistic dose levels (Steps 56–62). Hits are then tested on adult worms (Steps 72–78) to select compounds with which to pursue in vivo testing (Steps 79–86).

In vivo studies

Drug candidates are tested in laboratory mice harboring an *S. mansoni* infection. Different rodent strains can be used (Supplementary Table 1). We infect 3- to 4-week-old female NMRI mice with *S. mansoni* cercariae (Steps 35–38). To evaluate the activity of a compound, drug candidates are administered 7 to a maximum of 8 weeks post infection, the time it takes for adults to develop in the mouse model (Steps 79–82).

To test the activity of a drug candidate on juvenile worms, the mice should instead be treated 3 weeks post infection. In addition, drugs can be tested for their protective efficacy by administering the drug before the infection (i.e., day −2 up to day 0) or for efficacy against migrating schistosomula[56]. In both cases, the value used to assess the activity of a drug is the worm burden reduction (WBR). It is determined by comparing the number of live worms found in the treated mice to the numbers of live worms in the control group (Steps 83–86).

Controls

The negative controls for the in vitro procedure are parasites incubated in appropriate medium with the drug solvent only, in general 0.1% (vol/vol) DMSO. For positive-control wells, the experimenter can use auranofin or mefloquine for the NTS assays (Step 54) or praziquantel for the adult worm assays (Step 77). The control mice for in vivo experiments are either untreated or administered with the drug vehicle only (Step 82).

Materials

Biological materials

! CAUTION National and institutional guidelines on animal experimentation must be followed. Refer to the ‘Experimental design’ section. For all our experiments involving laboratory animals, we were granted ethical and experimental approval from both the Canton of Basel-Stadt and the Swiss federal veterinary authorities (license no. 2070). A certification in animal experimentation was required for all the operators involved.

- *B. glabrata* snails (these can be initially obtained from, e.g., the NIAID Schistosomiasis Resource Center, https://www.niaid.nih.gov/research/schistosomiasis-resource-center)
- Hamster or mouse infected with *S. mansoni* worms (these can be initially ordered from the NIAID Schistosomiasis Resource Center, https://www.niaid.nih.gov/research/schistosomiasis-resource-center)
- RJHan:AURA male hamsters (3 weeks old, e.g., Janvier Labs, cat. no. HAMST-M)
- NMRI female mice (3 weeks old, e.g., Charles River, cat. no. 605NMRI)

Reagents

- ‘Pond water’ (filtered dechlorinated tap water)
- Fresh lettuce and spinach leaves
- 70% (vol/vol) Ethanol (EtOH; Merck, Switzerland, cat. no. 1.00983.6025) in water
- Milli-Q water (Merck, e.g., Milli-Q Advantage A10 Water Purification System, cat. no. Z00Q0V0WW)
- NaCl (Merck, cat. no. 1.06404.1000)
- Hank’s Balanced Salt Solution (1× HBSS; Gibco, cat. no. 24020117)
- Penicillin–streptomycin (pen–strep; 10,000 U/mL; Sigma-Aldrich, cat. no. P4333-100ML)
- Medium 199 (Gibco, cat. no. 22340-020)
- Fetal calf serum (FCS; Bioconcept, cat. no. 2-01F30-1)
- Kanamycin (Fluka, cat. no. 60615)
- Penicillin G (Sigma, cat. no. P3032-10MU)
- 5-Fluorocytosine (Sigma, cat. no. F7129)
- Chloramphenicol (Fluka, cat. no. 23275)
- dH_2O
- Dimethyl sulfoxide (DMSO; Sigma-Aldrich, cat. no. 276855-2L)
- RPMI 1640 (Gibco, cat. no. 51800-043)
- Tween 80 (Fluka, cat. no. 23908273)
- Absolute ethanol (Merck, cat. no. 1.00983.6025)

Equipment

- Personal protective equipment: nitrile gloves, lab coat, sleeve protection, long gloves, facial shield and laboratory goggles
- 5-gallon standard fish tank or a simple, transparent rectangular plastic bin
- Simple fish tank mesh lid (should completely cover the fish tank opening)
- Simple fish tank air pump
- Flat polystyrene (in square pieces of 8–9 cm)

- CO_2 chamber for euthanizing rodents
- Dissection board
- Pins for dissection
- Scissors
- Forceps
- Hamster polycarbonate type 4 cages (Tecniplast, cat. no. 1354G)
- Mouse polycarbonate type 3 cages (Tecniplast, cat no. 1290D)
- Four stainless-steel sieves with pore sizes of 425, 180, 106 and 45 µm (Fig. 2a; VWR, cat. nos. VWRI510-0586, VWRI510-0576, VWRI510-0570 and VWRI510-0560)
- Laboratory immersion blender with variable speed (variable-speed laboratory blender; Waring, cat. no. Z272183)
- Pressure garden sprayer with brass lance and brass nozzle pump (5 L)
- 1-L side-arm flask (e.g., Sigma-Aldrich, cat. no. Z290459-1EA; alternatively, fit an Erlenmeyer filter flask with a custom-made L-shaped adapter (Fig. 2b))
- Water bath (Julabo VC)
- A fitted cardboard or wooden box to cover the side-arm flask (or aluminum foil)
- Transparent plastic foil (Semadeni, cat. no. 2457)
- Incandescent bulb (40 W; Osram)
- Dissecting microscope (Optika, model no. Lab 20)
- Eppendorf pipettes (P20, P200 and P1000; Eppendorf)
- Pyrex glass beakers (10, 30 and 1,000 mL; Corning, cat. nos. CLS100010, CLS100030 and CLS10001L)
- 24-, 48- and 96-well plates (Sarstedt, cat. nos. 83.3922, 83.3923 and 83.3924)
- Light source for cercaria shedding: neon lamp (36 W, 4,000 K, 3,350 lumens, G13; Osram, cat. no. 4050300517872)
- Tweezers (flat tip, no teeth; Fisherbrand, cat. no. 16100127)
- Hypodermic 25-gauge syringe needle (0.5 × 16 mm, sterile; Braun Medical, cat. no. 4657853)
- Filter for sterilization (0.2 µm, Filtropur S 0.2; Sarstedt, cat. no. 83.1826.001)
- Conical graduated cylinder (Dynalon, cat. no. 1211Y42)
- Stericup (0.22 µm, 500 mL; Corning, cat. no. 431097-COR)
- Nylon filters (100 µm, nylon, VWR, cat. no. 732-2759)
- 15- and 50-mL Test tubes (Sarstedt, Germany, cat. nos. 62.547.004 and 62.554.002)
- Serological pipettes (5, 10 and 25 mL; Sarstedt, Germany, cat. nos. 86.1253.001, 86.1254.025 and 86.1685.001)
- Syringes with Luer-Lok tips (10 mL; BD, cat. no. BD 309695)
- Luer-Lok connector (Discofix; B. Braun, cat. no. 40951111)
- Petri dish, 94 × 16 mm (Greiner, cat. no. 633102)
- Upright bright-field microscope with 4, 10 and 20× lenses (Primovert)
- Pyrex borosilicate glass Petri dishes (55-mm diameter; Fisher Scientific, cat. no. 12013333)
- Oral gavage needle (straight; Carl Roth, cat. no. HPY8.1)
- Pasteur pipette (Pastette; Alpha Laboratories, cat. no. LW4111)
- 1-mL Sterile plastic syringes (B. Braun, cat. no. 9161406V)
- Waterproof markers (Stabilo, cat. no. 842/41)
- Mouse identification marker: picric acid solution (1.3% (vol/vol) in H_2O; Sigma-Aldrich, cat. no. P6744-1GA)

Reagent setup

S. mansoni egg rinsing solution

S. mansoni egg rinsing solution is 4 °C physiological saline solution (0.9 or 1.2% NaCl in Milli-Q H_2O at 4 °C). Prepare fresh solution before each experiment.

Hank's Balanced Salt Solution

Hank's Balanced Salt Solution (HBSS 1×) should be supplemented with 1% (vol/vol) pen–strep. It can be stored at 4 °C for up to 4 weeks.

NTS culture medium

M199 medium should be supplemented with 5% (vol/vol) FCS, 1% (vol/vol) pen–strep and 1% (vol/vol) antibacterial/antifungal mix (see preparation below) with 45% (vol/vol) kanamycin, 27% (vol/vol) penicillin G, 23% (vol/vol) 5-fluorocytosine and 5% (vol/vol) chloramphenicol. It can be stored at 4 °C for 2–4 weeks.

Antibacterial/antifungal mix for 10-mL solution

Antibacterial/antifungal mix should be prepared as shown below. It can be stored at −20 °C for up to 3–6 months[57].

- Weigh 10 mg of chloramphenicol and dissolve it in 143 μL of 70% (vol/vol) EtOH.
- Weigh 50 mg of 5-fluorocytosine and dissolve it in 9,857 μL of dH_2O in a 15-mL tube.
- Weigh 100 mg of kanamycin.
- Weigh 60 mg of penicillin G.
- Mix all ingredients together in a 15-mL tube.
- Sterilize by 0.2-μm filtration.
- Prepare aliquots of the solution for convenience.

Adult worm culture medium

RPMI 1640 medium supplemented with 5% (vol/vol) FCS and 1% (vol/vol) pen–strep. It can be stored at 4 °C for 2–4 weeks.

Drug solution for oral administration

Drug solution for oral administration is 70:30 Tween 80/absolute ethanol solution dissolved in Milli-Q H_2O (10% (vol/vol)). Prepare fresh solution before each experiment.

Procedure

Establishing and maintaining a snail cycle ● Timing 30 min

1 Fill the aquarium tank three-quarters full with pond water warmed to 26–28 °C.

! CAUTION Water quality is important: charcoal-filtered water must be used in the case that the water quality is untested. Water must always be dechlorinated. As it will be frequently used, we recommend setting up a large reservoir of pond water: simply fill a large tub with tap water and add a simple air pump.

2 Insert the air pump and turn it on such that bubbles form and float to the top to prevent water fouling.

▲ CRITICAL STEP Never allow the water to become stagnant. Check the air flow in the tanks periodically.

3 Place between 200 and 300 snails of different sizes in the tank and add a few leaves of lettuce and/or spinach.

4 Cover the tank with a weighted mesh lid and place the aquarium under neon lamps.

5 Set and maintain the room temperature (RT) at 26–28 °C.

6 Maintain a 12-h day and night light cycle by, for example, automatically setting lights to turn on at 6 AM and turn off at 6 PM.

7 Feed the snails once daily with fresh lettuce and spinach, and clean the tanks weekly.

▲ CRITICAL STEP The fresh vegetables should not remain longer than 1 d in the tank, as they will start to rot. Feed only as much as the snails consume. Store the food in a wine cooler refrigerator, as this works best for lettuce and spinach.

8 At the time of snail infection, select snails that have reached the adult stage (size ≥4–6 mm) and transfer these to a new tank, filled with 26 –28 °C pond water. Those snails will be infected with *S. mansoni* miracidia (Steps 11–28). This new tank is referred to as the 'infection tank'. Take the remaining snails and place them into a second new tank filled with 26–28 °C pond water. This tank, known as the 'breeding tank', will be used to produce offspring (Steps 1–10).

! CAUTION This step should be performed once for each batch of snails. Therefore, in the breeding tank(s), snails of different sizes will be present. Each tank should have no more than 200–300 snails.

9 Put an 8- to 9-cm^2 flat piece of polystyrene into each breeding tank(s) with the smooth side upside down, so the snails can lay their eggs on the surface. Move the polystyrene pieces with the eggs to a new tank filled with pond water, for breeding the snails.

! CAUTION Snails might lay eggs on the walls of the tank. Collect these eggs and add them to the breeding tank(s). Alternatively, siliconized surface materials can be used to prevent the eggs from attaching.

? TROUBLESHOOTING

10 Set up the new tanks as described in Steps 1 and 2, and maintain them as described in Steps 4–7.

! CAUTION Infecting a new batch of snails every 2–3 weeks is recommended for continuous availability of cercariae.

? TROUBLESHOOTING

Hatching miracidia and infecting snails ● Timing 30 min to collect eggs plus overnight release of eggs; 2.5 h to hatch and infect; maintain tank for 5–6 weeks

! CAUTION National and institutional guidelines on animal experimentation must be followed. Refer to the 'Experimental design' section. For all our experiments involving laboratory animals, we were granted ethical and experimental approval from both the Canton Basel-Stadt and Swiss federal veterinary authorities (license no. 2070). A certification in animal experimentation was required for all the operators involved.

11 Euthanize two infected hamsters by CO_2 inhalation (see the 'Materials' section, or infected mice can be used, from Step 38).

! CAUTION The number of hamsters for *S. mansoni* egg isolation depends on the investigator's needs. The hamsters can be kept between 2 and 12 months post infection at maximum.

12 After checking for the absence of vital signs and reflexes, dissect each hamster upward from the lower abdomen to expose the liver (Fig. 5a).

13 Excise the liver and place it into cold (4 °C) physiological saline overnight (see 'Materials' for saline preperation). This will create small tissue cracks in the liver, which will increase the release of *S. mansoni* eggs.

14 The next day, blend the cracked livers with cold (4 °C) saline solution, using a variable-speed blender progressively from 0 to ~9,000*g* for 10 s. Repeat this step three times.

▲ CRITICAL STEP The blending must ensure that the liver is very well homogenized, so that the maximum number of *S. mansoni* eggs are released. However, it must not be too rough, or the eggs will be destroyed in the blending process.

? TROUBLESHOOTING

15 Pour the liver homogenate sequentially through four sieves (Fig. 2a) in the following order of pore size: 425, 180, 106 and 45 μm. Rinse all the sieves with the cold (4 °C) saline solution using the pump sprayer, until the smallest filter is reached.

▲ CRITICAL STEP If the saline solution becomes warm (25–28 °C), the miracidia could hatch; therefore, it is important to keep the solution cold (at 4 °C) during the filtering process.

? TROUBLESHOOTING

16 Collect the unfiltered fractions from the 425- and 180-μm sieves into a 1,000-mL beaker by rinsing them with the 4 °C saline solution using the pump sprayer; then blend and sieve the unfiltered fractions by repeating Steps 14 and 15 three times.

17 The eggs will have been collected on the 45-μm sieve, as they do not pass through this sieve. Rinse the eggs from the 45-μm sieves into a 1,000-mL beaker by using 50–100 mL of cold (4 °C) saline solution, using the pump sprayer.

18 For hatching, pour the egg suspension into the side-arm flask (Fig. 2b). Add dechlorinated tap water (28 °C) until it reaches and fills the side arm of the flask.

19 Place the side-arm flask into a 30 °C water bath and place an incandescent lamp above. Wait until you see by eye the first hatched miracidia (10–20 min).

? TROUBLESHOOTING

20 Cover the entire side-arm flask with a carton box (or aluminum foil), except for the side arm.

21 Expose the side arm of the flask to the light. The miracidia will concentrate in the side arm, attracted by the light, and will swim up to the surface.

22 Collect the entire volume of miracidial suspension from the side arm with a P1000 pipette and place it in a 30-mL beaker. Check for the presence of miracidia under a bright-field microscope.

23 Determine the concentration of miracidia by sampling 5 × 10-μL drops of the miracidial suspension, placing them in a Petri dish and counting the number of miracidia in each drop.

▲ CRITICAL STEP Miracidia tend to sediment, so shake the solution before each sampling to ensure a homogeneous distribution.

24 Fill each well of a 48-well plate halfway with pond water.

25 Transfer each snail from the infection tank (saved for infection in Step 8) and place one snail per well of the plate prepared in Step 24.

! CAUTION Use flat-tip tweezers carefully to avoid damaging the snails.

▲ CRITICAL STEP Selecting snails that are smaller or larger in diameter than 4–6 mm will result in an unsuccessful or mild infection, and, on average, early mortality of small snails.

26 Add a volume of the miracidial suspension that would correspond to six to eight miracidia per well.

27 Place the 48-well plate under a 40-W incandescent bulb and leave it for 2–3 h at RT. In our experience, this ensures a proper infection of the snails by the miracidia.

28 Place the infected snails into a new tank, referred as the 'working tank', set up as described in Steps 1 and 2, and maintain as described in Steps 4–7.

Shedding and collecting of the cercariae ● Timing 30–60 min

▲**CRITICAL** A record of each infection should be kept, with infection rate (number of snails infected per batch) and the intensity of infection (average number of cercariae shedding per snail).

29 After 5–6 weeks post infection, the snails from the working tank (Step 28) should be ready to shed cercariae. Fill each well of a 24-well plate with 1 mL of pond water.

! CAUTION Cercariae can infect humans via direct skin contact. Wear protective clothing that includes a lab coat, nitrile gloves and laboratory goggles. Note: simple hospital latex gloves are potentially insufficient for protection.

30 Place one snail into each well (carefully using flat-tip tweezers). Put the lid on the plate and leave it under a neon lamp for 3–4 h (Fig. 3 (**i**)).

! CAUTION As the procedure is a source of stress for the snails, we recommend that it not be repeated more than twice a week. Alternatively, if several snail batches are available, we recommend using them in rotation.

▲**CRITICAL STEP** Cercarial shedding from the snail follows a circadian rhythm, so it is essential that the snails be placed under light in the morning and retrieved 3–4 h later in the afternoon. In our laboratory, the snails are placed under the light before 9 AM, but each lab should track the cercarial shedding pattern once the cycle is established.

31 Retrieve the plate and examine for cercariae, using a bright-field microscope with a ×10 or ×20 magnification.

? TROUBLESHOOTING

32 Place all the infected snails back into the working tank (Step 28) until the next cercarial shedding.

! CAUTION Steps 29–34 can be repeated six to eight times with the same snails. Snails that are not shedding cercariae after 8 weeks should be killed by placing them into soapy water. Do not use a batch of infected snails more than twice a week (better only once). The snails should have time to recover; otherwise the parasite yield could decrease.

▲**CRITICAL STEP** Only uninfected snails lay eggs, but do not keep the snails that are not shedding cercariae for breeding, as this would decrease the overall genetic susceptibility of the breeding pool to *S. mansoni* infection.

33 Use a Pasteur pipette to collect the cercariae from the 24-well plate into a 150-mL conical-bottom beaker at RT before pouring the cercarial suspension through a 100-µm filter into 50-mL tube(s). At this point, the cercarial solution is either immediately adjusted for animal infection and injected (Steps 35–38) or is transformed into NTS (Steps 39–50).

34 Count the cercarial concentration by sampling 5 × 10 µL drops of the suspension on a Petri dish. Use a bright-field microscope to count and average the number of cercariae for 10 µL.

Infecting rodents ● Timing 30 min–2 h, depending on the number of rodents

! CAUTION National and institutional guidelines on animal experimentation must be followed. Refer to the 'Experimental design' section. For all our experiments involving laboratory animals, we were granted ethical and experimental approval from both the Canton Basel-Stadt and Swiss federal veterinary authorities (license no. 2070). A certification in animal experimentation was required for all the operators involved.

35 Adjust the cercarial concentration to 100 cercariae/100 µL by either adding the appropriate volume of pond water to dilute the suspension from Step 33, or by centrifuging it (211*g*, 3 min, RT) and removing the appropriate volume of supernatant to concentrate the suspension.

36 Aspirate 100 µL of the cercarial suspension with the 1-mL syringe, ensuring there are no air bubbles in the aspirate. Make sure to stir the suspension before aspirating.

37 Inject the suspension subcutaneously into the mouse/hamster neck. The number of mice/hamsters to infect depends on the cercarial yield and/or the investigator's needs.

! CAUTION In the case that a higher number of *S. mansoni* adult worms is required, we recommend infecting some of the mice with 200 cercariae instead of 100, or infecting hamsters with a dose of up to 800 cercariae. Although this will increase the yield of adult worms, we do not recommend using the highly infected mice for drug testing, as they will probably not be able to withstand the testing period.

38 After infection, house the animals at 25 °C with a 12-h day/night cycle with free access to rodent diet and water in enriched cages. At 7 weeks post infection, the adult parasite infection is established and the egg production is initiated. For perpetuating the life cycle, return to Step 11. For adult worm collection, refer to Steps 67–71.

? TROUBLESHOOTING

Transformation of cercariae to NTS ● Timing 3–4 h

39 Place the suspension from Step 33 on ice for 30 min to immobilize the cercariae (Fig. 3 (**iv**)).

40 Centrifuge the tube for 3 min at 211*g* at RT.

41 Use a Pasteur pipette to remove the supernatant and discard it.

42 Resuspend the pellet in 7 mL of ice-cold HBSS supplemented with 1% (vol/vol) pen–strep. Alternatively, supplemented M199 medium at 37 °C can be used.

43 Fill a 10-mL syringe with the 7-mL cercarial suspension obtained in Step 42 and connect it to the Luer-Lok (Fig. 4a,b (inset). Connect another empty syringe to the opposite side of the Luer-Lok. Push the liquid back and forth three to four times vigorously (Fig. 4b). The transformation yield can immediately be viewed under the bright-field microscope. The tails must have been separated from the heads for at least 90% of the parasites (Fig. 4c). If this is not the case, repeat this step three to four times more and check for any improvement under the bright-field microscope.

! CAUTION Test the syringe-Luer-Lok connection by passing some water or HBSS before you proceed. An incorrect connection can result in a splattering of infectious cercarial suspension. Personal protection, including a face shield, must be worn in case of spills. Wearing two pairs of gloves, with a long-sleeved pair over the top is advisable.

44 Pour the suspension into 15-mL tubes. Place them on ice and in the dark for 7 min to allow the sedimentation of the heads.

45 Remove the supernatant (and therefore the tails), by slowly pipetting, and discard. Avoid disturbing the sedimented heads (hereafter referred to as NTS).

? TROUBLESHOOTING

46 Resuspend the NTS in 4 °C HBSS supplemented with 1% (vol/vol) pen–strep to wash them.

47 Repeat Steps 44–46 three times to eliminate the remaining tails. Observe the successful separation of the tails from the heads under a bright-field microscope (Fig. 4c).

▲CRITICAL STEP It is imperative to reduce the number of tails and untransformed cercariae as much as possible, as they can harm the NTS with their rapid whipping movements.

48 Remove the wash solution by pipetting and resuspend the sediment in 5–10 mL of supplemented M199 by inverting the tube or gently pipetting up and down.

! CAUTION Do not vortex, as additional mechanical stress could damage the parasites and negatively influence their overall viability.

49 Count the NTS by sampling 5 × 10-μL drops from the NTS suspension. Pipette each drop into a Petri dish (Fig. 4d) and observe under a bright-field microscope.

▲CRITICAL STEP To obtain a homogeneous NTS suspension, mix it gently by inverting the tube before each sampling.

50 Adjust the suspension to the appropriate NTS concentration. To increase the concentration of NTS, place the tubes in a vertical position for 5 min to allow them to sediment. The proper volume of medium can then be removed by gently pipetting away the supernatant. For decreasing the concentration, simply top up with an appropriate volume of supplemented M199 medium.

▲CRITICAL STEP We recommend that the NTS be suspended in an appropriate volume of medium for a maximum concentration of 2,000 NTS/mL.

■PAUSE POINT Before being used in drug assays, the NTS should be left overnight in the incubator (37 °C, 5% CO_2) for 12 to a maximum of 24 h. This allows the parasites to complete the necessary biochemical and metabolic changes to emulate the larval stage of the parasite in the definitive host[46].

Drug-screening assay with NTS ● Timing 2–3 h

▲CRITICAL Because not 100% of the cercariae will be transformed, it is important to wear laboratory goggles and use proper biosafety level 2 (BSL 2) equipment.

51 Dilute the initial 10 mM drug stock solution (in DMSO) to a 100 μM solution in supplemented M199 medium.

52 Add 175 μL of supplemented M199 medium per well of a 96-well plate.

53 Add 25 μL of the 100 μM drug solution to each well, then 50 μL of the 2,000 NTS/mL suspension (from Step 50) for a final drug concentration of 10 μM and a final count of ~100 NTS per well. Each drug should be tested in duplicates or triplicates.

54 Repeat Steps 52 and 53 for the control wells, using the solvent (DMSO) instead of the drug. One can also include a positive control such as auranofin or mefloquine, but this is not required for assays based on visual scoring as assessment.

! CAUTION Praziquantel is not a good positive control for NTS in vitro assays because it is not very active on the larval stages of the parasite.

▲ CRITICAL STEP If the drugs are dissolved in DMSO, the final assay concentrations of DMSO should never exceed >1.5% (vol/vol), as this can decrease the parasites' viability.

55 Place the plate in the incubator (37 °C, 5% CO_2). Score the NTS viability every 24 h for up to 72 h to evaluate the drug effect compared to the controls. The evaluation procedure is described below (Steps 56–66).

? TROUBLESHOOTING

Determination of compound IC_{50} values ● Timing 2–3 h

! CAUTION The desired drug concentration range varies from assay to assay. Here, we provide a sample protocol that is used in our lab as a guiding example. The procedure below is for a starting concentration of 10 μM and a dilution factor of 1:2.

56 To determine the IC_{50} values of any drug, first prepare in a 96-well plate a drug dilution series that is ten times higher than the desired final assay concentration. Thereafter, the whole assay is diluted 10× in another 96-well plate, where the NTS are added. To prepare this pre-dilution plate, fill row A of a 96-well plate with 180 μL of supplemented M199 medium and add 20 μL of a 1 mM drug working solution to reach a concentration of 100 μM (one drug per well).

57 To rows B to G, add 100 μL of supplemented M199 medium. Pipette 100 μL from row A to row B for a 1:2 dilution and mix well. Continue by pipetting from row B to row C, and so on. Reject the last 100 μL from row G. This results in concentrations of 100, 50, 25, 12.5, 6.25, 3.13 and 1.56 μM.

58 In row H, prepare DMSO controls by adding 20 μL of 10% (vol/vol) DMSO in 180 μL of supplemented M199 medium for a final concentration of 1% (vol/vol) DMSO in the well.

59 In another 96-well plate (test plate), add 175 μL of supplemented M199 medium to all wells. Assign three columns of the plate to each drug dilution (in order to have three replicates for each drug).

60 Transfer 25 μL of column 1 from the pre-dilution plate to columns 1, 2 and 3 of the new plate. Repeat for each drug (e.g., column 2 of the pre-dilution plate to columns 4, 5 and 6 of the new plate, and so on).

61 Add 50 μL of NTS suspension (Step 50) to each well of the new plate. The result is a drug dilution assay with concentrations of 10, 5, 2.5, 1.25, 0.63, 0.31 and 0.16 μM and control wells with 0.1% (vol/vol) DMSO.

62 Incubate at 37 °C and 5% CO_2 and evaluate at 24, 48 and 72 h post drug incubation (Steps 63–66).

? TROUBLESHOOTING

Assessment of the parasites in vitro ● Timing 2 h

63 Evaluate each well, using a bright-field microscope (×4 or ×10 magnification), and assign a score to each well that reflects the phenotype of the majority of the parasites. Score the control wells first. In Figs. 6 and 7, we present the viability score scale and sample phenotypes for NTS and adult worms, respectively. The motility is the most important parameter to take into account when assigning a score. Living parasites move smoothly. An abnormally decreased or enhanced motility, a loss of plasticity, saccades or wobbles would lead to a lower score. The second important aspect to consider is the morphology and the integrity of the tegument. Impaired parasites may lose their original shape by shrinkage or swelling. Blebs on the tegument or a darkened pigmentation can also appear (Figs. 6 and 7, and Supplementary Videos 1–12).

! CAUTION Do not keep the plates outside the incubator for longer than 15 min. The NTS movement decreases when the medium cools; this might bias the scores.

▲ CRITICAL STEP Control wells should have a minimum score of 2 to ensure that the NTS were sufficiently viable for the assay. If not, the assay should be rejected and repeated.

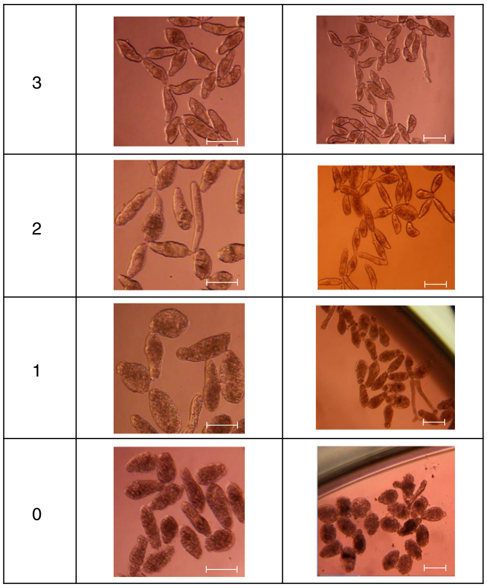

Fig. 6 | NTS phenotypes corresponding to each viability score. 3 = motile, no changes to morphology or transparency; 2 = reduced motility and/or some damage to tegument noted, as well as reduced transparency and granularity; 1 = severe reduction of motility and/or damage to tegument observed, with high opacity and high granularity; 0 = dead. The images of the NTS in the left column were taken with a ×20 magnification. The images in the right column were obtained using a ×10 magnification (Step 63). Scale bars, ~100 μm. See also Supplementary Videos 9–12.

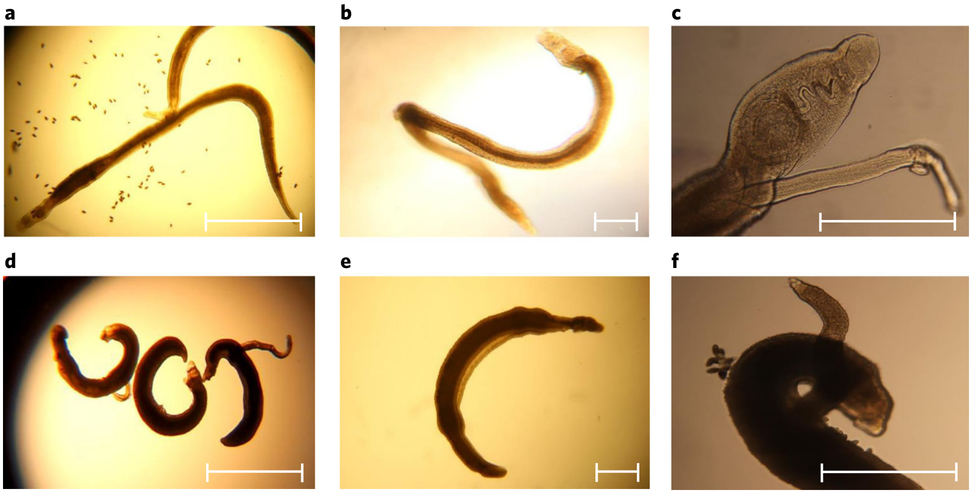

Fig. 7 | Adult worm phenotypes. a–c, The viability scores of 3 = motile, no changes to morphology, transparency and intact tegument, active ventral and oral sucker (see also Supplementary Videos 7 and 8) and (**d–f**) 0 = dead, the worms appear darkened and motility of the ventral and oral sucker is absent (see also Supplementary Videos 1 and 2). Additional characteristics can also help to assign a score (see also Supplementary Videos 3–6 for examples of scores 1 and 2). For instance, the ventral sucker of impaired worms (score <2) is often detached from the bottom of the well, whereas the presence of eggs can be used as a sign of good viability of the worm (score >2). The images were taken with ×4 (**a**,**d**), ×10 (**b**,**e**) or ×20 (**c**,**f**) lenses (Step 63). Scale bars, 1 mm (**b**,**c**,**e**,**f**); 2.5 mm (**a**,**d**).

64 Report all the data in a spreadsheet and calculate the effect score of each drug by normalizing the drug scores to the control well scores, using the following formula: average (Test) is the average score of all test wells containing the drug and Average (Control) is the average score of the control wells.

$$\%\text{Effect} = 100 - \frac{\text{Average}(\text{Test}) \times 100}{\text{Average}(\text{Control})}.$$

65 With a single concentration assay (Steps 51–55), determine the threshold effect for what you will consider to be a hit. Usually, this threshold reflects either total mortality of the parasite (100% effect) or substantially reduced parasite viability (e.g., 75% effect).

66 For dose–response assays (Steps 56–62), plot the effect scores against the drug concentrations to generate a dose–response curve in order to determine the IC_{50} value. There are many tools for this; an easy and freely available tool is CompuSyn (http://www.combosyn.com/).

S. mansoni adult worm recovery ● Timing 15–30 min per mouse

! CAUTION National and institutional guidelines on animal experimentation must be followed. Refer to the 'Experimental design' section. For all our experiments involving laboratory animals, we were granted ethical and experimental approval from both the Canton Basel-Stadt and Swiss federal veterinary authorities (license no. 2070). A certification in animal experimentation was required for all the operators involved.

67 Euthanize the infected mice from Steps 34 to 38 with CO_2 for 5 min (see 'Materials' section).

68 After checking for the absence of vital signs and reflexes, dissect the mice by cutting from the lower abdomen up to the sternum to expose the intestines and liver (Fig. 5a).

69 Resect the liver, then excise the intestines and place them into a Petri dish. At this point, the liver can also be removed. Manually, press the liver between two pieces of transparent plastic foil in order to obtain a thin layer of tissue so that the worms can be visualized, counted and sexed under a dissecting microscope. A pair is counted as two worms. Draw a grid on the plastic foil with a marker to facilitate the localization of the worms (Fig. 5b). The live worms can be collected with flat-tip tweezers and placed in 37 °C supplemented RPMI 1640 medium. For in vitro assays, refer to Steps 72–78.

▲ CRITICAL STEP The portal vein must be located and pinched firmly with tweezers in order to prevent the worms from spilling out, because *S. mansoni* are mostly located in the portal vein (Fig. 5a).

? TROUBLESHOOTING

70 Place the intestines under the dissection microscope and, using flat-tip tweezers, gently open the veins and pick out the worms (Fig. 5c,d). Place the recovered worms in supplemented RPMI 1640 medium. Count and sex the worms as in Step 69. Transfer them to a new Petri dish filled with supplemented RPMI 1640 medium and incubate them at 37 °C, 5% CO_2.

▲ CRITICAL STEP It is important to avoid damaging the worms with the flat-tip tweezers during collection. Do not tug the worms.

■ PAUSE POINT Worms can be kept in an incubator for up to 10 d if the medium is replaced regularly (every 3 d). To allow sufficient nutrient supply, a maximum of 15 worms should be placed in a single Petri dish.

? TROUBLESHOOTING

71 Use the worms recovered from Steps 69 to 70 for in vitro assays (Steps 72–78). The worm counts can be used to determine the WBR (Steps 83–86).

In vitro assay of *S. mansoni* adult worms ● Timing 40–60 min

72 From a 10 mM drug stock solution in 100% (vol/vol) DMSO, prepare a 1 mM working solution in supplemented RPMI 1640 medium. We recommend the use of a 10 µM drug concentration as a starting concentration (unless natural crude extracts are being screened). Higher concentrations are unlikely to be achieved in vivo.

73 In each well of a 24-well plate, pipette 15 µL of the 1 mM drug solution, and add 1,485 µL of supplemented RPMI 1640 medium. Each compound should be tested in duplicate or triplicate when possible.

▲ CRITICAL STEP To ensure that the worms remain clearly viable throughout the assay, the volume to add to the well should not be <1.5 mL.

74 Prepare a 10% (vol/vol) DMSO (or any other solvent) solution in supplemented RPMI 1640 medium and transfer 15 µL of it to the control wells to have a final concentration of 0.1% (vol/vol) of the solvent. Praziquantel can be used for positive control wells in this assay; follow Steps 72 and 73.

75 Carefully, place two pairs or three random worms of both sexes per well, using flat-tip tweezers.
▲CRITICAL STEP To avoid contaminations, clean the flat-tip tweezers by dipping them first into a solution of 70% (vol/vol) ethanol–water and then into supplemented RPMI 1640 as frequently as possible.

76 Check the assay to ensure that each well has the correct number of worms. Place the assay in the incubator (37 °C, 5% CO_2).

77 Score each of the worms individually. Record both the sex and the phenotypic score every 24 h for up to 72 h (Steps 63–66 and Fig. 7).

78 Compounds that are active can then be further tested in a drug dose–response assay to determine their IC_{50} value. The same assay setup is used (Steps 72–78) with a 1:2 or 1:3 serial drug dilution, and at least three drug concentrations.

In vivo drug administration ● Timing >4 h

! CAUTION National and institutional guidelines on animal experimentation must be followed. Refer to the 'Experimental design' section. For all our experiments involving laboratory animals, we were granted ethical and experimental approval from both the Canton Basel-Stadt and Swiss federal veterinary authorities (license no. 2070). A certification in animal experimentation was required for all the operators involved.

79 Prepare the drug solution for oral administration in Tween 80/EtOH solution (or any other vehicle). Intraperitoneal or intravenous administration can also be considered. The drug dosage depends on the researcher's needs, and it should be adapted accordingly.
▲CRITICAL STEP Make sure that the drug is well dissolved; otherwise, you risk administering different concentrations to each mouse.
? TROUBLESHOOTING

80 Weigh each infected mouse from Step 38 individually.
! CAUTION The mice must be individually identifiable and marked before drug administration using any standard identification (ID) method. We recommend noninvasive and painless methods such as skin or fur marking in order to comply the 3Rs principles[58]. We use picric acid solution (a yellow synthetic marker) on the mouse's back for labeling.

81 Calculate the drug volume to administer to each mouse using the following formula:

$$\text{Volume administration} = (\text{target dose (mg/kg)} \times \text{mouse mass (kg)})/\text{drug concentration (mg/mL)}.$$

82 Prepare the administration volume in a 1-mL syringe. Administer the drug to the infected mouse. The control mice for the experiment can be administered with the vehicle only or left untreated.
▲CRITICAL STEP Do not administer >100 µL for every 10 g of weight, keeping in mind that it is better to work with small volumes. It is important to administer each drug to several mice. The number of mice used depends on the experimental design[59].
? TROUBLESHOOTING

Data recovery for in vivo results ● Timing >2–3 h

83 After a maximum of 21 d after drug administration, euthanize the mice as in Steps 67–71.

84 Dissect the mice and recover the liver and the intestines as described previously (Steps 67–70). The granuloma distribution and the hepatosplenomegaly provide important information on the magnitude of the infection of each mouse.

85 Evaluate the presence of live adult worms in the pressed liver and in the mesenteric veins of test and control mice (Steps 69–70). Sex, count and include them in the WBR evaluation formula (Step 86).

86 Calculate the WBR using the following equation:

$$\text{WBR}(\%) = 100\% - (100\%/\text{WB Control} \times \text{WB treatments}),$$

which compares the average number of live worms in the treated mice to the live worms found in the mouse control group.
? TROUBLESHOOTING

Troubleshooting

Troubleshooting advice can be found in Table 1.

Table 1 | Troubleshooting table

Step	Problem	Possible reason	Solution
9	No/poor snail egg deposition	• Poor water quality • Poor water tank airflow • Poor-quality snail food • Stagnant water	• Use filtered water • Check air flow • Use fresh leaves (we suggest spinach) • Check water quality
1–10	Snails die	• Poor water quality • Not enough food • Too many snails in the same tank	• Use filtered water • Avoid allowing food to rot in the tanks and change it daily • Subdivide the snail population into separate tanks, keeping the population between 200 and 300 snails
14, 15	Damaged *S. mansoni* eggs	• Too-aggressive blending of the liver(s)	• Reduce the time and/or speed of each blending step
19	No miracidia hatching	• Too-aggressive blending of the liver(s) • Water temperature not correct	• Reduce the time and/or speed of each blending step • Ensure water temperature is 30 °C • Increase the exposure time by 10–15 min
31	No/poor cercarial shedding	• Snails are not permissive • Snails are too old • Circadian cycle is not adequate • Too many cercariae collections	• Make a freshly infected batch of snails • After 6–8 weeks, infected snails should be replaced • Consider starting the light cercarial induction earlier in the morning • Increase the collection time span to ensure one cercarial shedding per week
38	Mice die after infection with *S. mansoni*	• Too many cercariae were injected	• Adjust the cercariae concentration to 100 cercariae/100 μL and inject smaller volumes
45	The NTS pellet is taken away or disturbed	• Pipetting error	• Repeat the washing step (Steps 46 and 47)
55	Dead NTS in the assay control wells	• Overly aggressive transformation • Too many NTS in medium kept overnight • Incorrect medium used	• Reduce the number of syringe passages (three or four instead of four to six) • Control the medium formulation and concentration
62	No changes in NTS viability after testing a known active drug (positive control)	• Suboptimal concentration used, low solubility of the compound and/or low activity on NTS (e.g., praziquantel)	• Increase the drug concentration and/or improve solubility (e.g., by changing the solvent)
69, 70	Dead adult worms recovered from untreated mice	• Worms were recovered too late • Worms were damaged during collection	• Collect the worms at an earlier time point • Avoid pressure with tweezers during worm collection
79, 86	Erratic worm burden in vivo	• Multiple operators perform the mouse infection • Biological variation	• Consider using a single operator for infections • Include a randomization step
82	Mice die a few days after drug treatment	• Too many cercariae • The drug dose was too high • The compound is toxic	• Adjust cercariae concentration for mouse infection • Lower the administered dose

Timing

Steps 1–10, establishing and maintaining a snail cycle—initial setup: 30 min
Steps 11–28, hatching miracidia and infecting snails: 30 min to collect eggs plus overnight release of eggs; 2.5 h to hatch and infect; maintain tank for 5–6 weeks
Steps 29–34, shedding and collection of cercariae: 30–60 min
Steps 35–38, infecting rodents: 30 min–2 h, depending on the number of rodents
Steps 39–50, transformation of cercariae to NTS: 3–4 h
Steps 51–55, drug-screening assay with NTS: 2–3 h
Steps 56–62, determination of IC_{50}: 2–3 h

Steps 63–66, assessment of parasites in vitro: 2 h
Steps 67–71, *S. mansoni* adult worm recovery: 15–30 min per mouse
Steps 72–78, in vitro assay of *S. mansoni* adult worms: 40–60 min
Steps 79–82, in vivo drug administration: >4 h
Steps 83–86, data recovery for in vivo results: >2–3 h

Anticipated results

This protocol describes the establishment of an *S. mansoni* life cycle, which is the basis for conducting in vitro and in vivo drug sensitivity assays. Once a schistosome life cycle has been established in the laboratory, cercariae should be shed by the snails into the water on a regular basis for 5–8 weeks. There is, however, no typical volume of cercarial yield, as this depends on the number of snails, their infection level and the age of the snail infection. In our experience, a cercarial suspension with a minimum range of 250–1,000 cercariae per milliliter is required for performing an effective transformation. Practically, a satisfactory cercarial yield can be visualized under a bright-field microscope, directly in the wells containing the shedding snails, before starting the transformation. Although some cercariae can be very motile, not all are active. The transformation should therefore be attempted even in the absence of fully active cercariae.

The described phenotypic drug assays can be used for testing compounds and libraries in a low-throughput manner, as described in previous studies[7,9,10,25]. These assays allow determination of dose–response relationship or IC_{50} values essential to identifying hits and selecting early lead drug candidates to be tested in vivo. The worm burden obtained from infected mice or hamsters is variable, but in our experience, 10–50 adult worms can be recovered 7 weeks post infection with 100 cercariae (as described in Steps 76 and 77). Some examples of in vivo results for antischistosomal drug discovery can be found in our previous studies[7,9,10,25]. Although anemia and loss of weight are often observed in infected mice, they can survive for a maximum of 5 weeks post treatment without presenting major symptoms or behavioral changes. As a consequence of egg deposition, infected animals usually present an enlarged granulomatous liver and spleen (hepatosplenomegaly, Fig. 5a).

Reporting Summary

Further information on research design is available in the Nature Research Reporting Summary.

References

1. Bergquist, R., Utzinger, J. & Keiser, J. Controlling schistosomiasis with praziquantel: how much longer without a viable alternative? *Infect. Dis. Poverty* **6**, 74 (2017).
2. Vale, N. et al. Praziquantel for schistosomiasis: single-drug metabolism revisited, mode of action, and resistance. *J. Antimicrob. Chemother.* **61**, e02582–e02516 (2017).
3. Pedrique, B. et al. The drug and vaccine landscape for neglected diseases (2000-11): a systematic assessment. *Lancet Glob. Health* **1**, E371–E379 (2013).
4. Neves, B., Andrade, C. & Cravo, P. Natural products as leads in schistosome drug discovery. *Molecules* **20**, 1872–1903 (2015).
5. Caffrey, C. R. & Secor, W. E. Schistosomiasis: from drug deployment to drug development. *Curr. Opin. Infect. Dis.* **24**, 410–417 (2011).
6. Paveley, R. A. et al. Whole organism high-content screening by label-free, image-based Bayesian classification for parasitic diseases. *PLoS Negl. Trop. Dis.* **6**, e1762 (2012).
7. Cowan, N. & Keiser, J. Repurposing of anticancer drugs: in vitro and in vivo activities against *Schistosoma mansoni*. *Parasit. Vectors* **8**, 417 (2015).
8. Aerts, C., Sunyoto, T., Tediosi, F. & Sicuri, E. Are public-private partnerships the solution to tackle neglected tropical diseases? A systematic review of the literature. *Health Policy* **121**, 745–754 (2017).
9. Pasche, V., Laleu, B. & Keiser, J. Screening a repurposing library, the Medicines for Malaria Venture Stasis Box, against *Schistosoma mansoni*. *Parasit. Vectors* **11**, 298 (2018).
10. Ingram-Sieber, K. et al. Orally active antischistosomal early leads identified from the open access Malaria Box. *PLoS Negl. Trop. Dis.* **8**, e2610 (2014).
11. Keiser, J. In vitro and in vivo trematode models for chemotherapeutic studies. *Parasitology* **137**, 589–603 (2010).
12. Lee, C. L. & Lewert, R. M. Maintenance of *Schistosoma mansoni* in the laboratory. *J. Infect. Dis.* **99**, 15–20 (1956).
13. Eveland, L. K. & Haseeb, M. A. in *Biomphalaria Snails and Larval Trematodes* 33–55 (Springer, New York, 2011).
14. Basch, P. F. Cultivation of *Schistosoma mansoni* in vitro establishment of cultures from cercariae and development until pairing. *J. Parasitol.* **67**, 179–185 (1981).

15. Hackett, F. The culture of *Schistosoma mansoni* and production of life cycle stages. *Methods Mol. Biol.* **21**, 89–99 (1993).
16. Tucker, M. S., Karunaratne, L. B., Lewis, F. A., Freitas, T. C. & Liang, Y. S. Schistosomiasis. *Curr. Protoc. Immunol.* **103**, 19.11.11–19.11.58 (2013).
17. Colley, D. G. & Wikel, S. K. *Schistosoma mansoni*: simplified method for the production of schistosomules. *Exp. Parasitol.* **35**, 44–51 (1974).
18. Ramalho-Pinto, F. J. et al. *Schistosoma mansoni*: defined system for stepwise transformation of cercaria to schistosomule in vitro. *Exp. Parasitol.* **36**, 360–372 (1974).
19. James, E. R. & Taylor, M. G. Transformation of cercariae to schistosomula: a quantitative comparison of transformation techniques and of infectivity by different injection routes of the organisms produced. *J. Helminthol.* **50**, 223–233 (1976).
20. Milligan, J. N. & Jolly, E. R. Cercarial transformation and in vitro cultivation of *Schistosoma mansoni* schistosomules. *J. Vis. Exp.* **2011**, e3191 (2011).
21. Ramirez, B. et al. Schistosomes: challenges in compound screening. *Expert Opin. Drug Discov.* **2**, S53–S61 (2007).
22. Abdulla, M.-H. et al. Drug discovery for schistosomiasis: hit and lead compounds identified in a library of known drugs by medium-throughput phenotypic screening. *PLoS Negl. Trop. Dis.* **3**, e478 (2009).
23. Mansour, N. R. & Bickle, Q. D. Comparison of microscopy and Alamar blue reduction in a larval based assay for schistosome drug screening. *PLoS Negl. Trop. Dis.* **4**, e795 (2010).
24. Manneck, T., Haggenmüller, Y. & Keiser, J. Morphological effects and tegumental alterations induced by mefloquine on schistosomula and adult flukes of *Schistosoma mansoni*. *Parasitology* **137**, 85–98 (2010).
25. Panic, G., Vargas, M., Scandale, I. & Keiser, J. Activity profile of an FDA-approved compound library against *Schistosoma mansoni*. *PLoS Negl. Trop. Dis.* **9**, e0003962 (2015).
26. Meister, I. et al. Activity of praziquantel enantiomers and main metabolites against *Schistosoma mansoni*. *Antimicrob. Agents Chemother.* **58**, 5466–5472 (2014).
27. Lazdins, J. K., Stein, M. J., David, J. R. & Sher, A. *Schistosoma mansoni* - rapid isolation and purification of schistosomula of different developmental stages by centrifugation on discontinuous density gradients of Percoll. *Exp. Parasitol.* **53**, 39–44 (1982).
28. Hughes, J. P., Rees, S., Kalindjian, S. B. & Philpott, K. L. Principles of early drug discovery. *Br. J. Pharmacol.* **162**, 1239–1249 (2011).
29. Lalli, C. et al. Development and validation of a luminescence-based, medium-throughput assay for drug screening in *Schistosoma mansoni*. *PLoS Negl. Trop. Dis.* **9**, e0003484 (2015).
30. Panic, G., Flores, D., Ingram-Sieber, K. & Keiser, J. Fluorescence/luminescence-based markers for the assessment of *Schistosoma mansoni* schistosomula drug assays. *Parasit. Vectors* **8**, 624 (2015).
31. Peak, E., Chalmers, I. W. & Hoffmann, K. F. Development and validation of a quantitative, high-throughput, fluorescent-based bioassay to detect *Schistosoma* viability. *PLoS Negl. Trop. Dis.* **4**, e759 (2010).
32. Manneck, T., Braissant, O., Haggenmuller, Y. & Keiser, J. Isothermal microcalorimetry to study drugs against *Schistosoma mansoni*. *J. Clin. Microbiol.* **49**, 1217–1225 (2011).
33. Rinaldi, G., Loukas, A., Brindley, P. J., Irelan, J. T. & Smout, M. J. Viability of developmental stages of *Schistosoma mansoni* quantified with xCELLigence worm real-time motility assay (xWORM). *Int. J. Parasitol. Drugs Drug Resist.* **5**, 141–148 (2015).
34. Smout, M. J., Kotze, A. C., McCarthy, J. S. & Loukas, A. A novel high throughput assay for anthelmintic drug screening and resistance diagnosis by real-time monitoring of parasite motility. *PLoS Negl. Trop. Dis.* **4**, e885 (2010).
35. Lee, H. et al. Quantification and clustering of phenotypic screening data using time-series analysis for chemotherapy of schistosomiasis. *BMC Genomics* **13**, S4 (2012).
36. Mansour, N. R. et al. High throughput screening identifies novel lead compounds with activity against larval, juvenile and adult *Schistosoma mansoni*. *PLoS Negl. Trop. Dis.* **10**, e0004659 (2016).
37. Cheever, A. W. et al. Variation of hepatic-fibrosis and granuloma size among mouse strains infected with *Schistosoma mansoni*. *Am. J. Trop. Med. Hyg.* **37**, 85–97 (1987).
38. Bickle, Q., Long, E., James, E., Doenhoff, M. & Festing, M. *Schistosoma mansoni*: influence of the mouse host's sex, age, and strain on resistance to reinfection. *Exp. Parasitol.* **50**, 222–232 (1980).
39. Olivier, L. A comparison of infections in mice with three species of schistosomes, *Schistosoma mansoni*, *Schistosoma japonicum* and *Schistosomatium douthitti*. *Am. J. Hyg.* **55**, 22–35 (1952).
40. Dettman, C. D., Higgins-Opitz, S. B. & Saikoolal, A. Enhanced efficacy of the paddling method for schistosome infection of rodents by a four-step pre-soaking procedure. *Parasitol. Res.* **76**, 183–184 (1989).
41. Yolles, T. K., Moore, D. V., Degiusti, D. L., Ripsom, C. A. & Meleney, H. E. A technique for the perfusion of laboratory animals for the recovery of schistosomes. *J. Parasitol.* **33**, 419–426 (1947).
42. Adema, C. M. et al. Whole genome analysis of a schistosomiasis-transmitting freshwater snail. *Nat. Commun.* **8**, 15451 (2017).
43. Theron, A. Early and late shedding patterns of *Schistosoma mansoni* cercariae: ecological significance in transmission to human and murine hosts. *J. Parasitol.* **70**, 652–655 (1984).
44. Geyer, K. K. et al. The *Biomphalaria glabrata* DNA methylation machinery displays spatial tissue expression, is differentially active in distinct snail populations and is modulated by interactions with *Schistosoma mansoni*. *PLoS Negl. Trop. Dis.* **11**, e0005246 (2017).

45. Davies, C. M., Fairbrother, E. & Webster, J. P. Mixed strain schistosome infections of snails and the evolution of parasite virulence. *Parasitology* **124**, 31–38 (2002).
46. Protasio, A. V., Dunne, D. W. & Berriman, M. Comparative study of transcriptome profiles of mechanical- and skin-transformed *Schistosoma mansoni* schistosomula. *PLoS Negl. Trop. Dis.* **7**, e2091 (2013).
47. Protasio, A. V. et al. A systematically improved high quality genome and transcriptome of the human blood fluke *Schistosoma mansoni*. *PLoS Negl. Trop. Dis.* **6**, e1455 (2012).
48. Stefanic, S. et al. RNA Interference in *Schistosoma mansoni* schistosomula: selectivity, sensitivity and operation for larger-scale screening. *PLoS Negl. Trop. Dis.* **4**, e850 (2010).
49. Samuelson, J. C., Caulfield, J. P. & David, J. R. *Schistosoma mansoni*: post-transformational surface changes in schistosomula grown in vitro and in mice. *Exp. Parasitol.* **50**, 369–383 (1980).
50. Brink, L. H., McLaren, D. J. & Smithers, S. R. *Schistosoma mansoni*: a comparative study of artificially transformed schistosomula and schistosomula recovered after cercarial penetration of isolated skin. *Parasitology* **74**, 73–86 (1977).
51. Wilson, M. S. et al. Immunopathology of schistosomiasis. *Immunol. Cell Biol.* **85**, 148–154 (2006).
52. Ricciardi, A. & Ndao, M. Still hope for schistosomiasis vaccine. *Hum. Vaccin. Immunother.* **11**, 2504–2508 (2015).
53. Skelly, P. J. The use of imaging to detect schistosomes and diagnose schistosomiasis. *Parasite Immunol.* **35**, 295–301 (2013).
54. Swinney, D. C. Phenotypic vs. target-based drug discovery for first-in-class medicines. *Clin. Pharmacol. Ther.* **93**, 299–301 (2013).
55. Kilkenny, C., Browne, W. J., Cuthill, I. C., Emerson, M. & Altman, D. G. Improving bioscience research reporting: the ARRIVE guidelines for reporting animal research. *PLoS Biol.* **8**, e1000412 (2010).
56. Keiser, J. et al. Aryl hydantoin Ro 13-3978, a broad-spectrum antischistosomal. *J. Antimicrob. Chemother.* **70**, 1788–1797 (2015).
57. Mäser, P., Grether-Bühler, Y., Kaminsky, R. & Brun, R. An anti-contamination cocktail for the in vitro isolation andcultivation of parasitic protozoa. *Parasitol. Res.* **88**, 172–174 (2002).
58. Dahlborn, K. et al. Report of the Federation of European Laboratory Animal Science Associations Working Group on animal identification. *Lab Anim.* **47**, 2–11 (2013).
59. Charan, J. & Kantharia, N. D. How to calculate sample size in animal studies? *J. Pharmacol. Pharmacother.* **4**,303–306 (2013).

Acknowledgements

J.K. is grateful to the European Research Council (ERC) (grant no. ERC-2013-CoG 614739-A_HERO) for financial support. We are grateful to C. Häberli for scientific support.

Author contributions

J.K., F.C.L., V.P. and G.P. developed the concept of the protocol. F.C.L., V.P., G.P. and Y.E. drafted the first version of this manuscript, and J.K. revised the manuscript. Videos and images were taken by F.C.L. and V.P.

Competing interests

The authors declare no competing interests.

Additional information

Supplementary information is available for this paper at https://doi.org/10.1038/s41596-018-0101-y.

Reprints and permissions information is available at www.nature.com/reprints.

Correspondence and requests for materials should be addressed to J.K.

Publisher's note: Springer Nature remains neutral with regard to jurisdictional claims in published maps and institutional affiliations.

Published online: 4 January 2019

Related links

Key references using this protocol

Pasche, V., Laleu, B. & Keiser, J. *Parasit. Vectors* **11**, 298 (2018): https://doi.org/10.1186/s13071-018-2855-z

Panic, G., Vargas, M., Scandale, I. & Keiser, J. *PLoS Negl. Trop. Dis.* **9**, e0003962 (2015): https://doi.org/10.1371/journal.pntd.0003962

Cowan, N. & Keiser, J. *Parasit. Vectors* **8**, 417 (2015): https://doi.org/10.1186/s13071-015-1023-y

Chapter II:

Parallelized Impedance-Based Platform for Continuous Dose-Response Characterization of Antischistosomal Drugs

ADVANCED BIOSYSTEMS
www.adv-biosys.co

Parallelized Impedance-Based Platform for Continuous Dose-Response Characterization of Antischistosomal Drugs

Paolo S. Ravaynia, Flavio C. Lombardo, Stefan Biendl, Matthias A. Dupuch, Jennifer Keiser,* Andreas Hierlemann, and Mario M. Modena*

Schistosomiasis is an acute and chronic disease caused by tropical parasitic worms of the genus *Schistosoma*, which parasitizes annually over 200 million people worldwide. Screening of antischistosomal compounds is hampered by the low throughput and potential subjectivity of the visual evaluation of the parasite phenotypes, which affects the current drug assays. Here, an impedance-based platform, capable of assessing the viability of *Schistosoma mansoni* schistosomula exposed to drugs, is presented. This automated and parallelized platform enables unbiased and continuous measurements of dose–response relationships for more than 48 h. The platform performance is established by exposure of schistosomula to three test compounds, praziquantel, oxethazaine, and mefloquine, which are known to affect the larvae phenotypes. The system is thereafter used to investigate the response of schistosomula to methiothepine, an antipsychotic compound, which causes complex drug-induced effects. Continuous monitoring of the parasites reveals transient behavioral phenotypes and allows for extracting temporal characteristics of dose–response curves, which are essential for selecting drugs that feature high activity and fast kinetics of action. These measurements demonstrate that impedance-based detection provides a wealth of information for the in vitro characterization of candidate antischistosomals and, represents a promising tool for the identification of new lead compounds.

1. Introduction

Efficient and reliable screening methods are an essential tool for the discovery of novel drug candidates. The demand for improving the identification of promising compounds is particularly high in the field of neglected tropical diseases (NTDs), where funding and commercial investments are typically low.[1,2] Among the frequently occurring NTDs, schistosomiasis is a tropical disease caused by worms of the genus *Schistosoma*, which infect over 200 million people worldwide, predominantly children living in poor rural areas of Sub-Saharan Africa.[3,4] If left untreated, the infection slowly develops into a debilitating chronic disease, which leads to fibrosis of the liver, intestines and/or bladder, anemia, urogenital cancers and, eventually, death.[4] Despite the high prevalence of schistosomiasis, the current anthelmintic drug discovery pipeline is alarmingly unproductive.[5] For over 40 years, praziquantel has been the treatment of choice for schistosomiasis and has been widely used as chemotherapeutic agent in mass drug-administration campaigns.[3] Hundreds of millions of treatments are administered to children and populations at risk each year,[6] raising a significant potential public-health threat due to the emergence of praziquantel drug resistance.[5,7,8] In addition, reported cases of reduced efficacy of praziquantel have been associated with multiple rounds of mass drug administration, highlighting the need for new antischistosomal drugs.[9]

Compound libraries of pharmaceutical and academic organizations offer a potential source for identification of candidate therapeutics. However, the large number of drugs that need to be tested requires the use of medium- or high-throughput assays to implement an efficient and cost-effective screening.[10,11] In addition to drug efficacy, information on pharmacodynamics would allow to select lead candidates. High activity, fast action, and low toxicity represent key parameters for the selection of promising leads during the in vitro screening process.[10,12,13] Despite these requirements, the current gold standard for antischistosomal drug screening is based on worm phenotypic evaluation using operator-based microscopy, which is limited in throughput, labor-intensive, and subjective. Therefore, the

---

P. S. Ravaynia, Prof. A. Hierlemann, Dr. M. M. Modena
Bioengineering Laboratory
Department of Biosystems Science and Engineering
ETH Zürich, Mattenstrasse 26, Basel 4058, Switzerland
E-mail: paolo.ravaynia@bsse.ethz.ch

F. C. Lombardo, S. Biendl, Prof. J. Keiser
Swiss Tropical and Public Health Institute
Department of Medical Parasitology and Infection Biology
University of Basel
Socinstrasse 57, Basel 4051, Switzerland
E-mail: jennifer.keiser@swisstph.ch

M. A. Dupuch
Micro and Nanosystems
Department of Mechanical and Process Engineering
ETH Zürich, Tannenstrasse 3, Zurich 8092, Switzerland

The ORCID identification number(s) for the author(s) of this article can be found under https://doi.org/10.1002/adbi.201900304.

DOI: 10.1002/adbi.201900304

© 2020 WILEY-VCH Verlag GmbH & Co. KGaA, Weinheim

development of advanced screening methods for the identification of new promising lead compounds is of high importance and priority.

In the last years, the more abundant *Schistosoma mansoni* larval-stage worms, or newly transformed schistosomula (NTS), have been used for the preselection of lead compounds prior to testing in adult parasites and to overcome the limitations related to the handling of adult worms for large-scale screenings.[14,15] The advent of NTS-based screenings has set the stage for the development of automated and higher-throughput systems, and several screening methods have been explored. Microcalorimetry was found to be a useful tool to thoroughly analyze drug effects on adult and larval stage helminths in real-time, however it requires a large number of NTS per sample (at least 400).[16,17] An alternate approach based on an image-based automated microscopy system was described as a label-free method to evaluate helminth viability based on morphology and motility.[18,19] Nonetheless, it has not been adopted for systematic dose-response assays and real-time monitoring, as the high computational burden and the low level of parallelization limit its use for routine analysis. The impedance-based xCelligence system, which detects parasite viability in a 96-well plate format, has been applied to adult-stage *S. mansoni* but not to the highly abundant NTS.[20] In summary, no drug screening system, which can automatically measure NTS viability and continuously assess dose-response effects, is currently available.

To address these current limitations, a first version of an in vitro impedance-based microfluidic assay for drug screening on NTS has been developed.[21] Electrical impedance spectroscopy (EIS) is a noninvasive and label-free technique for investigating the dielectric properties of a sample and its potential variations within a specific frequency range.[22,23] We previously demonstrated that the confinement of NTS in small sensing regions and the use of electrodes featuring dimensions comparable to those of the parasite larvae enable to assess NTS motility by means of EIS, and that this motility characterization may be a good indicator of NTS viability in drug screening applications.[21] However, the rather complex microfluidic structures ultimately limited the analysis throughput, the measurements still required considerable sample handling by an operator, and the system did not allow for long-term culturing and real-time detection of drug-induced effects.

In this paper, we present a parallelized impedance-based platform to continuously assess dose-response effects of drugs on NTS. The electrical-impedance microwell (EIM) platform includes 32 analysis units to allow for simultaneous execution of several measurement replicates and to increase throughput. To achieve high sensitivity of the detection method without physical confinement of the parasites in channels of sub-millimeter dimensions, we used sensing electrodes with dimensions comparable to the NTS size, which resulted in a sensing volume of ≈25 nL or ≈100 µm height, given the well dimensions. This configuration enabled the use of a large medium reservoir over the sensing region to achieve long-term culturing of the parasites without affecting the detection characteristics of the system with respect to NTS motility. In addition, the chip design features simple loading of the parasites, which are driven into the nanoliter sensing volume by sedimentation. To validate our platform, we first measured the NTS response to three antischistosomal compounds, oxethazaine, praziquantel, and mefloquine, which have already been shown to cause different phenotypical behaviors in vitro, that is, they reduce parasite motility, stimulate hyperactivity or induce both effects, respectively.[24–28] As a case study, we then analyzed the activity of an antipsychotic drug, methiothepine, which belongs to the emerging class of tricyclic compounds and serotonin modulators, which have been investigated as potential therapeutic agents against schistosomiasis.[24,29] The obtained results indicate that the EIM platform can provide continuous dose-dependent viability and activity patterns of NTS on-chip and can be a suitable component for antischistosomal drug screening.

2. Results

2.1. EIM Platform Function and Operation

The overall concept of the EIM platform is illustrated in **Figure 1**. To provide continuous impedance-based recordings of parasite motility in parallel to optical inspection, the analysis unit was fabricated from two transparent components: a PDMS (polydimethylsiloxane) microwell and a glass slide patterned with platinum electrodes. Each culture unit was loaded with 60 µL of NTS suspension (≈10–15 NTS per 60 µL) by using a pipette (Figure 1A-II). The NTS rapidly (≈1 min) settled to the bottom of the microwell (chamber) on the patterned glass substrate. Each microwell was equipped with a pair of coplanar electrodes for detecting NTS motility by measuring conductivity variations that were caused by parasite movements between the electrodes. To measure the signal fluctuations upon NTS activity and movements, an AC voltage was applied to the left co-planar electrode, and the current flowing through the sensing volume was then measured at the right electrode and converted to voltage through a trans-impedance amplifier (Figure 1A-III). Motile and non-motile parasites were evaluated separately in the device to detect differences in the voltage signal during 1-min acquisition. Because of the parasite movements, the high-pass-filtered signal output of motile NTS exhibits clear fluctuations around zero (Figure 1A-IV), while non-motile NTS do not cause signal variations, and the trace only shows the readout background noise (in the µV range, Figure S1, Supporting Information).

To assign a motility value as a function of signal fluctuations in a time window of 60 s, we computed the signal power in a bandwidth of 1–3 Hz. Figure 1B shows an example of the separation between the normalized signal power generated by motile and non-motile NTS, evaluated every 15 min during 1 h. The signal power measured with alive and motile parasites (–13.1 ± 1.1 dBµ, ≈0.05 a.u.) was, therefore, constantly two orders of magnitude higher than the signal power obtained from the non-motile counterpart (–34.7 ± 0.6 dBµ, in the range of 0.0005 a.u.), which evidences the robust recognition and differentiation of worm motility by using our platform.

The motility of the parasites was also qualitatively evaluated by visual inspection under an inverted microscope, as the chip was optically transparent and openings were included in the chip holder. The sequence of bright-field images clearly shows the contraction/extension movements of the alive NTS in

© 2020 WILEY-VCH Verlag GmbH & Co. KGaA, Weinheim

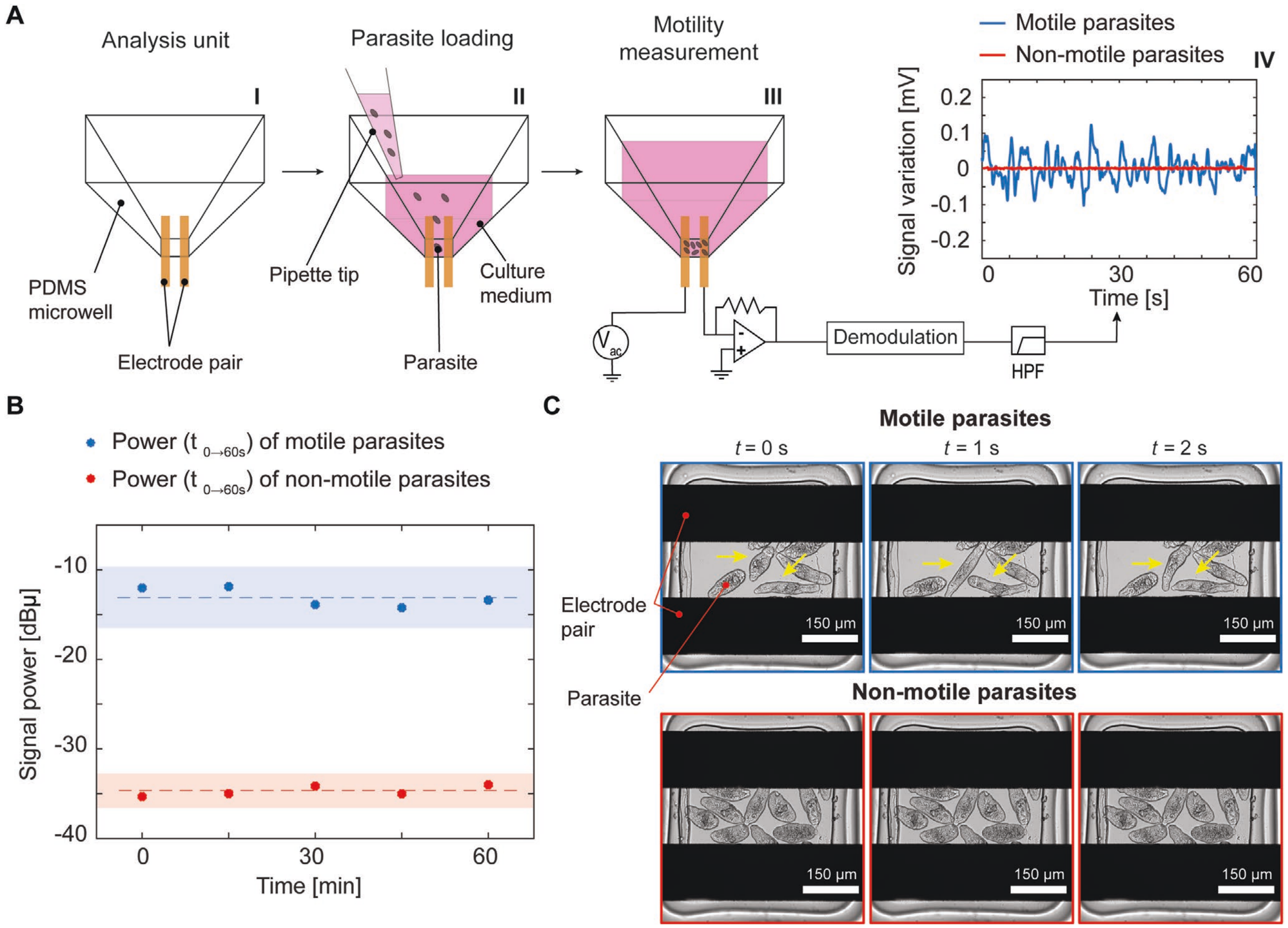

Figure 1. Detection of NTS parasite motility by the EIM platform. A) The analysis unit of the EIM platform consists of an inverted-pyramid-shape PDMS part, aligned with a pair of platinum electrodes I). After loading and sedimentation of the schistosomula in the inverted-pyramid-shape PDMS well II), the impedance-based motility measurement of NTS was carried out III). Signal fluctuations, caused by impedance variations between the electrodes owing to larvae movements, were acquired using a 500 kHz sinusoidal excitation. The graph shows an example of 60 s of signal recordings for both, motile and non-motile parasites IV). The signal was filtered using a 0.2 Hz high-pass filter to remove the signal baseline. B) The power of the signals acquired from motile and non-motile NTS parasites was calculated in a bandwidth of 1–3 Hz during a time window of 1 min and measured every 15 min. The dotted line indicates the mean value of the signal power for motile (blue) and non-motile (red) NTS. The shaded areas show ±3 standard deviations. The power unit refers to 10^{-6} a.u. C) Bright-field microscopy images of motile and non-motile NTS parasites in the analysis units. The yellow arrows indicate parasites that contract and elongate between frames.

between the electrode pair, while non-motile NTS do not move or change position (Figure 1C). The microscopy observations correlated with the impedance-based recordings and confirmed that the impedance signal fluctuations arose from the parasite movements.

2.2. Higher-Throughput EIM Platform Design

The higher-throughput EIM platform was designed to achieve parallelized and automated monitoring of the motility of NTS exposed to different test conditions. The platform included three components (**Figure 2**A): 1) A custom-made printed circuit board (PCB) for signal routing; 2) four analysis chips; 3) a device holder to accommodate the chips and provide connections between the PCB and the electrode pads on the chips. All these parts were designed according to a 96-well-standard format to ensure compatibility with standard lab equipment and automated imaging and analysis tools. The PCB enabled the multiplexing of the analog input/output signals of the impedance spectroscopy unit to any of the 32 parasite chambers. The PCB featured two analog multiplexers to separately switch the 32 input and output electrodes, spring-contact connectors for interfacing with the fluidic chips, a mini-HDMI plug to connect to the controller board outside of the incubator, and two analog SMA connectors to the input/output ports of the impedance spectroscope. The chips were inserted in a 3D-printed device holder with four insertion sites. Each chip included a top PDMS layer, containing the microfluidic structures that defined the 8 analysis units (microwell) and a bottom glass slide patterned with 16 co-planar platinum electrodes. To prevent absorption of small hydrophobic molecules

© 2020 WILEY-VCH Verlag GmbH & Co. KGaA, Weinheim

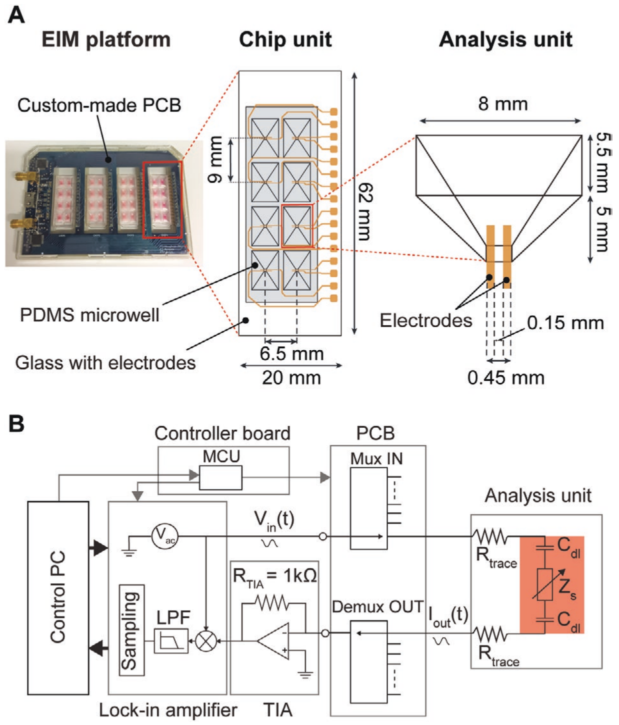

Figure 2. Design of the EIM platform. A) The EIM platform can accommodate up to four chip units, which were placed on a custom-made PCB. A single chip (highlighted with dashed red line) hosted eight PDMS analysis units that were plasma-bonded to a glass substrate featuring platinum electrodes. The PDMS cavity featured an inverted-pyramid shape to promote sedimentation of the parasites to the sensing volume over the coplanar electrodes. B) The electrical equivalent circuit of the experimental setup, which included a lock-in amplifier for generating the AC stimulation signal (V_{in}), a custom-made PCB for routing the AC signal to the selected analysis unit, and a trans-impedance amplifier (TIA) for current-to-voltage conversion. The voltage signal was sampled by the lock-in amplifier and recorded. A controller board featuring a microcontroller (MCU) was used for synchronizing the switching between the analysis units and the lock-in amplifier.

from the solution into the PDMS during the drug assays, all chips were coated with a parylene-C layer (Figures S2 and S3, Supporting Information).[30] Moreover, the microwells were arranged at 9 mm pitch to allow for loading of the parasites and of the medium by means of a standard multichannel pipette to simplify platform operation. Each analysis unit was shaped as an inverted pyramid to bring the parasites down to the micro-sensing area (450×450 µm^2) through sedimentation and to provide enough medium volume (60 µL) for multi-day experiments. Despite the considerable liquid volume over the sensing area, the electrode dimensions limited the sensing volume to the first 100 µm in height, which corresponds to the approximate size of the NTS (≈50×100 µm^2) (Figure S4, Supporting Information). The overall sensing volume (≈25 nL) was defined to enable testing with ≈10–15 NTS per condition, which represents an ≈tenfold reduction in sample consumption with respect to standard visual evaluation methods.[12]

The automated multiplexing in the platform allowed to simultaneously record from up to 32 analysis units. From an electrical point of view, each sample can be described as a variable impedance Z_s, representing the NTS suspension between the electrodes, in series with two double-layer capacitances, C_{dl}, which form at the interface between the electrodes and the medium (Figure 2B). The variations of Z_s over time were caused by the movement of the NTS in between the electrodes, while the Z_s average value depended on the solution conductivity and on the number of parasites between the electrodes. A multiplexing and switching architecture was used to route the output of the lock-in amplifier to each of the 32 parasite chamber units. Correspondingly, a de-multiplexing stage was used to route the output signals of each chamber to the input of the trans-impedance amplifier (TIA). The frequency of the sinusoidal carrier signal (500 kHz) was selected to enable fast multiplexing and to minimize the signal attenuation in the EIM platform (≈−32 dBV, Figure S5, Supporting Information). The switching interval and the selection of the electrode pairs were defined by a custom-made Python script, which interfaced to a microcontroller (MCU, on the controller board) that controlled the de/multiplexers on the PCB. To achieve continuous and quasi-parallel impedance measurements of the NTS in the 32 chambers, we performed short recordings (1 ms) at each electrode pair and fast switching (1.5 µs) between all the units in a round-robin fashion, which resulted in an effective sampling frequency of ≈32 Hz per chamber unit.

2.3. Monitoring of Parasite Motility Under Drug Treatment

To validate the ability of the EIM platform to detect NTS motility and to discriminate between different schistosomula movement characteristics, we measured the signal fluctuations caused by the parasites following incubation with two compounds, known to affect schistosomula phenotypes. We selected oxethazaine, a fast-acting in vitro compound that reduces parasite motility,[24] and praziquantel, which, although mostly effective against adult parasites, is known to have an excitatory effect on NTS in vitro.[26] The parasites were exposed to different concentrations of these test compounds, and we tested our impedance-based motility readout. As controls, we measured also the motility of NTS under standard medium conditions and in medium containing the drug vehicle (DMSO). The parasite larvae were first loaded in the chips under standard medium condition using a multichannel pipette. We then performed impedance measurements of all the chambers during 1 h to evaluate the motility of the untreated parasites and to confirm their initial viability (**Figure** 3A). After baseline acquisition, the different drug concentrations were added to the chamber units and NTS motility was recorded over time. This procedure enabled us to normalize the power of the signal fluctuations to the power of the first 1-h window for each condition and to extract a motility index. This normalization also allowed for comparing measurements from chambers with different numbers of parasites, as the absolute signal power depends on the number of loaded parasites.

Our platform allowed to differentiate the inhibitory and excitatory effects, induced by the two test compounds (Figure 3B). After addition of oxethazaine ($t = 0$ h) at all concentrations tested, the NTS exhibited a considerable decrease in motility, compared to the vehicle control condition, during 48 h

© 2020 WILEY-VCH Verlag GmbH & Co. KGaA, Weinheim

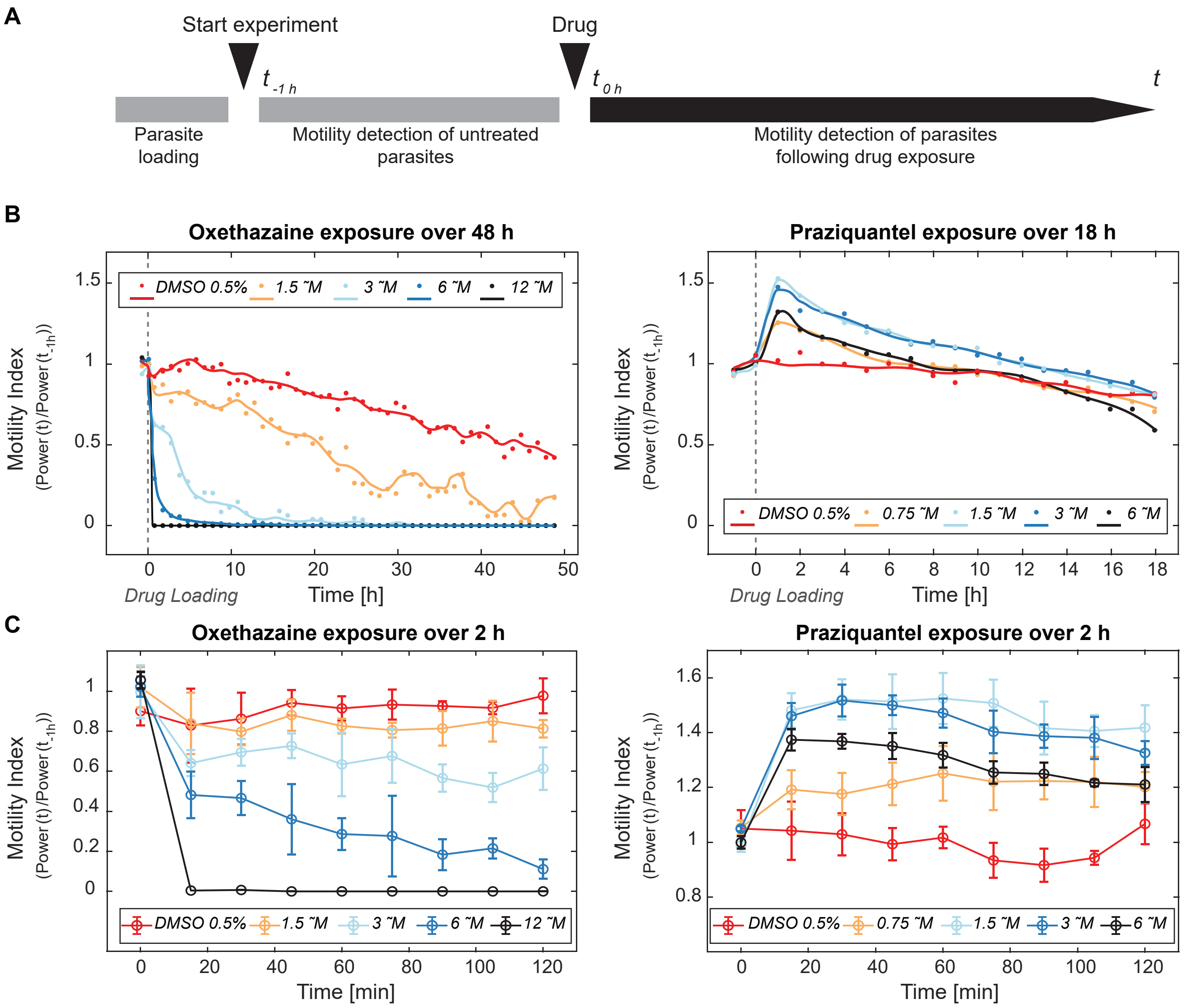

Figure 3. Measurements of drug-induced NTS parasite motility via impedance-based recording. A) The flow diagram shows the main steps for performing an impedance-based drug assay. First, 30 µL of NTS solutions were loaded into all analysis-unit chambers. After 1 h of impedance-based motility detection, the measurement was stopped and additional 30 µL of drug solution were dispensed into each chamber. Afterward, the impedance detection was restarted and recordings of drug-induced motility variations continued until the end of the assay. B) The graphs show the variations in the motility index of the vehicle-control sample (exposed to 0.5% v/v DMSO) and of NTS exposed to four different concentrations of oxenthazaine (left) and praziquantel (right). For clarity, one point per hour is displayed, and each point indicates the mean value of the motility index determined from three analysis units. Five trend lines were superimposed to the points to guide the eye for the different tested conditions. C) The motility graphs of the first 2 h of recording for both, oxenthazaine and praziquantel. Each point represents the mean value of the motility index simultaneously measured with three analysis units, while the error bars represent the standard error of the mean.

of continuous measurements. The reduction of NTS motility showed a drug-dose dependence: the motility index for 6 µM oxethazaine reached zero (i.e., no motility) in 12 h, whereas the 3 µM condition required about 24 h to achieve the same effect. The highest drug concentration, 12 µM, inhibited the larvae movement within the first 15 min upon addition of the compound. Contrarily, praziquantel showed a drastic increase in NTS motility, which is in line with the phenotypical evaluations of drug effects reported in literature.[25,26] Higher motility index values (≈1.5) were obtained for 1.5 and 3 µM of praziquantel. After reaching a peak of the motility index, all the drug–dose curves exhibited a gradual decrease in motility and approached the vehicle-control behavior in about 18 h. Moreover, the effect of both drugs was also confirmed in a 96 well-plate by the standard visual method (Movies S1 and S2, Supporting Information).

By focusing on the first 2 h of the motility detection for both compounds, we evaluated the sensitivity of the platform in discriminating motility changes caused by different drug concentrations (Figure 3C). To observe drug-induced rapid variations of NTS behavior, the motility index was computed for 1-min windows every 15 min during the entire recording. We achieved a robust discrimination of the effects induced by 3, 6, and 12 µM of oxethazaine after 75 min compared to the 0.5% v/v DMSO and 1.5 µM oxethazaine conditions. For praziquantel, we observed a significant increase in motility after 30 min for all tested concentrations in comparison to the vehicle-control condition.

2.4. Long-Term Dose-Response Analysis

To evaluate the performance of our platform in continuously assessing NTS viability and generating real-time dose–response curves, we exposed the parasite larvae for 48 h to six serially diluted concentrations (1.5, 3, 6, 12, 25, 50 µM) of two compounds, oxethazaine and mefloquine, which are known for their antischistosomal activity in vitro.[24,28] The impedance-based parasite viability was calculated by normalizing the motility index of each drug condition to the motility index of the vehicle control at each time point along two days of drug exposure.

By measuring parasite viability exposed to oxethazaine via the EIM platform, no signal fluctuations were detected for the NTS incubated with the highest drug concentrations (12, 25, and 50 µM) after 30 min, indicating that the NTS were dead (**Figure 4**A). For the same time point, the viability upon dosage of 6 µM was already reduced to ≈0.5, which indicates that a significant fraction of the NTS population has deceased or lost its motility. After 17 h, only the parasites exposed to 1.5 µM showed

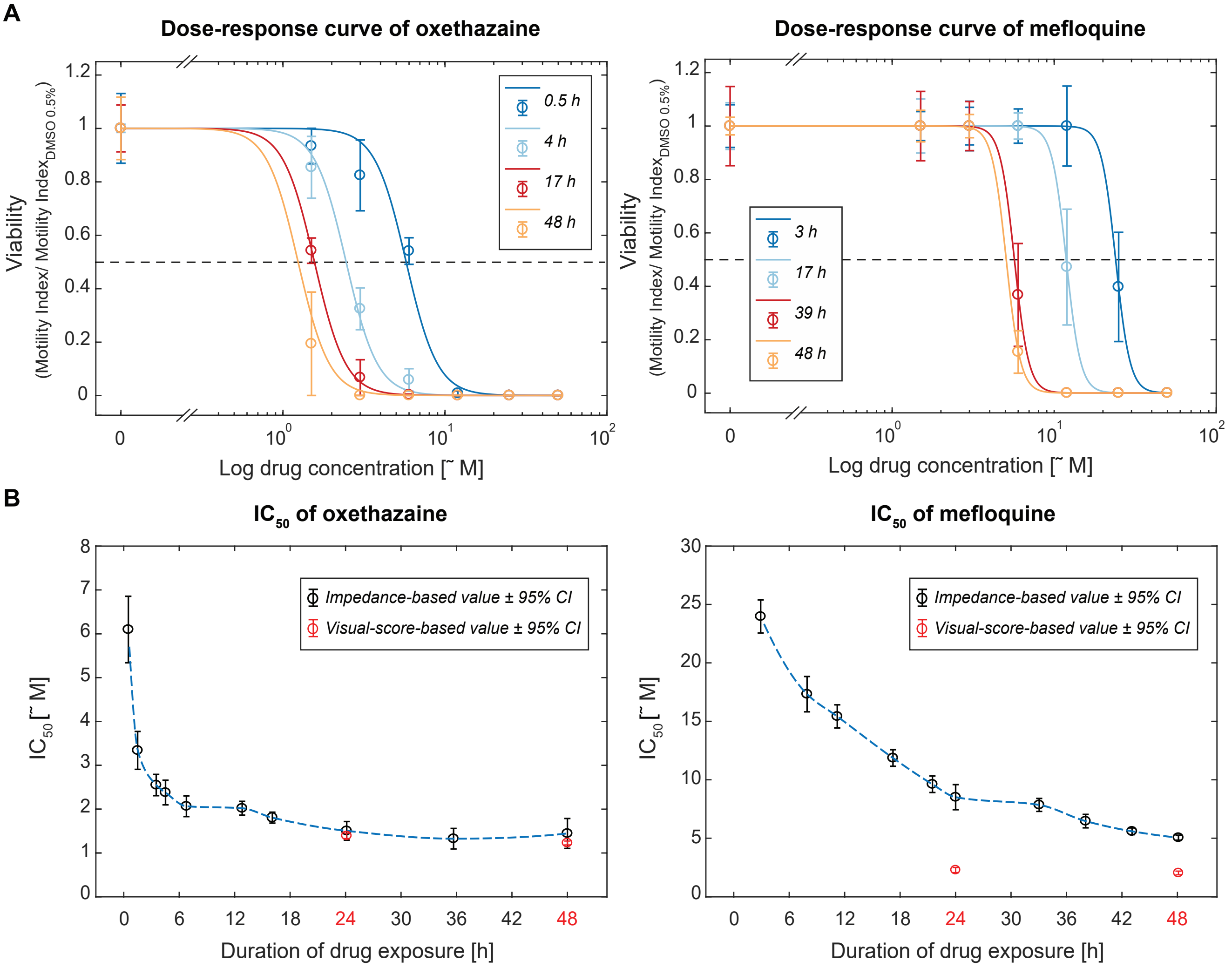

Figure 4. Temporal evolution of the dose–response curves determined through continuous long-term monitoring of NTS viability by impedance-based detection. A) The graphs show the impedance-based estimations of the NTS viability at four selected time points as a function of drug concentration. The NTS was exposed to six different concentrations (1.5, 3, 6, 12, 25, and 50 µM) of oxethazaine (left) and mefloquine (right) during 48 h. Each circle represents the mean value of the viabilities of three replicates, and the error bars represent the standard error of the mean. The four sigmoid fits, used to calculate the IC$_{50}$, values are superimposed to the viability measurements. B) The temporal evolution of the IC$_{50}$ values for oxethazaine and mefloquine as determined by using impedance-based detection. The IC$_{50}$ values obtained through standard visual scoring at 24 and 48 h are shown for comparison (marked in red). The circles represent the values obtained through the sigmoidal fits, while the error bars show the 95% confidence intervals.

© 2020 WILEY-VCH Verlag GmbH & Co. KGaA, Weinheim

a viability above 0.5 (0.54 ± 0.05), which further decreased to ≈0.2 (0.2 ± 0.19) at 48 h of incubation with the drug. By testing the activity of mefloquine on the NTS, we obtained dose–response curves along time that evidenced a lower potency compared to oxethazaine. After 3 h, only the parasites exposed to 50 µm were dead, whereas those exposed to 25 µm showed a viability slightly below 0.5 (0.39 ± 0.21). Toward the end of the drug assay (39 h), only the parasites exposed to 6 µm displayed a viability of 0.37 ± 0.19, which further decreased to 0.15 ± 0.08 at 48 h. Parasites exposed to drug concentrations lower than 6 µm were viable and showed a high level of motility during the entire assay.

We used the viability calculations to extract IC_{50} values of oxethazaine and mefloquine (Figure 4B). IC_{50} corresponds to the drug concentration at which the larvae were compromised in their activity and moving 50% less. Sigmoid fits (shown in Figure 4A) were used to calculate the IC_{50} values over time. The IC_{50} values obtained from the impedance-based viability measurements showed that oxethazaine featured an IC_{50} of 6.1 ± 0.76 µm at 30 min incubation. The IC_{50} value rapidly decreased and reached 2.02 ± 0.16 µm after 12 h of drug exposure. Between 24 and 48 h, the IC_{50} did not change significantly anymore (1.51 ± 0.21 µm and 1.45 ± 0.34 µm, respectively). In the case of mefloquine, the impedance-based estimations evidenced an IC_{50} of 24 ± 1.42 µm after 3 h of exposure, which decreased linearly to 8.51 ± 1.07 µm during 24 h of incubation. Finally, the IC_{50} calculated at 48 h using the EIM platform was 5.05 ± 0.21 µm.

The parasite viability was also evaluated using the standard visual scoring method at 24 and 48 h in a 96-well plate to validate the IC_{50} estimations obtained with the EIM platform (Movies S1–S3, Supporting Information). The IC_{50} concentrations of oxethazaine obtained from the visual evaluation were 1.39 ± 0.06 µm after 24 h and 1.23 ± 0.04 µm after 48 h. In the case of mefloquine, the IC_{50} estimations from the visual method were 2.28 ± 0.22 µm at 24 h, and 2.03 ± 0.16 µm at 48 h. The visual-score-based evaluations were in good accordance and within the same order of magnitude as the results obtained with the impedance-based method (Figure S6, Supporting Information).

2.5. Characterization of Methiothepine Effect on NTS

As a case study, we challenged our system by investigating the effect of methiothepine on schistosomula. Methiothepine is a tricyclic antipsychotic compound whose behavior on NTS has not been fully characterized in vitro.[24] Tricyclic antipsychotic compounds bind to the serotonin transporter (SERT) of helminths and have been studied for their antischistosomal effects.[31] It has been previously shown that SERT antagonists can cause either persistent or transient hyperactivity of helminths and, eventually, can affect parasite viability.[32] To explore the temporal evolution of the dose-response effect, we measured the motility index and the viability of NTS exposed to six different methiothepine concentrations (1.5, 3, 6, 12, 25, 50 µm) for 48 h. We observed an excitatory effect lasting ≈24 h that was induced by the drug at sub-lethal concentrations (<25 µm at 24 h; **Figure 5**A), which is in line with previous observations of NTS exposed to other members of the tryclic-compound family.[31,32] Live imaging of parasites in the chamber unit confirmed the hyperactivity of NTS that were incubated with sub-lethal methiothepine concentrations (Figure 5B).

After 4 h of incubation, only the 50 µm-condition caused a drastic decrease in NTS viability (0.2 ± 0.09; Figure 5C). A comparably high level of NTS viability was maintained over 30 h for lower doses, while, for longer exposure times, methiothepine showed a slow-acting and dose-dependent killing behavior. At the end of the assay, after 48 h of incubation with the drug, all concentrations higher than 1.5 µm exhibited a viability below 0.5. The extraction of the IC_{50} over time also showed the slow efficacy of methiothepine in killing the NTS (Figure 5D). To inhibit the parasite viability by 50% during the first 24 h, a concentration of more than 26.81 ± 0.94 µm of methiothepine was required. The IC_{50} calculated after 48 h using the EIM platform was 2.45 ± 0.9 µm. The IC_{50} values extracted by the standard visual evaluation amounted to 10.88 ± 2.05 µm at 24 h and 2.22 ± 0.31 µm at 48 h. Differences in IC_{50} values obtained at 24 h by the two methods were expected, as the hyperactivity of the NTS introduces additional difficulties to visually score the parasite status for the operator (Movie S4, Supporting Information). Nevertheless, the IC_{50} values obtained at 48 h with the two different methods are in good accordance.

3. Discussion

Advancing the development of automated and medium- or high-throughput approaches for antischistosomal drug screening is of fundamental importance for the identification of new compound candidates. In this work, we introduced a novel platform with integrated electrodes for the automated detection of schistosomula viability by means of an impedance-based method. In particular, we showed how this label-free technique offers an unbiased method to quantitatively score parasite viability, and that the impedance method enables long-term and continuous assessment of drug efficacy.

The EIM platform allows for robust and simple screening of the viability of NTS that have been exposed to different drug concentrations, and it requires minimal operator interference. The use of micron-size electrodes and the small detection volumes reduces the number of NTS that are needed for analysis ≈tenfold in comparison to the current standard visual evaluation method,[12] and up to 30-fold in comparison to luminescence- and fluorescence-based assays reported in literature.[33,34] The arrangement of the pyramid-shape wells facilitates the loading of the parasite samples with standard multichannel pipettes and ensures the positioning of the parasites on top of the electrodes for over 48 h. In addition, the 96-well format of the platform enables compatibility with standard lab automation tools, such as automated liquid handlers, which further improves automation and increases the throughput.

The impedance-based readout allows to overcome major limitations associated with the currently used visual evaluation method, which include limited throughput, potential subjectivity, and bias in the operator's scoring.[14,35] In a previous proof-of-principle study, we showed the possibility to use impedance measurements of NTS motility as proxy for

© 2020 WILEY-VCH Verlag GmbH & Co. KGaA, Weinheim

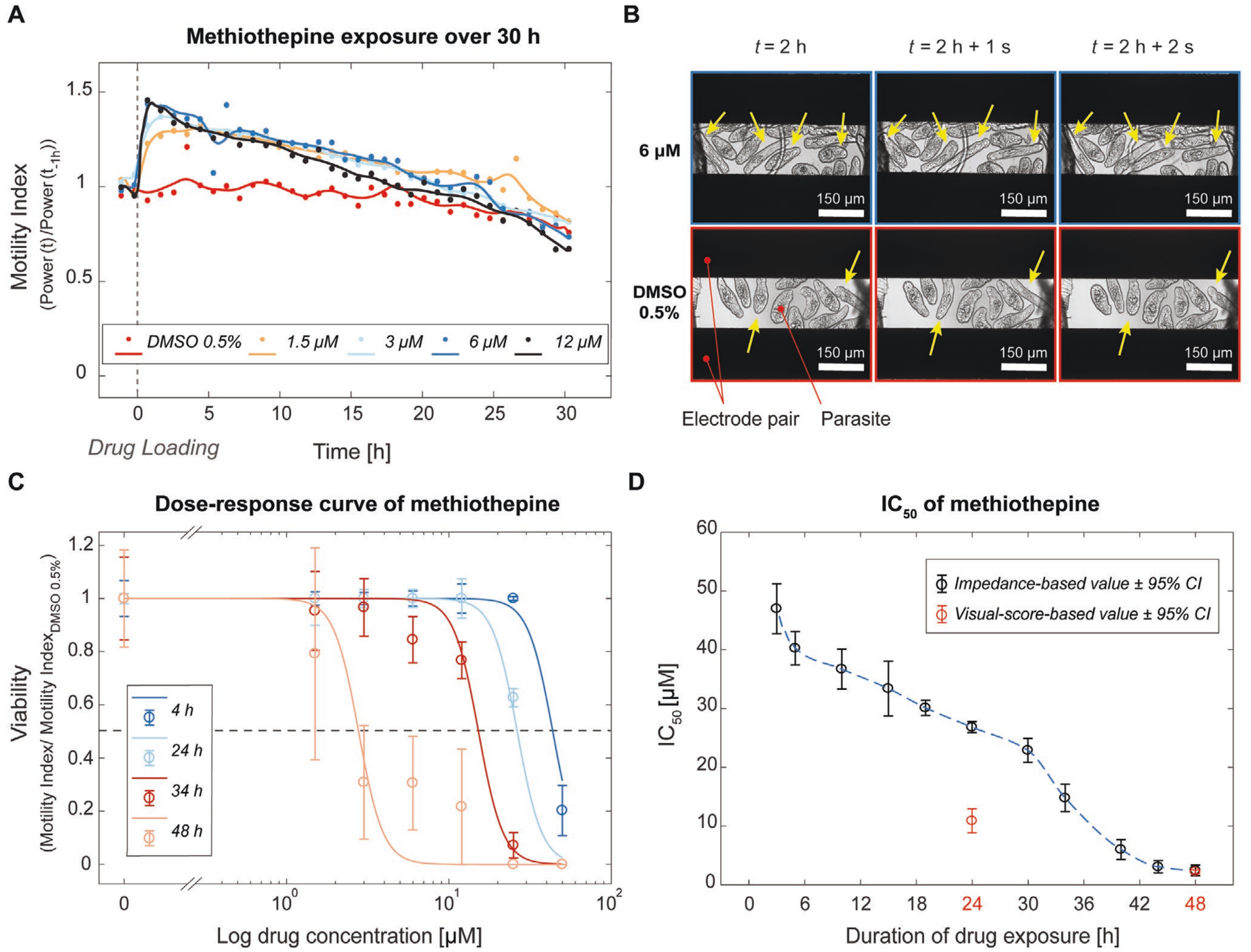

Figure 5. Characterization of NTS parasite motility and viability during long-term exposure to methiothepine. A) The motility values of the NTS, exposed to four different concentrations of methiothepine, are shown and compared to the motility indices of the vehicle-control sample (NTS exposed to 0.5% v/v DMSO). Each point represents the mean value of the motility indices of three replicates. Trend lines were superimposed to the points to guide the eye for the different tested conditions. B) Time-lapse images of NTS showed qualitative movement differences between NTS exposed to 6 µM methiothepine and to 0.5% v/v DMSO. The yellow arrows indicate parasites that moved between the different frames. C) The impedance-based viability measurements of NTS at four selected time points are plotted as a function of the drug concentration. The NTS was incubated with six different concentrations of methiothepine (1.5, 3, 6, 12, 25, and 50 µM) during 48 h. Each circle represents the mean viability value of three replicates, and the error bars represent the standard error of the mean. The sigmoid fit was used to calculate the IC_{50} value at each time point. D) IC_{50} values, calculated from the impedance-based detection of NTS viability, are compared with IC_{50} values obtained by standard visual scoring at 24 and 48 h (marked in red). The circles represent the values determined from the sigmoid fits, while the error bars show the 95% confidence intervals.

parasite viability.[21] However, the previous system did not allow for long-term culturing of NTS and could only provide end-point evaluation of the larvae viability. Furthermore, the complex fluidic structure that was used to confine the larvae in the sensing area and to increase the signal-to-noise ratio of the measurements strongly limited the analysis throughput to four recordings in parallel. Here, we were able to preserve the previously demonstrated high sensitivity of the impedance-based characterization by confining the larvae to a small detection volume in an easy-to-operate open fluidic structure. This solution enabled to simplify the platform operation and increase the analysis throughput to up to 32 recordings in parallel. We also determined the Z′-factor, which indicates the quality of an assay based on the difference of mean values of positive and negative controls in reference to the corresponding standard deviations.[36,37] The developed system showed a Z′-factor of 0.63 (calculated from 32 × 4 measurements of pre-treated motile and dead parasites of the impedance-based assays, $\text{power}_{\text{motile}} = -12.8 \pm 1.9$ dBμ and $\text{power}_{\text{dead}} = -34.5 \pm 0.8$ dBμ), which highlights the potential of the platform as a robust and higher throughput antischistosomal screening method according to NIH guidelines.[36] The novel design also enabled the long-term culturing of the parasite larvae to realize a real-time evaluation of drug activity, which is important for providing insights into drug kinetics and for selecting fast-acting compounds.[38] High and fast drug activity along with low toxicity are relevant criteria to select promising antischistosomal lead compounds.[24]

The constant decrease of motility in the control samples during long-term in vitro culture, a common behavior of NTS also observed in standard assays, may introduce artifacts in the evaluation of compound efficacy in multi-day drug-exposure experiments using motility-based parasite evaluation. Therefore, medium exchanges may be considered to extend the viability time of the NTS in the platform for long-term assays.

We first validated the EIM platform by recording variations in NTS motility upon dosage of three active drugs triggering antischistosomal effects (Figure S7, Supporting Information). By analyzing the effect of praziquantel on NTS motility, we were able to reproduce the in vitro excitatory action of the drug on parasites, which lasted for over 18 hours. This hypermotility is caused by the activity of praziquantel as calcium channel agonist, which increases the calcium concentration in the schistosomula body within minutes of exposure and causes intense and sustained muscular contraction of the parasites.[26,39] In contrast, the exposure of NTS to oxethazaine caused a fast-acting inhibitory effect on their motility.[24] Motility reduction is most likely caused by the high affinity of the drug to the sodium channels of the NTS, which has been shown to have an in vitro inhibitory effect on the schistosomula smooth muscles by blocking the action of serotonin.[27] Via our impedance-based detection, we were able to confirm the fast action and the high efficacy of the drug in vitro, which showed an IC_{50} value of 3.48 µm already after 1 h of incubation. To investigate complex antischistosomal drug response, we studied the effect of mefloquine on NTS with the EIM platform. This antimalarial compound is known to induce hyperactivity and to affect NTS viability in vitro, which may be attributed to its potential role as an inhibitor of glycolysis and interference with schistosomula metabolic activity.[40] Our impedance-based IC_{50} estimations confirmed the reported lethal effect of mefloquine on NTS showing values below 10 µm after 20 h of drug exposure.[21] Differences in IC_{50} values, obtained with impedance-based and visual methods were expected for mefloquine at 24 h, as the morphology of the NTS was highly affected at high drug concentrations, and it was difficult to detect subtle movements of the larvae by eye, which, however, remained detectable using the impedance system.[21,28]

After validating the ability of our method in detecting changes of NTS motility caused by drugs with known in vitro effects, we used the EIM platform to analyze the response of the schistosomula to methiothepine. The complex dose- and time-dependent response of the NTS to the compound underlines the importance of continuous monitoring of parasites when investigating the efficacy of new drugs. Methiothepine is an antipsychotic drug of the tricyclic group, which acts as an inhibitor of both the serotonin receptor and the SERT, depending on the dose.[24,29] A transient increase in schistosomula motility was detected for sub-lethal drug concentrations (<12 µm of methiothepine for the first 24 h of incubation). This result corroborates the effects observed for two classical SERT inhibitors, fluoxetine and clomipramine, which were shown to induce strongly hyperactive phenotypes.[41] Recently, incubation of NTS with paroxetine, another *S. mansoni* SERT inhibitor, in the 1–10 µm concentration range was reported to have a similar hypermotility effect during the first 24 h of incubation, while the motility then decreased for longer exposure times.[32] Our measurements demonstrate that methiothepine has a similar effect on NTS for an analogous concentration range, as the schistosomula showed decreased motility after 24 h. Higher concentrations of methiothepine (>12 µm) resulted in a rapid loss of motility and a consequent reduction in larvae viability,[42] which confirmed earlier findings[24] and was similar to what has been previously reported for high concentrations of paroxetine.[32]

In summary, we developed a parallelized and automatable drug-screening platform, which continuously provides dose-dependent viability scores of NTS. The drug-dose responses of the parasites to four different antischistosomal compounds that were obtained through impedance detection show good agreement with those obtained from standard visual scoring of NTS motility. This agreement evidences that the impedance-based approach constitutes a reliable alternative method to identify novel drug candidates in vitro. The current platform layout enables the operator to use up to 4 chips, which include 32 analysis units in parallel, with a single instrument. The electrical detection method allows for further parallelization to achieve increased throughput with minimal experimental-setup modifications. The chip design, implemented in PDMS, can be easily realized with standard plastic materials to avoid issues related to compound ad/absorption in PDMS, and fabrication processes for mass production, such as injection molding, can be used. Finally, the EIM platform can be readily adapted to other relevant motile schistosome stages, such as cercariae, juvenile and adult parasites, or to different parasite species by simple modification of the sensing-area design, which will contribute to improve anthelmintic drug-screening applications.

4. Experimental Section

Culture Medium and Drugs: M199 medium was obtained from Gibco (cat. no. 22340-020, Thermo Fisher Scientific, Waltham, USA). Penicillin/streptomycin 10′000 U mL^{-1} (pen/strep, cat. no. P4333-100ML, Sigma-Aldrich, Buchs, Switzerland) and inactivated fetal calf serum (iFCS, cat. no. 2-01F30-I, Bioconcept AG, Allschwil, Switzerland) were purchased from Bioconcept AG. All media were sterilized by filtration using a 0.22 µm filter bottle (cat. no. 431097-COR, Vitaris AG, Baar, Switzerland). Oxethazaine (cat. no. O5380-5G, Sigma-Aldrich, Buchs, Switzerland), praziquantel (cat. no. P4668-5G, Sigma-Aldrich, Buchs, Switzerland), mefloquine (cat. no. M2319-100MG, Sigma-Aldrich, Buchs, Switzerland), and methiothepine (cat. no. M149-100MG, Sigma-Aldrich, Buchs, Switzerland) were all purchased as racemic powders from Merck (Sigma-Aldrich).

Parasite Culture and Transformation: *S. mansoni* culturing and NTS transformation were performed according to protocols previously described in literature.[12,43] In brief, *S. mansoni* -infected *Biomphalaria glabrata* snails were placed singularly in 24-well plates and exposed to a neon lamp (36 W, 4000 K, 3350 lumens), for 3–4 h, to induce the shedding of cercariae. The supernatant was collected and filtered to remove impurities in the solution. The mechanical transformation of the cercariae into NTS was performed by physically removing the tail by constricted passage through a Luer-Lok tip in between two 12 mL syringes. The NTS was resuspended in M199 medium supplemented with 5% v/v iFCS, 1% pen/strep, and 1% antifungal mix.

In Vitro Antischistosomal Drug Assay: The drug assay in the EIM platform was performed by first dispensing 30 µL of NTS solution with 1 NTS 2 μL^{-1}. After 1 h recording of the NTS-induced fluctuations as

© 2020 WILEY-VCH Verlag GmbH & Co. KGaA, Weinheim

baseline activity, 30 µL of drug solution (1.5–50 µm in NTS medium) were added, yielding a total volume of 60 µL in each analysis unit. Final drug concentrations ranged between 0.75 and 25 µm in a 2× dilution series. In each assay, 0.5% v/v DMSO (vehicle control) and blank M199 medium controls were included. All conditions were measured in quadruplicates. NTS viability under each test condition was measured every 15 min for 48 h in the EIM platform. A viability score ranging from 0 to 1 (0 = non motile and dead parasite, 1 = motile and alive parasite) was assigned to each test condition and per time point, according to the relative motility of the parasites with respect to the vehicle control motility (see Data Analysis for more information).

In parallel, identical drug concentrations were set up in a 96-well plate (cat. no. 83.3924, Sarstedt, Nümbrecht, Germany) to perform the same experiment by using the standard visual scoring method to compare the results obtained via standard viability detection with the impedance-based characterization. 50 µL of 2 NTS 1 µL^{-1} suspension were dispensed in each well, and subsequently 50 µL of drug-concentration solutions were added to reach a final drug concentration ranging from 0.75 to 25 µm. Each condition was prepared in duplicates or triplicates. A trained operator evaluated the viability of the NTS in the different drug solutions assigning a score from 0 to 3 on a quarter-of-a-point scale. In this scale, 0 represents NTS with complete loss of motility, while 3 represents NTS with good motility, good overall viability, and healthy behavior.[12] Visual scoring was carried out after 24 and 48 h of drug incubation.

Each drug test was performed in a separate experiment.

Chip Fabrication: The analysis chip consisted of two parts: a polydimethylsiloxane (PDMS) layer containing the microfluidic structures and a glass slide with a patterned metal layer. The PDMS layer was cast from a 3D-printed master mold (fabricated in Accura SL 5530, Protolabs, Feldkirchen, Germany) by using soft lithography. The silicone and curing agent (Sylgard 184, Dow Corning Corp., Midland, USA) were mixed at a 10:1 w/w ratio, degassed, and poured onto the master mold. After curing or 2 h at 85 °C, the PDMS layer was peeled off the master mold and cut into individual chips.

The 200-nm-thick platinum electrodes were deposited on a 6-in., 500-µm-thick borosilicate glass wafer via a lift-off process. Briefly, the wafer was spin-coated with lift-off resist (LOR3B, Microchem Corp., Newton, USA), followed by a positive photoresist (S1813, Rohm-Haas, Schwalbach, Germany), and patterned using photolithography. After Pt deposition, the lift-off of the metal was carried out by using Mr-Rem-400 remover (micro resist technology GmbH, Berlin, Germany). Finally, the glass wafer was diced into individual glass slides (20 mm × 62 mm).

Each PDMS chip and patterned glass slide were aligned using a custom-made alignment tool and irreversibly bonded together after surface treatment using oxygen plasma (Harrick Plasma PDC-002, Harrick Plasma, Ithaca, USA).

Parylene Coating of PDMS Chip: To prevent drug absorption by PDMS during long-term compound incubation (48 h), we coated the chip surface with parylene-C polymer.[30,44] All microfluidic chips were coated using a parylene coating system (Parylene P6, Diener Electronic GmbH, Ebhausen, Germany). The devices were placed in the center of the rotating trays in the deposition chamber. 10 g of parylene-C dimer powder (parylene, Diener Electronic GmbH, Ebhausen, Germany) were placed into the evaporator. The system was evacuated to 0.012 mbar before the deposition was initiated. The powder was evaporated in a temperature range of up to 170 °C, cleaved in the pyrolysis tube at 720 °C, and deposited onto the samples at 80 °C and 0.03 mbar over the course of 4.2 h (Figure S2A, Supporting Information). After the evaporation of the parylene powder, the deposition chamber was cooled down to 41 °C and the devices were then removed from the coating system.

The thickness of the deposited parylene-C layer was evaluated by using a 3D optical surface profiler (Zygo Corporation, Middlefield, USA) on a microscope slide (Menzel-Gläser, Thermo Scientific, Dreieich, Germany), placed in the chamber with the devices (Figure S2B, Supporting Information). For this purpose, the parylene layer was cut, one part was pealed from the glass slide, and the thickness was measured along the cut.

Rhodamine Absorption Evaluation: To compare the dye absorption in parylene-coated PDMS and bare PDMS chips, 30 µL of rhodamine B (83689, Sigma-Aldrich, Buchs, Switzerland) solution (0.1 mm in DI water) were loaded into each well chamber. Fluorescence images inside the chambers were captured before the loading of the dye, at 5 min, 1 and 2 h after sample loading using an inverted microscope (Nikon Ti-E, Nikon, Egg, Switzerland). During the measurements, the chips were kept in the dark to prevent photobleaching and at 37 °C, 5% CO_2 using a stage-top incubator. The microscope was controlled using Youscope software, and offline image analysis was performed using ImageJ (Figure S3, Supporting Information).

EIM Platform Assembly: The chips were placed between a custom-made printed-circuit board (PCB) and a chip holder (Figure S8, Supporting Information). The PCB was designed in Altium Designer 17.0 and ordered from PCBWay (Hangzhou, China). Electrical connections between the PCB and the analysis chips were obtained by contacting the electrode pads from above using spring-loaded pins (0956-0-15-20-75-14-11-0, Mill-Max Mfg. Corp., Oyster Bay, USA). The PCB featured four window-like openings (15 mm × 58 mm) to allow for visual access to the chips without disassembling the platform.

The chip holder was 3D-printed by means of stereolithography (Protolabs, Feldkirchen, Germany) in ABS-like material (Accura Xtreme White 200, Protolabs, Feldkirchen, Germany). The printing material was selected as to withstand the high-humidity conditions in the incubator and the high force levels required for reliable chip connection. The chip holder also featured four openings to allow for visual examination of the parasites using a standard inverted microscope.

Neodymium block magnets (Q-10-03-02-HN, Supermagnete, Uster, Switzerland) were used to align and keep the chip holder and PCB in position, and to provide the force necessary for pressing the spring-loaded pins onto the electrode pads on the chips for stable electrical connection. The magnets were attached to the chip holder and the PCB with a 2-component white epoxy adhesive (EA 9492, Henkel, Düsseldorf, Germany). Finally, the platform was covered with an omniTray lid (Nunc OmniTray Single-Well Plate, Thermo Fisher Scientific, Reinach, Switzerland) to prevent medium evaporation from the culture units.

Impedance Measurement: Impedance measurements were performed using a HF2-LI impedance spectroscope (Zurich Instruments AG, Zurich, Switzerland). The analysis chips were contacted via a custom-made PCB to route the connections from the impedance spectroscope to the integrated electrodes. An AC voltage with an amplitude of 100 mV and a frequency of 500 kHz was applied between the selected pair of coplanar electrodes. The current flowing through the system was then converted to voltage through a trans-impedance amplifier (HF2TA, Zurich Instruments AG, Zurich, Switzerland) with a 1-kΩ feedback resistor and sampled by the HF2-LI with a sampling frequency of 14 kHz. The acquired signal was filtered with a 2.2-kHz low-pass filter in the impedance spectroscope. The amplitude variation of the sampled current-to-voltage signal was then used for further analysis. A custom-made software, written in Python, was used to control the selection of the electrode pair and to control the signal acquisition.

Microscopy: During the recording of the impedance signals, the platform was placed on the stage of an automated microscope. Microscopic images were obtained using an inverted microscope (Nikon Ti-E, Nikon, Egg, Switzerland), placed in an environmental control box, which maintained a stable temperature of 37 °C, CO_2 of 5%, and a relative humidity of ≈90%. Bright-field images were captured on the Nikon microscope using a Nikon Plan Fluor 10X objective (NA 0.3, WD 16 mm). Automated imaging was performed for 20 s every hour from each analysis unit during the entire experiment. The live micrographs were recorded to compare the results of the gold-standard evaluation (visual scoring) with those obtained by the impedance-based readout. The microscope was controlled using Youscope software, and offline image analysis was performed using ImageJ.

For standard visual assessment, the parasites were incubated in culture medium with the test compounds in a 96-well plate in duplicates/triplicates for 48 h. Every 24 h, the drug effects on the parasites were

© 2020 WILEY-VCH Verlag GmbH & Co. KGaA, Weinheim

assessed by visual scoring with a light microscope using a magnification of 4–10×.

Computational Modeling: A finite-element-method (FEM) model was used to verify the current-density distribution in the microwell (Figure S4A, Supporting Information). The current passing through the electrodes in the measurement chamber was calculated by integrating the current density over the middle orthogonal cross section area of the microwell in Comsol Multiphysics 5.4 (COMSOL AB, Stockholm, Sweden). To evaluate the current density across the entire depth of the microwell, the current was derived over the microwell height (Figure S4B, Supporting Information).

Data Analysis: The voltage-converted current signals were processed and analyzed in MATLAB (The MathWorks Inc., Natick, USA). The recorded signals were filtered using a 0.2-Hz high-pass filter to remove slow signal variation due to solution evaporation. Each analysis unit may exhibit different baseline values due to differences in solution conductivity caused, for example, by different drug compounds or drug concentrations, or by subtle variations in the alignment of the electrodes with the microwell base. To reduce the influence of such effects, the high-pass-filtered traces were normalized with respect to the mean baseline signal of the respective unit. To quantify the signal fluctuations induced by the parasites, the power of the filtered and normalized signal was computed in a 1–3 Hz bandwidth. This approach minimizes the effect of readout noise, which is present at higher frequencies, while it preserves the signal power that is related to the movement of the NTS between the electrodes. To confirm that the sample was correctly loaded in the microwell, the signal power was first measured during 1 h prior to addition of the drug compound. Only analysis units, the signal power of which ranged between (–18.5, –7.1) dBμ (± 3 standard deviations of the average NTS motile value, –12.8 ± 1.9 dBμ), were further analyzed. The runtime calculated power of the measured fluctuations in each unit was normalized to its initial power magnitude (t_{-1hr}) in order to compare measurements with different numbers of NTS in the sensing compartments and to extract motility index parameters. To evaluate NTS viability, the motility index of every condition was normalized to the motility index of the vehicle control. This procedure followed the normalization performed in the standard drug assay using visual scoring and it helped to remove NTS phenotype variations caused by the vehicle.[21] In addition, a viability value of 1 was assigned to all the microwells in which the NTS showed a motility equal or higher than that in the vehicle control microwells.

The viability scores obtained from visual evaluation were averaged across replicates and normalized to the vehicle-control viability score.

The half-maximum inhibitory concentration (IC_{50}) values of the tested drugs were determined for both visual-inspection-based and impedance-based viability scores by applying a nonlinear least-squares analysis. A two-parameter sigmoid function with a constant hill slope was fitted to the viability scoring data. A single average slope was first computed across all experimental time points for each drug and then applied to the fit for the estimation of the IC_{50} during the continuous long-term measurements.

The Z′-factor of the impedance-based assays was computed to determine the suitability of the EIM platform for high-throughput screening applications.[36,37] The Z′-factor is defined as

$$Z' - \text{factor} = 1 - \frac{3\sigma_{+} + 3\sigma_{-}}{|\mu_{+} - \mu_{-}|}$$

where $\mu+$ and $\mu-$ indicate the mean signal power of alive (motile and pre-treated) and dead (non-motile) schistosomula and $\sigma+$ and $\sigma-$ the corresponding standard deviations.

Supporting Information

Supporting Information is available from the Wiley Online Library or from the author.

Acknowledgements

P.S.R. and F.C.L. contributed equally to this work. The work was financially supported by Swiss National Science Foundation under contract CR32I2_166329: “Infected body-on-chip” and the Swiss Commission for Technology and Innovation under contract 25727.1 PFLS-LS: “Broadband high-accuracy impedance analyzer.” The authors acknowledge the clean-room facility at D-BSSE, ETH Zurich, for help and support. Further, the authors would like to thank Carlo Cosimo Campa, Fernando Cardes, Nassim Rousset, and Vijay Viswam, all at D-BSSE of ETH Zurich, for their scientific input and support throughout the project.

Conflict of Interest

The authors declare no conflict of interest.

Keywords

drug screening, microfluidic impedance-based system, pharmacodynamics, *Schistosoma mansoni*, schistosomiasis

Received: December 20, 2019
Revised: May 19, 2020
Published online: June 8, 2020

---

[1] L. Conteh, T. Engels, D. H. Molyneux, *Lancet* **2010**, *375*, 239.
[2] H.-B. Weng, H.-X. Chen, M.-W. Wang, *Infect. Dis. Poverty* **2018**, *7*, 67.
[3] D. P. McManus, D. W. Dunne, M. Sacko, J. Utzinger, B. J. Vennervald, X.-N. Zhou, *Nat. Rev. Dis. Primers* **2018**, *4*, 13.
[4] B. Gryseels, K. Polman, J. Clerinx, L. Kestens, *Lancet* **2006**, *368*, 1106.
[5] D. G. Colley, A. L. Bustinduy, W. E. Secor, C. H. King, *Lancet* **2014**, *383*, 2253.
[6] J. F. Friedman, R. M. Olveda, M. H. Mirochnick, A. L. Bustinduy, A. M. Elliott, *Bull. W. H O.* **2018**, *96*, 59.
[7] D. Cioli, L. Pica-Mattoccia, A. Basso, A. Guidi, *Mol. Biochem. Parasitol.* **2014**, *195*, 23.
[8] D. Cioli, L. Pica-Mattoccia, *Parasitol. Res.* **2003**, *90*, S3.
[9] A. C. Mafud, M. P. N. Silva, G. B. L. Nunes, M. A. R. de Oliveira, L. F. Batista, T. I. Rubio, A. C. Mengarda, E. M. Lago, R. P. Xavier, S. J. C. Gutierrez, P. L. S. Pinto, A. A. da Silva Filho, Y. P. Mascarenhas, J. de Moraes, *Toxicol. In Vitro* **2018**, *50*, 1.
[10] R. A. Paveley, Q. D. Bickle, *Parasite Immunol.* **2013**, *35*, 302.
[11] A. M. C. Canavaci, J. M. Bustamante, A. M. Padilla, C. M. Perez Brandan, L. J. Simpson, D. Xu, C. L. Boehlke, R. L. Tarleton, *PLoS Negl. Trop. Dis.* **2010**, *4*, e740.
[12] F. C. Lombardo, V. Pasche, G. Panic, Y. Endriss, J. Keiser, *Nat. Protoc.* **2019**, *14*, 461.
[13] J. Keiser, *Parasitology* **2010**, *137*, 589.
[14] E. Peak, K. F. Hoffmann, *An. Acad. Bras. Ciênc.* **2011**, *83*, 649.
[15] D. Das, V. Ramachandra, S. Islam, H. Bhattacharjee, J. Biswas, A. Koul, P. Deka, A. Deka, *Indian J. Ophthalmol.* **2016**, *64*, 794.
[16] T. Manneck, O. Braissant, Y. Haggenmuller, J. Keiser, *J. Clin. Microbiol.* **2011**, *49*, 1217.
[17] L. Tritten, A. Silbereisen, J. Keiser, *Int. J. Parasitol.* **2012**, *2*, 98.
[18] R. A. Paveley, N. R. Mansour, I. Hallyburton, L. S. Bleicher, A. E. Benn, I. Mikic, A. Guidi, I. H. Gilbert, A. L. Hopkins, Q. D. Bickle, *PLoS Negl. Trop. Dis.* **2012**, *6*, e1762.
[19] N. R. Mansour, Q. D. Bickle, *PLoS Negl. Trop. Dis.* **2010**, *4*, e795.
[20] G. Rinaldi, A. Loukas, P. J. Brindley, J. T. Irelan, M. J. Smout, *Int. J. Parasitol.* **2015**, *5*, 141.

[21] K. Chawla, M. M. Modena, P. S. Ravaynia, F. C. Lombardo, M. Leonhardt, G. Panic, S. C. Bürgel, J. Keiser, A. Hierlemann, *ACS Sens.* **2018**, *3*, 2613.

[22] T. Sun, H. Morgan, *Microfluid. Nanofluid.* **2010**, *8*, 423.

[23] S. C. Bürgel, L. Diener, O. Frey, J. Y. Kim, A. Hierlemann, *Anal. Chem.* **2016**, *88*, 10876.

[24] G. Panic, M. Vargas, I. Scandale, J. Keiser, *PLOS Negl. Trop. Dis.* **2015**, *9*, e0003962.

[25] N. Vale, M. J. Gouveia, G. Rinaldi, P. J. Brindley, F. Gärtner, J. M. Correia da Costa, *Antimicrob. Agents Chemother.* **2017**, *61*, e02582-16.

[26] V. Silva-Moraes, F. F. B. Couto, M. M. Vasconcelos, N. Araújo, P. M. Z. Coelho, N. Katz, R. F. Q. Grenfell, *Mem. Inst. Oswaldo Cruz* **2013**, *108*, 600.

[27] R. K. Parakh, N. S. Patil, *Int. J. Res. Med. Sci.* **2018**, *6*, 383.

[28] J. Keiser, T. Manneck, M. Vargas, *J. Antimicrob. Chemother.* **2011**, *66*, 1791.

[29] A. C. K. Fontana, M. S. Sonders, O. S. Pereira-Junior, M. Knight, J. A. Javitch, V. Rodrigues, S. G. Amara, O. V. Mortensen, *Eur. J. Pharmacol.* **2009**, *616*, 48.

[30] H. Sasaki, H. Onoe, T. Osaki, R. Kawano, S. Takeuchi, *Sens. Actuators, B* **2010**, *150*, 478.

[31] M.-H. Abdulla, D. S. Ruelas, B. Wolff, J. Snedecor, K.-C. Lim, F. Xu, A. R. Renslo, J. Williams, J. H. McKerrow, C. R. Caffrey, *PLoS Negl. Trop. Dis.* **2009**, *3*, e478.

[32] B. J. Neves, R. F. Dantas, M. R. Senger, W. C. G. Valente, J. D. M. Rezende-Neto, W. T. Chaves, L. Kamentsky, A. Carpenter, F. P. Silva-Junior, C. H. Andrade, *MedChemComm* **2016**, *7*, 1176.

[33] E. Peak, I. W. Chalmers, K. F. Hoffmann, *PLoS Negl. Trop. Dis.* **2010**, *4*, e759.

[34] C. Lalli, A. Guidi, N. Gennari, S. Altamura, A. Bresciani, G. Ruberti, *PLoS Negl. Trop. Dis.* **2015**, *9*, e0003484.

[35] B. Ramirez, Q. Bickle, F. Yousif, F. Fakorede, M.-A. Mouries, S. Nwaka, *Expert Opin. Drug Discov.* **2007**, *2*, S53.

[36] G. S. Sittampalam, N. P. Coussens, M. Arkin, D. Auld, C. Austin, B. Bejcek, M. Glicksman, J. Inglese, P. W. Iversen, J. Mcgee, O. Mcmanus, L. Minor, A. Napper, J. M. Peltier, T. Riss, O. J. Trask, J. Weidner (Eds) in *Assay Guidance Manual*, Eli Lilly & Company and the National Center For Advancing Translational Sciences, Bethesda, MD **2004**.

[37] J. H. Zhang, T. D. Y. Chung, K. R. Oldenburg, *J. Biomol. Screen.* **1999**, *4*, 67.

[38] M. J. Smout, A. C. Kotze, J. S. McCarthy, A. Loukas, *PLoS Negl. Trop. Dis.* **2010**, *4*, e885.

[39] R. Pax, R. Fetterer, J. L. Bennett, *Comp. Biochem. Physiol. Part C Comp. Pharmacol.* **1979**, *64*, 123.

[40] T. Manneck, J. Keiser, J. Müller, *Parasitology* **2012**, *139*, 497.

[41] N. Patocka, P. Ribeiro, *Mol. Biochem. Parasitol.* **2013**, *187*, 32.

[42] J. P. Boyle, T. P. Yoshino, *J. Parasitol.* **2005**, *91*, 542.

[43] J. N. Milligan, E. R. Jolly, *J. Vis. Exp.* **2011**, *54*, 3191.

[44] M. W. Toepke, D. J. Beebe, *Lab Chip* **2006**, *6*, 1484.

© 2020 WILEY-VCH Verlag GmbH & Co. KGaA, Weinheim

Chapter III:

Evaluation of human liver microtissues for drug screening on *Schistosoma mansoni* schistosomula

ACS Infectious Diseases

pubs.acs.org/journal/aidcbc

Article

Evaluation of Human Liver Microtissues for Drug Screening on *Schistosoma mansoni* Schistosomula

Flavio C. Lombardo, Paolo S. Ravaynia, Mario M. Modena, Andreas Hierlemann, and Jennifer Keiser*

Cite This: https://dx.doi.org/10.1021/acsinfecdis.0c00614

Read Online

ACCESS | Metrics & More | Article Recommendations | Supporting Information

Downloaded via UNIV OF BASEL on November 3, 2020 at 15:28:04 (UTC).
See https://pubs.acs.org/sharingguidelines for options on how to legitimately share published articles.

ABSTRACT: Schistosomiasis is a major neglected tropical disease with more than 200 million infections annually. Despite only one drug, praziquantel, being available, the drug pipeline against schistosomiasis is empty, and drug screening tools have limitations. We evaluated the potential of human liver microtissues (hLiMTs) in antischistosomal drug discovery. Because hLiMTs express all human P450 enzymes, they are an excellent tool to evaluate compounds' bioinactivation, bioactivation, and toxicity. To validate the metabolic conversion capacity of hLiMTs, we first quantified (*R*)- and (*S*)-praziquantel and the main metabolite *trans*-OH-praziquantel following incubation with 0.032−50 μM (0.01−15.62 μg/mL) praziquantel for up to 72 h by a validated LC-MS/MS method. We cocultured hLiMTs with newly transformed schistosomula (NTS) and evaluated the antischistosomal activity and cytotoxicity of three prodrugs terfenadine, tamoxifen citrate, and flutamide. HLiMTs converted 300−350 ng (*R*)-praziquantel within 24 h into *trans*-OH-praziquantel. We observed changes in the IC_{50} values for terfenadine, flutamide, and tamoxifen citrate in comparison to the standard NTS assay *in vitro*. Cytotoxicity was observed at high concentrations of flutamide and tamoxifen citrate. An *in vitro* platform containing hLiMTs could serve as an advanced drug screening tool for *Schistosoma mansoni*, providing information on reduced or increased activity and toxicity.

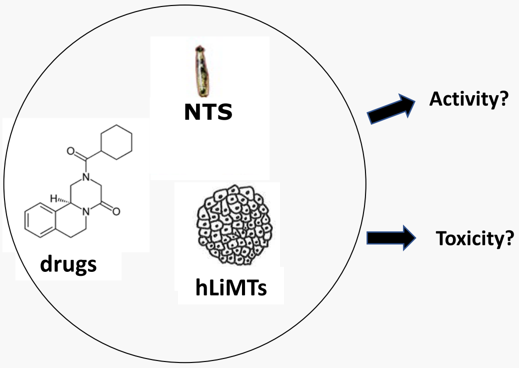

KEYWORDS: *Schistosoma mansoni, primary human liver microtissue, praziquantel, drug screening*

Schistosomiasis causes a tremendous public health burden, affecting annually more than 200 million people worldwide.[1,2] The parasites mainly responsible for the disease are *Schistosoma haematobium*, *S. japonicum*, and *S. mansoni*.[2,3] More than 90% of the cases occur in sub-Saharan Africa.[3] Only one drug, praziquantel, has been available for decades to treat schistosomiasis.[4,5] Oxamniquine had been commonly used against *S. mansoni* for about 40 years, but after massive use, especially in South America, resistant strains were frequently detected, leading to the abandonment of oxamniquine as treatment option.[6] Therefore, novel drug candidates to fill to the empty drug pipeline are urgently needed in case of emergence of praziquantel resistant strains.[1]

Currently, the research for antischistosomal compounds has limitations. The drug screening procedure is mainly based on phenotypic screenings, which are performed by microscopy-based visual scoring of the fitness of parasites by trained operators. This procedure is laborious, subjective, and slow.[7] However, the effect of a compound can be observed on the parasite directly rather than on an isolated component, which captures complex biological mechanisms. Moreover, this system can be relatively easily modified and sophisticated.

The human primary liver microtissues (hLiMTs) are a rather novel technology,[8] which has been explored in toxicology studies for evaluation of drug-induced liver injuries (DILIs),[9,10] because hLiMTs might indicate toxicity that otherwise might be overlooked in animal studies.[11] It has been shown that about 60% of drug-induced toxic effects could be predicted using microtissue-based liver systems, whereas standard rodent-based drug testing showed only roughly 40% of those toxic effects in comparative studies.[10,12]

Moreover, the three-dimensional structure of the microtissues triggers and enhances some physiological mechanisms that would not be reproduced in two-dimensional cell cultures, such as activity of the cytochrome P450 enzymes (CYP450) and cell polarization.[10,12,13] Microtissue models offer a microenvironment that better represents *in vivo* conditions with respect to cell shape, adhesion, behavior, topology, and morphology.[10,14] One important advantage offered by this 3D cell-culture technology is the possibility to coculture different cell types that can self-assemble and mimic tissue/organ organization.[10] Because these primary human hepatocytes

Special Issue: In Celebration of Jonathan Vennerstrom: A Pioneer in Neglected Tropical Diseases

Received: August 30, 2020

ACS Publications
© XXXX American Chemical Society

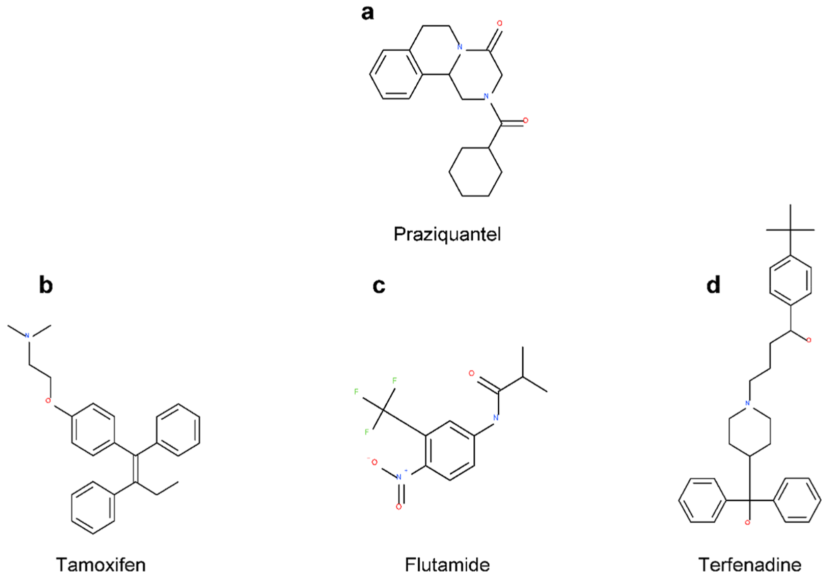

Figure 1. Structures of drugs tested in this study: (a) praziquantel, (b) tamoxifen, (c) flutamide, and (d) terfenadine.

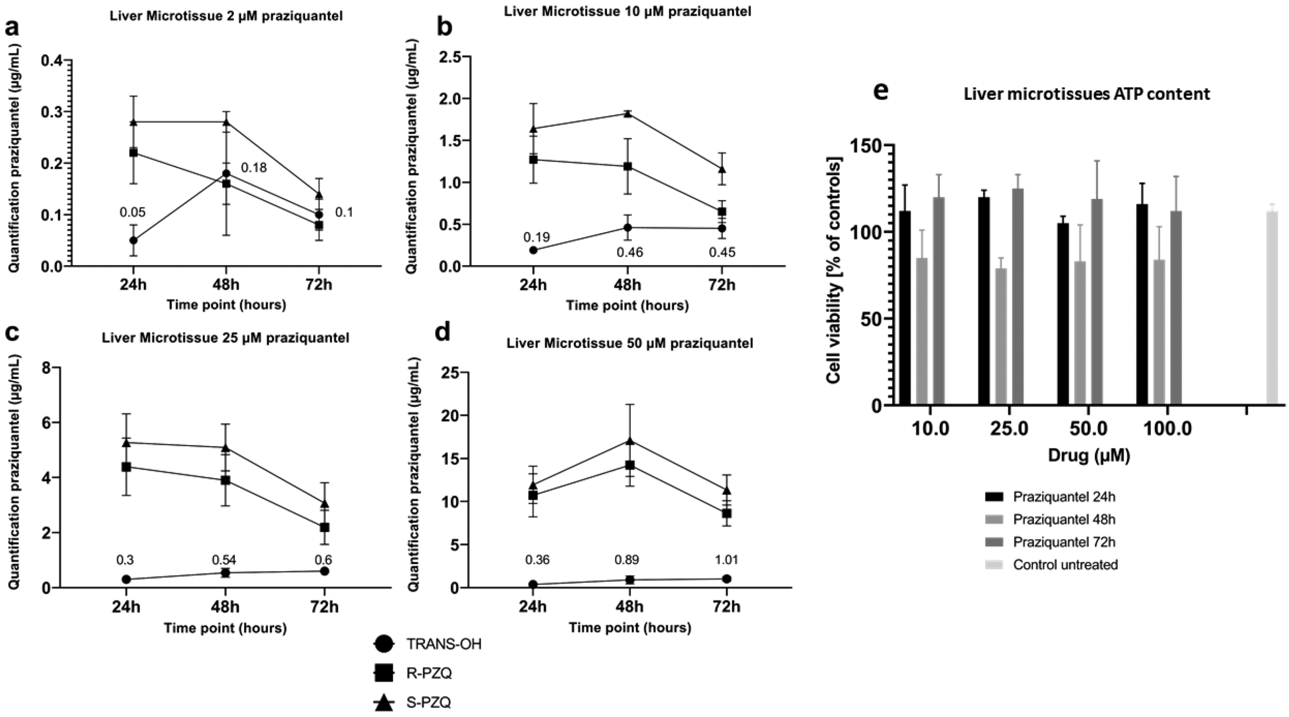

Figure 2. (*R*)-Praziquantel, (*S*)-praziquantel, and *trans*-OH-praziquantel quantified by LC-MS/MS following exposure of hLiMTs to praziquantel for a period of 3 days for (a) 2 μM praziquantel, (b) 10 μM praziquantel, (c) 25 μM praziquantel, and (d) 50 μM praziquantel. Error bars represent the standard deviation of three independent experiments. (e) ATP content of hLiMTs after 24, 48, and 72 h of incubation with praziquantel (without NTS); as reference, untreated separate parallel controls were used. The standard deviation is indicated as error bars from triplicate experiments.

(PHH) are harvested directly from human donors, they feature high expression levels of CYPP450 enzymes such as P450-4A3 and P450-2E9, which are comparable to the *in vivo* situation.[10]

In this study, we tested hLiMTs as a component of a phenotypic drug screening assay for schistosomiasis. We first established the system by incubating hLiMTs with newly transformed schistosomula (NTS). We next assessed the activity and metabolic conversion of the hLiMTs with the antischistosomal drug praziquantel, known to be quickly metabolized with P450 cytochromes into *trans*-4-hydrodoxypraziquantel by LC-MS/MS-based quantification. In a case study, we evaluated the effects of different doses of the prodrugs terfenadine, flutamide, and tamoxifen citrate (Figure 1) in the newly established system of an NTS and hLiMTs coculture. The compounds were selected for their known first pass liver metabolism and/or for their hepatoxicity. We measured ATP content of hLiMTs as proxy to test eventual drug cytotoxicity because ATP is a valid marker to measure cell viability. This new system could serve as an advanced preclinical tool to identify safe and active antischistosomal compounds.

■ RESULTS

Validation of the hLiMTs-Based Drug Screening with Praziquantel. To compare the liver microtissue-based system to the standard *in vitro* assay on NTS, we used praziquantel as a test drug, and in the first step assessed a potential toxicity. We exposed the cocultures of NTS and hLiMTs to different concentrations of praziquantel. To confirm that praziquantel was not detrimental to the hLiMTs, we studied the toxicity of praziquantel on the hLiMTs over a period of 72 h by measuring intracellular ATP content (Figure 2). The data suggest that the ATP content is stable (ranging from 74 to 135%) regardless of praziquantel concentration and evaluation time point for a period of 3 days.

LC-MS/MS Method Partial Validation. To reliably verify the robustness of the LC-MS/MS quantification method, we performed a partial interday validation, which was analyzed by comparing three separate and independent validation tests that were run on separate days. In every run, at least 75% of the calibration line samples were within a precision of ±15% (±20% for the LLOQ) to the nominal concentrations. The fitted linear regression values R^2 were >0.995 for every set. The accuracy was between 85 and 115% and 80−120% for the LLOQ. At least 67% of the QC samples were within a precision of ±15% and ±20% for the LLOQ. The accuracy was calculated to lie between 85 and 115% (LLOQ: 80−120%). We analyzed the coefficient of variation of the QC replicates in each set, and it was found to be below 7% intra-assay between separate sets (Table S1).

Evaluation of Accuracy, Precision, and Matrix Effect. We considered the samples below the LLOQ 10 ng/mL as 0, as indicated by the FDA guidelines.[15] Each set was within ±15% and ±20% for the LLOQ. The interassay accuracy was between 94 and 103%, with the highest variation of 9.2% observed at the high QC (2000 ng/mL) for (*S*)-praziquantel. The interday precision was between 3 and 7% for the LLOQ values and 5% for the ULOQ. The matrix effects were between 91 and 107% overall (Table S1). The highest matrix effect value was determined for the ULOQ QC (2000 ng/mL) for (*R*)-praziquantel and an intersample deviation of 5%. The matrix effect lowest value (91% for (*S*)-praziquantel) was calculated for the low LLOQ QC (10 ng/mL). In the low QC, we observed a standard deviation of 12% for (*R*)-, 10% for (*S*)-praziquantel, and 3% for *trans*-OH-praziquantel. The total recovery values were between 103 and 105% for (*R*)-praziquantel (lowest to highest concentration) and 89−104% for (*S*)-praziquantel. The total recovery of *trans*-OH-praziquantel was between 92 and 98%. Results are summarized in Table S 1.

Praziquantel and *trans*-OH-Praziquantel Quantification by LC-MS/MS. To evaluate the functionality of the metabolism of the hLiMTs, we sampled the supernatant from microtissues exposed to praziquantel every 24 h by LC-MS/MS, quantifying (*R*)-,(*S*)-, and the metabolite *trans*-OH-praziquantel. *trans*-OH-praziquantel was detected after 24 h, increasing from 323 ng/mL at 24 h to 828 ng/mL at 72 h when the microtissues were exposed to the highest concentration tested, 50 μM praziquantel (Figure 2). A similar trend was observed for the lower concentrations tested. In praziquantel control samples (no microtissues, incubation for 72 h at 37 °C) praziquantel was found to be stable (no *trans*-OH-praziquantel present) (Table S2).

Activity Evaluation of Tamoxifen Citrate, Flutamide, And Terfenadine. We evaluated the IC_{50} values of tamoxifen citrate, flutamide, and terfenadine in the hLiMTs assay and in the standard drug assay (Table 1). The evaluation was performed by visual screening as described elsewhere.[7] Tamoxifen citrate-treated-NTS showed over the course of 72 h a gradual decrease in movements and at 72 h a darkening of the tegument in both hLiMTs' coculture and standard drug screening; however, the changes were more accentuated in the standard NTS drug assay. Terfenadine-treated NTS revealed a darkening and reduction of movements, which was highly pronounced in the standard assay, while less visible in with the hLiMT assay. In the case of flutamide in the standard NTS assay, changes of motility and morphology became evident mostly at 72 h, while NTS coincubated with hLiMTs showed a reduction of movements after 24 h that gradually increased at 48 and 72 h.

Table 1. IC_{50} Values Calculated for Praziquantel and Three Test Drugs on NTS Using an Assay Containing hLiMTs versus the Standard Assay[a]

	IC_{50} microtissues (μM)			IC_{50} standard assay (μM)		
compound	24 h	48 h	72 h	24 h	48 h	72 h
praziquantel	1.9	1.8	3.1	1.4	2.5	2.5
flutamide	5.1*	16.0	16.2	>50	25.1	0.1
tamoxifen citrate	4.7*	6.5*	3.5*	3.2	1.8	0.5
terfenadine	1.5	1.6*	0.8*	1.7	0.8	0.4

[a] IC_{50} calculated from experiment triplicates every 24 h for 72 h. The values marked with * show a statistical significance in comparison with the same time point without liver microtissues with *p*-values <0.05 tested by a two-way ANOVA.

A significant difference in IC_{50} values was observed when comparing the two systems after 48 and 72 h for terfenadine (1.6 μM in hLiMTs versus 0.8 μM in the standard drug assay and 0.8 μM in hLiMTs versus 0.4 μM in the standard drug assay), tamoxifen citrate (6.5 μM in hLiMTs versus 1.8 μM in the standard drug assay and 3.5 μM in hLiMTs versus 0.5 μM in the standard drug assay), and at 72 h for flutamide (16.2 μM in hLiMTs versus 0.1 μM in the standard drug assay). Drug effect curves for each drug are shown in Figure S1. The mean drug activity of praziquantel and the three drugs on NTS recorded at different concentrations and time points is presented in Table S3.

ATP Quantification Following Incubation with Test Drugs. We evaluated the cell viability measuring ATP content of the hLiMTs after 72 h coincubation with the three test drugs. Tamoxifen citrate reduced the hepatocyte viability to 0 at 25 μM, while the other concentrations yielded a viability above 100%. ATP content following flutamide incubation ranged from 71 to 113%, while terfenadine incubation yielded a cell viability based on ATP content of over 100% at all concentrations tested, as shown in Figure 3.

■ DISCUSSION

In this study, we evaluated for the first time a primary human liver microtissue-based (hLiMTs) assay for drug screening on *S. mansoni* NTS.

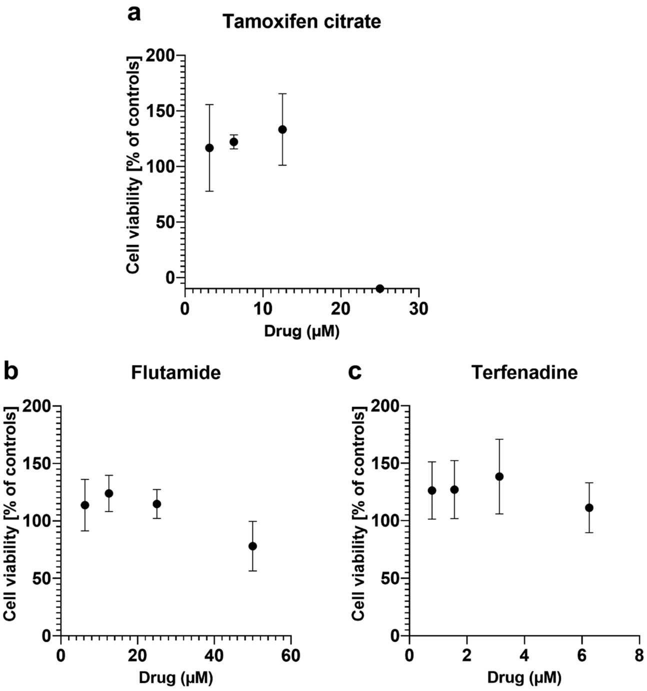

Figure 3. Viability of the liver microtissue is shown by ATP quantification after 72 h coincubation with hLiMTs and NTS for (a) tamoxifen citrate, (b) flutamide, and (c) terfenadine. The error bars indicate the standard deviation of triplicate experiments.

Recently, hLiMTs have been receiving increased attention as a valuable, highly sensitive tool in drug discovery. Compared to traditional approaches, hLiMTs achieve higher sensitivity to predict metabolism or toxicity.[10] For example, in a recent study, S9 liver fractions showed decreased CYP450s enzyme activity in comparison to human primary hepatocytes flat cell cultures.[16] Moreover, compared to the flat cells cultures, hLiMTs were also shown to be more sensitive to overall drug-induced cytotoxicity.[17]

We observed significant differences in the activity of the prodrugs in the microtissue assay versus our standard NTS assay. This finding corroborates the capability of hLiMTs in processing and metabolizing drugs, as demonstrated in the validation part of our study for praziquantel, which is metabolized at a rate of about 300−350 ng/day per single microtissue, and hence, metabolism can bioactivate compounds as well as reducing the activity of others.

In more detail, terfenadine is an antihistaminic drug, which was found to be active on *S. mansoni* NTS and adult worms in a previous study.[18] We observed an increase of the IC_{50} value after coculturing the drug with hLiMTs at 48 and 72 h, which is likely due to conversion of the parent drug into fexofenadin, which is inactive against *S. mansoni in vitro* and *in vivo*.[19,20]

Similarly, tamoxifen citrate, a chemotherapeutic, showed significantly higher IC_{50} in the presence of hLiMTs. The IC_{50} value in the NTS standard assay we obtained in this study is very similar to the one reported by Cowan et al.[21] Tamoxifen citrate is a prodrug and when it undergoes liver processing especially by CYP3A4 and CYP2C9, two metabolites, afimoxifene and endoxifen are formed, both selective estrogen receptor modulators. Our finding is supported by the study of Oliveira et al., where the authors found only 54% activity against adult *S. mansoni* after administration of tamoxifen or tamoxifen citrate *per os* or intraperitoneally in a murine-based study.[22] In the case of flutamide, we also observed a considerable difference in the IC_{50} values after coculturing NTS for 72 h with and without hLiMTs (16.2 μM versus 0.1 μM). Flutamide, a nonsteroidal selective androgen receptor antagonist, is an established prodrug used against prostate cancer,[23] which was reported to show low activity against *S. mansoni in vitro* and *in vivo*.[24] The compound was mainly chosen for its known hepatotoxicity.[23] Indeed, at the highest concentration tested, a decrease in cell viability was detected in the hLiMTs system.

Although we demonstrated that praziquantel is metabolized by hLiMTs when tested against NTS, the IC_{50} values were very similar between standard *in vitro* testing and after coincubation with liver microtissues. This could be due to the fact that praziquantel is active but not lethal, even at very low concentrations on NTS,[25] and slight differences on viability and phenotype might be hard to detect using a visual scoring method,[26] in particular when both the parent drug and metabolites are present in the same wells. Another possibility of the unchanged potency of praziquantel on NTS could be the disproportional reduction of fraction metabolized with increasing concentration of praziquantel as shown in Figure 2. In addition, there was a high uncertainty in the IC_{50} values for praziquantel due to the difficulty in scoring the parasites because of their increased motility and the darkened phenotype of the tegument.

A limitation of our study is that we did not quantify the metabolism of tamoxifen, terfenadine, and flutamide, which would provide additional information on the behavior of the compounds over time. Moreover, the liver microtissues in this study were used as single experimental units, but it might be possible to use multiple microtissues per well to increase the metabolic output. However, if microtissues are pooled together, they could merge and increase in size, which can be detrimental for both viability and drug intake during testing.[27] Furthermore, microtissues are costly, and the implementation at a larger scale can result in high costs. Hence, it is debatable whether a sophistication of a phenotypic stage is required already at this early stage of antischistosomal drug discovery. Lastly, additional studies underlining the advantages of the hLiMTs in comparison with 2d primary hepatocytes cultures for the discovery of novel antischistosomal compounds are necessary to evaluate the method's full potential.

■ CONCLUSION

Our liver-based screening assay represents the first study integrating hLiMTs in the drug screening process for schistosomiasis. The data indicate that the hLiMTs are useful for detecting changes in the activity of test drugs on NTS due to drug metabolism as well as toxicity in a single test system. More studies need to be conducted to confirm these findings with other drugs. An improved coculturing screening system might advance the research in helminth drug discovery by lessening the number of inactive compounds tested *in vivo*, in compliance with the 3R guidelines. Such a system can also better predict compounds' cytotoxicity.

■ METHODS

Newly Transformed Schistosomula (NTS). *Schistosoma mansoni* cercariae of a Liberian strain were harvested from light-exposed infected *Biomphalaria glabrata* snails. Once the cercariae were shed, they were mechanically transformed into NTS as described elsewhere.[7] They were then cultured at 37 °C, 5% CO_2 in M199 medium (Gibco, USA, cat. no. 22340-020), enriched with 5% v/v iFCS (Bioconcept AG, Switzerland, cat. no. 2-01F30-I), 1% v/v penicillin/streptomycin 10 000 U/mL (Sigma-Aldrich, Switzerland, cat. no. P4333-100 ML), 1% v/v antifungal and antibacterial cocktail, as described elsewhere.[7] All media were filter-sterilized prior usage by using a 0.22 μm filter bottle (Corning Stericup 500 mL, Vitaris AG, Switzerland, cat. no. 431097-COR).

Primary Human Liver Microtissue (hLiMT) System Handling. The multidonor (10) hLiMTs were purchased from Insphero AG (Schlieren, Switzerland). The handling was performed according to the manufacturer's guidelines. Briefly, upon arrival, the sealed Insphero Akura 96 Microtissue Delivery Plate was first centrifuged at 250*g* for 1 min and immediately removed from the inner sealing, followed by medium exchange with Insphero AF medium, prewarmed at 37 °C.

Compounds. All drug stock concentrations (10 mM) were freshly prepared in DMSO (Merck, Zug, Switzerland, cat. no. 276855-2L) before the experiments and kept at −20 °C. Praziquantel as racemic powder (cat. no. P4668-5G), terfenadine (cat. no. T9652-5G), flutamide (cat. no. F9397-1G) and tamoxifen citrate (cat. no. 579000-100MG) were purchased from Sigma-Aldrich (Buchs, Switzerland). Praziquantel was chosen for its fast first pass liver metabolism, while terfenadine, flutamide, and tamoxifen citrate were chosen because they are known prodrugs,[3,20,28] and flutamide reveals hepatotoxic effects.[23]

Coincubation of NTS Directly with hLiMTs. NTS were resuspended in Insphero Tox medium at a concentration of 1 NTS/1 μL. For each test condition, a volume of 10 μL of NTS solution was loaded directly into the Insphero Akura 96 Microtissue Delivery Plate. In parallel, NTS were tested by applying the same drug conditions using the standard drug assay procedure (without microtissues), as described elsewhere.[7] For praziquantel and tamoxifen citrate, we tested a drug concentration range between 3.13 and 25 μM; for terfenadine, we used a drug concentration range between 0.78 and 6.25 μM, and for flutamide, the concentrations ranged from 6.25 to 50 μM. These concentration ranges were preselected by testing the drug compounds on the NTS alone and by evaluating the IC_{50} value. A volume of 45 μL of each of the drug concentrations was added to 10 μL of NTS-suspension and resuspended in Insphero Tox medium at 1 NTS/μL. Finally, each well was filled with 25 μL of Insphero Tox medium, to a final volume of 80 μL. The parasites were incubated at 37 °C, 5% CO_2 and evaluated under the microscope every 24 h for a period of 3 days.

ATP Assay for Viability Evaluation of hLiMT after Drug Exposure. The viability of the hLiMTs alone after praziquantel exposure was evaluated at 24, 48, and 72 h by an ATP assay (Promega AG, Dübendorf, Switzerland, cat. no G9681). In a separate experiment, NTS coincubated with hLiMTs at 37 °C, 5% CO_2 were evaluated at 72 h post coincubation with praziquantel. The other compounds tested were evaluated at 72 h post drug exposure. The ATP quantification was performed by removing the medium and rinsing each well 3 times with 100 μL of sterile PBS to remove the medium and NTS. Later, 40 μL of Celltiter Glo 3D reagent, prediluted 1:1 v/v with sterile PBS, was dispensed into the Akura 96 microtissue plate. The solution was mixed up and down to ensure a homogeneous lysis of the microtissues and left for 30 min in the dark at room temperature within a thermomixer at 350 rpm (Themomixer C, Eppendorf, Hamburg, Germany). The solutions from the microtissue plates were collected and dispensed into 96 half-volume well plates (Corning, Root, Switzerland, cat. no. CLS4580-10EA). Each half-volume plate was then read with the Dynex MLX Luminometer (Dynex Technologies, Inc., Denkendorf, Germany) set for bioluminescence data acquisition. As standard for the assay quantification, adenosine 5′-triphosphate disodium salt hydrate (ATP) was used (Sigma-Aldrich, Buchs, Switzerland, cat. no. A7699-1G). The standard was diluted from 10 to 0.156 μM in duplicate. The ATP solutions were freshly prepared in filtered-sterile Milli-Q water to a final concentration of 100 μM before every experiment to avoid ATP decay. We calculated the relative variations in the microtissue cells' viability by the ratio of the quantified ATP under tested conditions and the quantified ATP under control conditions (DMSO 0.5% and blanks) as described elsewhere.[29]

Preparation of the Standards for Liquid Chromatography Tandem Spectroscopy (LC-MS/MS). Quality controls (QCs) and calibration line (CL) samples were freshly prepared before every experiment. One microliter of the appropriate concentration was used as spiking solution by mixing it with 19 μL of the 72-h blank conditioned Insphero TOX medium. The spiking solution was prepared in 10% v/v methanol and 90% v/v filtered Milli-Q water. The CL covered the following drug concentrations of praziquantel and *trans*-OH praziquantel: 0.01, 0.025, 0.05, 0.1, 0.25, 1.0, and 2.0 μg/mL. The QCs were prepared by spiking the following drug concentrations: 0.01, 0.1, 0.5, and 2.0 μg/mL of praziquantel and of *trans*-OH praziquantel. Each of the three validation sets contained the four QCs in six replicates plus a calibration line. The QCs covered the lower limit of quantification (LLOQ), low, middle, and high concentrations as recommended by the Food and Drug Administration (FDA) guidelines for industry for bioanalytical method validation.[15]

To prepare a praziquantel stock solution, praziquantel was dissolved in 100% methanol (Merck, Zug, Switzerland, cat. no. 1.06035.2500) to a final concentration of 5 mg/mL. To prepare the metabolite stock solution, *trans*-OH-praziquantel was dissolved in methanol at 10 mg/mL. This solution was used for preparing the QCs and CLs in the spiking solution. The internal standard (ISTD) stock solution was prepared in pure hyper-grade acetonitrile (Merck, Zug, Switzerland, cat. no. 1142912500) at a concentration of 500 ng/mL of d11-praziquantel (Toronto research, Canada, cat. no. cat. no. P702107). The ISTD stock solution was stored at −20 °C to avoid d11-praziquantel decay. The ISTD working solution was prepared in 20% v/v Milli-Q water, 80% acetonitrile v/v and contained d11-praziquantel at a final concentration of 400 ng/mL. The ISTD working solution was used as extraction solution for the samples.[30]

Validation of the LC-MS Method. A partial validation was performed by running three complete validation sets on three different days, as described elsewhere.[30] We adapted the quantification method from an already validated method for praziquantel quantification from mouse plasma.[30] The recovery was evaluated as spiked-sample concentration, compared to the nominal concentration in solution without matrix. FDA guidelines recommend limits for the quantification of analytes of high, middle, low concentration to be within ±15% of their nominal spiked concentration, or ±20% for the LLOQ.[15] The matrix effect was tested by comparing the normalized area under the curve (AUC) of the extracted and spiked samples of Tox Insphero medium to the AUC of spiked extraction solvent.

LC-MS/MS Method and Instrumentation. All measurements were performed using an Agilent 6460 Series triple quadrupole LC−MS/MS. The apparatus was run by Mass Hunter Workstation software suite (Agilent Technologies, United States, version: B.06.00), as described elsewhere.[30] The HPLC system's six-port switching valve was used to divert the flow to the MS/MS from 3 to 9.5 min. To prevent carry-over effect, we used a solution of 1:1 v/v filtered Milli-Q water and 2-propanol hypergrade (Merck, Zug, Switzerland, cat. no. 1027811000). This solution was used to wash the autosampler's needle after each injection. For every injection, a sample volume of 5 μL was injected for the analysis. A column-trapping system HALO C18, 4.6 × 5 mm, (Optimize Technologies, United States) was used before eluting to the main column for chiral separation, a Lux Cellulose-3 column (cellulose tris(3-chloro-4-methylphenylcarbamate) phase), 150 × 4.6 mm, 3 μm (Phenomenex, United States, cat. no. 00F-4456-B0).

Preparation of LC-MS/MS Samples. The samples were extracted with 180 μL of ISTD working solution containing 400 ng/mL d11-praziquantel in 4:1 v/v acetonitrile/Milli-Q water. After extraction, the samples were thermomixed at 20 °C for 30 min at 350 rpm (Eppendorf Themomixer C, Hamburg, Germany). The samples were filtered directly into 96-deep-well plates (500 μL) (Eppendorf, Switzerland, cat. no. 0030501101) by centrifugation (10 min at 2250*g* and 22 °C) of 2 μm PVDF membrane filter 96-well plates (Corning Life Sciences, CA, United States, cat. no. CLS3508-50EA). The 500 μL 96-deep-well plates were sealed with plastic sealing mats (Eppendorf, Germany, cat. no. 15319247) and immediately run.

Data Analysis and Statistics. For the data analysis, we used GraphPad Prism version 8. The half-maximal inhibitory concentration (IC_{50}) values were calculated by using a least-squares-fit model using a three-parameter nonlinear regression. The statistical model used to evaluate the statistical significance of the IC_{50} comparisons was a two-way ANOVA test with a confidence interval of 95%.

ASSOCIATED CONTENT

Supporting Information

The Supporting Information is available free of charge at https://pubs.acs.org/doi/10.1021/acsinfecdis.0c00614.

> S1: matrix effect and recovery of (*R*)-, (*S*)-, *trans*-OH-praziquantel; Table S2: stability of praziquantel after 96 h incubation at 37 °C with Tox medium; Table S3: mean and standard deviation of the drug effect on NTS at 24, 48, and 72 h post drug exposure; Table S4: dose effect curve parameters; Figure S1: dose effect curves for praziquantel, tamoxifen, terfenadine, and flutamide (PDF)

AUTHOR INFORMATION

Corresponding Author

Jennifer Keiser − *Swiss Tropical and Public Health Institute, CH-4002 Basel, Switzerland; Universität Basel, CH-4001 Basel, Switzerland;* orcid.org/0000-0003-0290-3521; Email: jennifer.keiser@swisstph.ch

Authors

Flavio C. Lombardo − *Swiss Tropical and Public Health Institute, CH-4002 Basel, Switzerland; Universität Basel, CH-4001 Basel, Switzerland*

Paolo S. Ravaynia − *Department of Biosystems Science and Engineering (D-BSSE), ETH Zurich, 4058 Basel, Switzerland*

Mario M. Modena − *Department of Biosystems Science and Engineering (D-BSSE), ETH Zurich, 4058 Basel, Switzerland;* orcid.org/0000-0002-4218-0404

Andreas Hierlemann − *Department of Biosystems Science and Engineering (D-BSSE), ETH Zurich, 4058 Basel, Switzerland;* orcid.org/0000-0002-3838-2468

Complete contact information is available at: https://pubs.acs.org/10.1021/acsinfecdis.0c00614

Author Contributions

F.L., J.K., A.H., M.M., and P.R. designed the study. F.L. performed the experiments, analyzed the data, and wrote the first draft of the manuscript. P.R. and M.M. supported the experiments. All authors revised the manuscript.

Notes

The authors declare no competing financial interest.

ACKNOWLEDGMENTS

We thank Insphero for providing the liver plates and their support. We are grateful to the Swiss National Science Foundation for financial support (CR32I2_166329).

ABBREVIATIONS:

PHH, primary human hepatocytes; hLiMTs, human primary liver microtissues; DILIs, drug-induced liver injuries; CYP450, cytochrome P450; NTS, newly transformed schistosomula; LLOQ, lower limit of quantification; FDA, Food and Drug Administration; ISTD, internal standard

REFERENCES

(1) Keiser, J. (2010) *In vitro* and *in vivo* trematode models for chemotherapeutic studies. *Parasitology 137*, 589−603.

(2) McManus, D. P., Dunne, D. W., Sacko, M., Utzinger, J., Vennervald, B. J., and Zhou, X. N. (2018) Schistosomiasis. *Nat. Rev. Dis Primers 4*, 13.

(3) Gryseels, B., Polman, K., Clerinx, J., and Kestens, L. (2006) Human schistosomiasis. *Lancet 368*, 1106−1118.

(4) Vale, N., Gouveia, M. J., Rinaldi, G., Brindley, P. J., Gartner, F., and Correia da Costa, J. M. (2017) Praziquantel for Schistosomiasis: Single-Drug Metabolism Revisited, Mode of Action and Resistance. *Antimicrob. Agents Chemother. 61*, e02582−16.

(5) Bergquist, R., Utzinger, J., and Keiser, J. (2017) Controlling schistosomiasis with praziquantel: How much longer without a viable alternative? *Infect Dis Poverty 6*, 74.

(6) Valentim, C. L., Cioli, D., Chevalier, F. D., Cao, X., Taylor, A. B., Holloway, S. P., Pica-Mattoccia, L., Guidi, A., Basso, A., Tsai, I. J., Berriman, M., Carvalho-Queiroz, C., Almeida, M., Aguilar, H., Frantz, D. E., Hart, P. J., LoVerde, P. T., and Anderson, T. J. (2013) Genetic and molecular basis of drug resistance and species-specific drug action in schistosome parasites. *Science 342*, 1385−1389.

(7) Lombardo, F. C., Pasche, V., Panic, G., Endriss, Y., and Keiser, J. (2019) Life cycle maintenance and drug-sensitivity assays for early drug discovery in *Schistosoma mansoni*. *Nat. Protoc. 14*, 461−481.

(8) Messner, S., Agarkova, I., Moritz, W., and Kelm, J. M. (2013) Multi-cell type human liver microtissues for hepatotoxicity testing. *Arch. Toxicol. 87*, 209−213.

(9) Tóth, K., Sirok, D., Kiss, Á., Mayer, A., Pátfalusi, M., Hirka, G., and Monostory, K. (2018) Utility of *in vitro* clearance in primary

hepatocyte model for prediction of *in vivo* hepatic clearance of psychopharmacons. *Microchem. J. 136*, 193−199.

(10) Proctor, W. R., Foster, A. J., Vogt, J., Summers, C., Middleton, B., Pilling, M. A., Shienson, D., Kijanska, M., Strobel, S., Kelm, J. M., Morgan, P., Messner, S., and Williams, D. (2017) Utility of spherical human liver microtissues for prediction of clinical drug-induced liver injury. *Arch. Toxicol. 91*, 2849−2863.

(11) Bale, S. S., Vernetti, L., Senutovitch, N., Jindal, R., Hegde, M., Gough, A., McCarty, W. J., Bakan, A., Bhushan, A., Shun, T. Y., Golberg, I., DeBiasio, R., Usta, B. O., Taylor, D. L., and Yarmush, M. L. (2014) *In vitro* platforms for evaluating liver toxicity. *Exp. Biol. Med. (London, U. K.) 239*, 1180−1191.

(12) Olson, H., Betton, G., Robinson, D., Thomas, K., Monro, A., Kolaja, G., Lilly, P., Sanders, J., Sipes, G., Bracken, W., Dorato, M., Van Deun, K., Smith, P., Berger, B., and Heller, A. (2000) Concordance of the toxicity of pharmaceuticals in humans and in animals. *Regul. Toxicol. Pharmacol. 32*, 56−67.

(13) Hendriks, D. F., Fredriksson Puigvert, L., Messner, S., Mortiz, W., and Ingelman-Sundberg, M. (2016) Hepatic 3D spheroid models for the detection and study of compounds with cholestatic liability. *Sci. Rep. 6*, 35434.

(14) Messner, S., Fredriksson, L., Lauschke, V. M., Roessger, K., Escher, C., Bober, M., Kelm, J. M., Ingelman-Sundberg, M., and Moritz, W. (2018) Transcriptomic, Proteomic, and Functional Long-Term Characterization of Multicellular Three-Dimensional Human Liver Microtissues. *Appl. In Vitro Toxicol 4*, 1−12.

(15) FDA (2018) *Bioanalytical Method Validation Guidance for Industry*.

(16) Vernetti, L. A., Vogt, A., Gough, A., and Taylor, D. L. (2017) Evolution of Experimental Models of the Liver to Predict Human Drug Hepatotoxicity and Efficacy. *Clin Liver Dis 21*, 197−214.

(17) Bell, C. C., Dankers, A. C. A., Lauschke, V. M., Sison-Young, R., Jenkins, R., Rowe, C., Goldring, C. E., Park, K., Regan, S. L., Walker, T., Schofield, C., Baze, A., Foster, A. J., Williams, D. P., van de Ven, A. W. M., Jacobs, F., Houdt, J. V., Lahteenmaki, T., Snoeys, J., Juhila, S., Richert, L., and Ingelman-Sundberg, M. (2018) Comparison of hepatic 2d sandwich cultures and 3d spheroids for long-term toxicity applications: a multicenter study. *Toxicol. Sci. 162*, 655−667.

(18) Panic, G., Vargas, M., Scandale, I., and Keiser, J. (2015) Activity Profile of an FDA-Approved Compound Library against Schistosoma mansoni. *PLoS Neglected Trop. Dis. 9*, No. e0003962.

(19) Perlmutter, J. I., Forbes, L. T., Krysan, D. J., Ebsworth-Mojica, K., Colquhoun, J. M., Wang, J. L., Dunman, P. M., and Flaherty, D. P. (2014) Repurposing the antihistamine terfenadine for antimicrobial activity against *Staphylococcus aureus*. *J. Med. Chem. 57*, 8540−8562.

(20) Jeong, D., Park, H. G., Lim, Y. R., Lee, Y., Kim, V., Cho, M. A., and Kim, D. (2018) Terfenadine metabolism of human cytochrome P450 2J2 containing genetic variations (G312R, P351L and P115L). *Drug Metab. Pharmacokinet. 33*, 61−66.

(21) Cowan, N., and Keiser, J. (2015) Repurposing of anticancer drugs: *in vitro* and *in vivo* activities against *Schistosoma mansoni*. *Parasites Vectors 8*, 417.

(22) Oliveira, R. N., Correa, S. A. P., Vieira, K. M., Mendes, T., Allegretti, S. M., and Miguel, D. C. (2019) In vitro schistosomicidal activity of tamoxifen and its effectiveness in a murine model of schistosomiasis at a single dose. *Parasitol. Res. 118*, 1625−1631.

(23) Choucha Snouber, L., Bunescu, A., Naudot, M., Legallais, C., Brochot, C., Dumas, M. E., Elena-Herrmann, B., and Leclerc, E. (2013) Metabolomics-on-a-chip of hepatotoxicity induced by anticancer drug flutamide and Its active metabolite hydroxyflutamide using HepG2/C3a microfluidic biochips. *Toxicol. Sci. 132*, 8−20.

(24) Keiser, J., Vargas, M., and Vennerstrom, J. L. (2010) Activity of antiandrogens against juvenile and adult *Schistosoma mansoni* in mice. *J. Antimicrob. Chemother. 65*, 1991−1995.

(25) Meister, I., Ingram-Sieber, K., Cowan, N., Todd, M., Robertson, M. N., Meli, C., Patra, M., Gasser, G., and Keiser, J. (2014) Activity of praziquantel enantiomers and main metabolites against Schistosoma mansoni. *Antimicrob. Agents Chemother. 58*, 5466−5472.

(26) Xiao, S. H., Catto, B. A., and Webster, L. T., Jr. (1985) Effects of praziquantel on different developmental stages of *Schistosoma mansoni in vitro* and *in vivo*. *J. Infect. Dis. 151*, 1130−1137.

(27) Verjans, E. T., Doijen, J., Luyten, W., Landuyt, B., and Schoofs, L. (2018) Three-dimensional cell culture models for anticancer drug screening: Worth the effort? *J. Cell. Physiol. 233*, 2993−3003.

(28) Harbut, M. B., Vilcheze, C., Luo, X., Hensler, M. E., Guo, H., Yang, B., Chatterjee, A. K., Nizet, V., Jacobs, W. R., Jr., Schultz, P. G., and Wang, F. (2015) Auranofin exerts broad-spectrum bactericidal activities by targeting thiol-redox homeostasis. *Proc. Natl. Acad. Sci. U. S. A. 112*, 4453−4458.

(29) Kijanska, M., and Kelm, J. (2004) In vitro 3D Spheroids and Microtissues: ATP-based Cell Viability and Toxicity Assays. In *Assay Guidance Manual (Internet)*, Markossian, S., Sittampalam, G. S., Grossman, A., Brimacombe, K., Arkin, M., Auld, D., Austin, C. P., Baell, J., Caaveiro, J. M. M., Chung, T. D. Y., Coussens, N. P., Dahlin, J. L., Devanaryan, V., Foley, T. L., Glicksman, M., Hall, M. D., Haas, J. V., Hoare, S. R. J., Inglese, J., Iversen, P. W., Kahl, S. D., Kales, S. C., Kirshner, S., Lal-Nag, M., Li, Z., McGee, J., McManus, O., Riss, T., Saradjian, P., Trask, O. J., Weidner, J. R., Wildey, M. J., Xia, M., and Xu, X., Eds.; Eli Lilly & Company and the National Center for Advancing Translational Sciences, Bethesda, MD.

(30) Lombardo, F. C., Perissutti, B., and Keiser, J. (2019) Activity and pharmacokinetics of a praziquantel crystalline polymorph in the *Schistosoma mansoni* mouse model. *Eur. J. Pharm. Biopharm. 142*, 240−246.

Chapter IV:

Activity and pharmacokinetics of a praziquantel crystalline polymorph in the *Schistosoma mansoni* mouse model

European Journal of Pharmaceutics and Biopharmaceutics 142 (2019) 240–246

Contents lists available at ScienceDirect

European Journal of Pharmaceutics and Biopharmaceutics

journal homepage: www.elsevier.com/locate/ejpb

Research paper

Activity and pharmacokinetics of a praziquantel crystalline polymorph in the *Schistosoma mansoni* mouse model

Flavio C. Lombardo[a,b], Beatrice Perissutti[c], Jennifer Keiser[a,b,*]

[a] Swiss Tropical and Public Health Institute, Socinstrasse 57, CH-4002 Basel, Switzerland
[b] Universität Basel, Petersplatz 1, CH-4001 Basel, Switzerland
[c] Department of Chemical and Pharmaceutical Sciences, University of Trieste, p.le Europa 1, 34127 Trieste, Italy

ARTICLE INFO

Keywords:
Schistosoma mansoni
Praziquantel
Polymorph B
Pharmacokinetics
Activity

ABSTRACT

Schistosomiasis is a global disease of significant public health relevance. Only one racemic drug, praziquantel, characterized by low bioavailability, low water solubility and extensive first pass metabolism, is currently available. We studied a new praziquantel formulation (polymorph B), which is based on a racemic praziquantel crystalline polymorph (TELCEU01). Its *in vitro* activity was tested on newly transformed schistosomula (NTS) and adult *Schistosoma mansoni*. *In vivo* studies were conducted in mice harboring chronic *S. mansoni* infections. Pharmacokinetic (PK) profiles of R- and S-praziquantel and R- and S- polymorph B following oral administration with both formulations were generated by sampling mice at 30, 60, 240 min and 24 h post-treatment, followed by LC-MS/MS analysis. PK parameters were calculated using a non-compartmental analysis with a linear trapezoidal model. *In vitro,* commercial praziquantel and the polymorph B performed similarly on both NTS (IC_{50} = 2.58 and 2.40 µg/mL at 72 h) and adults (IC_{50} = 0.05 and 0.07 µg/mL at 72 h). Praziquantel showed higher *in vivo* efficacy with an ED_{50} of 58.75 mg/kg compared to an ED_{50} of 122.61 mg/kg for the polymorph B. The PK profiles of the two drugs exhibited differences: R-praziquantel showed an overall 40% higher area under the plasma drug concentration–time curve ($AUC_{0\rightarrow 24}$) (R-praziquantel = 3.42; R-polymorph B = 2.05 h*µg/mL) and an overall 30% lower apparent clearance (Cl/F) (R-praziquantel = 70.68 and R-polymorph B = 97.63 (mg)/(µg/mL)/h). Despite the lack of improved activity and PK properties of polymorph B against *S. mansoni*, here presented; research on pharmaceutical polymorphism remains a valid and cost-effective option for the development of new praziquantel formulations with enhanced properties such as increased solubility and/or dissolution.

1. Introduction

Schistosomiasis is a global disease, which predominantly affects countries in Sub-Saharan Africa and some parts of Asia and South America [1,2]. An estimated 779 million people are at risk of infection, of which more than 50% are children [3]. More than 200 million people are infected [3,4], with *Schistosoma haematobium*, *S. mansoni* and *S. japonicum* being responsible for the bulk of infections [1]. There is no vaccine available and the only drug marketed for treatment against *Schistosoma* spp. infections is praziquantel. Alarmingly, the drug pipeline against schistosomiasis is empty. Praziquantel is commonly used in mass drug administration (MDA), so-called preventive chemotherapy [1,5]. For example, in 2016 alone, about 89 million doses of praziquantel were distributed in Sub-Saharan Africa [6,7]. However, it is not a perfect drug, primarily because of its low efficacy against juvenile stages of *Schistosoma* spp., high inter-individual variability of effects and poor compliance [8-11]. Praziquantel is a racemic compound, composed by 50% of R-praziquantel and 50% of S-praziquantel. Of these two enantiomers, R-praziquantel is the main active form. S-praziquantel shows less activity, while being responsible for the bitter taste [12,13].

According to the biopharmaceutical classification system (BCS), praziquantel belongs to the class II drug category, because of its high permeability and low solubility (0.4 mg/mL) [14,15]. Praziquantel also has a high first pass metabolism (1–3 h), which converts the active R-praziquantel into inactive metabolites very rapidly [10,16]. To overcome the low bioavailability, a crystalline polymorph of racemic praziquantel was prepared. The novel polymorph, polymorph B, as well as commercial praziquantel, consists of a mixture of R- and S- enantiomers.

---

* Corresponding author at: Swiss Tropical and Public Health Institute, Socinstrasse 57, CH-4002 Basel, Switzerland.
E-mail address: jennifer.keiser@swisstph.ch (J. Keiser).

https://doi.org/10.1016/j.ejpb.2019.06.029
Received 22 February 2019; Received in revised form 3 June 2019; Accepted 28 June 2019
Available online 29 June 2019
0939-6411/ © 2019 Elsevier B.V. All rights reserved.

For the preparation of the polymorph B, standard praziquantel was milled by neat grinding in a vibrational mill [17]. During the milling process in suitable conditions, in absence of solvents, the standard praziquantel turns into a new polymorphic anhydrous crystalline form, polymorph B [17], indexed as TELCEU01 in the Cambridge Structural Database [18]. As widely known, a polymorphic variety has different physical properties with respect to the standard crystal form, due to the different crystalline lattice [19–22]. In this case, polymorph B, forming a monotropic pair with commercial praziquantel crystal form, is characterized by double water solubility, and doubled intrinsic dissolution rate in comparison to the starting solid form [17]. In addition, it is a promising product because it is physically stable at the solid state for at least 1 year at ambient temperature [17]. Moreover, the polymorph B showed promising results in preliminary *in vitro* and *in vivo* studies on adult *S. mansoni* [17].

The aim of the present study was to thoroughly evaluate whether polymorph B would offer benefits over standard praziquantel such as increased efficacy and improved pharmacokinetic (PK) parameters. We conducted an in-depth side by side comparison of praziquantel and the polymorph B formulation (as aqueous suspensions). Both *in vitro* and *in vivo* studies as well as a PK analysis of the praziquantel polymorph B and standard praziquantel were performed. *In vitro* studies were conducted on the larval and adult stages of *S. mansoni*. ED_{50} values were determined in mice harboring a chronic *S. mansoni* infection. Finally, we determined PK parameters of R- and S-praziquantel and R- and S-polymorph B following treatment with both formulations in mice using a validated liquid chromatography (LC) tandem mass spectrometry (MS-MS) method (LC-MS/MS).

2. Materials and methods

2.1. Reagents

Ammonium formate (cat. no 70221-25G-F), formic acid (cat. no 5.33002.0050), ammonium acetate (cat. no. 73594-25G-F), methanol (cat. no. 1.06035.2500), acetonitrile (cat. no. 1.00029.2500), and 2-propanol (cat. no. 1.02781.1000) were MS grade. All MS reagents were purchased from Sigma-Aldrich (Buchs, Switzerland). Dimethylsulfoxide (DMSO) was the product of Sigma-Aldrich, Buchs, Switzerland, (cat. no. 276855-2L). Ultrapure water was filtered using a Millipore MilliQ water purification system (Merck Millipore, MA, USA). Human blood was supplied in lithium heparin-coated vacutainer tubes (Becton Dickinson (BD), Allschwil, Switzerland, cat. no. 367962) by the local blood donation center (Basel, Switzerland). Internal standard (ISTD) praziquantel d11 was purchased from Toronto research (Toronto, Canada, cat. no. P702097). Praziquantel as racemic powder was purchased from Sigma Aldrich (Buchs, Switzerland, cat. no. P4668-5G).

Penicillin/Streptomycin 10′000 U/mL (Sigma-Aldrich, Buchs, Switzerland, cat. no. P4333-100ML) and inactivated fetal calf serum (iFCS, Bioconcept AG, Allschwil, cat. no. 2-01F30-I) were purchased from Bioconcept AG (Allschwil, Switzerland). M199 medium and RPMI 1640 were obtained from Gibco (Waltham, USA cat. no. 22340-020). All media were filter sterilized using a 0.22 µm filter bottle (Corning Stericup 500 mL, Vitaris AG, Allschwil, Switzerland, cat. no. 431097-COR).

2.2. Praziquantel polymorph B

The preparation of the crystalline polymorph B was realized via a neat grinding process of standard racemic praziquantel in a vibrational mill as described elsewhere [17]. Briefly, this treatment resulted in the high yield and low costs production of a racemic crystalline polymorph B, physically stable for at least one year. The crystalline form of the praziquantel underwent chemical analysis by HPLC, NMR and polarimetry, confirming that the chemical entity of the praziquantel remained the same. Further analysis reported different physical properties of the polymorph B compared to standard praziquantel, such as increased water solubility and lower melting point [17].

2.3. In vitro studies with newly transformed schistosomula (NTS)

Biomphalaria glabrata snails infected with a Liberian strain of *S. mansoni* were placed under a neon light to allow cercarial shedding for 3–4 h. The cercarial suspension was then transformed using a technique based on the mechanical transformation proposed by Milligan & Jolly [23]. The obtained NTS were incubated at 37 °C with 5% CO_2 overnight. The NTS were resuspended at 2 NTS/µL in M199 medium supplemented with 1% v/v penicillin/streptomycin, 5% v/v iFCS. The proper volume of medium was added to each well of a 96-well-plate and supplemented with the appropriate volume of drug. A volume of 50 µL of NTS solution (100 NTS) was dispensed into each well [24]. Both praziquantel formulations were first suspended in DMSO to a working concentration of 10 mg/mL. The drug aliquots were kept at −20 °C until use. Polymorph B and praziquantel concentrations evaluated ranged from 100 to 0.78 µg/mL (320–2.50 µM). For the negative controls (in triplicates), DMSO was used at a final volume of 1% v/v. Each assay was evaluated every 24 h [25–27]. The parasites were given a score between 0 and 3, depending on their viability. On this scale, 0 represents dead parasites and 3 indicates alive and undamaged parasites [28,29]. The scores are then used to compute the IC_{50} curves with Compusyn® [24,30].

2.4. In vitro studies with adult S. mansoni

Schistosoma mansoni adult worms were recovered from female NMRI mice 7 weeks post infection. Mice were dissected after CO_2 euthanasia and cervical dislocation. The intestines and the liver were excised and analyzed with a dissection microscope. The adult worms were recovered from the organs by manual picking, using flat-tip tweezers. Alive worms were recovered and incubated in a Petri dish in supplemented RPMI 1640 at 37 °C with 5% CO_2, for up to 3 days. For the IC_{50} calculation, 2 worm pairs or 3 single worms were randomly chosen from the Petri dishes. The worms were then placed in 24 well plates at a final volume of 1.6 mL in fully supplemented RPMI 1640. Duplicates or triplicates, depending on the worm availability, were performed for every condition. Negative control wells consisted of medium with 1% v/v DMSO. The polymorph B and the standard praziquantel were tested using a concentration range of 0.45–0.05 µg/mL (1.44–0.16 µM). The drug effect was evaluated every 24 h by visual scoring with a light microscope, as described above, using a magnification of 4-10X. Similarly to the NTS, the adult *S. mansoni* were given a score from 0 to 3, depending on their viability. On this scale, 0 represents dead parasites and 3 indicates alive and undamaged individuals [24]. As for the NTS procedure, the IC_{50} values were calculated using Compusyn® [30].

2.5. In-vivo studies

All animals were ordered from Charles-River (Sulzfeld, Germany). Animal experiments were conducted in accordance with the local cantonal veterinary guidelines, license number 2070. A total of 66 three-week-old female NMRI mice were used for this study. Upon arrival, the animals were left for one week for acclimatization. The animals were housed at 25 °C in a controlled environment (temperature ~ 25 °C; humidity ~ 70%; 12-hour light and 12-hour dark cycle) with free access to water and rodent diet. The mice were infected subcutaneously with 100 *S. mansoni* cercaria in the neck area. Seven weeks post-infection, mice were treated with 400, 300, 200, 100, 50 mg/kg of the polymorph B or praziquantel. The oral suspensions were freshly prepared in a vehicle, composed of 90% v/v tap water and 10% v/v ethanol-Tween 80 (7% v/v Tween 80 and 3% v/v absolute ethanol). The administered volume was calculated for each mouse weight, as described elsewhere [27]. Each treatment arm had four mice, randomly chosen within the same infected batch. After treatment, the mice were monitored daily, for the next 21 days, before undergoing CO_2 euthanasia. The mice were then dissected and their livers were excised. Adult worms were picked, sexed and counted as described above. The worm burden reduction (WBR) was calculated by comparing the average number of recovered worms from each treatment arm to the control arm. The detailed *in vivo* procedure is described elsewhere [24]. The following formula was used for the evaluation of the WBR [27], where WB represents the average worm burden.

$$WBR(\%) = 100 - \left(\left(\frac{100}{WB_{Average_{Control}}}\right) * WB_{Average_{Test}}\right)$$

ED_{50} values were determined using the WBR and the doses using CompuSyn.[1]

2.6. Blood micro sampling for establishing pharmacokinetic profiles in mice

The day of drug administration of the polymorph B or praziquantel, plasma samples were collected from the infected mice by tail microsampling using 75 mm sodium hepatized microhaematocrit capillary tubes (Paul Marienfeld, cat: TX79.1, Lauda-Königshofen, Germany) at 30, 60, 240 min, and 24 h post-drug-administration. Volumes of 50 µL of whole blood were collected into capillary tubes. Each capillary tube was sealed on one side with one cm of wax by pressing them gently on a wax plate (Paul Marienfeld, Lauda-Königshofen, Germany, cat. no. 2960409). The tubes were placed in a microcentrifuge (Sigma-Zentrifugen, 1-16 special edition, Osterode am Harz, Germany) and centrifuged for 5 min at 5000 rpm at room temperature. The plasma was pipetted into a previously labelled 1.5 mL tube (Eppendorf, Hamburg, Germany). Finally, the tubes were stored at −80 °C until further analysis.

2.7. Preparation of the standards for LC-MS/MS

Quality controls (QCs) and calibration line (CL) samples were freshly prepared before every experiment. 2 µL of blank mouse plasma were mixed with 6 µL of blank human plasma. The blank mouse plasma was obtained from the control mice by heart puncture. Blank human plasma was obtained from the local blood donation centre (Basel, Switzerland). The plasma mixture was spiked with 2 µL of the appropriate drug concentration. The spiking solution was prepared in 10% v/v methanol and 90% v/v milliQ water. The CL covered the following drug concentrations: 0.01, 0.025, 0.05, 0.1, 0.25, 1.0, 2.0, 4.0 µg/mL. The QCs were prepared by adding the appropriate volume to obtain the following drug concentrations: 0.01, 0.1, 0.5, 2.0 µg/mL. Each validation set contained the 4 quality control (QCs) concentrations in 6 replicates each, plus a calibration line with 9 points. The QCs covered the lower limit of quantification (LLOQ), low, middle and high concentrations as recommended by the Food and Drug Administration (FDA) guideline for industry for bioanalytical method validation [31]. Each set was accepted within the partial validation criteria described below. Praziquantel was dissolved in 100% methanol to a final concentration of 5 mg/mL. This solution was used for preparing the QCs and CLs. The stock of internal standard (ISTD) was resuspended at a concentration of 1.25 mg/mL in methanol. The ISTD working solution was prepared in 20% v/v milliQ water, 80% acetonitrile and 400 ng/mL d11-PZQ and it was used as extraction solution for the samples. The spiking solution used was in 10% methanol v/v and 90% milliQ water v/v.

2.8. Validation of the LC-MS method

The quantification of the praziquantel enantiomers in this study was adapted from an already validated method for human plasma using a lower sample volume and a slightly changed matrix [32]. The adapted matrix for this study was a mixture of human and mice plasma at a ratio 3:1. A partial validation was performed by running 3 complete validation sets on three different days. Inter-day precision, accuracy, matrix-effect and recovery were evaluated.

The accuracy was calculated as the percentage of the measured concentration compared to the nominal spiked concentration. The precision was calculated as the percentage of the standard deviation of multiples compared to their average value. The recovery was evaluated as the calculated spiked sample's concentration, compared to the nominal one in solution without matrix. We followed the US FDA-guidelines [31]. The guidelines recommend limits for the quantification of analytes of high, middle, low concentration to be within ± 15% of their nominal spiked concentration, or ± 20% for the LLOQ. The matrix effect was tested by comparing the normalized area under the curve (AUC) of the spiked plasma samples to the AUC of the extracted samples of blank plasma, which were added to extraction solvent.

2.9. LC-MS/MS method LC-MS/MS instrumentation

All measurements were performed using an Agilent 6460 Series triple quadrupole LC–MS/MS. Mass Hunter Workstation (Agilent Technologies, CA, USA, version: B.06.00) was used to operate the instrument and for data analysis. The Agilent triple quadrupole 6460 instrument was coupled with an Agilent 1200 HPLC system. The MS was equipped with an electrospray system (ESI). The HPLC system (Agilent Technologies, CA, USA) consisted of four LC-20AD pumps, a G1367E auto-sampler (Agilent Technologies, CA, USA) and a G1322A degasser (Agilent Technologies, CA, USA). A column-trapping system HALO C–18, 4.6 × 5 mm, (Optimize Technologies, OR, USA) was used before eluting to the main chiral column, a Lux Cellulose-3 column (cellulose tris(3-chloro-4-methylphenylcarbamate) phase), 150 × 4.6 mm, 3 µm (Phenomenex, CA, USA, cat. no. 00F-4456-B0) for the analyte separation.

The elution gradient was defined as follows: 1–3 min A 0–100%; 3–9.5 min, B 0–100%; 9.5–10.5 min A 0–100%. The flow rate was 0.3 mL/min. The six-port switching valve was used to divert the flow from the HPLC columns to the mass spectrometer during 0–3 and 9.5–10.5 min of each sample run.

The mobile phase A consisted of a solution of ammonium acetate 10 mM in milliQ water with 0.015% v/v formic acid. The solution was filtered and degassed using 500 mL 0.22 µm filter bottles. The mobile phase B was based on a mixture of ammonium formate 20 mM in milliQ water 20% v/v and acetonitrile 80% v/v.

The columns were kept at 20 °C. For every sample, 5 µL were injected as sample volume. The product ions were tracked in multiple reactions monitoring (MRM) at 204 and 203 *m/z* for the ISTD and praziquantel, respectively. The gas temperature was set to 400 °C, with a flow rate of 12 L/min.

Carry-over was prevented by rinsing the auto-sampler syringe after each injection with 50% v/v milliQ water and 50% v/v isopropanol.

2.10. Preparation of LC-MS/MS samples

The samples were extracted with 200 µL of extraction solution containing 400 ng/mL d11-PZQ. After extraction, the samples were thermomixed at 20 °C for 20 min at 750 RPM (Eppendorf Themomixer C, Hamburg, Germany). The samples were filtered directly into 96-deep-well plates (500 µL) (Eppendorf, Switzerland, cat. no. 0030501101) by centrifugation (10 min at 2250*g* and 22 °C) of 2 µm PVDF membrane filter 96-well plates (Corning Life Sciences, CA, USA, cat. no. CLS3508-50EA). The 96-deep-well plates were sealed with plastic sealing mats (Eppendorf, Germany, cat. no. 15319247) and stored, for a maximum of 24 h, at 4 °C.

---

[1] ®.

2.11. Sample analysis

Precision was evaluated using the coefficient of variation (CV) between the replicates, and accuracy was calculated as the percentage ratio of the measured concentration to the nominal concentration. Calibration curves were normalized by the ISTD peak areas and fitted by linear regression. The weighting factor for the linear regression ($1/x^2$) was selected to yield the lowest total error. In every set, a calibration line (CL) ranging from 0.01 to 4 µg/mL was included, with a regression fitting coefficient R^2 above 0.996. Additionally, 6 replicates of QCs LLOQ, low, middle and high concentration were included in each set.

2.12. ISR (incurred sample reanalysis)

10% of the mice plasma samples were randomly chosen for incurred sample reanalysis (ISR). The criterion for ISR acceptance is that two-thirds (67%) of the repeated sample results should be within 20% between the first and the second measurement. The percentage difference of the results is determined with the following equation: ((Repeat – Original) * 100/Mean).

2.13. Statistics and pharmacokinetic parameters

All the data were handled with R version 3.4 and R-studio V 1.1.453 [33]. Statistics were performed with R-studio. Kruskal-Wallis rank sum test was used for the statistical analysis (Supplementary Fig. 1), non-compartmental analysis (NCA) was used to calculate the area under the curve 0-infinity ($AUC_{0-\infty}$), maximum concentration (C_{max}), time to maximum concentration (T_{max}), half-life ($t_{1/2}$), area under the curve 0–24 h ($AUC_{0\text{-}24h}$) and the apparent oral clearance (Cl/F) for both the R- and S- enantiomers of praziquantel and R- and S-enantiomers of polymorph B.

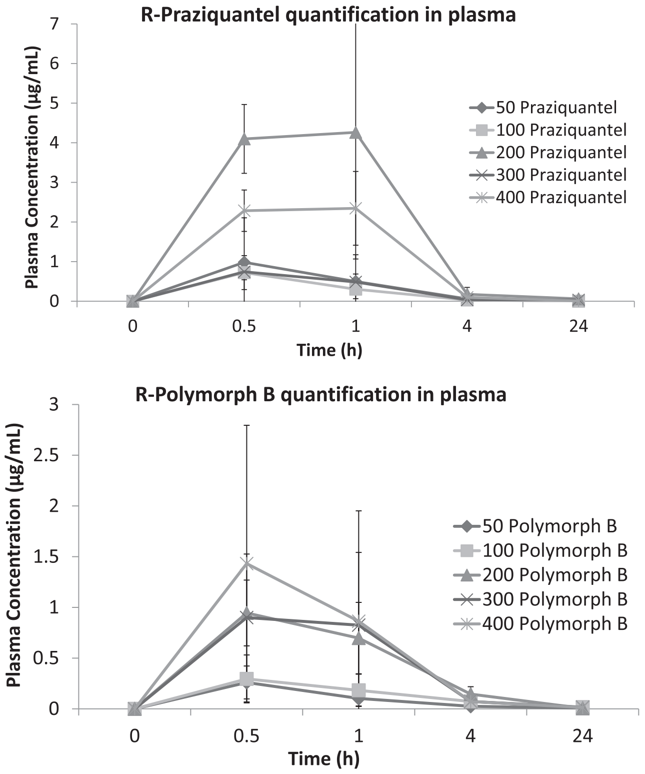

Fig. 1. Plasma concentration profiles of the standard R-praziquantel (a) and of R-polymorph B (b), Concentration time profile of the standard R-praziquantel (a) and of R-polymorph B (b) after quantification by LC-MS/MS. The error lines represent the standard deviation of the samples.

Table 1
IC_{50} values *in vitro* on *S. mansoni* newly transformed schistosomula (NTS).

IC_{50} (µg/mL)	24 h	SD	48 h	SD	72 h	SD
Polymorph B	16.45	4.88	4.45	2.96	2.40	0.50
Praziquantel	12.64	2.33	4.48	3.5	2.58	0.36

Data obtained as average of three independent experiments. SD = standard deviation.

3. Results

3.1. In vitro results with S. mansoni newly transformed schistosomula (NTS)

After 72 h, the calculated IC_{50} value for standard praziquantel on NTS was 2.58 µg/mL (8.26 µM), while for the polymorph B it was 2.40 µg/mL (7.68 µM) (Table 1). Both formulations showed decreased IC_{50} values over time, from 16.45 µg/mL (52.66 µM) (24 h) to 2.40 µg/mL (7.68 µM) (72 h) for the polymorph B and from 12.64 (24 h) to 2.58 (72 h) µg/mL (39.69 to 8.26 µM) for standard praziquantel (Table 1).

3.2. In vitro results with S. mansoni adults

The IC_{50} values determined after 24 h were 0.14 µg/mL (0.45 µM) for standard praziquantel and 0.23 µg/mL (0.74 µM) for the polymorph B. After 72 h, similar IC_{50} values of 0.07 µg/mL (0.22 µM) for the polymorph B and 0.05 µg/mL (0.16 µM) for the standard praziquantel were calculated (Table 2).

3.3. In vivo results

There was no significant difference between the number of female and male adult worms recovered from infected mice treated with praziquantel or the polymorph B for any of the treatment groups. However, both the polymorph B and standard praziquantel reduced the overall worm burden significantly (p value < 0.05) compared to the control mice (Table 3, Supplementary Fig. 1). The highest WBR was achieved at 300 mg/kg for both treatment arms (polymorph B = 89%; praziquantel = 87%). The lowest WBR was observed at 50 mg/kg dose for both standard praziquantel and the polymorph B (33.3% and 12.5% mg/kg, respectively) (Table 3). The 50% effective dose (ED_{50}) was determined as 58.75 and 122.61 mg/kg for standard praziquantel and the polymorph B, respectively.

3.4. LC-MS/MS partial validation and incurred samples reanalysis (ISR)

At least 75% of the CL were within a precision of ± 15% (LLOQ): ± 20%) and an accuracy between 85% and 115% (LLOQ: 80–120%). In every set, a minimum 75% of the CL samples showed linearity with a fitted linear regression R^2 value of above 0.996. At least four quality controls (QCs) (or 67%) were within precision of ± 15% (LLOQ: ± 20%) and an accuracy between 85% and 115% (LLOQ: 80–120%).

During the partial validation process, the complete sets with QCs and CLs were run on different days (inter-day validation) and analysed. The coefficient of variation between the QC replicates was below 7%.

Table 2
IC_{50} values *in vitro* on adult *S. mansoni* worms.

IC50 (µg/mL)	24 h	SD	48 h	SD	72 h	SD
Polymorph B	0.23	0.20	0.08	0.11	0.07	0.05
Praziquantel	0.14	0.16	0.06	0.09	0.05	0.06

Data obtained as average of three independent experiments. SD = standard deviation.

Table 3
Effect of standard praziquantel and polymorph B on the worm burden in mice harboring a chronic *S. mansoni* infection.

			Worm burden			Worm Burden Reduction (WBR %)		
Compound	Dose (mg/kg)	No. of mice	Female	Male	Total	Female	Male	Total (SD)
Control_mice_1	Untreated	8	12.6	12.4	25.0	–	–	–
Control_mice_2	Untreated	8	10.5	11.5	22.0	–	–	–
Control_mice_3	Untreated	8	2.1	1.9	4.0	–	–	–
Polymorph B***	50	4	10.5	10.5	21.0	13	12	13 (25)
Praziquantel***	50	3	4.8	4.8	9.5	33	33	33 (58)
Polymorph B**	100	4	3.3	4.3	7.5	69	63	66 (21)
Praziquantel**	100	4	1.5	2.3	3.8	86	80	83 (20)
Polymorph B*	200	4	2.5	8.5	11.0	80	31	56 (33)
Praziquantel*	200	4	3.3	5.5	8.8	74	56	65 (17)
Polymorph B*	300	4	0.8	2.0	2.8	94	84	89 (14)
Praziquantel*	300	4	1.3	2.0	3.3	90	84	87 (5)
Polymorph B*	400	5	3.0	3.4	6.4	76	73	74 (13)
Praziquantel*	400	4	1.5	2.5	4.0	88	80	84 (23)

* Indicates that the WBR was calculated based on mice batch 1.

** Indicates that mice batch 2 was used to calculate the WBR.

*** Indicates that mice batch 3 was used to calculate the WBR. In the group of 50 mg/kg praziquantel, one mouse was excluded from the analysis as outlier, because it was not infected. SD = Standard deviation.

The observed matrix effect values were between 93% and 114% for R-praziquantel (lowest to highest concentration) and 97% to 104% for S-praziquantel. The total recovery values were between 87% and 97% for R-praziquantel (lowest to highest concentration). A total recovery of 87% to 91% was observed for S-praziquantel (lowest to highest concentration). The 10% of ISR (17 samples) randomly chosen were within the ± 20 variation, as recommended by the FDA guidelines.

3.5. Accuracy, precision, and matrix effect

During the analysis about 2.5% of the samples exceeded the upper limit of quantification (ULOQ) (4 µg/mL). These samples were diluted three times in the extraction solution without ISTD and re-run within the same run. The samples below the LLOQ (0.01 µg/mL) were considered as 0, as recommended by the Food and Drug Administration (FDA) guidelines [31].

The inter-day accuracy of the analytical method was measured in every individual set as described above. Each set was within ± 15% and ± 20% for the LLOQ. The highest deviation was observed on the LLOQ in all three sets. The inter-assay accuracy was between 96% and 112%, with the highest variation of 12% observed at LLOQ. The inter-day precision was between 2% and 12% for the LLOQ values.

The matrix effect is summarized in Supplementary Table 1. The matrix effect of R praziquantel was 93.4% with a standard deviation of 10% for lower concentrations; at higher concentrations (2.5 µg/mL) the matrix effect was 113.6%, with a standard deviation of 1.6%. The R-praziquantel recovery was between 87% and 97% (low to high concentrations), with a maximum standard deviation of 10% at low concentrations. For S-praziquantel, the total recovery was 86.6% with a standard deviation of 16.7% for lower concentrations, while at high concentrations it was 104.3% with a standard deviation of 2.4%.

3.6. Pharmacokinetic parameters

Pharmacokinetic parameters for R and S-praziquantel and the R and S-polymorph B are summarized in Table 4. Median T_{max} values between 0.5 and 0.75 h were determined for both the R-, S-polymorph B and R-, S-praziquantel. The median values of C_{max} ranged between 0.67 and 2.73 µg/mL (2.14 to 8.74 µM) for R-praziquantel and between 0.18 and 1.56 µg/mL (0.58 to 5 µM) for R-polymorph B at 50–400 mg/kg. The C_{max} values for the S-polymorph B and S-praziquantel show a similar trend. The median values for the $t_{1/2}$ for R-praziquantel were between 2.64 and 5.93 h and between 4.02 and 10.56 h for the R-polymorph B. At the 100 mg/kg dose R-praziquantel showed a 4 times lower $t_{1/2}$ than the R-polymorph B, while the other doses showed similar $t_{1/2}$ profiles for the two formulations (Table 4). The median values for the $AUC_{0\to 24h}$ ranged between 1.25 and 6.28 h*µg/mL for R-praziquantel, with the maximum value observed at the 400 mg/kg dose and the lowest value at the 100 mg/kg dose. The $AUC_{0\to 24h}$ for the R-polymorph B reached the maximum level at 300 mg/kg (3.1 h*µg/mL) and the minimum at 50 mg/kg (0.3 h*µg/mL). The values for the S- polymorph B and S-praziquantel were lower. The apparent clearance for the R-polymorph B and R-praziquantel median values were between 22.25 and 123.94 and between 53.08 and 134.7 (mg)/(µg/mL)/h, indicating a ~30% variation in the overall profiles of the two formulations (Table 4). No relationship was observed between WBR and $AUC_{0\to 24h}$ or C_{max}. (Supplementary Fig. 2).

4. Discussion

For over 30 years, praziquantel has been the only available drug against schistosomiasis together with oxamniquine [10,34]. Oxamniquine was used extensively in South America until 10 years ago, when it was withdrawn due to resistance development [34]. In the present study, a crystalline polymorph of standard praziquantel, revealing improved physical characteristics, such as increased water solubility and dissolution, together with an appreciable physical stability, was thoroughly tested, given initial promising *in vitro* and *in vivo* findings [17]. Moreover, we conducted PK studies, for which we successfully adapted and validated an LC-MS/MS method for mouse plasma.

Indeed, different studies have demonstrated that improved praziquantel formulations are able to influence the *in vivo* drug performance. For example, a study by El-Feky *et al.* (2015) [35] showed that a clay-based nanoformulation praziquantel increased the efficacy of the drug. Moreover, El-Lakkany *et al.* (2012) showed an increased efficacy of a praziquantel–polyvinylpyrrolidone (PVP) solid dispersion, by increasing the bioavailability of praziquantel in a PK study [36].

Our results, based on *in vitro* and *in vivo* studies using the *S. mansoni* mouse model, show that the polymorph B has no benefit in terms of efficacy over the current formulation. No significant differences were observed in the *in vitro* and *in vivo* studies, contrary to preliminary *in vitro* and *in vivo* results which showed higher efficacy of the formulation derivative compared to the standard praziquantel [17].

The ED_{50} value of 58.45 mg/kg for the standard praziquantel calculated in this study is in line with previously reported values for susceptible *S. mansoni* strains ranging from 70 to 100 mg/kg [35–38] but lower than the one previously determined in our laboratory (246.5 mg/

Table 4
Pharmacokinetic parameters calculated for R- and S-praziquantel following treatment of mice infected with *S. mansoni* with praziquantel and the polymorph B.

Parameter	50 mg/kg	100 mg/kg	200 mg/kg	300 mg/kg	400 mg/kg	
$t_{1/2}$ [h]	5.9 (5.3; 9.8)	2.6 (2.3; 3.5)	3.3 (2.7; 6.5)	5.9 (4.1; 8.2)	3.3 (3.0; 3.7)	**R-Praziquantel**
T_{max} [h]	0.5 (0.5; 0.5)	0.5 (0.5; 0.5)	0.8 (0.5; 1)	0.5 (0.5; 0.5)	0.8 (0.5; 1)	
C_{max} [µg/mL]	0.7 (0.2; 1.4)	0.7 (0.4; 1.0)	2.1 (1.2; 4.5)	0.8 (0.7; 0.9)	2.7 (2.1; 3.1)	
AUC $_{0\text{-}24h}$ [h*µg/mL]	1.5 (0.8; 3)	1.2 (0.5; 1.9)	5.9 (4.5; 10.4)	2.2 (1.8; 2.4)	6.3 (4.7; 8.1)	
AUC_∞ [h*µg/mL]	2.2 (1.9; 4.3)	1.3 (0.6; 1.9)	7.1 (6.5; 10.4)	2.5 (1.8; 3.1)	6.4 (4.7; 8.2)	
Cl/F$_{\_obs}$ (mg)/(µg/mL)/h	22.3 (15; 26.9)	112.8 (51.8; 180.3)	28.1 (23.4; 31.8)	123.9 (98.5; 186.5)	66.3 (49.3; 85)	
$t_{1/2}$ [h]	5.4 (3.3; 7)	10.6 (8.9; 11.1)	3.1 (2.9; 3.6)	4 (3.8; 6.3)	5.3 (4.3; 6.5)	**R-Polymorph B**
T_{max} [h]	0.5 (0.5; 0.5)	0.5 (0.5; 0.5)	0.5 (0.5; 0.5)	0.8 (0.5; 1)	0.5 (0.5; 0.9)	
C_{max} [µg/mL]	0.2 (0.1; 0.3)	0.3 (0.2; 0.4)	0.9 (0.7; 1.1)	0.9 (0.6; 1.3)	1.6 (0.3; 2.7)	
AUC $_{0\text{-}24h}$ [h*µg/mL]	0.3 (0.3; 0.5)	1.4 (0.9; 2)	2.9 (1.9; 3.8)	3.1 (2.3; 3.6)	2.5 (1.1; 4.5)	
AUC_∞ [h*µg/mL]	0.4 (0.3; 0.5)	1.9 (1.3; 2.4)	3 (2.2; 3.9)	3.1 (2.5; 3.7)	3.1 (2.4; 5.1)	
Cl/F$_{\_obs}$ (mg)/(µg/mL)/h	134.7 (109.3; 147.3)	53.1 (41.4; 113.7)	72.6 (51.9; 91.6)	96.7 (82.8; 125.4)	131.1 (78.3; 170.1)	
$t_{1/2}$ [h]	5.5 (4.7; 6.3)	0.4 (0.4; 0.4)	6 (5.0; 7.0)	6.4 (3.1; 9.7)	4.7 (4.5; 4.8)	**S-Praziquantel**
T_{max} [h]	0.5 (0.5; 0.6)	0.5 (0.5; 0.6)	0.8 (0.5; 1.0)	0.5 (0.5; 0.5)	0.8 (0.5; 1)	
C_{max} [µg/mL]	0.2 (0.1; 0.8)	0.1 (0.1; 0.2)	2.9 (2.4; 3.2)	0.3 (0.2; 0.3)	0.5 (0.4; 0.7)	
AUC $_{0\text{-}24h}$ [h*µg/mL]	2.2 (1.0; 3.8)	0.2 (0.1; 0.8)	7.2 (5.0; 9.4)	0.8 (0.6; 0.9)	1.8 (1.3; 2.1)	
AUC_∞ [h*µg/mL]	3.6 (2.5; 4.7)	0.3 (0.3; 0.3)	11.5 (11.1; 11.9)	1 (0.7; 1.2)	1.9 (1.3; 2.2)	
Cl/F$_{\_obs}$ (mg)/(µg/mL)/h	22.6 (15.6; 29.6)	316.2 (316.2; 316.2)	17.4 (16.8; 18)	314.3 (251.8; 804.5)	222.4 (182.8; 335.1)	
$t_{1/2}$ [h]	5.4 (1.1; 47.4)	20.4 (17.2; 21.2)	1.5 (1.0; 2.7)	5.4 (4.7; 7)	7.1 (5.1; 13.2)	**S-Polymorph B**
T_{max} [h]	0.5 (0.5; 0.6)	0.5 (0.5; 0.5)	0.5 (0.5; 0.5)	0.8 (0.5; 1)	0.5 (0.5; 0.9)	
C_{max} [µg/mL]	0.1 (0; 0.2)	0.1 (0.1; 0.2)	0.4 (0.2; 0.6)	0.2 (0.2; 0.3)	0.7 (0.2; 0.8)	
AUC $_{0\text{-}24h}$ [h*µg/mL]	0.2 (0.1; 0.8)	0.6 (0.6; 1.4)	0.9 (0.4; 1.5)	0.8 (0.5; 1.1)	1.3 (0.5; 1.5)	
AUC_∞ [h*µg/mL]	0.3 (0.2; 8.2)	1.6 (1.3; 3.2)	1 (0.6; 1.6)	0.9 (0.6; 1.1)	1.5 (1.5; 1.6)	
Cl/F$_{\_obs}$ (mg)/(µg/mL)/h	196.5 (127; 385.5)	61.7 (41.1; 82.6)	236.1 (129.4; 366.4)	371.5 (271.1; 507.9)	260.8 (245.4; 269.7)	

Median values are reported, and an interquartile range is provided: 1st quartile and 3rd quartile.

kg) [39]. While a slightly higher ED_{50} of 122.61 mg/kg was calculated for the polymorph B (mainly due to a slightly lower activity at 50 mg/kg) no significant difference was observed between the two treatments (as aqueous suspensions) at the individual dosages.

One limitation of our study, which might explain this finding, was the comparison of the two crystalline forms as water suspension: Once the drugs were suspended in water for the oral administration, the conformation of the polymorph B might have changed, thereby possibly altering its properties. To fully exclude this possibility it would have been advantageous to use the crystalline polymorph and the standard praziquantel as powders embedded in mini gelatin capsules or loaded in microparticles suitable for oral administration. However, the high praziquantel doses required to achieve antischistosomal activity (up to 400 mg/kg) are not compatible with mini capsule usage in the mouse model (the main animal model for research on schistosomiasis [40]), since the maximum capacity of each commercially available mini-capsule is 2–4 mg. Capsules can only be administered to rodents larger than 150 g. Therefore, comparison of liquid formulations, as done in this study, is a widely used approach in drug formulations and delivery studies in rodents [41].

The praziquantel quantification method in mouse plasma was successfully adapted from a human-based validated LC-MS/MS quantification method [32,42]. The PK analysis was based on a non-compartmental analysis using a trapezoidal linear model, given the small number of time points used in the study (30, 60, 240 min and 24 h). The trapezoidal linear model was preferred to the log-linear model due to the general opinion of this model being more accurate in the calculation for drugs with a fast metabolism [43]. A limitation of the PK study was the rather small sample size for each treatment arm (four mice) which could influence the error rate in the study. To limit this experimental error, the test and the control mice were chosen randomly within the same infection batch.

The data presented here show that, surprisingly, the polymorph B has an overall lower exposure profile for both R- and S- enantiomers, indicating a lower bioavailability of the drug, in comparison with standard praziquantel. Moreover, the polymorph B shows lower plasma peak concentrations of the R- and S-enantiomers compared to standard praziquantel formulation (Table 4). The polymorph B has previously been shown to have a faster dissolution rate compared to standard praziquantel [17,44] and therefore a better absorption would have been expected [45]. However, the fast first pass metabolism typical of praziquantel, might result in lower disposition profiles of the drug over time [16,37,46]. Earlier PK sampling time points (e.g. 5 min) should have been considered to obtain a better picture of the absorption phase.

Though the AUC was 40% lower for the polymorph B compared to standard praziquantel, the WBR observed was similar (Table 3). No relationship was observed between AUC and C_{max} and WBR (Supplementary Fig. 2), confirming previous findings from Abla *et al.* (2017), hypothesizing that the portal vein drug concentration is primarily responsible for the activity of praziquantel [37].

Similar to other studies a great variability was observed for both compounds in the PK profiles and parameters among individual mice [37]. Overall, the short praziquantel T_{max} value obtained in this study is in agreement with other *in vivo* studies, while in humans the T_{max} is generally ranging between 3 and 4 h [46,47]. The C_{max} values we found (0.21–4.55 µg/mL (0.67 – 14.56 µM) for R-praziquantel) are considerably lower than the ones found in other studies, as for example El-Feky et al. (2015) and Botros et al. (2006) [35,48], which report values of 24.36 and 33.33 µg/mL (77.98 and 106.59 µM), respectively, based on PK analysis of Swiss albino mice's plasma. However, both groups are reporting those results following a 500 mg/kg dose only, which makes a direct comparison difficult. The overall lower C_{max} observed in our study could be explained by the different strains and sex of the mice used in the different studies and, as mentioned, the slightly lower doses used, but also by other parameters, such as infection rate and mouse age [16,46,48–50]. However, we obtained a similar C_{max} as the reported values from Abla et al. (2017) for the dose of 200 mg/kg of standard praziquantel (about 1.3 µg/mL) and a similar value for the WBR (about 68%) [37]. However, interestingly the AUC value of R praziquantel reported by the same group is 2.6 times lower than the ones reported in this study at the dose of 200 mg/kg (median value of 5.93 h*µg/mL in our study compared to 2.2 h*µg/mL reported by Abla and colleagues) even though experimental conditions were identical (Table 3 and Table 4).

5. Conclusion

In this study we generated activity and PK data on a new alternative praziquantel formulation based on a crystalline polymorph of the racemic drug, the polymorph B, obtained via a solvent-free process of neat grinding. The polymorph B showed similar *in vivo* efficacy to the standard praziquantel formulation, but in general lower plasma levels. However, due to the excellent physical stability and doubled water solubility of the polymorph, this product remains a valid option to enhance the pharmaceutical performance of the antischistosomal drug praziquantel. Indeed, the possibility to generate additional praziquantel solid forms or other suitable formulations may represent new interesting approaches for overcoming the numerous praziquantel pharmaceutical and biopharmaceutical drawbacks.

Acknowledgements

This work was supported by a grant from the European Research Council (ERC 614739-A_HERO).

Appendix A. Supplementary material

Supplementary data to this article can be found online at https://doi.org/10.1016/j.ejpb.2019.06.029.

References

[1] R. Bergquist, J. Utzinger, J. Keiser, Controlling schistosomiasis with praziquantel: How much longer without a viable alternative? Infect. Dis. Poverty 6 (2017) 74.
[2] B. Gryseels, K. Polman, J. Clerinx, L. Kestens, Human schistosomiasis, The Lancet 368 (2006) 1106–1118.
[3] D.G. Colley, A.L. Bustinduy, W.E. Secor, C.H. King, Human schistosomiasis, The Lancet 383 (2014) 2253–2264.
[4] M.J. Doenhoff, J.R. Kusel, G.C. Coles, D. Cioli, Resistance of *Schistosoma mansoni* to praziquantel: is there a problem? Trans. R. Soc. Trop. Med. Hyg. 96 (2002) 465–469.
[5] M.J. Doenhoff, L. Pica-Mattoccia, Praziquantel for the treatment of schistosomiasis: its use for control in areas with endemic disease and prospects for drug resistance, Expert Rev. Anti-infective Therapy 4 (2006) 199–210.
[6] W. Wang, Y. Liang, Mass drug administration (MDA) for schistosomiasis, J. Infect. Dis. 211 (2015) 848–849.
[7] WHO. 201Schistosomiasis and soil-transmitted helminthiases: number of people treated in 2016.
[8] J.T. Coulibaly, G. Panic, K.D. Silue, J. Kovac, J. Hattendorf, J. Keiser, Efficacy and safety of praziquantel in preschool-aged and school-aged children infected with *Schistosoma mansoni*: a randomised controlled, parallel-group, dose-ranging, phase 2 trial, Lancet Global Health 5 (2017) E688–E698.
[9] J.T. Coulibaly, M. Ouattara, B. Barda, J. Utzinger, E.K. N'Goran, J. Keiser, A rapid appraisal of factors influencing praziquantel treatment compliance in two communities endemic for schistosomiasis in Cote d'Ivoire, Trop. Med. Infect. Dis. 3 (2018).
[10] D.P. McManus, D.W. Dunne, M. Sacko, J. Utzinger, B.J. Vennervald, X.-N. Zhou, Schistosomiasis, Nat. Rev. Dis. Primers 4 (2018) 13.
[11] R. Shawahna, Pediatric biopharmaceutical classification system: using age-appropriate initial gastric volume, AAPS J. 18 (2016) 728–736.
[12] S.M. Alsaqabi, Praziquantel: A review, J. Veter. Sci. Technol. 05 (2014).
[13] J. Kovac, M. Vargas, J. Keiser, *In vitro* and *in vivo* activity of R- and S- praziquantel enantiomers and the main human metabolite trans-4-hydroxy-praziquantel against *Schistosoma haematobium*, Parasit Vectors 10 (2017) 365.
[14] M. Lindenberg, S. Kopp, J.B. Dressman, Classification of orally administered drugs on the World Health Organization Model list of Essential Medicines according to the biopharmaceutics classification system, Eur. J. Pharm. Biopharm. 58 (2004) 265–278.
[15] N. Passerini, B. Albertini, B. Perissutti, L. Rodriguez, Evaluation of melt granulation and ultrasonic spray congealing as techniques to enhance the dissolution of praziquantel, Int. J. Pharm. 318 (2006) 92–102.
[16] D. Cioli, L. Pica-Mattoccia, Praziquantel, Parasitol. Res. 90 (2003) S3–S9.
[17] D. Zanolla, B. Perissutti, N. Passerini, M.R. Chierotti, D. Hasa, D. Voinovich, L. Gigli, N. Demitri, S. Geremia, J. Keiser, P. Cerreia Vioglio, B. Albertini, A new soluble and bioactive polymorph of praziquantel, Eur. J. Pharm. Biopharm. 127 (2018) 19–28.
[18] C.R. Groom, I.J. Bruno, M.P. Lightfoot, S.C. Ward, The cambridge structural database, Acta Crystallogr. Sect. B: Struct. Sci., Crystal Eng. Mater. 72 (2016) 171–179.
[19] D. Singhal, Drug polymorphism and dosage form design: a practical perspective, Adv. Drug Deliv. Rev. 56 (2004) 335–347.
[20] S.R. Byrn Jr. RRP, J.G. Stowell. 1999. Solid-state chemistry of drugs, 2 ed. SSCI, West Lafayette, IN.
[21] H.G. Brittain, Polymorphism and solvatomorphism 2010, J. Pharm. Sci. 101 (2012) 464–484.
[22] K. Raza, Polymorphism: the phenomenon affecting the performance of drugs, SOJ Pharm. Pharm. Sci. (2014), https://doi.org/10.15226/2374-6866/1/2/00111.
[23] J.N. Milligan, E.R. Jolly, Cercarial transformation and *in vitro* cultivation of *Schistosoma mansoni* schistosomules, J. Visual. Exp.: JoVE (2011).
[24] F.C. Lombardo, V. Pasche, G. Panic, Y. Endriss, J. Keiser, Life cycle maintenance and drug-sensitivity assays for early drug discovery in *Schistosoma mansoni*, Nat. Protoc. 14 (2019) 461–481.
[25] M.H. Abdulla, D.S. Ruelas, B. Wolff, J. Snedecor, K.C. Lim, F. Xu, A.R. Renslo, J. Williams, J.H. McKerrow, C.R. Caffrey, Drug discovery for schistosomiasis: hit and lead compounds identified in a library of known drugs by medium-throughput phenotypic screening, PLoS Negl.Trop. Dis. 3 (2009) e478.
[26] J. Keiser, G. Panic, R. Adelfio, N. Cowan, M. Vargas, I. Scandale, Evaluation of an FDA approved library against laboratory models of human intestinal nematode infections, Parasites Vectors 9 (2016) 376.
[27] G. Panic, M. Vargas, I. Scandale, J. Keiser, Activity profile of an FDA-approved compound library against *Schistosoma mansoni*, PLoS Negl. Trop. Dis. 9 (2015) e0003962.
[28] T. Manneck, O. Braissant, Y. Haggenmuller, J. Keiser, Isothermal microcalorimetry to study drugs against *Schistosoma mansoni*, J. Clin. Microbiol. 49 (2011) 1217–1225.
[29] T. Manneck, Y. Haggenmuller, J. Keiser, Morphological effects and tegumental alterations induced by mefloquine on schistosomula and adult flukes of *Schistosoma mansoni*, Parasitology 137 (2010) 85–98.
[30] T.C. Chou, Theoretical basis, experimental design, and computerized simulation of synergism and antagonism in drug combination studies, Pharmacol. Rev. 58 (2006) 621–681.
[31] FDA. 2018. Bioanalytical Method Validation Guidance for Industry. https://www.fda.gov/downloads/drugs/guidances/ucm070107.Pdf.
[32] I. Meister, A. Leonidova, J. Kovač, U. Duthaler, J. Keiser, J. Huwyler, Development and validation of an enantioselective LC–MS/MS method for the analysis of the anthelmintic drug praziquantel and its main metabolite in human plasma, blood and dried blood spots, J. Pharm. Biomed. Anal. 118 (2016) 81–88.
[33] R. A language and environment for statistical computing. R Foundation for Statistical Computing, Vienna, Austria, https://www.R-project.org/.
[34] F.D. Chevalier, W. Le Clec'h, N. Eng, A.R. Rugel, R.Rd. Assis, G. Oliveira, S.P. Holloway, X. Cao, P.J. Hart, P.T. LoVerde, T.J.C. Anderson, Independent origins of loss-of-function mutations conferring oxamniquine resistance in a Brazilian schistosome population, Int. J. Parasitol. 46 (2016) 417–424.
[35] G.S. El-Feky, W.S. Mohamed, H.E. Nasr, N.M. El-Lakkany, S.H. Seif El-Din, S.S. Botros, Praziquantel in a clay nanoformulation shows more bioavailability and higher efficacy against murine *Schistosoma mansoni* infection, Antimicrob. Agents Chemother. 59 (2015) 3501–3508.
[36] N. El-Lakkany, S.H. Seif El-Din, L. Heikal, Bioavailability and *in vivo* efficacy of a praziquantel-polyvinylpyrrolidone solid dispersion in *Schistosoma mansoni*-infected mice, Eur. J. Drug Metab. Pharmacokinet. 37 (2012) 289–299.
[37] N. Abla, J. Keiser, M. Vargas, N. Reimers, H. Haas, T. Spangenberg, Evaluation of the pharmacokinetic-pharmacodynamic relationship of praziquantel in the *Schistosoma mansoni* mouse model, PLoS Negl. Trop. Dis. 11 (2017) e0005942.
[38] S. William, S. Botros, Validation of sensitivity to praziquantel using *Schistosoma mansoni* worm muscle tension and Ca2+-uptake as possible *in vitro* correlates to *in vivo* ED50 determination, Int. J. Parasitol. 34 (2004) 971–977.
[39] I. Meister, K. Ingram-Sieber, N. Cowan, M. Todd, M.N. Robertson, C. Meli, M. Patra, G. Gasser, J. Keiser, Activity of praziquantel enantiomers and main metabolites against *Schistosoma mansoni*, Antimicrob. Agents Chemother. 58 (2014) 5466–5472.
[40] J. Keiser, *In vitro* and *in vivo* trematode models for chemotherapeutic studies, Parasitology 137 (2010) 589–603.
[41] P.V. Turner, C. Pekow, M.A. Vasbinder, T. Brabb, Administration of substances to laboratory animals: equipment considerations, vehicle selection, and solute preparation, J. Am. Assoc. Lab. Anim. Sci. 50 (2011) 614–627.
[42] J. Kovač, G. Panic, A. Neodo, I. Meister, J.T. Coulibaly, J.D. Schulz, J. Keiser, Evaluation of a novel micro-sampling device, Mitra™, in comparison to dried blood spots, for analysis of praziquantel in *Schistosoma haematobium*-infected children in rural Côte d'Ivoire, J. Pharm. Biomed. Anal. 151 (2018) 339–346.
[43] J. Gabrielsson, D. Weiner, Non-compartmental analysis, Methods Mol. Biol. 929 (2012) 377–389.
[44] A.V. Yadav, A.S. Shete, A.P. Dabke, P.V. Kulkarni, S.S. Sakhare, Co-crystals: a novel approach to modify physicochemical properties of active pharmaceutical ingredients, Indian J. Pharm. Sci. 71 (2009) 359–370.
[45] K. Greco, R. Bogner, Solution-mediated phase transformation: significance during dissolution and implications for bioavailability, J. Pharm. Sci. 101 (2012) 2996–3018.
[46] P. Olliaro, P. Delgado-Romero, J. Keiser, The little we know about the pharmacokinetics and pharmacodynamics of praziquantel (racemate and R-enantiomer), J. Antimicrob. Chemother. 69 (2014) 863–870.
[47] A.D. Dayan, Albendazole, mebendazole and praziquantel. Review of non-clinical toxicity and pharmacokinetics, Acta Trop. 86 (2003) 141–159.
[48] S.S. Botros, S.H. El-Din, N.M. El-Lakkany, A.N. Sabra, F.A. Ebeid, Drug-metabolizing enzymes and praziquantel bioavailability in mice harboring *Schistosoma mansoni* isolates of different drug susceptibilities, J. Parasitol. 92 (2006) 1344–1349.
[49] M.E. Mandour, H. el Turabi, M.M. Homeida, T. el Sadig, H.M. Ali, J.L. Bennett, W.J. Leahey, D.W. Harron, Pharmacokinetics of praziquantel in healthy volunteers and patients with schistosomiasis, Trans. R. Soc. Trop. Med. Hyg. 84 (1990) 389–393.
[50] G. Watt, N.J. White, L. Padre, W. Ritter, M.T. Fernando, C.P. Ranoa, L.W. Laughlin, Praziquantel pharmacokinetics and side effects in *Schistosoma japonicum*-infected patients with liver disease, J. Infect. Dis. 157 (1988) 530–535.

2. Discussion

During my PhD, I had the opportunity to gain insight into the interesting and highly relevant field of drug development and to understand drawbacks of the current drug screening procedures against NTDs and schistosomiasis. I worked on a collection of protocols for drug screening on *Schistosoma mansoni*, with the aim to spread the current methodology that we employ in the laboratory here at Swiss TPH across other research settings (Chapter I). We examined the entire procedure and underlined its drawbacks. In this thesis we reflect on the drug discovery pipeline for schistosomiasis, which is empty due to its many constraints, such as low parasite yield, subjective drug screening, and the time-consuming harvest of adult parasites which requires an *in vivo* life cycle that needs 7 weeks to fully develop.

Here I will discuss a series of projects aimed at solving or lessening some of these drawbacks. Solving or reducing some of the problems related to the drug screening on *S. mansoni* might lead to faster drug screenings. Furthermore, solving the issue of the drug screening subjectivity would increase the concordance of hits between different laboratories, which might be as low as 20% (Panic et al., 2015). These improvements in the drug screening against schistosomiasis might contribute to fill the empty pipeline with novel promising compounds. Contributing to the empty drug pipeline is of fundamental importance, because at the moment praziquantel and -to some extent- oxamniquine are the only available active compounds against schistosomiasis. Nonetheless, other improvements of the current drug screening pipeline can be found in other emerging technologies, such as *in silico* drug screenings and *in silico* drug development.

The *de facto* gold standard approach to find novel drugs -the phenotypic screening- is old, maybe a bit out-dated, but due to the relatively small knowledge on all the proteins in the eukaryote kingdom, it is still a necessary approach to find novel drugs (Swinney and Anthony, 2011). As Swinney reported in a comparative study, phenotypical drug screening is the leading method for finding novel first-class drugs. The follower compounds are more frequently found by the target screening approach, because the biological details have been explained by the discovery of the first-class drug (Swinney and Anthony, 2011). The lack of knowledge is evident in the antischistosomal drug development field, where the mechanism of action of praziquantel is still unclear. This could stall research and the development of praziquantel alternatives (Marxer et al., 2012).

Parasitic organisms are very complex; they have co-evolved with their hosts for millions of years and many parts of their genome are still unknown. Therefore, more research is required to find possible new drug targets (Young et al., 2012, Berriman et al., 2009). In parasitic diseases, the interactions with human proteins are essential for the establishment and development of the parasites (Han et al., 2009, Jones, 2014, Schistosoma japonicum Genome and Functional Analysis, 2009). There is a new initiative started by Mullard and other researchers - Target 2035 - for finding a specific probe for each component of the human proteome within 2035, in order to foster the knowledge of all the human protein functions and molecular interactions (Mullard, 2019). Some of these proteins might be used to target molecular targets of the host required by the parasites for their development. The knowledge of the human proteome could lead to an increased usage of target-based screening -instead of the phenotypic screening- to find novel first-class drug candidates (Mullard, 2019).

I will discuss the advances in *in silico* drug discovery to highlight the latest evolutions and paradigm shifts in the drug discovery field by employing new technologies, which could be used in search for novel compounds (section 1.1). In section 1.2, I will discuss the project in which we aim to mitigate the drawbacks of the gold standard drug screening method by developing an impedance-based drug screening system. In section 1.3 I will discuss the possibility to include a primary human liver microtissue-based system to expand the current drug screening capacity in order to test prodrugs, to evaluate drug metabolites and to analyse drug- related cytotoxicity. Finally, in section 1.4, I will discuss and contextualise the project in which we compare the activity of a praziquantel polymorph-based derivative to commercial praziquantel.

2.1 Advances in *in silico* drug screenings

In recent years, with the advance of the computational power and increased knowledge of protein structures in freely available public databases (e.g. SwissProt, Expasys), drug discovery has been moving more and more to the direction of *in silico* molecular docking, *in situ* binding and *ex-novo* design, which are based on advanced 3D structural protein models. In this context, drug discovery and drug design for millions of possible compounds can be performed in days and not anymore in months/years (Wishart et al., 2006, Terstappen and Reggiani, 2001). In the anti-helminthic drug discovery field this is very beneficial because an *in vitro* based screen of thousands of compounds is very time-consuming and costly with some ethical aspects to consider. Parasites are obtained in low yield and their complex life cycle makes it laborious to test many compounds *in vitro* (Lombardo et al., 2019a, Pasche et al., 2018b, Pasche et al., 2018a, Panic et al., 2015). *Schistosoma spp*. cannot be grown from eggs to parasites *in vitro*, because the parasites require the intermediate and the definitive host to mature (Keiser, 2010). The novel technological improvements in machine learning and neural networks can greatly help the discovery and design of novel drug entities or the remodelling of existing drugs into better compounds by using both structure-based drug design (SBDD) and ligand-based drug design (LBDD). Those are the two types of computer-aided drug design (CADD) (Yu and MacKerell, 2017). The recent elucidation of the genomes of *Schistosoma mansoni*, *S. haematobium* and *S. japonicum* (Berriman et al., 2009, Schistosoma japonicum Genome and Functional Analysis, 2009, Young et al., 2012) makes CADD approaches very useful to specifically design a compound targeting the known structural molecular elements of the parasites. The freely available databases that offer potential drug targets, such as TDR Targets Database, Therapeutic Targets Database (TTD), DrugBank as well as the sequenced *Schistosoma mansoni* and other *Schistosoma* spp. genomes can be used to evaluate potential new drug targets. Identified drug targets can be used to screen hundreds of known molecular structures *in silico* to evaluate potential fits and estimate structure activity relations (SAR). For example, Torini *et al.* structurally characterized the key component of the purine salvage pathway, the Adenosine Phosphorylase/5'-Methylthioadenosine Phosphorylase, encoded by the gene *Sm*MTAP (Torini et al., 2016). This enzyme was predicted to be a good drug target because *S. mansoni* parasites do not have *de novo* purine pathways but rely on the purine salvage pathway (Torini et al., 2016). Therefore, targeting such a pathway would inevitably harm the parasites' ability to synthesise DNA. However, targeting such structural elements is challenging, as they often have homologs in the host (Boumis et al., 2011).

The research and development of novel compounds to be used in human medicine requires 10-12 years and it is estimated to cost between 500 and 2000 million USD (Adams and Brantner, 2006). Therefore, the repurposing strategy coupled by *in silico* prediction of drug candidates already in the market for human medicine for other diseases, with the aim to repurpose them against schistosomiasis, would be most favourable in the field of NTDs, that, by definition, lacks sufficient funding (Macleod et al., 2019). The strategy offers an excellent cost-benefit ratio by diminishing the time and money that would otherwise be required for the development of new compounds to bring them to the market (Panic et al., 2014).

There are some examples of *in silico* drug repurposing for *S. mansoni*, such as the study in which over 20 different compound candidates were identified, targeting metabolically active pathways in *S. mansoni* (Calixto et al., 2019). *In silico* based drug repurposing was used in genomic studies (Ziniel et al., 2016), in which the one member of the cytochrome P450 family (SmCYP450) found in *S. mansoni* was identified as potential drug target. Given the essential role of SmCYP450 in the development of the parasites, the authors identified miconazole as inhibitor of the SmCYP450 enzyme, leading to a high *in vitro* activity of the compound against *S. mansoni* parasites (Ziniel et al., 2016). In another study, over 115 potential drug candidates were found by *in silico* prediction, 20 of which were confirmed to be active on *S. mansoni* (Neves et al., 2015).

In conclusion, *in silico* drug screening or *in silico* drug repurposing can be very interesting methods that could be applied to facilitate drug screenings, for example by choosing only the most promising compounds out of huge compound libraries. The facilitation is of particular importance in a field like schistosomiasis where the funding is a problem and where the *in vitro* model does not allow high throughput screenings because of the low parasite yield. However, the *in silico* drug screenings and cheminformatics in general have their limitations. One of the most important limitations is the computational power required by such an approach, because oftentimes computational facilities providing cloud computing systems are needed and this could require big investments that are not possible to all laboratories. Finally, the current algorithms might also predict false positive hits that are not active *in vitro*, reducing the advantages offered by these computational models. However, *in silico* drug screening and *in silico* drug repurposing would still hold advantages over traditional high throughput screening in terms of time and money (Sacan et al., 2012). Ideally, a non-profit research and development organization, such as Drugs for Neglected Diseases initiative (DNDi) would finance and organize the development of a computational facility where other partners and laboratories could remotely join and take advantage of the novel *in silico* drug screening and *in silico* drug design benefits for the development of novel drug candidates against schistosomiasis.

2.2 EIS-based real time drug screening on *Schistosoma mansoni*

One of the most challenging parts of drug screening against schistosomiasis is the lack of automation and the subjectivity of the gold standard drug screening method on *Schistosoma spp.,* which is based on phenotypic evaluation by visual scoring of NTS viability (Keiser, 2010) (Chapter I). In the project further explained in Chapter II, we addressed these issues. Together with the Bio Engineering Laboratory (BEL) at the ETH in Basel, led by Prof. Andreas Hierlemann, we developed a novel platform to evaluate *in vitro* drug activity on NTS in real time. We employed electrical impedance spectroscopy (EIS) for the investigation of the dielectric properties of NTS. The big advantage of EIS is that it is a non-destructive technique, it is a label free method and it can be integrated into other platforms with relative ease. Those were the main reasons for which we decided to use this technology for the development of a novel promising way to analyse NTS viability for drug screening.

To develop the EIS platform, we adopted a polydimethylsiloxan (PDMS) matrix, in order to develop a biocompatible prototyping platform to record NTS-viability. The EIS based platform helped us evaluate the drug activity onset on NTS in more detail and at better time-resolution, providing real time measurement of the parasites' motility after drug administration. In addition, the platform allowed for microscopical evaluation of the parasites' morphology simultaneous to the EIS measurement.

EIS has been implemented already with a variety of biological samples in solution, such as single cells (Sun and Morgan, 2010) and plants for detection of viability of seeds (Repo et al., 2002). EIS has been used for organisms such as *C. elegans* (Zhu et al., 2018) and for *S. mansoni* (Rinaldi et al., 2015). The latter study evaluated the use of xCELLigence technology for the assessment of motility in *S. mansoni* adult worms, cercariae and hatching eggs. Although it was possible to determine the motility of adult worms, cercariae and hatching eggs, the 96-well plate format of this technique precluded accurate assessment of NTS motility. This could likely be explained by a lower sensitivity of this platform, due to an increased surface area of measurement, in contrast to our platform that has a smaller surface area. Moreover, due to the lower sensitivity of the xCELLigence in the evaluation of the parasites' motility, thousands of cercariae or eggs or several adult worms are required. In contrast, the EIS platform we developed allows for using 10 times fewer parasites than the standard drug screening assay on NTS and hundreds of times less parasites than would be necessary with xCELLigence. Moreover, in contrast to the costly and non-reusable xCELLigence plates, our EIS based platform can be autoclaved and reused multiple times.

We developed two EIS-based platforms. The first one was used as a method validation for the implementation of EIS to evaluate parasite viability. We assembled a device that was based on microfluidics, PDMS and EIS (Chawla et al., 2018). We tested two compounds to compare the EIS-based platform with the already established visual scoring (Chapter I) in order to assess the robustness of the novel method on NTS. In this device, we were able to record viability through motility assessment of NTS, and we used microscopy to evaluate their phenotype and number to confirm the findings of the EIS (Chawla et al., 2018) (Figure 7). However, with this version of the platform we had some limitations, such as the low throughput, because the measurements could not be parallelized with more than three chambers simultaneously. In addition, the parasite loading was cumbersome, and it could influence the parasites' viability. A recurrent issue with the first platform was that the parasites were not directly co-cultured with the drug within the platform, but they were transferred into it at 24 and 72 hour endpoints. At those time-points, the parasites' motility was measured as a proxy for viability. During the parasites' loading from the inlet port (Figure 7), the flow generated within the device did not consistently transport all the NTS into the measurement area between the electrodes; many were spread in the channel. Furthermore, a lot of handling was required to correctly load the parasites into the device and to not make them clog the channel. All these issues led to decreased parasite viability already before the measurements.

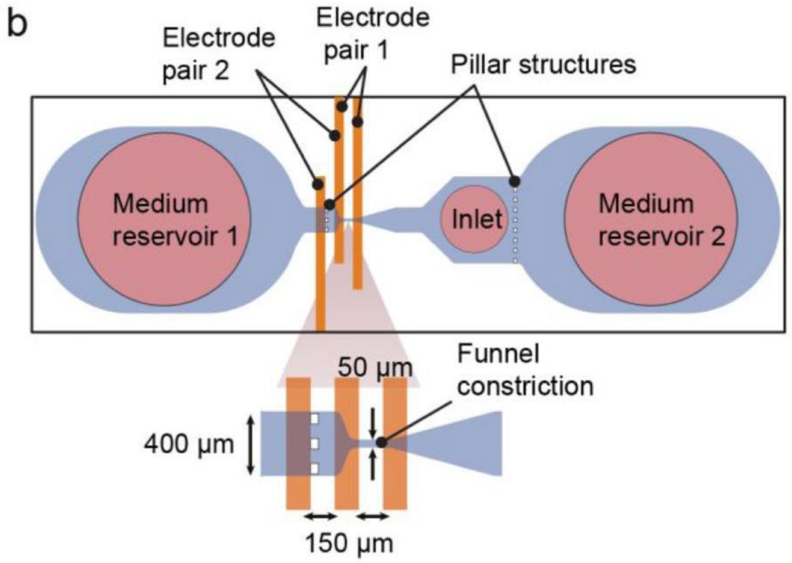

Figure 7: Figure showing the schematic of the first EIS based platform. The two co-planar electrodes pairs are depicted in orange.

To solve this first platform's limitations, we designed a second platform after multiple rounds of design changes and testing (Chapter II). The microfluidic component of the platform was removed. This ameliorated parasite loading and handling and it allowed much more rapid workflows. The larger measurement area -that now more closely resembles a standard half-area 96 well plate surface- ensured a higher viability of the parasites over time, allowing culturing of the NTS within the platform for over 48 hours. The increased measurement area and the absence of constraining structures, as in the first platform, were essential for the real-time measurement of the drug's activity on the NTS, since the novel platform layout did not show detrimental effects on the overall NTS viability (Figure 8).

However, the long-term NTS incubation for over 48 hours in the platform introduced a new issue: the problem of drug absorption by the PDMS, which is a known drawback of the PDMS matrix (Toepke and Beebe, 2006, Van Meer et al., 2016, Sasaki et al., 2010). This issue had not been relevant in the previous platform, since the NTS motility recordings were only performed at end-points of 24 and 72 hours. Some studies analysed intermediate substances that could be used on top of the PDMS to reduce its drug absorption: Sasaki *et al.* used substances such as hydrophobic polymers of poly(p-xylylene) –parylene to mitigate the absorption problem, showing a drastic reduction in the absorption of rhodamine B, once the parylene matrix was deposited on top of PDMS (Sasaki et al., 2010). Therefore, we adopted the same approach as Sasaki *et al.,* by coating the PDMS matrix with parylene. The approach was successful and we drastically reduced the absorption of rhodamine B, which is a good indicator of the absorption for the compounds we used (Chapter II).

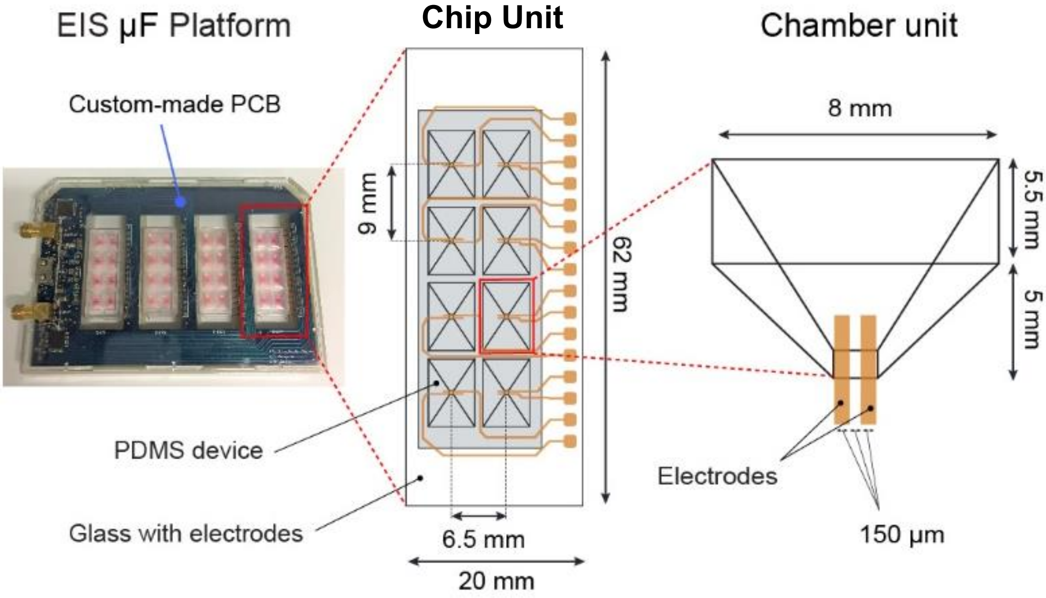

Figure 8: The schematic of the second platform. The printed circuit board (PCB) is illustrated in the left part of the figure; the polydimethylsiloxane (PDMS) chip unit is depicted in more detail in the middle and right part of the schematics. On the right side of the schematic, the chamber unit and the measurement area on top of the electrodes are illustrated.

For the second EIS-platform we decided to select some compounds with evident, yet varying activity *in vitro* on NTS. In this study with the second platform, we aimed to prove the EIS-based platform a good alternative to the standard visual scoring. To demonstrate this, we chose a fast acting compound that would kill the parasites immediately, such as oxethazaine, and one compound, methiothepin, that would increase drastically the parasites' motility (hypermotility). Hypermotility is in fact difficult to be scored by visual scoring (Chapter I). We performed in parallel standard visual scoring in 96 well plates for both compounds, in order to compare the dose response curves and IC_{50}.

Oxethazaine showed high and fast activity *in vitro*, confirming previous findings from Panic *et al.* (2015). With the EIS platform, we observed the compound's onset of action on NTS already at 30 min post drug exposure. Oxethazaine is commonly used in human medicine as potent local anaesthetic and as therapy against esophagitis and other gastro-intestinal diseases. The mechanism of action of oxethazaine is based on reducing the tendency of voltage-dependent sodium channels to activate (PubChem). Possibly, the blockage of the sodium voltage dependent channels is the reason for the fast activity of the compound on NTS, causing the parasites' complete paralysis within one hour after treatment.

Methiothepin had a fast onset of action on NTS, but it showed lethality only in the high range of the tested concentrations in both EIS and visual scoring on standard plates. Methiothepin has a role as an antipsychotic agent by antagonizing serotonin receptors (5-HT1, 5-HT2). The onset of activity was observed to be within 15 minutes after co-incubation of the NTS with the compound. The compound had already been tested against the sporocyst stage and adult stage of the *S. mansoni* parasites as shown by Boyle *et al.* (2000, 2005) (Boyle and Yoshino, 2005, Boyle et al., 2000). Methiothepin inhibited the parasites' movements, according to the authors by blocking serotonin intake, which plays a crucial role in the parasitic movements (Boyle et al., 2000). In contrast, we observed hypermotility once the drug was tested on NTS, therefore indicating an excitatory effect of the methiothepin on the NTS and not inhibition of the movements as described by Boyle *et al.* on the sporocyst stage and adult stage of *S. mansoni* parasites. One possible explanation for this difference could be the genetic differences between the *S. mansoni* Liberian strain used in our experiments and the Puerto Rican strain used by Boyle *et al.*, as well as the differences between the sporocyst and adult stages of the parasites, as used by Boyle *et al.*, and the NTS stage, which we used in our experiments. (Boyle et al., 2000, Boyle and Yoshino, 2005). Other studies demonstrated that bromocriptine and rotundine, selective inhibitors of 5HT, induced hypermotility on NTS (Chan et al., 2016). They showed similar results to the ones we obtained using different compounds acting in a similar way as methiothepin on NTS. This might indicate a common pathway in which bromocriptine and methiothepin could exert their mechanism of action (MOA), maybe by targeting a common receptor for the 5-HT or by targeting different parts of the same molecular pathway. In short, methiothepin and oxethazaine had different effects on NTS and those could be observed in both the EIS platform and visual scoring. However, the EIS platform provided objective evaluation; while the standard assay was less precise. In the case of oxethazaine, the results were very similar, while the methiothepin results were more discordant between the two drug screening methods (Chapter II).

To make the comparison to the standard assay more complete, we evaluated the effect of praziquantel in a side-by-side comparison between the EIS based platform and the standard drug screening on NTS. Praziquantel is active *in vitro* on NTS but not lethal; the drug induces changes in the behaviour and morphology of NTS. Among those changes, we observed an increase in motility within 30 minutes after drug administration, a darkening of the tegument including evident blebs on the parasites' tegument and contractions of the parasites' length. However, because the effect of praziquantel *in vitro* on juvenile stages of the parasites is mild, praziquantel's effect *in vitro* is hard to evaluate by visual scoring and it requires a trained operator to score the characteristic drug-induced phenotype on NTS accurately. The comparison between the two techniques resulted again in a similar precision, but the EIS scoring was objective and automated, in contrast to the standard visual scoring.

The EIS based platform could be useful also in the context of exploration of the compound's MOA, because providing real time information on the compound's activity could help define specific time-points in which the compound can be found bound to its molecular target(s) and this could facilitate the identification of those targets. Coupling the platform with confocal microscopy and the usage of fluorescent probes could help resolve the molecular location(s) to which the compound of interest is bound. Another advantage of the EIS platform is the possible selection of very active compounds only, because the compound onset of action can be determined in real time. Until now, in fact, selecting fast-acting compounds was challenging and required a lot of operator time, because the screening time points had to be increased.

In conclusion, we demonstrated the usage of EIS as a suitable alternative method to the standard visual scoring for drug screening on NTS. We obtained similar dose response curves and similar IC_{50} demonstrating the usability of this technology as possible replacement for the visual scoring on NTS. The EIS platform we developed has many advantages over the standard drug screening assay on NTS as discussed above, but it is not free from drawbacks. For example, the cost for the preparation of the chips and the necessity of a clean room to prepare the electrodes for the measurements can be major constraints for the adoption of this technology in other laboratory settings. In addition, the transimpedance recorder can be very expensive and out of budget for many laboratories working on NTDs. It is possible to reduce the costs related to this platform by plastic fabrication in the future, using for example an injection molding. In addition, the transimpedance device can be less sensitive than the one we have used in this study, and therefore cheaper. However, to reduce the costs associated with the production and the usage of this platform, it would need to be mass produced. Further studies are required to assess the feasibility of this. At the current stage, the platform allows only the readout of the NTS stage of *S. mansoni*, but it could be potentially adapted to other stages and/or parasites, to maximise the cost-usability of the platform. More research on the latter point is necessary to establish the EIS platform usage for other parasites and/or stages.

2.3 Incorporation of liver microtissues into the drug screening procedure

Many of the compounds that are tested in our laboratory show interesting activity *in vitro* against NTS and adults, but fail to show activity *in vivo*. There are many possible reasons to explain this phenomenon, such as unknown administration dosage and high first pass metabolism that could inactivate the compound before reaching the systemic circulation. There are some compounds such as prodrugs that can hardly be pre-screened *in vitro*, because they need to be pre-activated by the liver enzymes first. Prodrugs can lessen some of the drawbacks commonly seen in standard compounds, such as low water solubility, high first pass metabolism and increased resistance to pH. Prodrugs are precursors of the API, conjugated with additional chemical groups. Once the additional groups are removed from the API by the liver CYPs, the compound is active. This strategy is increasingly being considered for novel drug candidates, because it can increase the compounds' bioavailability and it reduces the first pass metabolism and at the same time it increases the duration of action of the compounds (Ortiz de Montellano, 2013).

In addition, a liver-based drug screening system could provide important information on a compound's cytotoxicity, such as drug induced liver injuries (DILI) evaluation by analysis of some of the specific liver-related markers for this condition such as miR-122 and miR-192. Including liver microtissues into the drug screening process could also provide information on the drug metabolism, for example by evidencing the compound's metabolites. Furthermore, such a system can provide information on a compound's cytotoxicity by quantification of intracellular ATP (Proctor et al., 2017, Hendriks et al., 2016). The liver human primary microtissues technology extends the capability offered by the standard primary liver culture, by prolonging the functionality of the cells, thereby extending the stable expression of CYP enzymes for more than four weeks, in comparison to just two weeks for flat cell cultures (Proctor et al., 2017, Simon et al., 2018). This becomes important when testing long drug exposure effects such as DILI, which with the standard cell cultures is not feasible after two weeks (Proctor et al., 2017). In addition, liver microtissues resemble the human liver and are capable of metabolizing most of the compounds with their high expression of CYPs (Bale et al., 2014).

We tested primary human liver microtissues to evaluate whether they could bioactivate or bioinactivate drugs and prodrugs to test *in vitro* on *S. mansoni* NTS. I compared the IC_{50} of the liver microtissues' medium after co-exposure with compounds to the IC_{50} obtained in the standard drug screening assay on NTS to assess the functionality of such a platform in drug screening. We evaluated the cytotoxicity of praziquantel and the other tested compounds by intracellular ATP quantification. In addition, we evaluated the metabolism of praziquantel by LC-MS/MS quantification of praziquantel's main metabolite trans-OH-praziquantel (Chapter III).

Microtissues with praziquantel were tested to evaluate the liver microtissues' metabolism by quantification of the trans-OH-praziquantel metabolite at 24, 48 and 72 hours post exposure of the liver microtissues to 50, 25, 10, 2 µM of praziquantel. We analysed the conditioned medium for quantification of the R- and S- and trans-OH praziquantel for every time point by LC-MS/MS. We found that liver microtissues have an active metabolism that allows quantifying the trans-OH-praziquantel metabolised. We quantified about 250-300 ng/day of trans-OH-praziquantel. The presence of less active praziquantel metabolites was notably in contrast with the unchanged IC_{50} we observed after NTS direct co-incubation with liver microtissues. The reason for this divergence between expectation and observation could be explained by the fact that due to the very low concentration of praziquantel needed to cause a phenotypic change in NTS (as low as 2 µM and below could damage the NTS), there would always be enough parent compound present in solution so that the operator would score those phenotypic changes on NTS with low scores. In addition, the resolution of the visual scoring is very low for minimal changes in the parasites' phenotype, making the exact effect evaluation difficult.

The first step in planning such experiments is to carefully select potentially useful or informative drugs and in the following sections I will elaborate on why we chose the drugs that eventually were tested.

Auranofin is in fact a known active compound *in vitro* and we wanted to test whether the exposure to liver microtissues could alter its activity *in vitro* on NTS. The compound had been shown to be inactive *in vivo* on *S. mansoni* in infected mice. Perhaps a decrease in the compound's activity *in vivo* after exposure of the compound to the liver CYPs could be predicted *in vitro* with the microtissues approach. Auranofin is a gold salt that is used in human medicine as disease-modifying antirheumatic drug (DMARDs). Its mechanism of action has not been characterized but it is assumed that it acts as an inhibitor of kappab kinase and thioredoxin reductase (Roder and Thomson, 2015, Harbut et al., 2015). Auranofin is an example of a repurposed drug, being originally designed to treat DMARD, its use was expanded to the treatment of amoebiasis and tuberculosis (Roder and Thomson, 2015).

We tested tamoxifen citrate and terfenadine, since their high activity *in vitro* on NTS had previously been shown (Cowan and Keiser, 2015, Panic et al., 2015). We evaluated if the liver enzymes could bioactivate or bioinactivate them, thereby reducing or increasing their IC_{50} *in vitro* on NTS. Tamoxifen citrate is a prodrug classified as an essential drug for the treatment of oestrogen-receptor-positive breast cancer. Tamoxifen is metabolized by the cytochrome P450 isoforms CYP3A4, CYP2C9, and CYP2D6 into two active metabolites afimoxifene and endoxifen, both selective oestrogen receptor modulators (Sanchez-Spitman et al., 2019). Terfenadine is used as a peripherally selective antihistamine or antagonist of the histamine H1 receptor. It is a prodrug, completely metabolized to the active form fexofenadine in the liver by the enzyme cytochrome P450 3A4. (Perlmutter et al., 2014, Jeong et al., 2018).

Some of the main problems of the liver microtissue system are the high costs and the difficulty in prediction of pharmacokinetics. In fact, the liver microtissues are spheroids in a static medium, and the dynamics of the drug entering inside a sphere are not as simple as in flat cell cultures, where there are various models predicting pharmacokinetic parameters such as hepatic clearance and half-life ($t_{1/2}$) (Tóth et al., 2018). There are currently no models explaining exactly how and if the drug enters in the inner part of the liver spheroids and how different the permeability of the outer spheroids is from the inner spheroids. Another important factor to consider is the liver spheroids' albumin production (10-20 ng/spheroid/day). The albumin in our static system, for example, could bind the compounds in solution and retain them from permeating the NTS and by doing so, prevent their activity, which could be the reason for lower IC_{50} as we demonstrated for some of the tested compounds, such as tamoxifen (Chapter III). However, most likely the influence of the albumin produced by the liver microtissue system was negligible, because the microtissues only produce 10-20 ng/per day of albumin.

Nonetheless, there are solutions to make the system more dynamic. For example, in a next study, it would be interesting to integrate the microtissues in a microfluidic device with a gravity driven flow or a micro pump. In such a solution, multiple liver microtissues could be connected and exchange metabolites and other markers more efficiently than by using just one liver spheroid as we did in our study (Lohasz et al., 2017, Mittal et al., 2019). Furthermore, in such a platform, the prediction of the drugs' behaviour could be easier than in a static microtissue system, because inside this microfluidic device the fluid viscosity could resemble the one in the body and the albumin level could be adjusted to resemble the physiological plasma concentration in blood (45 g/Litre).

In future studies, the liver microtissue system could be combined with the EIS based platform (Chaper II) to gather more information on the compounds’ activity, dynamics and cytotoxicity simultaneously. In addition, more studies could help assembling an *in vitro* system resembling closely the *in vivo* settings of a human being. For example, multiple microtissue types, such as cardiac microtissue, lung microtissue and liver microtissues could be combined with the EIS technology. This "organ-on-a-chip" approach might facilitate the accurate prediction of pharmacokinetics and pharmacodynamics and provide information on compound testing more representative to human beings than animal models. Furthermore, such a system could be established to evaluate compounds' activity in more detail, for example providing precise information on the dynamics of action and the compound. Such a platform with microtissues from different organs involved in the parasite development, such as lungs, endothelial cells, heart and liver, might also be used to study the growth of *S. mansoni* NTS from juvenile into adult stages. This would allow to discover the essential unknown factors that do not allow the growth of the parasites *in vitro*. Growing parasites *in vitro* would increase the drug screening output and more testing could be performed on adult *S. mansoni*, perhaps making high throughput screening on adult *S. mansoni* parasites reality. However, more studies on this technology need to be conducted in order to fully exploit the potential offered by this novel cell culture type.

In conclusion, with this study, we are the first to explore the liver microtissue technology as a tool to improve the current drug screening against schistosomiasis. The liver microtissue system not only offers information on the effect of the cytochrome P450 family activity on prodrugs, but it is also able to provide important information on a compound’s toxicity and metabolites simultaneously. By enabling the selection of promising, non-toxic compounds for further assessment *in vivo*, the liver microtissue system could lead to a decreased usage of animal models in preclinical studies, thereby reducing the costs and the ethical issues related with drug screening and development.

2.4 Praziquantel and derivatives

One of the most important breakthroughs in the anthelminthic drug discovery history is praziquantel, a compound that complies with the Lipinski rule of five and that belongs to the Biopharmaceutics Classification System (BCS) class II compounds, because of its low solubility and high permeability. Praziquantel was developed in the early ‘70s for veterinary usage and used for human medicine a few years later (Alsaqabi, 2014, Cioli and Pica-Mattoccia, 2003).

Nowadays, praziquantel is massively used in the mass drug administration (MDA) campaigns organised by the WHO, with over 200 million doses of praziquantel given to individuals annually since the ‘80s (Wang and Liang, 2015, Olveda et al., 2016). This was possible thanks to private companies such as Merck and non-profit organisations such as WHO, which donated millions of doses, and the fact that a dose of praziquantel can currently be purchased for less than 0.30$ in some countries (Cioli and Pica-Mattoccia, 2003).

Praziquantel has not always been the sole drug candidate against schistosomiasis. For over 30 years, oxamniquine was the first-line drug in countries such as Brazil (Valentim et al., 2013). The drug was working very well, but in contrast to praziquantel, its mechanism of action was specific for *Schistosoma mansoni* only. This is because oxamniquine targets a specific sulfotransferase enzyme present in *S. mansoni* (Valentim et al., 2013). This was likely the main reason why the massive use of oxamniquine led to the rise of a resistant strain that rapidly spread across South America, making its use obsolete in 2010 (Fallon and Doenhoff, 1994, Bruce et al., 1987).

MDA campaigns have the purpose of controlling schistosomiasis to finally achieve elimination of the disease by 2020 (Wang and Liang, 2015, Olveda et al., 2016). This objective will not be reached. It is more likely that the objective might be achieved by 2030, as indicated by the sustainable development goals (SDGs) of the United Nations (UN) (Knopp et al., 2019). The reasons for missing the objective was the lack of re-infection prevention due to the limitations of praziquantel and the lack of proper sanitation, which is one of the main drivers of infection and reinfection in the first place (Fenwick and Jourdan, 2016, Secor and Montgomery, 2015).

Praziquantel is the main drug to fight schistosomiasis, but it is not without drawbacks, such as low water solubility and extensive first pass liver metabolism that limit the compound’s bioavailability (Olliaro et al., 2014). There are reports showing big inter-individual variability, with erratic absorption profiles, as reported (Kovac et al., 2018). This finding is confirmed by other comparative studies on praziquantel (El-Feky et al., 2015, El-Lakkany et al., 2012), underlining the inter-individual variability observed in praziquantel-treated individuals (Olliaro et al., 2014, Schneeberger et al., 2018). Genetic variation of the parasites might contribute to this inter-individual variability (Norton et al., 2010, Coeli et al., 2013). Others have suggested that the human microbiota is involved. (Sady et al., 2015) (Jenkins et al., 2018, Schneeberger et al., 2018). Generally, the effective time of the active pharmaceutical ingredient (API) in the blood circulation (duration of action) is short and the AUC (indicating the blood API concentration) is low. Praziquantel is rapidly absorbed (80% to 100%), but undergoes extensive first-pass hepatic metabolism. This results in inactive metabolites so that most of the active drug does not reach the systemic circulation (Secor and Montgomery, 2015, Kemal et al., 2019, Chan et al., 2017, Colley et al., 2014, McCarthy and Moore, 2015). Moreover, there are indications that the efficacy of praziquantel against schistosomiasis is decreasing, especially in countries where praziquantel has been used the longest, such as Egypt and Sudan (Doenhoff et al., 2008, Doenhoff and Pica-Mattoccia, 2006). The reason for this could be related to the selection of praziquantel resistant *Schistosoma spp.* in countries where MDA campaigns are common, due to the very high selective pressure to which the parasites are exposed (Coeli et al., 2013, Sady et al., 2015).

To alleviate the low water solubility and the extensive first pass metabolism, many improvements of the standard praziquantel formulation have been suggested. Solubility of praziquantel can be improved by administering a praziquantel -polyvinylpyrrolidone solid dispersion, by encapsulating it into clay, by using nanoparticles or by co-administration of praziquantel with other drugs that could eventually improving praziquantel bioavailability (El-Lakkany et al., 2012, El-Feky et al., 2015, Elmasry et al., 2017, Campelo et al., 2017). Praziquantel derivatives are being developed and tested, such as organometallic derivatives, and two praziquantel derivatives conjugated with $Cr(CO)_3$ showed interesting *in vitro* and *in vivo* results (Hess et al., 2015).

Here I elaborate on my research on the effects of a polymorph co-crystal-based formulation derivative on *S. mansoni*. A polymorph is defined as a solid material that can have different crystalline forms and different special rearrangements of the crystal lattice. The polymorphic crystals differ in their physicochemical properties such as dissolution rate, solubility, stability and hygroscopicity compared to their amorphous state (Raza, 2014). In this work, we tested the praziquantel derivative *in vitro* on NTS as well as adult worms and *in vivo* in a side by side comparison with the standard praziquantel. We found that the novel compound was less effective than the standard praziquantel in terms of absolute WBR. However, we did observe differences in pharmacokinetics and pharmacodynamics. *In vivo* WBR that we observed with the polymorph was 60%, while the standard praziquantel had a WBR of 68% overall (Figure 9). One of the reasons for this result could be its administration as a solution: This might have altered the co-crystal formulation of the compound, perhaps lessening its advantages. It might have been advantageous to administer the compound in microcapsules *in vivo* in order to not solubilize the compound before reaching the gastro-intestinal (GI) tract. A microcapsule administration of the praziquantel polymorph might have prevented the transition to the standard conformation, thereby enhancing the water solubility advantage offered by the polymorphic formulation (Lombardo et al., 2019b).

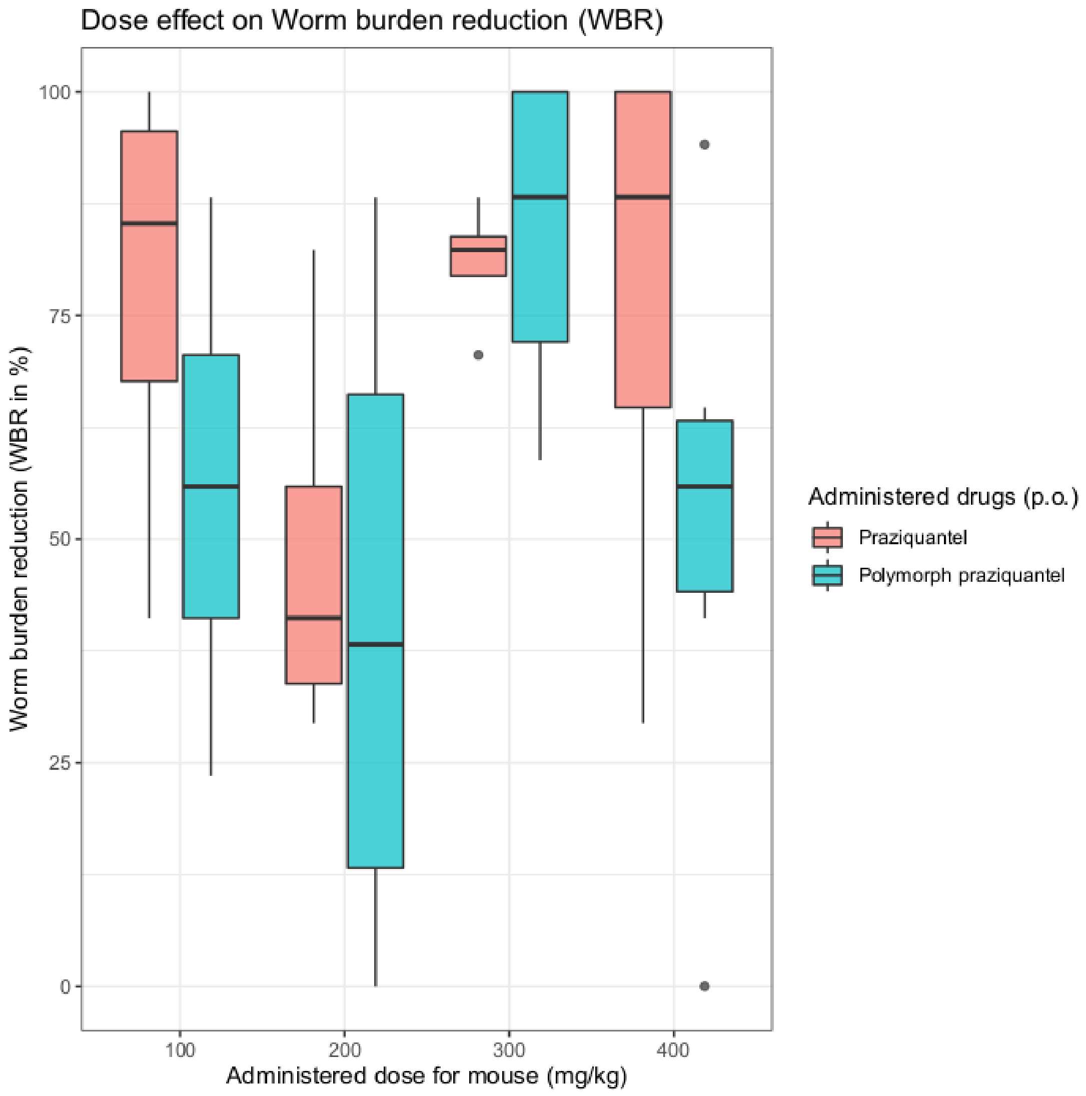

Figure 9: Worm burden reduction by dose. The box plot indicates the WBR by each of the tested concentrations *in vivo* for the standard praziquantel and polymorph praziquantel.

The praziquantel formulation derivative was absorbed slower than the standard praziquantel and the maximum concentration (C_{max}) in the circulation did not reach the C_{max} obtained by the standard praziquantel. We did not find correlations between the C_{max} and the WBR, which indicates that other factors might be important for the drug activity *in vivo*. For example, in other studies the portal vein drug concentration was considered the main parameter for the determination of the effect of praziquantel: the portal vein drug concentration can be considered as the active part of the compound effectively affecting the blood flukes *Schistosoma spp.*, because the blood flukes reside in the mesenteric veins. (Abla et al., 2017).

Praziquantel is a racemate in which both R- and S- enantiomers are present at 50%. The active principle is the R-praziquantel, while the S-praziquantel is inactive and it is responsible for the bitter taste of the formulation. We evaluated the pharmacokinetics of the R- and S- praziquantel in murine plasma by LC-MS/MS and found the concentration of R-praziquantel to be superior to the one of S-praziquantel in both formulations (Figure 4). In humans the opposite trend can be found (Meister et al., 2016). The different concentration of the API between human and mice could be due to different P450 cytochromes and ADME parameters in mice and humans. Humans have seven genetic clusters with 27 active genes that encode CYP enzymes; mice have 72 active genes distributed in seven clusters (Nelson et al., 2004). It is possible that the enzymatic kinetics of some of the enzymes differ between species. More research should be conducted in order to establish the exact behaviour of praziquantel in mice and in other animal models, in order to better understand its mechanism of action.

In conclusion, polymorphs could represent a valid opportunity to further develop existing drugs without undergoing the time and money requirements of developing a completely new compound. McCrone’s law states that “every compound has different polymorphic forms, and that, in general, the number of forms known for a given compound is proportional to the time and money spent in research on that compound.”(McCrone, 1965). Praziquantel is the mainstay treatment against schistosomiasis. However, its drawbacks and the decrease of the compound efficacy in endemic areas indicate the importance to develop novel anthelmintics. In order to develop praziquantel derivatives that have an impact on schistosomiasis, it is important to accurately define praziquantel's mechanisms of action and identify all the molecular targets of the compound. Although the praziquantel polymorph we tested in this study had no superior efficacy to the standard praziquantel, polymorphs are still an interesting possibility that could be explored for novel drug candidates’ development.

3. Conclusion and outlook

Drug discovery and development are essential elements for human and animal health. Schistosomiasis currently relies on a single drug for treatment of millions of people, praziquantel. Since praziquantel has been used for 40 years, the emergence of resistance poses a threat to the wellbeing of millions of people, therefore there is a necessity to find alternative drugs to accompany and potentially replace the only one available at the moment. However, this is quite a challenging task due to the complex parasite life cycle, the resulting limited drug screening throughput and the socio-economic status of NTDs, being associated with the poorest regions of the world. We tried to tackle these issues by providing novel solutions to increase drug screening throughput and lower the costs associated with it.

This work consists of several projects that I worked on: the development of a novel drug screening platform; the inclusion of liver microtissues in the drug screening process and the testing of a derivative version of praziquantel.

The EIS based platform can be used to increase the drug screening throughput and the objectivity of the drug screening on NTS, which would foster common ground between labs working with the same drug screening technology. The EIS based platform can be mass-produced by plastic-based injection printing of the current template and is reusable, which would make the platform cheap and easy to adopt in various research settings. Also, the real-time evaluation of the parasites' viability made possible by this platform might expedite the identification of fast acting compounds.

The human primary liver microtissues based project aimed at extending the output of the standard drug screening by making use of the liver P450 cytochromes' metabolism to process drugs into metabolites that are active or inactive on NTS. This approach, although it could cause considerable costs, would allow simultaneous drug screening, hepatotoxicity evaluation and metabolite studies of interesting active compounds. Moreover, the liver microtissues, with more research being done on that subject, could be used as predictor for potential lead compounds’ pharmacokinetics and dose finding.

Finally, we worked on a praziquantel polymorph and gained interesting insight on its metabolism in the mouse model. We did not find this compound to be more active than the standard praziquantel, but the idea of developing polymorphs could be an affordable way to produce more drug candidates with potentially new chemical-physical properties. Further research on other praziquantel polymorphs or co-crystal derivatives might lead to optimisations of the drug's properties, as well as the development of novel *in vivo* formulation strategies, such as nanoformulation.

With these projects we contributed significantly to the field of helminth drug discovery and I am confident that by providing these novel ideas, solutions and proof-of-concepts, we paved the way for faster, cheaper and more efficient drug screening and development against *S. mansoni*.

REFERENCES:

ABLA, N., KEISER, J., VARGAS, M., REIMERS, N., HAAS, H. & SPANGENBERG, T. 2017. Evaluation of the pharmacokinetic-pharmacodynamic relationship of praziquantel in the *Schistosoma mansoni* mouse model. *PLOS Neglected Tropical Diseases,* 11**,** e0005942.

ADAMS, C. P. & BRANTNER, V. V. 2006. Estimating the cost of new drug development: is it really 802 million dollars? *Health Aff (Millwood),* 25**,** 420-8.

ALSAQABI, S. M. 2014. Praziquantel: A Review. *Journal of Veterinary Science & Technology,* 05.

BALE, S. S., VERNETTI, L., SENUTOVITCH, N., JINDAL, R., HEGDE, M., GOUGH, A., MCCARTY, W. J., BAKAN, A., BHUSHAN, A., SHUN, T. Y., GOLBERG, I., DEBIASIO, R., USTA, B. O., TAYLOR, D. L. & YARMUSH, M. L. 2014. *In vitro* platforms for evaluating liver toxicity. *Exp Biol Med (Maywood),* 239**,** 1180-1191.

BERRIMAN, M., HAAS, B. J., LOVERDE, P. T., WILSON, R. A., DILLON, G. P., CERQUEIRA, G. C., MASHIYAMA, S. T., AL-LAZIKANI, B., ANDRADE, L. F., ASHTON, P. D., ASLETT, M. A., BARTHOLOMEU, D. C., BLANDIN, G., CAFFREY, C. R., COGHLAN, A., COULSON, R., DAY, T. A., DELCHER, A., DEMARCO, R., DJIKENG, A., EYRE, T., GAMBLE, J. A., GHEDIN, E., GU, Y., HERTZ-FOWLER, C., HIRAI, H., HIRAI, Y., HOUSTON, R., IVENS, A., JOHNSTON, D. A., LACERDA, D., MACEDO, C. D., MCVEIGH, P., NING, Z., OLIVEIRA, G., OVERINGTON, J. P., PARKHILL, J., PERTEA, M., PIERCE, R. J., PROTASIO, A. V., QUAIL, M. A., RAJANDREAM, M.-A., ROGERS, J., SAJID, M., SALZBERG, S. L., STANKE, M., TIVEY, A. R., WHITE, O., WILLIAMS, D. L., WORTMAN, J., WU, W., ZAMANIAN, M., ZERLOTINI, A., FRASER-LIGGETT, C. M., BARRELL, B. G. & EL-SAYED, N. M. 2009. The genome of the blood fluke Schistosoma mansoni. *Nature,* 460**,** 352-358.

BOUMIS, G., ANGELUCCI, F., BELLELLI, A., BRUNORI, M., DIMASTROGIOVANNI, D. & MIELE, A. E. 2011. Structural and functional characterization of *Schistosoma mansoni* Thioredoxin. 20**,** 1069-1076.

BOYLE, J. P. & YOSHINO, T. P. 2005. Serotonin-induced muscular activity in *Schistosoma mansoni* larval stages: importance of 5-HT transport and role in daughter sporocyst production. *J Parasitol,* 91**,** 542-50.

BOYLE, J. P., ZAIDE, J. V. & YOSHINO, T. P. 2000. *Schistosoma mansoni*: effects of serotonin and serotonin receptor antagonists on motility and length of primary sporocysts *in vitro*. *Exp Parasitol,* 94**,** 217-26.

BRUCE, J. I., DIAS, L. C., LIANG, Y. S. & COLES, G. C. 1987. Drug resistance in schistosomiasis: a review. *Memorias Do Instituto Oswaldo Cruz,* 82 Suppl 4**,** 143-150.

CALIXTO, N. M., DOS SANTOS, D. B., BEZERRA, J. C. B. & SILVA, L. D. A. 2019. *In silico* repositioning of approved drugs against *Schistosoma mansoni* energy metabolism targets. *PLOS ONE,* 13**,** e0203340.

CAMPELO, Y. D. M., MAFUD, A. C., VÉRAS, L. M. C., GUIMARÃES, M. A., YAMAGUCHI, L. F., LIMA, D. F., ARCANJO, D. D. R., KATO, M. J., MENDONÇA, R. Z., PINTO, P. L. S., MASCARENHAS, Y. P., SILVA, M. P. N., DE MORAES, J., EATON, P. & DE SOUZA DE ALMEIDA LEITE, J. R. 2017. Synergistic effects of *in vitro* combinations of piplartine, epiisopiloturine and praziquantel against *Schistosoma mansoni*. *Biomedicine & Pharmacotherapy,* 88**,** 488-499.

CHAN, J. D., CUPIT, P. M., GUNARATNE, G. S., MCCORVY, J. D., YANG, Y., STOLTZ, K., WEBB, T. R., DOSA, P. I., ROTH, B. L., ABAGYAN, R., CUNNINGHAM, C. & MARCHANT, J. S. 2017. The anthelmintic praziquantel is a human serotoninergic G-protein-coupled receptor ligand. *Nat Commun,* 8**,** 1910.

CHAN, J. D., MCCORVY, J. D., ACHARYA, S., JOHNS, M. E., DAY, T. A., ROTH, B. L. & MARCHANT, J. S. 2016. A miniaturized screen of a *Schistosoma mansoni* serotonergic G protein-coupled receptor identifies novel classes of parasite-selective inhibitors. *PLOS Pathogens,* 12**,** e1005651.

CHAWLA, K., MODENA, M. M., RAVAYNIA, P. S., LOMBARDO, F. C., LEONHARDT, M., PANIC, G., BURGEL, S. C., KEISER, J. & HIERLEMANN, A. 2018. Impedance-based microfluidic assay for automated antischistosomal drug screening. *ACS Sens*.

CIOLI, D. & PICA-MATTOCCIA, L. 2003. Praziquantel. *Parasitology Research,* 90**,** S3–S9.

COELI, R., BABA, E. H., ARAUJO, N., COELHO, P. M. Z. & OLIVEIRA, G. 2013. Praziquantel Treatment Decreases *Schistosoma mansoni* Genetic Diversity in Experimental Infections. *PLOS Neglected Tropical Diseases,* 7**,** e2596.

COLLEY, D. G., BUSTINDUY, A. L., SECOR, W. E. & KING, C. H. 2014. Human schistosomiasis. *The Lancet,* 383**,** 2253-64.

COWAN, N. & KEISER, J. 2015. Repurposing of anticancer drugs: *in vitro* and *in vivo* activities against *Schistosoma mansoni*. *Parasites & Vectors,* 8**,** 417.

DOENHOFF, M. J., CIOLI, D. & UTZINGER, J. 2008. Praziquantel: mechanisms of action, resistance and new derivatives for schistosomiasis. *Curr Opin Infect Dis,* 21**,** 659-67.

DOENHOFF, M. J. & PICA-MATTOCCIA, L. J. E. R. O. A.-I. T. 2006. Praziquantel for the treatment of schistosomiasis: its use for control in areas with endemic disease and prospects for drug resistance. 4**,** 199-210.

EL-FEKY, G. S., MOHAMED, W. S., NASR, H. E., EL-LAKKANY, N. M., SEIF EL-DIN, S. H. & BOTROS, S. S. 2015. Praziquantel in a clay nanoformulation shows more bioavailability and higher efficacy against murine *Schistosoma mansoni* infection. *Antimicrobial Agents and Chemotherapy,* 59**,** 3501-8.

EL-LAKKANY, N., SEIF EL-DIN, S. H. & HEIKAL, L. 2012. Bioavailability and *in vivo* efficacy of a praziquantel-polyvinylpyrrolidone solid dispersion in *Schistosoma mansoni*-infected mice. *European Journal of Drug Metabolism and Pharmacokinetics,* 37**,** 289-99.

ELMASRY, A., ALADEEB, N. M., ELKAREF, A. & ABOULFOTOUH, N. 2017. Simvastatin exerts antifibrotic effect and potentiates the antischistosomal effects of praziquantel in a murine model: Role of IL10. *Biomedicine & Pharmacotherapy,* 96**,** 215-221.

FALLON, P. G. & DOENHOFF, M. J. 1994. Drug-Resistant Schistosomiasis: Resistance to Praziquantel and Oxamniquine Induced in *Schistosoma mansoni* in Mice is Drug Specific. *The American Journal of Tropical Medicine and Hygiene,* 51**,** 83-88.

FENWICK, A. & JOURDAN, P. 2016. Schistosomiasis elimination by 2020 or 2030? *Int J Parasitol,* 46**,** 385-8.

HAN, Z.-G., BRINDLEY, P. J., WANG, S.-Y., CHEN, Z. J. A. R. O. G. & GENETICS, H. 2009. *Schistosoma* genomics: new perspectives on schistosome biology and host-parasite interaction. 10**,** 211-240.

HARBUT, M. B., VILCHÈZE, C., LUO, X., HENSLER, M. E., GUO, H., YANG, B., CHATTERJEE, A. K., NIZET, V., JACOBS, W. R. & SCHULTZ, P. G. 2015. Auranofin exerts broad-spectrum bactericidal activities by targeting thiol-redox homeostasis. *J Proceedings of the National Academy of Sciences,* 112**,** 4453-4458.

HENDRIKS, D. F., FREDRIKSSON PUIGVERT, L., MESSNER, S., MORTIZ, W. & INGELMAN-SUNDBERG, M. 2016. Hepatic 3D spheroid models for the detection and study of compounds with cholestatic liability. *Sci Rep,* 6**,** 35434.

HESS, J., KEISER, J. & GASSER, G. 2015. Toward organometallic antischistosomal drug candidates. *Future Med Chem,* 7**,** 821-30.

JENKINS, T. P., PEACHEY, L. E., AJAMI, N. J., MACDONALD, A. S., HSIEH, M. H., BRINDLEY, P. J., CANTACESSI, C. & RINALDI, G. 2018. *Schistosoma mansoni* infection is associated with quantitative and qualitative modifications of the mammalian intestinal microbiota. *Scientific Reports,* 8**,** 12072.

JEONG, D., PARK, H. G., LIM, Y. R., LEE, Y., KIM, V., CHO, M. A. & KIM, D. 2018. Terfenadine metabolism of human cytochrome P450 2J2 containing genetic variations (G312R, P351L and P115L). *Drug Metab Pharmacokinet,* 33**,** 61-66.

JONES, B. 2014. Exploring gene function and parasite–host protein interactions. *Nature Reviews Genetics,* 15**,** 646.

KEISER, J. 2010. *In vitro* and *in vivo* trematode models for chemotherapeutic studies. *Parasitology,* 137**,** 589-603.

KEMAL, M., TADESSE, G., ESMAEL, A., ABAY, S. M. & KEBEDE, T. 2019. *Schistosoma mansoni* infection among preschool age children attending Erer Health Center, Ethiopia and the response rate to praziquantel. *BMC Res Notes,* 12**,** 211.

KNOPP, S., PERSON, B., AME, S. M., ALI, S. M., HATTENDORF, J., JUMA, S., MUHSIN, J., KHAMIS, I. S., MOHAMMED, K. A., UTZINGER, J., HOLLENBERG, E., KABOLE, F. & ROLLINSON, D. 2019. Evaluation of integrated interventions layered on mass drug administration for urogenital schistosomiasis elimination: a cluster-randomised trial. *Lancet Glob Health*.

KOVAC, J., MEISTER, I., NEODO, A., PANIC, G., COULIBALY, J. T., FALCOZ, C. & KEISER, J. 2018. Pharmacokinetics of praziquantel in *Schistosoma mansoni*- and *Schistosoma haematobium*-Infected School- and Preschool-Aged Children. *Antimicrob Agents Chemother,* 62.

LOHASZ, C., FREY, O., RENGGLI, K. & HIERLEMANN, A. 2017. A Tubing-Free, Microfluidic Platform for the Realization of Physiologically Relevant Dosing Curves on Cellular Models. 1**,** 497.

LOMBARDO, F. C., PASCHE, V., PANIC, G., ENDRISS, Y. & KEISER, J. 2019a. Life cycle maintenance and drug-sensitivity assays for early drug discovery in *Schistosoma mansoni*. *Nature Protocols,* 14**,** 461-481.

LOMBARDO, F. C., PERISSUTTI, B. & KEISER, J. 2019b. Activity and pharmacokinetics of a praziquantel crystalline polymorph in the *Schistosoma mansoni* mouse model. *Eur J Pharm Biopharm*.

MACLEOD, C. K., BRIGHT, P., STEER, A. C., KIM, J., MABEY, D. & PARKS, T. 2019. Neglecting the neglected: the objective evidence of underfunding in rheumatic heart disease. *Transactions of The Royal Society of Tropical Medicine and Hygiene,* 113**,** 287-290.

MARXER, M., INGRAM, K. & KEISER, J. 2012. Development of an in vitro drug screening assay using *Schistosoma haematobium* schistosomula. *Parasites & Vectors,* 5**,** 165.

MCCARTHY, J. S. & MOORE, T. A. 2015. 42 - Drugs for Helminths. *In:* BENNETT, J. E., DOLIN, R. & BLASER, M. J. (eds.) *Mandell, Douglas, and Bennett's Principles and Practice of Infectious Diseases (Eighth Edition).* Philadelphia: Content Repository Only!

MCCRONE, W. C. 1965. Polymorphism. *Physics and chemistry of the organic solid state,* 2, 725-767.

MEISTER, I., KOVAC, J., DUTHALER, U., ODERMATT, P., HUWYLER, J., VANOBBERGHEN, F., SAYASONE, S. & KEISER, J. 2016. Pharmacokinetic Study of Praziquantel Enantiomers and Its Main Metabolite R-trans-4-OH-PZQ in Plasma, Blood and Dried Blood Spots in *Opisthorchis viverrini*-Infected Patients. *PLoS Negl Trop Dis,* 10, e0004700.

MITTAL, R., WOO, F. W., CASTRO, C. S., COHEN, M. A., KARANXHA, J., MITTAL, J., CHHIBBER, T. & JHAVERI, V. M. 2019. Organ-on-chip models: Implications in drug discovery and clinical applications. *J Cell Physiol,* 234, 8352-8380.

MULLARD, A. 2019. A probe for every protein. *Nature Drug discovery reviews*.

NELSON, D. R., ZELDIN, D. C., HOFFMAN, S. M., MALTAIS, L. J., WAIN, H. M. & NEBERT, D. W. 2004. Comparison of cytochrome P450 (CYP) genes from the mouse and human genomes, including nomenclature recommendations for genes, pseudogenes and alternative-splice variants. *Pharmacogenetics,* 14, 1-18.

NEVES, B. J., BRAGA, R. C., BEZERRA, J. C. B., CRAVO, P. V. L. & ANDRADE, C. H. 2015. *In silico* repositioning-chemogenomics strategy identifies new drugs with potential activity against multiple life stages of *Schistosoma mansoni*. *PLOS Neglected Tropical Diseases,* 9, e3435.

NORTON, A. J., GOWER, C. M., LAMBERTON, P. H., WEBSTER, B. L., LWAMBO, N. J., BLAIR, L., FENWICK, A. & WEBSTER, J. P. 2010. Genetic consequences of mass human chemotherapy for *Schistosoma mansoni*: population structure pre- and post-praziquantel treatment in Tanzania. *Am J Trop Med Hyg,* 83, 951-7.

OLLIARO, P., DELGADO-ROMERO, P. & KEISER, J. 2014. The little we know about the pharmacokinetics and pharmacodynamics of praziquantel (racemate and R-enantiomer). *Journal of Antimicrobial Chemotherapy,* 69, 863-870.

OLVEDA, D. U., MCMANUS, D. P. & ROSS, A. G. P. 2016. Mass drug administration and the global control of schistosomiasis: successes, limitations and clinical outcomes. *Current Opinion in Infectious Diseases,* 29, 595-608.

ORTIZ DE MONTELLANO, P. R. 2013. Cytochrome P450-activated prodrugs. *Future Med Chem,* 5, 213-28.

PANIC, G., DUTHALER, U., SPEICH, B. & KEISER, J. 2014. Repurposing drugs for the treatment and control of helminth infections. *Int J Parasitol Drugs Drug Resist,* 4, 185-200.

PANIC, G., VARGAS, M., SCANDALE, I. & KEISER, J. 2015. Activity Profile of an FDA-Approved Compound Library against *Schistosoma mansoni*. *PLOS Neglected Tropical Diseases,* 9, e0003962.

PASCHE, V., LALEU, B. & KEISER, J. 2018a. Early antischistosomal leads identified from *in vitro* and *in vivo* screening of the Medicines for Malaria Venture Pathogen Box. *ACS Infectious Diseases*.

PASCHE, V., LALEU, B. & KEISER, J. 2018b. Screening a repurposing library, the Medicines for Malaria Venture Stasis Box, against *Schistosoma mansoni*. *Parasit. Vectors.,* 11, 298.

PERLMUTTER, J. I., FORBES, L. T., KRYSAN, D. J., EBSWORTH-MOJICA, K., COLQUHOUN, J. M., WANG, J. L., DUNMAN, P. M. & FLAHERTY, D. P. 2014. Repurposing the antihistamine terfenadine for antimicrobial activity against *Staphylococcus aureus*. *J Med Chem,* 57, 8540-62.

PROCTOR, W. R., FOSTER, A. J., VOGT, J., SUMMERS, C., MIDDLETON, B., PILLING, M. A., SHIENSON, D., KIJANSKA, M., STROBEL, S., KELM, J. M., MORGAN, P., MESSNER, S. & WILLIAMS, D. 2017. Utility of spherical human liver microtissues for prediction of clinical drug-induced liver injury. *Archives of Toxicology,* 91**,** 2849-2863.

PUBCHEM. *Oxethazaine, CID=4621* [Online]. Available: https://pubchem.ncbi.nlm.nih.gov/compound/Oxethazaine [Accessed 01/10 2019].

RAZA, K. 2014. Polymorphism: The Phenomenon Affecting the Performance of Drugs. *SOJ Pharmacy & Pharmaceutical Sciences*.

REPO, T., PAINE, D. H. & TAYLOR, A. G. 2002. Electrical impedance spectroscopy in relation to seed viability and moisture content in snap bean (Phaseolus vulgaris L.). *Seed Science Research,* 12**,** 17-29.

RINALDI, G., LOUKAS, A., BRINDLEY, P. J., IRELAN, J. T. & SMOUT, M. J. 2015. Viability of developmental stages of *Schistosoma mansoni* quantified with xCELLigence worm real-time motility assay (xWORM). *International Journal for Parasitology: Drugs and Drug Resistance,* 5**,** 141-148.

RODER, C. & THOMSON, M. J. 2015. Auranofin: repurposing an old drug for a golden new age. *Drugs R D,* 15**,** 13-20.

SACAN, A., EKINS, S. & KORTAGERE, S. 2012. Applications and limitations of *In silico* models in drug discovery. *In:* LARSON, R. S. (ed.) *Bioinformatics and Drug Discovery.* Totowa, NJ: Humana Press.

SADY, H., AL-MEKHLAFI, H. M., WEBSTER, B. L., NGUI, R., ATROOSH, W. M., AL-DELAIMY, A. K., NASR, N. A., CHUA, K. H., LIM, Y. A. L. & SURIN, J. 2015. New insights into the genetic diversity of *Schistosoma mansoni* and *S. haematobiumin* Yemen. *Parasites & vectors,* 8**,** 544-544.

SANCHEZ-SPITMAN, A. B., SWEN, J. J., DEZENTJE, V. O., MOES, D. J. A. R., GELDERBLOM, H. & GUCHELAAR, H. J. 2019. Clinical pharmacokinetics and pharmacogenetics of tamoxifen and endoxifen. *Expert Review of Clinical Pharmacology,* 12**,** 523-536.

SASAKI, H., ONOE, H., OSAKI, T., KAWANO, R. & TAKEUCHI, S. 2010. Parylene-coating in PDMS microfluidic channels prevents the absorption of fluorescent dyes. *Sensors and Actuators B-Chemical,* 150**,** 478-482.

SCHISTOSOMA JAPONICUM GENOME, S. & FUNCTIONAL ANALYSIS, C. 2009. The *Schistosoma japonicum* genome reveals features of host-parasite interplay. *Nature,* 460**,** 345-51.

SCHNEEBERGER, P. H. H., COULIBALY, J. T., PANIC, G., DAUBENBERGER, C., GUEUNING, M., FREY, J. E. & KEISER, J. 2018. Investigations on the interplays between *Schistosoma mansoni*, praziquantel and the gut microbiome. *Parasit Vectors,* 11**,** 168.

SECOR, W. E. & MONTGOMERY, S. P. 2015. Something old, something new: is praziquantel enough for schistosomiasis control? *Future Med Chem,* 7**,** 681-4.

SIMON, M., LISA, F., M., L. V., KATRIN, R., CLAUDIA, E., MAGDALENA, B., M., K. J., MAGNUS, I.-S. & WOLFGANG, M. 2018. Transcriptomic, proteomic, and functional long-term characterization of multicellular three-dimensional human liver microtissues. *Applied In Vitro Toxicology,* 4**,** 1-12.

SUN, T. & MORGAN, H. 2010. Single-cell microfluidic impedance cytometry: a review. *Microfluidics and Nanofluidics,* 8**,** 423-443.

SWINNEY, D. C. & ANTHONY, J. 2011. How were new medicines discovered? *Nature Reviews Drug Discovery,* 10**,** 507-519.

TERSTAPPEN, G. C. & REGGIANI, A. 2001. *In silico* research in drug discovery. *Trends in Pharmacological Sciences,* 22**,** 23-26.

TOEPKE, M. W. & BEEBE, D. J. J. L. O. A. C. 2006. PDMS absorption of small molecules and consequences in microfluidic applications. 6, 1484-1486.

TORINI, J. R., BRANDÃO-NETO, J., DEMARCO, R. & PEREIRA, H. D. M. 2016. Crystal Structure of *Schistosoma mansoni* Adenosine Phosphorylase/5'-Methylthioadenosine Phosphorylase and Its Importance on Adenosine Salvage Pathway. *PLOS Neglected Tropical Diseases,* 10, e0005178.

TÓTH, K., SIROK, D., KISS, Á., MAYER, A., PÁTFALUSI, M., HIRKA, G. & MONOSTORY, K. 2018. Utility of *in vitro* clearance in primary hepatocyte model for prediction of *in vivo* hepatic clearance of psychopharmacons. *Microchemical Journal,* 136, 193-199.

VALENTIM, C. L., CIOLI, D., CHEVALIER, F. D., CAO, X., TAYLOR, A. B., HOLLOWAY, S. P., PICA-MATTOCCIA, L., GUIDI, A., BASSO, A., TSAI, I. J., BERRIMAN, M., CARVALHO-QUEIROZ, C., ALMEIDA, M., AGUILAR, H., FRANTZ, D. E., HART, P. J., LOVERDE, P. T. & ANDERSON, T. J. 2013. Genetic and molecular basis of drug resistance and species-specific drug action in schistosome parasites. *Science,* 342, 1385-9.

VAN MEER, B., DE VRIES, H., FIRTH, K., WEERD, J., TERTOOLEN, L. G. J., KARPERIEN, H. B. J., JONKHEIJM, P., DENNING, C., IJZERMAN, A. P. & MUMMERY, C. L. 2016. Small molecule absorption by PDMS in the context of drug response bioassays. *Biochemical and Biophysical Research Communications,* 482.

WANG, W. & LIANG, Y. 2015. Mass drug administration (MDA) for schistosomiasis. *The Journal of Infectious Diseases,* 211, 848-9.

WISHART, D. S., KNOX, C., GUO, A. C., SHRIVASTAVA, S., HASSANALI, M., STOTHARD, P., CHANG, Z. & WOOLSEY, J. J. N. A. R. 2006. DrugBank: a comprehensive resource for *in silico* drug discovery and exploration. 34, D668-D672.

YOUNG, N. D., JEX, A. R., LI, B., LIU, S., YANG, L., XIONG, Z., LI, Y., CANTACESSI, C., HALL, R. S., XU, X., CHEN, F., WU, X., ZERLOTINI, A., OLIVEIRA, G., HOFMANN, A., ZHANG, G., FANG, X., KANG, Y., CAMPBELL, B. E., LOUKAS, A., RANGANATHAN, S., ROLLINSON, D., RINALDI, G., BRINDLEY, P. J., YANG, H., WANG, J., WANG, J. & GASSER, R. B. 2012. Whole-genome sequence of *Schistosoma haematobium*. *Nat Genet,* 44, 221-5.

YU, W. & MACKERELL, A. D., JR. 2017. Computer-Aided Drug Design Methods. *Methods in molecular biology (Clifton, N.J.),* 1520, 85-106.

ZHU, Z., CHEN, W. J., TIAN, B. T., LUO, Y. L., LAN, J. F., WU, D., CHEN, D., WANG, Z. X. & PAN, D. J. 2018. Using microfluidic impedance cytometry to measure *C. elegans* worms and identify their developmental stages. *Sensors and Actuators B-Chemical,* 275, 470-482.

ZINIEL, P. D., KARUMUDI, B., BARNARD, A. H., FISHER, E. M. S., THATCHER, G. R. J., PODUST, L. M. & WILLIAMS, D. L. 2016. The *Schistosoma mansoni* Cytochrome P450 (CYP3050A1) is essential for worm survival and egg development. *PLOS Neglected Tropical Diseases,* 9, e0004279.

Curriculum vitae

Flavio Lombardo

Date of Birth: 08.04.1987

Nationality: Italian

Address: Swiss TPH
Socinstrasse 57
4051 Basel

E-mail address: flavio.lombardo@unibas.ch

EDUCATION

10/2016-12/2019	**PhD in microbiology**, University of Basel, Basel, CH Thesis: Development of novel strategies to fill the empty drug pipeline for schistosomiasis: from drug sensitivity assay development to preclinical studies
11/2011-10/2014	**MSc biotechnology**, University of Bologna, Bologna, IT
11/2006-03/2011	**BSc molecular biology**, University of Catania, Catania, IT

PUBLICATIONS

Evaluation of Human Liver Microtissues for Drug Screening on Schistosoma mansoni Schistosomula
Lombardo, et al, ACS infection diseases, 2020

Parallelized Impedance-Based Platform for Continuous Dose-Response Characterization of Antischistosomal Drugs
PS Ravaynia & FC Lombardo, et al, Advanced Biosystems, 1900304, 2020

Life cycle maintenance and drug-sensitivity assays for early drug discovery in Schistosoma mansoni
FC Lombardo, V Pasche, G Panic, Y Endriss, J Keiser, Nature protocols 14 (2), 461-481, 2019

Combining mechanochemistry and spray congealing for new praziquantel pediatric formulations in schistosomiasis treatment
B Albertini, B Perissutti, S Bertoni, D Zanolla, E Franceschinis, Voinovich D, Lombardo FC, et al, International journal of molecular sciences 20 (5), 1233, 2019

Impedance-based microfluidic assay for automated antischistosomal drug screening
K Chawla, MM Modena, PS Ravaynia, FC Lombardo, et al, ACS sensors 3 (12), 2613-2620, 2019

Activity and pharmacokinetics of a praziquantel crystalline polymorph in the Schistosoma mansoni mouse model
FC Lombardo, B Perissutti, J Keiser, European Journal of Pharmaceutics and Biopharmaceutics 142, 240-246, 2019

EXPERIENCE

Experimental	LC-MS/MS method validation
	LC-MS/MS chiral separation
	Human primary liver microtissue cultures
	Cytotoxicity assays
	ELISA, PCR, ELISPOT
	Multicolor flow cytometry
Bioinformatics	LC-MS/MS data processing and analysis
	Analysis and visualization of PK/PD data
	R, Python, Shell

Languages

English: Fluent
Italian: Mother tongue
Portuguese: Intermediate
Spanish: Intermediate
German: Conversational